

Model-based measurement and control of fluidised bed spray granulation processes

Dissertation

zur Erlangung des akademischen Grades

**Doktoringenieur
(Dr.-Ing.)**

von Dipl.-Ing. Andreas Bück
geb. am 03.06.1982 in Magdeburg

genehmigt durch die Fakultät für Verfahrens- und Systemtechnik
der Otto-von-Guericke-Universität Magdeburg

Promotionskommission: Prof. Dr.-Ing. habil. Eckehard Specht (Vorsitz)
Prof. Dr.-Ing. habil. Evangelos Tsotsas (Gutachter)
Prof. Dr.-Ing. habil. Achim Kienle (Gutachter)
Hon.-Prof. Dr.-Ing. Mirko Peglow (Gutachter)

eingereicht am 12.06.2012

Promotionskolloquium am 05.11.2012

Foreword

*We are such stuff as dreams are made on;
and our little life is rounded with a sleep.*

W. Shakespeare, *The Tempest*, Act IV/I

This thesis is the result of research conducted as part of the research group *Nachwuchsforschungsgruppe Wirbelschichttechnik* (NaWiTec) at the Chair of Thermal Process Engineering at the Otto von Guericke University in Magdeburg from 2008 to 2012.

The research group NaWiTec was established in 2008 at the Chair of Thermal Process Engineering as part of the *InnoProfile* project *Unternehmen Region* and funded by the Germany Federal Ministry of Science and Education (BMBF), which is gratefully acknowledged.

Firstly, I want to express my gratitude to the head of the chair, Prof. Dr.-Ing. habil. Evangelos Tsotsas, and the head of the research group, Hon.-Prof. Dr.-Ing. Mirko Peglow – not only for being my advisors, but also for introducing a control engineer to the unexpected depths of drying technology and particle formulation, for creating a stimulating research environment and granting me the freedom to pursue other projects along the way.

I also thank Prof. Dr.-Ing. habil. Achim Kienle (Chair of Automation and Modelling) for the direct and indirect support over the last years, for his profound interest in the research and his willingness to review and evaluate the thesis. My thanks go also to Prof. Dr.-Ing. Eckehard Specht for chairing the defense of this thesis.

I also want to express my gratitude to my colleagues and friends in our group and at the Chair of Thermal Process Engineering for their support, especially: Dr.-Ing. Plamena Ihlow, Dipl.-Ing. Philipp Bachmann, Dipl.-Ing. Matthias Börner, Susanne Bögelsack, Dipl.-Ing. Mathias Dervedde, Dipl.-Ing. Christian Fischer, Dipl.-Ing. Neli Hampel and Dipl.-Ing. Torsten Hoffmann. Special thanks go to Dipl.-Ing. Franka Kretschmer with whom I have had the pleasure to share an office and many, many, many, many discussions on all things small and great in the last four years.

I am also grateful to Dr.-Ing. Stefan Palis for our joint efforts in shedding light on the mysterious and complex thing known as control of particulate processes.

Additionally, many thanks go to my friends for persistently performing the task of reminding me that there is a life *out there*. In order to minimise the danger of forgetting someone important, I refrain from naming them explicitly but with no intention to lessen my gratitude towards them all.

Last but not least, I would like to thank my family, especially my parents Leona and Rainer, and my brother Torsten, for their unconditional trust and support through all these years. It is to them that I dedicate this thesis.

Abstract

Particulate products play an important role in many industries and applications, for instance pharmaceuticals, fertilisers, or foods. Compared to the often liquid state of the raw materials, they are easier to transport, store and post-process. Furthermore, the transformation from liquid to solid allows for particle formulation, i.e. the production of particles with defined characteristics.

In general, the particles are not uniform, i.e. they possess a distribution in their properties, for instance size, shape, moisture content, or composition. This distribution also characterises the quality of the product. Increasing customer requirements give rise to the need to realise pre-defined, or required, property distributions of the particle in the process.

Widely used processes for the production of dustless, free-flowing powders from liquid raw materials are crystallisation and spray granulation in fluidised beds.

In fluidised bed spray granulation, which can be run batch-wise as well as in continuous mode, a solution, suspension or melt is sprayed onto a particle bed which is fluidised by heated air. Due to evaporation of the liquid in the spray, a particle growth can be observed as the solid in the spray solidifies on the particle surface. The combination of heat and mass transfer with particulate processes renders fluidised bed spray granulation a complex multiphase process. The realisation of a desired property distribution therefore necessitates the use of process control.

In this thesis a model-based scheme for the feedback control of particle size distributions as well as the particle temperature and moisture content in fluidised bed spray granulation is devised. The focus lies on the control of the particle properties in batch spray granulation and in continuous spray granulation with external classification by sieves and mills. Depending on the configuration of the external classification, i.e. the parametrisation of the sieves and the mill, a different dynamic behaviour is obtained: Whereas for some configurations a stable steady-state is attained, the steady-state is unstable for others. To achieve a steady-state with constant product mass flow for these cases, the unstable steady-states have to be stabilised by feedback control.

As a basis, mathematical process models for particle formation and heat and mass transfer in fluidised bed spray granulation are derived. In order to account for the distributed character of the particle properties the population balance approach is utilised yielding non-linear partial-integro differential equations for the temporal evolution of the particle size distribution. The models allows to analyse the dynamic behaviour of the process and build the core of the model-based feedback control scheme.

The implementation of feedback control requires information on the state of the process, for instance the particle size distribution. As this knowledge is not always available through direct measurements, model-based measurement systems, also known as state observers or estimators, are designed to reconstruct the particle size distribution from other measurements utilising the mathematical process models. It is demonstrated that the size distribution can be successfully reconstructed, for instance from measurements of the mean particle diameter.

Control of the particle size distribution in the batch and the continuous process is achieved by use of model predictive control: Based on the future evolution of the process calculated by the mathematical models, an optimal input trajectory is calculated yielding a required size distribution at the end of the batch and a stabilisation of unstable steady-states in the continuous process with external classification. Additionally, the particle moisture content and temperature is controlled by a multiple-input multiple-output controller.

The approach is tested in a first step using ideal measurements, i.e. it is assumed that all information required can be measured directly. In a second step this assumption is dropped and the designed model-based measurement systems and the controllers are combined into a model-based control scheme for feedback control of the particle properties. It is demonstrated that also this set-up is able to achieve the required control tasks.

Thus by using mathematical process models, the design of a model-based measurement scheme and model-based controllers allows to produce particles with pre-defined characteristics in fluidised bed spray granulation.

Zusammenfassung

Partikuläre Produkte sind von großer Bedeutung in vielen Industriezweigen und Anwendungsbereichen, z.B. der pharmazeutischen Industrie, der Landwirtschaft und der Lebensmittelproduktion. Im Vergleich zu ihren oftmals flüssigen Ausgangsstoffen weisen sie wesentliche Vorteile im Transport, der Lagerung und Weiterverarbeitung auf. Zusätzlich können bei der Umwandlung vom flüssigen in den festen Aggregatzustand den Partikeln bestimmte Eigenschaften aufgeprägt werden.

Im Allgemeinen sind die entstehenden Partikel jedoch nicht gleichartig, d.h. sie weisen Unterschiede in ihren Eigenschaften, z.B. der Größe, der Form, des Feuchtegehaltes oder der Zusammensetzung, auf. Diese Eigenschaftsverteilung der Partikel spiegelt sich auch in der Produktqualität wider, daher führen die stetig steigenden Kundenanforderung zu der Aufgabe partikuläre Produkte mit vordefinierten Eigenschaftsverteilungen herzustellen.

Für die Herstellung staubfreier, frei fließender Pulver werden oftmals Kristallisationsprozesse oder die Sprühgranulation in Wirbelschichten eingesetzt.

Bei der Sprühgranulation, die sowohl im Batch-Betrieb als auch in kontinuierlicher Fahrweise betrieben werden kann, wird eine Lösung, Suspension oder Schmelze auf eine Partikelschüttung eingedüst, die durch einen beheizten Gasstrom fluidisiert wird. Durch Verdampfung der Flüssigkeit kommt es zur Feststoffabscheidung auf der Partikeloberfläche und eine Größenänderung der Partikel kann beobachtet werden. Die Kombination aus Stoff- und Wärmeübergang und partikulären Prozessen gestaltet die Sprühgranulation zu einem komplexen Mehrphasenprozess. Für das Erreichen von gewünschten Produkteigenschaften ist daher der Einsatz von Prozessregelungen notwendig.

In dieser Arbeit wird ein modellbasiertes Konzept für die Regelung von Partikelgrößenverteilungen, die Partikelfeuchte und -temperatur in der Wirbelschichtsprühgranulation entwickelt. Der Fokus liegt dabei auf der Batch-Sprühgranulation sowie der kontinuierlichen Sprühgranulation mit externer Produktklassifikation und Partikelrückführung über einen Sieb-Mahl-Kreislauf. In Abhängigkeit der Konfiguration der Siebe und der Mühle liegt ein unterschiedliches dynamisches Verhalten des kontinuierlichen Prozesses vor: Während für einige Konfigurationen ein stabiler stationärer Zustand erreicht wird, ist der stationäre Zustand für andere Konfigurationen instabil. Um auch in diesen Fällen einen stationären Zustand mit konstanten Produktmassenstrom zu erhalten, ist eine Stabilisierung durch den Einsatz von Prozessregelungen erforderlich.

Als Grundlage fungieren mathematische Prozessmodelle für die Partikelprozesse und den Wärme- und Stoffübergang. Um dem verteilten Charakter der Partikelgröße Rechnung zu tragen, wird ein populationsdynamischer Ansatz zur Beschreibung der zeitlichen Entwicklung der Partikelgröße verfolgt. Dieser führt insgesamt auf partielle Integrodifferentialgleichungen zur Beschreibung des zeitlichen Verhaltens der Partikelgröße, -feuchte und -temperatur. Die abgeleiteten Prozessmodelle bilden den Kern des modellbasierten Regelungssystems.

Da die Implementierung von Prozessregelungen mitunter Informationen benötigt, die nicht di-

rekt oder nur sehr aufwendig gemessen werden können, wie z.B. die Partikelgrößenverteilung, werden in dieser Arbeit modellbasierte Messsysteme, auch bekannt als Zustandsbeobachter oder Zustandsschätzer, entworfen, die es erlauben, die Größenverteilung aus leichter zugänglichen Informationen dynamisch zu berechnen. Dies wird unter anderem durch die Rekonstruktion der Größenverteilung aus der Messung des mittleren Partikeldurchmessers und der Nutzung der Prozessmodelle demonstriert.

Zur Regelung der Partikelgrößenverteilung wird der Ansatz modellprädiktiver Regelungen verfolgt: Basierend auf einer mit Hilfe des mathematischen Prozessmodells berechneten zukünftigen Entwicklung des Sprühgranulationsprozesses wird durch die Lösung eines dynamischen Optimierungsproblems der optimale Stellgrößenverlauf ermittelt, der die gewünschte Größenverteilung am Ende des Batches bzw. die Stabilisierung eines instabilen Arbeitspunktes im kontinuierlichen Prozess mit Sieb-Mahlkreislauf ermöglicht. Für die Regelung der Partikelfeuchte und -temperatur werden Mehrgrößenregler eingesetzt, die die interne Verkopplung der Regelgrößen berücksichtigen.

Zunächst wird unter der Annahme idealer Messungen, d.h. alle zum Einsatz der Regler benötigten Größen können direkt gemessen werden, gezeigt, dass die entworfenen Regler in der Lage sind, die gestellten Ziele zu erreichen. Die Annahme wird dann fallen gelassen und durch Kombination der modellbasierten Messsysteme mit den entworfenen Reglern wird ein modellbasiertes Regelungssystem erschaffen, das in der Lage ist, die gestellten Regelungsziele auch unter Vorlage nicht-idealer Messinformationen, z.B. des mittleren Partikeldurchmessers an Stelle der Größenverteilung, zu erreichen.

Durch die Nutzung der mathematischen Prozessmodelle und dem Entwurf von modellbasierten Messsystemen und Regelungen wird damit ein modellbasiertes Regelungssystem entworfen, das die Realisierung von wichtigen gewünschten Partikeleigenschaften in der Wirbelschichtsprühgranulation ermöglicht.

Contents

1	Introduction	1
1.1	Motivation and scope of the thesis	1
1.2	Previous works	4
1.3	Outline of the thesis	7
2	Mathematical modelling of fluidised bed spray granulation processes	9
2.1	Fluidised bed processes	9
2.2	Fluidised bed spray granulation	11
2.3	Fundamentals of population balance modelling	13
2.4	Modelling of batch spray granulation	16
2.5	Modelling of continuous spray granulation with particle recycle	19
2.6	Derivation of the steady-state distribution in continuous spray granulation	23
2.7	Mathematical analysis of particle dynamics	26
2.7.1	Batch spray granulation	26
2.7.2	Continuous spray granulation with particle recycle	28
2.8	Modelling of heat and mass transfer	31
3	Model-based measurement of particle property distributions	36
3.1	Introduction	36
3.2	Fundamentals of model-based measurement systems	40
3.3	Design methods for model-based measurement systems	44
3.3.1	Design methods for state observers	45
3.3.2	Design methods for state estimators	50
3.4	Model-based measurement of size distributions	60
3.4.1	Structural observability of the spray granulation process	60
3.4.2	Application to batch fluidised bed spray granulation	63
3.4.3	Application to continuous spray granulation with particle recycle	80
4	Model-based feedback control of fluidised bed spray granulation processes	96

4.1	Introduction	96
4.2	Stabilisation of the continuous process with particle recycle	100
4.2.1	Linearisation of the model equations	101
4.2.2	Proportional-integral feedback control	102
4.2.3	LQ-optimal feedback control	104
4.2.4	Model predictive control	105
4.2.5	Feedback control results	113
4.3	Feedback control of batch fluidised bed spray granulation	126
4.4	Feedback control of heat and mass transfer	130
4.5	Model-based control systems for fluidised bed spray granulation processes	139
4.5.1	Batch fluidised bed spray granulation	140
4.5.2	Continuous fluidised bed spray granulation	144
4.5.3	Summary	150
5	Summary	152
A	Hydro- and thermodynamics of fluidised bed processes	158
A.1	Hydrodynamic correlations	158
A.2	Heat and mass transfer correlations	159
A.2.1	Heat and mass transfer between particles and suspension gas	159
A.2.2	Heat transfer between particles and wall	159
A.2.3	Heat transfer between gas and wall	160
A.2.4	Heat transfer between wall and environment	160
A.3	Material properties	161
A.3.1	Material properties of dry air	161
A.3.2	Material properties of water	162
A.3.3	Material properties of water vapour	164
B	Elements of graph theory	166
C	Method of characteristics	167
D	Discretisation of population balance equations	169
D.1	Finite volume method	170
D.2	Spectral methods	172
D.3	Convergence of discretisations	174
E	Root-locus method for feedback controller design	175

List of symbols

This thesis draws from a variety of fields of mathematics and engineering. In order to retain as much standard notation from each field as possible, the symbols used in the main text, and the appendices, are defined chapter-wise. When a symbol is re-defined in one chapter, it takes precedence over the definitions in previous chapters. If ambiguity may arise in the use of a symbol its meaning is re-stated at the point of use.

Chapter 2

Symbol	Description	Unit
c_p	specific heat capacity	$\text{J kg}^{-1} \text{K}^{-1}$
e	property coordinate	various
h	height	m
m	mass	kg
n	number density function	depending on e and x
q_0	normalised number density function	m^{-1}
p	net production density	depending on e and x
r	radius	m
s	solid, steady-state	
t	time	s
u	velocity	m s^{-1}
x	spatial coordinate	m
A	surface area	m^2
B	number flow rate of particles	s^{-1}
G	particle growth velocity	m s^{-1}
H	total enthalpy	J
\dot{H}	enthalpy flow rate	J s^{-1}
K	outlet kinetics	s^{-1}
\dot{M}	mass flow rate	kg s^{-1}
N	total number of particles	
NTU	number of transfer units	
P	total net production of particles	s^{-1}
\dot{Q}	heat flow	J s^{-1}
S	surface of property space	
T	separation function	
V	volume	m^3
X, Y	moisture content	$(\text{kg liquid}) (\text{kg dry matter})^{-1}$
\mathbf{n}	outward normal vector	

Symbol	Description	Unit
α	heat transfer coefficient	$\text{W m}^{-2} \text{K}^{-1}$
β	mass transfer coefficient	m s^{-1}
η	mass transfer efficiency	
θ	temperature	$^{\circ}\text{C}$
λ	parameter	
μ	total moment of density function	depending on e and x
\dot{v}	normalised drying velocity	
ξ	particle size	m
ϱ	mass density	kg m^{-3}
ϕ	transport flux	depending on e and x
ψ	mean porosity	
Δh_{evap}	specific evaporation enthalpy	J kg^{-1}
Φ	total flow of particles	s^{-1}
Ω	property space	

Chapter 3

Symbol	Description	Unit
e	error	
k	state correction gain	
p	probability distribution	
s	chord length	m
u	input to system, manipulated variable	
v	bias (noise)	
w	weights	
x	state of dynamic system	
\hat{x}	estimate of x	
y	measured variable	
\hat{y}	measurement calculated from \hat{x}	
A, B, C, D	matrices of linear state space system	
E	integral error	
K	observer gain matrix	
M	number of measured outputs	
N	number of states	
O	observability matrix	
P, Q, R	covariance matrix	
S	Cholesky factor	
T	horizon length	s
U	number of inputs	
V	Lyapunov function candidate	
X	set of sigma points	
Y	set of transformed sigma points	
\mathcal{D}	finite-dimensional approximation of derivative operator	
α	design/tuning parameter	
η, ω	bias (noise)	
λ	eigenvalue of a matrix	
Δt	sampling interval	s

Chapter 4

Symbol	Description
d	disturbance signal
r	reference signal
u	manipulated variable
y	output signal (measured, controlled)
C, P	transfer function, matrix
G	transfer function matrix
J	cost functional
K	controller gain
N	number of horizons
Q, R	weight matrix
T	time constant, sampling time
C	controller (abstract)
\mathcal{P}	process (abstract)
α	coupling factor
Δ	deviation, increment
Ξ	decoupling network

Appendices

Symbol	Description	Unit
a	spectral weights	
Ar	Archimedes number	
Gr	Grashof number	
Le	Lewis number	
Nu	Nusselt number	
Pr	Prandtl number	
Ra	Raleigh number	
Re	Reynolds number	
Sc	Schmidt number	
Sh	Sherwood number	
δ	diffusion coefficient	$\text{m}^2 \text{s}^{-1}$
η	dynamic viscosity	$\text{kg m}^{-1} \text{s}^{-1}$
ϑ	temperature	$^{\circ}\text{C}$
λ	thermal conductivity	$\text{W m}^{-1} \text{K}^{-1}$
ν	kinematic viscosity	$\text{m}^2 \text{s}^{-1}$
ψ	spectral nodes	

Subscripts

Symbol	Description
0	smallest size considered, initial value
des	desired
elu	elutriation
evap	evaporation
g	gas
gp	gas – particle
gw	gas – wall
mf	minimal fluidisation
nf	noise-free
nuc	nuclei
opt	optimum
pw	particle – wall
rec	recycle
s	solid
sample	sampling
sat	saturation
sus	suspension, solution
v	vapour
CLD	chord-length distribution
E	internal property space
M	mill
X	external property space

Chapter 1

Introduction

1.1 Motivation and scope of the thesis

Major portions of all industrially processed goods exist in the form of particulate substances. If one generalises the term “particle” from the classical sense of grains to, for instance, solutions, suspensions (solid material in liquid), aerosols (liquid droplets in gas), or gas bubbles in a liquid, then up to three quarters of all processed goods fall into this category [99].

There are many examples of particulate products in everyday-life: milk powder, milled and roasted coffee, instant cacao powder, and sugar, to name just a few. Additionally, particulate products play an important role in other fields: health-care (e.g. in form of an active pharmaceutical ingredient pressed into a tablet), in agriculture in the form of fertilisers, or in the chemical industry as catalyst powders.

Particulate goods in the form of powders produced from liquid raw materials do have many advantages; they are for instance often easier to transport, store, and post-process than in their liquid form. One illustrative example is milk: In its liquid form it has to be kept cool at all times to keep it from spoiling. However, if it is spray-dried, i.e. the water is removed from the emulsion by drying, it can be stored at room temperature for a long time. The liquid form can easily be restored at all times by just adding water to the powder.

The product properties can often be characterised by the particle properties, or rather the particle properties affect the properties of the product. Important particle properties are for instance

- the particle size and form,
- the porosity of the particle,
- the moisture content, and
- the enthalpy (temperature).

The particle size and form determine for instance the *flow-ability* of a powder: If the particles in the powder are too small, then cohesive forces between the particles prevent a free flow. This can be observed by comparison of sugar powder and crystal sugar: Although both products consist of the same material, sugar powder flows less freely because of the smaller size of the particles. The size also has great influence on *safety and environmental issues*: If a particulate commodity is produced from toxic material and dust is produced and set free, the danger of inhaling the toxic substance exists, which may lead to long-term health degradation. On the environmental side, the

release of a herbicide dust may lead to the decease of essential insects if they consume the very fine particles. Additionally, very fine powders pose the danger of explosion, if they are dispersed in a gaseous medium.

Apart from these aspects, the particle size can have an influence on the *efficiency* of a product, e.g. in pharmaceuticals: Here, the aim may be the production of a tablet with a pre-defined dissolution characteristic of the active ingredient. This characteristic is influenced by the thickness of a coating layer that is applied to the active ingredient to shield it from the acids, mostly hydrochloric acid, in the stomach. The efficiency of the active ingredient strongly depends on the quality of the layer: If it is too thin, the ingredient becomes active before it reaches its desired destination (often the intestine) – if it is too thick, it may not dissolve at all.

The porosity of the particle also has influence on the product properties: If the particle is very porous then it may have a decreased *storage stability*, i.e. the particle may crumble under application of forces, for example the weight of other particles. This may lead to a layer of dust-like particles at the bottom of a storage container. It can also influence the efficiency of product: As was mentioned above, in pharmaceuticals the aim is to produce a product with a pre-defined dissolution characteristic. If the particle is too porous the active ingredient may be released too fast, leading in a worst case to an overdose, if it is too compact the release may be too slow, and the ingredient may have only a very limited effect.

Moisture content and temperature have an influence on the transport and the storage of the product. If the commodity is too moist it may form very large particles that cannot be used any further. One example is the production of sugar: If the sugar is put into a silo with too high a moisture content and temperature, it will form – by cooling – a particle with the size of the silo (in the worst case). To prevent such events a post-processing of the commodity is often necessary, i.e. drying and cooling. These are two energy-extensive processes with great influence on the cost of the production, i.e. the particle properties can have an influence on the *economics* of the product.

Additionally, the porosity of the formed particle is influenced by the humidity and the temperature during the process. This can be seen in Fig. 1.1 where particles with a different final porosity are produced. Depending on the product specifications, the moisture of the particles and the gas, and the temperature have to be regulated for the product to comply to the desired specifications.

For the production of particulate substances from liquid starting material (solutions, emulsions, or suspensions) various processes exist: e.g. crystallisation, granulation, and spray drying. These can be further specialised depending on the characteristic effect that is used for the transformation, for example cooling crystallisation or spray granulation.

Crystallisation and granulation are complex dynamic processes, involving multiple phases (fluid and solid), heat and mass transfer between these phases, as well as particle formation processes.

One process that is often used in industries, e.g. in pharmaceuticals, foods, and fertilisers, is *fluidised bed spray granulation*. It allows for the production of a dustless, free-flowing particles from liquid raw materials: The suspension (or solution) is sprayed onto particles in the process chamber and due to drying – the bed is fluidised by hot air – the liquid evaporates. The remaining solid builds up a new layer of solid material on the particles. A simplified schematics of this process is shown in Fig. 1.2.

Furthermore, fluidised bed spray granulation can be run in batch as well as continuous mode, and drying and particle formation processes can be coupled and run simultaneously in one apparatus. The structure of the apparatuses is simple, and due to the high heat and mass transfer between the phases induced by the fluidisation, compact plants – compared to other technologies – can be designed. A detailed presentation of fluidised bed spray granulation is postponed for the moment,

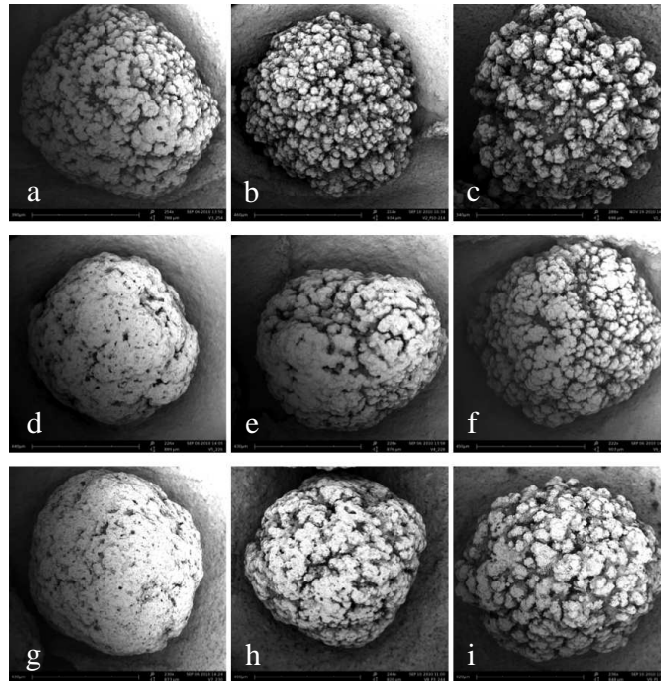


Figure 1.1: Influence of the humidity and the process temperature on the final structure of the produced particles [55]. From left to right: Increase in humidity; from top to bottom: increase in process temperature.

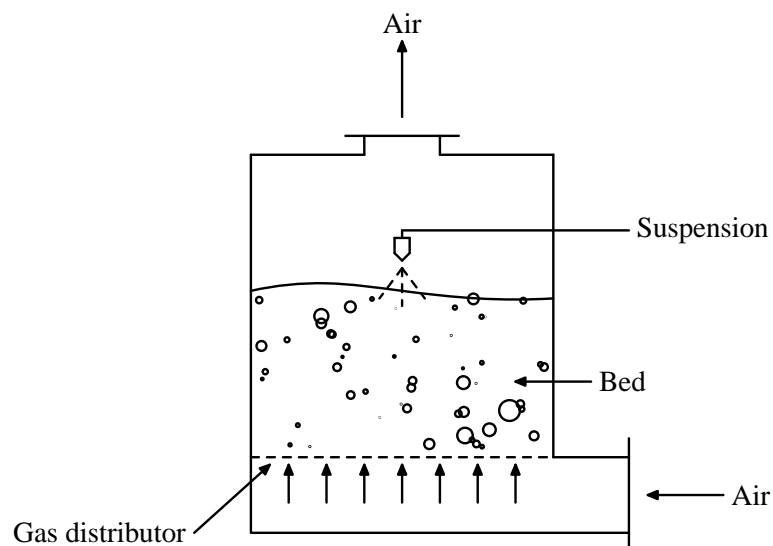


Figure 1.2: Simplified schematic of a fluidised bed spray granulation process. Instead of a suspension, solutions or melts are also sprayed in many applications.

but will be given in Chapter 2.

In the practical realisation of particle formation processes the following problem arises: The particles are not uniform, i.e. they differ in their properties, for instance in size, form, or colour. This means that the particles in the powder do possess a distribution with respect to their properties, and therefore the product also possesses a property distribution. Given a product specification then requires that the distribution lies within the limits posed by the specifications to be accepted by a customer.

The product specifications can be very strict, for instance in processes with costly raw materials or where the product is a hazardous good, and are further increasing. The need to guarantee that the product complies to the specification motivates the use of *process control* systems in particle processes. Today, practically implemented control systems mostly concentrate on the regulation of heat and mass transfer (e.g. product moisture and temperature), and integral values (e.g. total mass of product) or mean values (e.g. mean particle size) of the particles. Although the control schemes are for most part sufficient for their tasks, they cannot guarantee that the property distribution as a whole complies to the specifications. This means that in light of the increasing strictness of product specifications the control schemes have to be improved.

The basis for almost all control scheme design methods is formed by mathematical models that represent the dynamic behaviour of the processes – in this case of heat and mass transfer and particle formation.

The problem with these processes is that they are *distributed parameter systems*, and have to be modelled mathematically by non-linear partial differential equations to account for the distributed character. The mathematical analysis of this class of systems is in general intricate and the design of a control scheme for a property distribution is therefore a challenging task. The necessity for a controller to have information on the current state of the process, e.g. the current property distribution, leads to another challenging task: the measurement of property distributions.

In this thesis *model-based control schemes* for the control of particle size distributions in two practically relevant fluidised bed spray granulation processes – batch granulation and continuous granulation with external classification and particle recycle – are devised. The thesis focuses in a first part on the reconstruction of particle size distributions from process measurements by *model-based measurement systems*; in a second part the feedback control of particle size distributions, coupled with heat and mass transfer, by *model-based controllers* is considered.

1.2 Previous works

The topics of this thesis draw from several fields of mathematics and engineering. More precisely:

- Modelling of property-distributed systems
- Modelling of heat and mass transfer in fluidised beds
- Measurement of property distributions
- System theory and control of property-distributed systems

Modelling of property-distributed systems: In principle the modelling of property-distributed systems, i.e. the description of the dynamic behaviour of the property distribution of particles, can be carried out on two levels: microscopic and macroscopic. On the microscopic level all particle formation processes (e.g. interactions of the particles with other particles, or spray droplets) are

modelled and evaluated for every single particle in the system. For reviews on the state-of-the-art in microscopic modelling of particle formation processes, see for instance the articles of Iveson et al. [62] and Deen et al. [28].

In the microscopic modelling community, often discrete element methods (DEM) and Monte-Carlo methods are used for the description of the dynamic behaviour of the particulate systems, see for instance [30, 112, 6, 106] for application of discrete element methods, and for the application of Monte-Carlo methods [132, 76, 86, 153, 98, 135, 29].

Because of the explicit consideration of every single particle in the system, this approach has the potential to produce very accurate results. However, for the description of real-world problems, where the number of particles in the system can be extremely large, the actual computation of the properties for each particle is not feasible. The practical use of microscopic modelling can be found in the determination of the structure of kinetics of particle formation processes. Here, using statistical theory, only a small number of particles – compared to an industrial process – has to be considered.

Macroscopic modelling, on the other side, does not treat every particle separately: Particles with the same properties, for instance size, are collected in property classes. In the limit, i.e. infinitesimal classes, a property distribution is obtained. The modelling then describes the temporal evolution of a given property distribution under the occurring particle formation processes.

One well-established framework for the macroscopic modelling of property-distributed systems that is well-suited for the modelling of industrial-scale processes, is the *population balance approach*, introduced for problems in statistical mechanics by Hulburt and Katz in the 1960s [60]. To the field of particulate processes it was transported by the work of Randolph and Larson [115] (with a focus on crystallisation); it was advertised and established in a series of journal publications by D. Ramkrishna and co-workers. These publications were later turned into a book that is considered a standard reference [114].

In the literature, many successful applications of population balance modelling to particulate processes can be found, for instance in

- crystallisation [77, 63, 85, 57],
- granulation [144, 52, 100, 142, 79],
- drying [140, 108, 107], or
- aerosol processes [9, 67] .

As the focus of this work lies on the application to industrial-scale plants, the macroscopic modelling approach based on population balances will be used to describe the dynamic behaviour of the particle property distributions.

Modelling of heat and mass transfer in fluidised beds: Heat and mass transfer are classical topics in thermal process engineering, and thus extensively investigated. In fluidised bed processes, the heat and mass transfer is governed by the hydro- and thermodynamics of fluidised beds. They form a complex topic: The basis of the hydrodynamics is set by the Navier-Stokes equation (conservation of linear momentum of the fluid and the particles), the basis of thermodynamics is conservation of total energy in the system. Due to the complexity of these equations, most approaches do not use them directly, but derive empirical or semi-empirical models for the description of the hydro- and thermodynamics, see for instance the reference works of Kunii and Levenspiel [75] and Mörl et al. [100] for an extensive treatment of the hydrodynamics, and for example the works

of Schlünder and Tsotsas [127], Groenewold and Tsotsas [50], Burgschweiger and Tsotsas [14] for a presentation of the thermodynamics, or the recently published book series *Modern Drying Technology* [138] for a general treatment of heat and mass transfer in particulate systems.

Measurement of property distributions: In general, the task of measuring property distributions is multifaceted, and many different measurement principles exist. A recent overview and practical applications in various fields are given in the book of Merkus [99].

For the case of measuring the particle size distributions direct offline methods, e.g. sieving, and in-line methods, for example laser-diffraction or focused beam reflectance, or fibre-optical methods [66, 124, 40] are available. Although these methods become increasingly popular, they suffer from one important disadvantage: The probes do not measure the size distribution directly, but, for example, a chord-length distribution. This proves to be a major obstacle in the direct use of the measurements in process monitoring and control applications and makes the development of a transformation from the chord-length to the particle size distribution necessary. It turns out to be a difficult problem to which up until now only solutions for special cases have been found, see for instance [150, 66, 124, 40] for approaches, results, and limitations (e.g. the influence of measurement noise).

A model-based approach, that has been in use in other fields of chemical engineering for several decades, has in recent years emerged in particle size measurement: model-based measurement systems, also known as state observers or state estimators. The idea was conceived in the 1960s–1970s by Kalman [68] and Luenberger [82] and extended in the following decades. Application to various spatially distributed systems in chemical engineering can be found, see for instance [151, 69, 16, 90, 58, 152, 88] for applications in reaction engineering and fuel cells.

For particulate processes the methods are not yet established, but are gaining interest with the increase in property-distributed modelling, as evidenced by some recent work in crystallisation and fluidised bed spray granulation [91, 89, 13, 87].

As model-based measurement schemes can offer many advantages over classical and in-line measurement systems, that will be detailed in Chapter 3, the focus in this thesis will lie on this type of measurement systems.

Systems theory and control of property-distributed systems: Property-distributed systems are systems with distributed parameters and are from a systems-theoretic point of view infinite-dimensional. The mathematical theory is in general very complex. This is the main obstacle in the analysis and development of general control design methods for distributed parameter systems.

Over the decades various efforts have been taken to establish a systems theory for infinite-dimensional systems. So far, only the linear case is at a level comparable to finite-dimensional systems, major contributions are [147, 45, 42, 27, 103, 8, 26]. However, even in the linear case the theory is mathematically highly involved, drawing from operator theory, and functional analysis.

In the case of nonlinear distributed system the treatment is restricted in most cases to practically important process structures, see for instance [23, 128, 21, 22]. Nonetheless, control schemes are successfully designed for distributed parameter systems, for applications to spatially-distributed systems see for instance [69, 21, 22, 118, 3, 88, 2].

There are also contributions in the field of property-distributed processes available, for instance

- Kalani and Christofides [67]: nonlinear controller design applied to an aerosol process on the basis of a reduced model,
- Chiu and Christofides [20]: nonlinear controller applied to a crystallisation process on the basis of a reduced model.

- Pottmann et al. [110] design a model-predictive controller for a drum granulation system;
- Vollmer and Raisch [141] design a stabilising controller for an unstable crystallisation process using H_∞ -theory;
- Shi et al. [130] design a model-predictive controller for a batch crystallisation process;
- Dueñas Díez et al. [36] control inventories of a property-distributed process by passivity-based control.
- Villegas et al. [140] present a distributed control scheme in a batch fluidised bed dryer; and
- Glaser et al. [46] present the design of a model-predictive controller for continuous drum granulation.

Recently, Palis and Kienle [104, 105] presented results on stabilisation of unstable steady-states in continuous fluidised bed spray granulation using H_∞ -theory and discrepancy-based control, assuming that the size distribution of particles can be measured. Apart from this publication, the control of particle property distributions in fluidised bed spray granulation, especially in combination with model-based measurement systems, has not received much attention.

Because of the high practical importance of these processes, this thesis aims at closing the gap by developing a model-based feedback control system for fundamental product properties, for example the particle size distribution, the particle moisture content, and the particle temperature, in fluidised bed spray granulation in batch, as well as continuous processes. In addition to the task of designing suitable feedback controllers, a main focus lies on the reconstruction of particle property distributions from available plant measurements.

The basic components for all tasks which will form a control system are mathematical process models that describe the dynamic behaviour of the spray granulation process.

1.3 Outline of the thesis

This thesis consists of four chapters covering the mathematical modelling of fluidised bed spray granulation processes, the model-based measurement of particle size distributions, and the design of feedback controllers to achieve desired product properties. In detail:

In Chapter 2 the dynamic process models are derived: Starting with fluidised bed processes and their characteristics in general, spray granulation processes are presented. The modelling starts with the consideration of the particles in the process; all process assumptions used in the remainder of the text are motivated and stated. To describe the dynamic evolution of the particle property, i.e. the particle size, a population balance approach [114] is used. Afterwards, a mathematical analysis of the process dynamics for the batch and the continuous process with particle recycle is presented. The chapter ends with the modelling of heat and mass transfer during spray granulation.

In Chapter 3 various concepts for model-based measurement systems are presented and applied to the fluidised bed spray granulation processes with the aim of reconstructing the particle size distribution from limited or noised process measurements. Different concepts are evaluated and compared with each other.

Model-based feedback controllers for the particle size distributions in the granulation processes are designed in Chapter 4. Additionally, feedback controllers for the heat and mass transfer are designed. The feedback controllers and the model-based measurement systems are then linked to

form the final model-based control scheme. The feedback controllers and the model-based control scheme are evaluated and the results are discussed.

In Chapter 5, the main results of the thesis are summarised and an outlook to future research is given.

In the appendices methods and concepts from mathematics, control engineering, and hydro- and thermodynamics that are needed for certain sub-steps are summarised.

Chapter 2

Mathematical modelling of fluidised bed spray granulation processes

As was motivated in the introduction, the aim of this thesis is the control of product properties in fluidised bed spray granulation processes. The basis for controller design is a dynamic process model. In principle, the more accurate the process description the more can be said about the process result. But an overabundance of details may also drastically complicate the controller design process, so at some point assumptions are made, that will later on simplify the controller design without sacrificing too much in the accuracy of the process result.

In this chapter, at first a general overview on the principles and applications of fluidised bed processes is given. Afterwards a phenomenological description of spray granulation is presented. In section three the concepts of population balance modelling are introduced. In the subsequent sections these concepts are applied to a batch spray granulation and a continuous granulation process to describe the temporal evolution of the particle property distribution. After a discussion of the general dynamic behaviour of these processes, a dynamic model for the heat and mass transfer during spray granulation is derived.

2.1 Fluidised bed processes

An apparatus consisting of a process chamber with a distributor plate at its bottom, that can be passed by a flow of fluid (gas or liquid), is considered. On top of the distributor plate a *packed bed*, i.e. particles at rest (also: *fixed bed*), with mean porosity ψ is situated, Fig. 2.1(a).

Now a fluid flow is applied to the apparatus via the distributor plate. If a certain mass flow rate (corresponding to a fluid velocity) is reached, a loosening of the bed is observed, and the particles hover and move randomly in the bed. This state is called *fluidised bed* (Fig. 2.1(b)); the minimum velocity necessary to reach it is called minimum fluidisation velocity. An expansion of the bed height, compared to the initial fixed bed, and a change in porosity can also be observed. Further increasing the fluid flow yields a further expansion of the bed and an intensive mixing of the particles in the bed, see Fig. 2.1(c). Macroscopically, the particles behave like a fluid in this state. If the fluid flow is further increased, at some point the particles are transported out with the fluid flow. This state is called pneumatic transport or *elutriation of particles*; the corresponding fluid velocity is called elutriation velocity (Fig. 2.1(d)).

The range of existence for a fluidised bed is defined by the two limit velocities: It starts at the minimum fluidisation velocity and ends at the elutriation velocity [100].

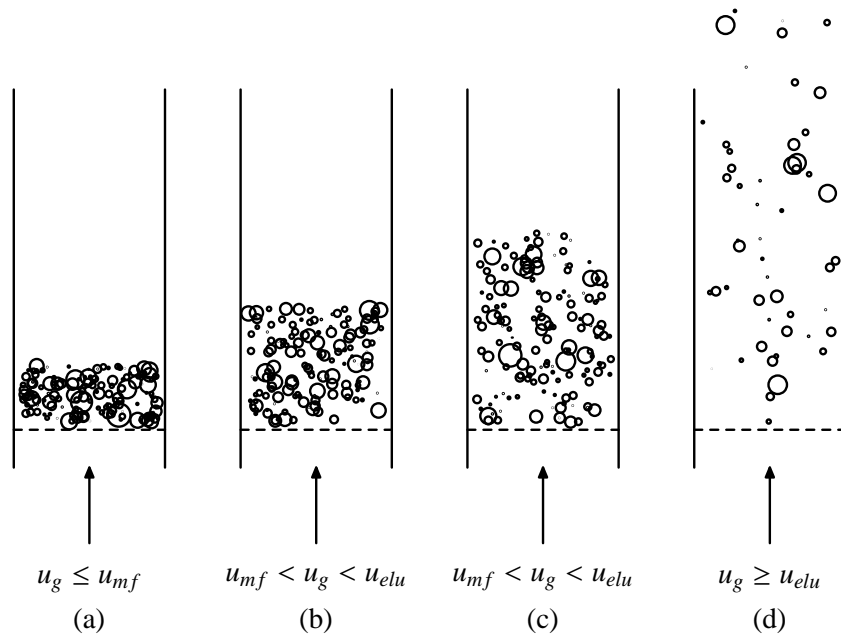


Figure 2.1: Different stages of a fluidised bed: (a) fixed bed; (b)–(c) fluidisation; (d) pneumatic transport (elutriation) [75].

Geldart [44] identified for two parameters, the mass density and the diameter of the particles in the bed, four groups (depicted in Fig. 2.2) with different fluidisation behaviour:

- *Group C*: Particles with a size less than $50\mu\text{m}$ fall into this group. They are very difficult to fluidise because of the strong cohesive forces between the particles.
- *Group A*: Particles in a range of $50 - 200\mu\text{m}$ and a mass density in a range of $700 - 1400\text{kgm}^{-3}$. These are not so difficult to fluidise but a strong expansion of the bed (even at minimum fluidisation velocity) is experienced. Additionally, hardly controllable gas bubbles build up in the bed.
- *Group B*: These particles with a range of $40 - 500\mu\text{m}$ and a density in between $1400 - 4000\text{kgm}^{-3}$ are preferred for fluidised bed applications. Although here also gas bubbles build up, the amount depends only on the fluid velocity and can easily be controlled.
- *Group D*: Particles with a very large size or with a very high mass density fall into this class. They are difficult to fluidise by the setup described above (owing to bubble formation), but can be fluidised quite well in a modified apparatus, the spouted bed.

There are several types of fluidised bed systems, e.g.

- gas-solid fluidised beds, and
- liquid-solid fluidised beds.

In order to use fluidised beds of particles of different sizes, the process chamber is widened at the top. This yields a reduction of fluid velocity and allows particles up to a certain size to sink back into the process chamber, thus reducing the amount of elutriated material. This extension of the process equipment is of great importance if a bed with a very wide range of sizes is to be fluidised,

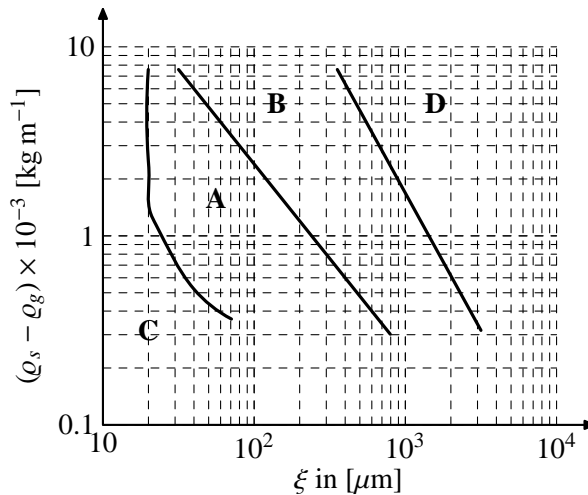


Figure 2.2: Classification of particles into four groups depending on their fluidisation behaviour after Geldart [44].

because as the minimum fluidisation velocity and the elutriation velocity depend on the particle size it might happen that for some particle sizes the elutriation velocity has already been reached, whereas for others the minimum velocity has barely been reached.

Fluidised bed processes are widely applied in different areas of chemical and process engineering, for instance:

- mixing of particulate materials,
- classifying and sorting of particles, or
- drying.

An important application of fluidised bed processes is the production of granules. It is promoted by the heat and mass transfer in the bed due to the mixing induced by the fluid flow. One way to realise the production of granules is by spray granulation, which will be presented in the next section.

2.2 Fluidised bed spray granulation

In fluidised bed spray granulation solid material, for instance in form of a suspension or a solution, is sprayed onto the particles that are fluidised by a gas flow. For that purpose a nozzle is installed in the process chamber. Most common configurations are: If the nozzle is installed above the particle bed (at rest), it is called top-spray configuration. If the nozzle is situated at the bottom of the process chamber, i.e. the particles are sprayed from below, it is called bottom spray configuration.

In both cases suspension (solution) droplets leave the nozzle and are deposited on the particles. Due to the external heating of the fluidisation gas flow the liquid in the suspension evaporates, the solid remains on the particle, see Fig. 2.3 where for two different process times particles taken from a spray granulation process are shown. Due to the intensive mixing of particles in the bed, the deposition of solid on a droplet can be considered uniform. Phenomenologically, a layering growth of the particles and an increase in size is observed. This mechanism is depicted in Fig. 2.4.

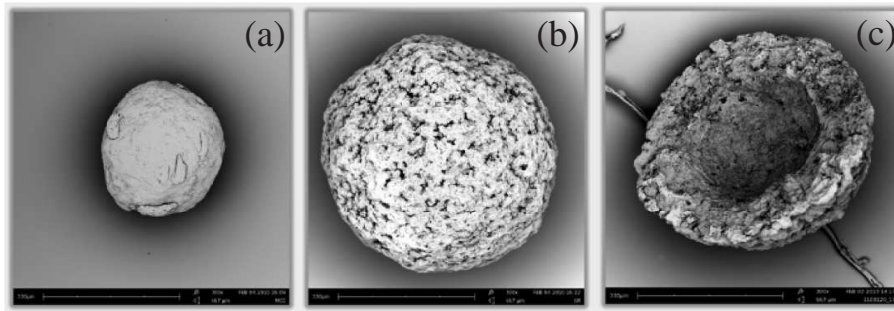


Figure 2.3: Evolution of a particle during spray granulation: (a) initial particle; (b) final particle; (c) formed layer.

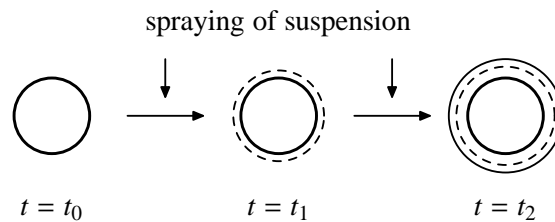


Figure 2.4: Schematic representation of layering growth of particles by spray granulation.

If the solid contained in the spray is identical to the material of the particles in the bed, the process is called *spray granulation*. It is used for instance in food industries and in the production of fertilisers (urea melt granulation). If the materials differ, the process is called *coating*. It finds wide application in pharmaceuticals, for instance in the coating of the active pharmaceutical ingredient with a protective layer, or in the production of tablets with several layers of different active ingredients. The mechanism in both cases, however is the same: A suspension or solution is sprayed onto some carrier particle, the liquid is evaporated and a new layer is formed.

Other effects that can occur during spray granulation are

- *Pre-drying of droplets*: When a droplet leaves the nozzle it comes almost instantaneously in contact with the heated fluidisation gas and evaporation of the liquid starts. If the distance to the bed is very large or drying is very fast, i.e. the gas flow is very hot and dry, the liquid will evaporate before the droplet can deposit on a particle in the bed. The droplet will then form a very small solid particle (a nucleus) on its own. This effect is called *nucleation*.
- If two particles with not completely dried surfaces collide in the bed, and the viscosity of the suspension on the surface is sufficiently high, a solid bridge between the particles will form. In the simplest case two particles will afterwards form a new, larger particle. This effect is called *agglomeration*. A criterion on the occurrence in fluidised bed processes has been given by Ennis et al. [37].
- An effect opposite to agglomeration occurs if an agglomerate collides with another particle or the walls of the process chamber. If the kinetic energy of contact cannot be absorbed by the solid bridges the agglomerate will break. The effect is therefore called *breakage*. The criteria when a bridge (or even a particle) will break are still investigated in solid process engineering.

In the following spray granulation, i.e. the layering of particles, will be considered in a two-phase setting: The solid particles are dispersed in the gas phase. In addition to the layering of particles

heat and mass transfer over the phase boundaries occurs. In order to simplify the subsequent modelling, the liquid is not considered as an individual phase but as a part of either the solid phase (in the form of liquid) or the gas phase (in the form of vapour).

In general the particles in the bed are not uniform; they may differ in their properties, e.g. size, enthalpy, moisture, porosity or form. Also the spatial position of each particle in the process chamber will be different. If all particles are considered as individuals of a particle population, and to each particle values for its properties are assigned that are chosen such that the product can be characterised easily, then the population possesses a *distribution* with respect to the chosen properties.

The modelling of the change of this property-distribution, and thus the modelling of the process, can be done by using the *population balance framework*. The fundamentals will be presented in the next section before it is applied to two configurations of fluidised bed spray granulation processes.

2.3 Fundamentals of population balance modelling

In the following a balance volume, for example, the process chamber of a fluidised bed process, with a particle population with a total number of N particles is considered. The change in number in the system can be modelled as

$$\frac{dN}{dt} = \Phi(t) + P(t) \quad (2.1)$$

where $\Phi(t)$ denotes the net flow of particles over the system boundary, and $P(t)$ is the net production rate of particles in the system, i.e. summing all sub-processes that create new particles and all sub-processes that consume particles.

This formulation, however, gives no information on the properties of the particles in the system. To this end the notion of a *number density function* is introduced: It describes the number of individuals (particles) that lie in the same infinitesimal property interval $[\tilde{e}, \tilde{e} + d\tilde{e}]$. The total number of all particles in the system can then be expressed by the number density function as follows:

$$N(t) = \int_{\Omega} n(t, \tilde{e}) d\tilde{e} . \quad (2.2)$$

Here Ω is the property-space of the particles, i.e. all possible values \tilde{e} can attain are included in Ω . By convention, the number density is non-negative, i.e. $n \geq 0$.

Population balance modelling is the description of the temporal evolution of the number density function (or other functions derived from it, e.g. mass density function). For this, all sub-processes have to be modelled in terms of the number density function. This concept was first introduced by Hulbert and Katz [60], and extended by Ramkrishna [114] in the field of particulate processes.

The state of a particle is characterised by its properties. In general, two types of coordinates are distinguished: external coordinates (the spatial position in the system, maximum of three), and internal coordinates (particle properties, e.g. the size). In total, these properties span a property state-space: Usually, during the process the properties of a particle will change; this corresponds to a movement in state-space. The modelling then describes the curve the particles trace out over process time. This idea is depicted in Fig. 2.5 for one external coordinate x and one internal coordinate e .

If the property state-space is written as the Cartesian product of the state-space of external properties Ω_X and the state-space of internal properties Ω_E , i.e. $\Omega = \Omega_X \times \Omega_E$, the total number can be

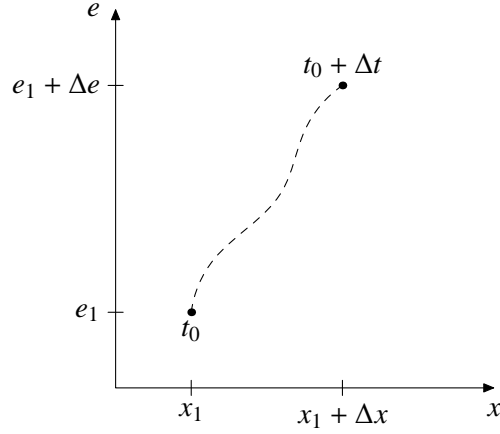


Figure 2.5: Movement of a particle in property state-space.

expressed as:

$$N(t) = \int_{\Omega_X} \int_{\Omega_E} n(t, x, e) de dx, \quad x \in \Omega_X, e \in \Omega_E. \quad (2.3)$$

The unit of the number density function is defined by the units of the properties:

$$[n] = \frac{1}{\prod_i [e_i] \prod_j [x_j]}. \quad (2.4)$$

In the special case of no external coordinates, i.e. $\dim(x) = 0$, corresponding to a well-mixed system, the following holds:

$$N(t) = V \int_{\Omega_E} n(t, e) de, \quad (2.5)$$

with $V = \text{vol}(\Omega_X)$ being the physical volume of the system.

In order to derive a balance, equation Eq. (2.3) is inserted into Eq. (2.1), yielding:

$$\frac{dN}{dt} = \frac{d}{dt} \int_{\Omega_X} \int_{\Omega_E} n(t, x, e) de dx = \Phi(t) + P(t). \quad (2.6)$$

If transport and production densities are introduced in an analogous way, i.e.

$$\Phi(t) = - \int_{S_X} \int_{S_E} \langle \varphi(t, x, e), n \rangle d\sigma_e d\sigma_x, \quad (2.7)$$

$$P(t) = \int_{\Omega_X} \int_{\Omega_E} p(t, x, e) de dx, \quad (2.8)$$

then the balance equation can be written as

$$\frac{d}{dt} \int_{\Omega_X} \int_{\Omega_E} n(t, x, e) de dx = - \int_{S_X} \int_{S_E} \langle \varphi(t, x, e), n \rangle d\sigma_e d\sigma_x + \int_{\Omega_X} \int_{\Omega_E} p(t, x, e) de dx. \quad (2.9)$$

In the definition of the transport density (transport flux) φ , it is accounted for that Φ only enters or leaves via the system boundary. Therefore the flux is defined as a surface integral over the system

boundary of the property state space. In order to account only for fluxes that leave or enter the system in direction of the outward normal to the boundary π , the standard Euclidean scalar product of the flux with this normal is taken. The minus sign is introduced to comply to the convention that outward-bound fluxes enter the balance equation with a negative sign, and inward-bound fluxes enter the equation with a positive sign.

In order to further manipulate the balance equation, the surface integral is transformed into a volume integral by Gauss' theorem [54], yielding:

$$\frac{d}{dt} \int_{\Omega_X} \int_{\Omega_E} n(t, x, e) de dx = - \int_{\Omega_X} \int_{\Omega_E} \text{div}(\varphi(t, x, e)) de dx + \int_{\Omega_X} \int_{\Omega_E} p(t, x, e) de dx. \quad (2.10)$$

This equation is called the *integral formulation* of the population balance equation.

If the volumes $\text{vol}(\Omega_X)$ and $\text{vol}(\Omega_E)$ are constant over time, differentiation and integration can be interchanged on the left-hand side of the equation:

$$\int_{\Omega_X} \int_{\Omega_E} \left(\frac{\partial n}{\partial t} + \text{div}(\varphi(t, x, e)) + p(t, x, e) \right) de dx = 0. \quad (2.11)$$

Observing that the integrals range over the same domain, and therefore the integrand must vanish in the interior of the domain, yields the differential or *local formulation* of the population balance equation:

$$\frac{\partial n}{\partial t} + \text{div}(\varphi(t, x, e)) + p(t, x, e) = 0. \quad (2.12)$$

In case that the volumes $\text{vol}(\Omega_X)$ or $\text{vol}(\Omega_E)$ are not constant over time, the local formulation can be derived by an application of Leibniz' rule [54] to the integral formulation. The result is a correction term that accounts for the change in number density due to the change in volume.

The result of this section is a formal balance law for the temporal change of the number density function n . Open are the expressions for the transport flux φ and the production rate p . They depend on the process to be modelled and therefore no general expression can be given. Further required are initial and boundary conditions, depending on the modelled process.

Before this concept is applied to two spray granulation processes in the next sections, an additional notion is introduced: the *moment of a distribution*. In general, it is difficult to interpret the number density function. However, there exist integral values of a density function (a distribution) that are easier to interpret. These quantities are called moments of the distribution. Limiting the scope to a density function with only one property, the j -th moment is defined by:

$$\mu_j(t) = \int_{\Omega_E} e^j n(t, e) de, \quad j \geq 0. \quad (2.13)$$

For certain j a physical interpretation is possible, for instance $j = 0$ gives the total number of particles, i.e. $\mu_0(t) = N(t)$. For higher moments the meaning of e has to be taken into account. If, for example, e is the particle size, then μ_1 is equal to the total length of particles (laid out and measured in a row), μ_2 is proportional to the surface area of all particles in the population, and μ_3 is proportional to the total volume of particles. The proportionality factors depend on the geometric shape of the particles.

On the basis of the population balance equation dynamic equations for the moments can be derived:

$$\frac{d\mu_j}{dt} = \int_{\Omega_E} e^j \frac{\partial n}{\partial t} de \quad (2.14)$$

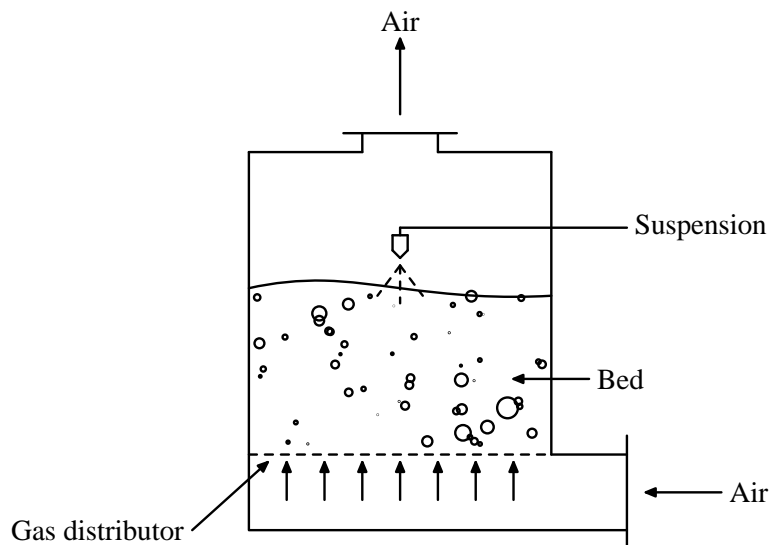


Figure 2.6: Simplified schematics of a batch fluidised bed spray granulation process.

$$= \int_{\Omega_E} e^j (-\text{div}(\varphi) + p) \, d\epsilon. \quad (2.15)$$

If the integral on the right-hand side can be evaluated for a given number j in such a way that it depends only on a finite number of lower-order moments $k \geq j$, then a closed moment system of the population balance equation can be derived which will provide valuable insight into the behaviour of the process.

2.4 Modelling of batch spray granulation

In the following a fluidised bed apparatus as depicted in Fig. 2.6 is considered: A suspension or solution is sprayed into the process chamber on a fluidised particle bed by a nozzle. The fluidisation gas is heated, so that the liquid in the suspension evaporates. The remaining solid builds up new layers on the particles.

Batch processes are widely applied in industries, for instance in pharmaceuticals for the coating of tablets, or in the production of fertilisers from bio-sludges [100]. From a practical point of view the property distribution of the formed granules at the end of the batch is of interest.

Particle properties of interest can be the particle size, the particle moisture, and the particle temperature. As was highlighted in the introduction these three properties can have significant influence on the product characteristics.

In the following population balance modelling of batch spray granulation is performed, i.e. a balance equation for the number density function of the particles in the process is derived.

The *main assumptions* used in the remainder of this thesis are:

- *The number density function does not depend on the spatial position in the process*, i.e. there do not exist spatial gradients, that is the system is well-mixed. Furthermore, *the process chamber is modelled as a single-compartment vessel*. This means that all particles can receive new solid material, regardless of their position inside the bed. This neglects the typical division of the process chamber into multiple compartments, for instance a zone where

particles receive new spray and a zone where only drying occurs. The particle movement between the compartments is rather complex and still under investigation [79, 56].

- The process parameters are chosen such that *only layering growth occurs in the process*, i.e. no agglomeration or breakage of particles. Nucleation, however, can occur and will be handled separately. A criterion on how to choose the process parameters to obtain layering growth was devised by Ennis et al. [37].
- *Only spherical particles are considered*, i.e. it is assumed that the initial particles are spheres and remain spherical at all times. This assumption is justified by many experimental results, see for instance the catalogue in Mörl et al. [100]. Based on this assumption, *only the characteristic size of a particle – the diameter – ξ is considered* to describe the size of the particles.
- *The formed layer of new material on the particle surface is assumed to be compact*. Experimental results show that the formed layer is porous, however, due to the lack of a verified functional relationship between the process conditions and the resulting porosity, the assumption of compact layers is made. In practical application, this means that the particle size in the process, where the porous layer is formed, is underestimated by the particle size in the model.
- It is further assumed that there is *no distribution of particles with respect to temperature θ_s and moisture content X* , i.e. all particles have the same mean temperature and mean moisture. This assumption can be motivated by the intensive mixing of particles and the high heat and mass transfer in the bed.

Using these assumptions, the particles can be described by the number density function $n(t, \xi)$ and the mean temperature θ_s and the mean moisture X . In the following the dynamic equation for the number density function is derived; the derivation of the mean temperature and the moisture content is postponed to section 2.8.

During spray granulation, and the formation of new layers of solid material on the surface of the particles, a growth in particle size ξ can be observed. The growth velocity G can be defined formally by

$$G = \frac{d\xi}{dt}, \quad (2.16)$$

i.e. the change of particle size with time.

In order to derive an expression for the transport flux φ the following reasoning can be used: Consider a particle at time t with size ξ . Due to layering growth, it will have at time $t_1 > t$ a size $\xi_1 > \xi$. This can be interpreted as a convective transport of the particle from the infinitesimal class ξ to the infinitesimal class ξ_1 . The distance $\xi_1 - \xi$ depends on the velocity G and the time interval $t_1 - t$. The transport flux is therefore expressed as

$$\varphi = Gn. \quad (2.17)$$

Depending on the structure of G different effects on a number density function can be observed. For instance, if $G \sim \xi$ larger particles will grow faster than smaller ones. This will yield a broadening of the initial size distribution over process time. The reverse is true if $G \sim \xi^{-1}$; here, the distribution will become narrower, in the limit $t \rightarrow \infty$ a mono-modal number density function will be obtained. If $G \sim 1$ then no particle size is preferred, i.e. all particles grow with the same velocity. The shape of the number density function is then preserved; it will only be shifted to larger sizes over time.

For the growth of spherical particles in fluidised bed spray granulation processes, Mörl et al. [100] derived a surface-proportional growth velocity that has been validated by many experimental results. A generalisation of their idea is the following: If solid is sprayed with a mass flow rate \dot{M}_{sus} on a bed of spherical particles, then the solid is distributed proportionally to some moment μ_j of the size distribution in the bed.

The change in mass of a single particle m_p can then be expressed as

$$\frac{dm_p}{dt} = \dot{M}_{solid} \frac{f(\xi)}{C_j \mu_j}. \quad (2.18)$$

Here, \dot{M}_{solid} is the mass flow of dry solid, that is sprayed into the system, i.e. the liquid medium is not considered. C_j is a constant factor such that $C_j \mu_j$ can be interpreted physically. The function $f(\xi)$ relates the integral quantity expressed by the moment to a single particle of size ξ , for example the surface area of a particle.

Then the following can be derived:

$$\varrho_s \frac{\pi}{6} \frac{d(\xi^3)}{dt} = \dot{M}_{solid} \frac{f(\xi)}{C_j \mu_j}, \quad (2.19)$$

$$3\xi^2 \frac{d\xi}{dt} = \frac{6\dot{M}_{solid}}{\varrho_s \pi C_j \mu_j} f(\xi), \quad (2.20)$$

$$\frac{d\xi}{dt} = \frac{2\dot{M}_{solid}}{\varrho_s \pi C_j \mu_j} \frac{f(\xi)}{\xi^2} := G_j. \quad (2.21)$$

In case of $j = 2$, i.e. a distribution of solid proportional to the surface area of the particles, the constant $C_2 = \pi$ and the function $f(\xi) = \pi\xi^2$, yielding the growth law

$$G_2 = \frac{d\xi}{dt} = \frac{2\dot{M}_{solid}}{\varrho_s \pi \mu_2}, \quad [G_2] = \text{m s}^{-1}. \quad (2.22)$$

as derived by Mörl et al. [100].

The growth velocity is not size-dependent, i.e. all particles in the bed grow with the same velocity. It is however time-dependent as the total surface area $\pi\mu_2$ of the particles will change over time.

This derivation yields the following population balance equation for the number density function:

$$\frac{\partial n}{\partial t} + \frac{\partial}{\partial \xi}(G_2 n) = 0. \quad (2.23)$$

In order to solve this equation, initial and boundary conditions have to be formulated. At the beginning of the process $t = 0$ the particles in the bed possess the number density function $n_0(\xi)$, therefore the initial condition is: $n(0, \xi) = n_0(\xi)$.

A condition has to be posed at the left boundary of the size coordinate, here the flux of particles entering the size range can be specified:

$$(G_2 n)(t, \xi_0) = B_0(t), \quad [B_0] = \text{s}^{-1}. \quad (2.24)$$

B_0 denotes the number flow of particles having the smallest size ξ_0 . This boundary condition can be used to model the external input of nuclei into the system (a semi-batch configuration) or the internal production of nuclei by spray drying, see for instance Vreman et al. [142].

From a mathematical point of view, this population balance model is a first-order non-linear partial differential equation. It is not linear due to the non-linear dependence of the growth velocity G

on μ_2 which depends linearly on the number density function n . An explicit analytical solution of this equation is rather difficult, but qualitative results can be obtained as will be shown later in Section 2.7.

This population balance model is a basic model for the description of batch spray granulation. As was mentioned before, extensions of the model can be made by consideration of different compartments in the process chamber, for instance a spray zone and a drying zone. Only in the spraying zone the particles receive new solid material; in the much larger drying zone the particles are only mixed and dried. Based on the characteristic residence time in the zones a transport of particles from one zone into the other occurs [79, 56].

Although compartment models are not easy to parametrise, especially the residence times and the sizes of the compartments, they allow for a modelling of dispersion effects (a widening) in the number density function by relatively simple growth laws, for instance surface-proportional growth. An alternative growth model that can be used to describe certain effects, e.g. dispersion, can be derived as a convex combination of the growth laws G_j defined above:

$$G = \sum_j \lambda_j G_j, \quad \sum_j \lambda_j = 1. \quad (2.25)$$

The constraint on the λ_j is necessary in order to have mass conservation in the model. The determination of the maximum index j and the λ_j has to be done experimentally, a direct relation to process parameters is still an open problem [56].

2.5 Modelling of continuous spray granulation with particle recycle

In comparison to a batch configuration, a continuous spray granulation offers many advantages: In batch processes between two batches the plant has to be shut-down, cleaned, and refilled with starting material. This leads to a discontinuous product flow. In a continuous spray granulation a continuous production is possible by adding new initial particles or recycling portions of the product flow. The continuous process attains a steady-state, thus guaranteeing a steady flow of product with steady properties. This is especially advantageous if large quantities of the product have to be produced. Additionally, energy and maintenance costs are known to be smaller than for comparable batch apparatuses.

In the following a continuous spray granulation process as depicted in Fig. 2.7 is considered. The core of this configuration is a process chamber with a nozzle as in the batch process. The process chamber is augmented by an outlet tube that is installed in the centre of the gas distributor plate. During granulation particles will leave the chamber by this tube. This mass flow is then screened twice: The over-sized particles from the first screen are sent to a mill where they are milled and then re-fed into the process chamber. The under-sized particles are screened once more. Here, the over-sized particles are accepted as product, whereas the undersized particles are also re-fed into the process chamber for further growth.

For population balance modelling of the number density function of particles in the bed, the same assumptions as in the batch configuration are used. This means that the population balance equation for the batch process can be used as a basis for the continuous process – it only has to be augmented by terms accounting for the particle outlet and the re-cycle of particles.

For that purpose the screens and the mill have to be modelled by population balances. Here the following simplifying assumptions are used:

- No hold-up of particles in the screens and the mill, i.e. they work quasi-stationary. This assumption is justified as long as the residence times of particles in the screens and the mill

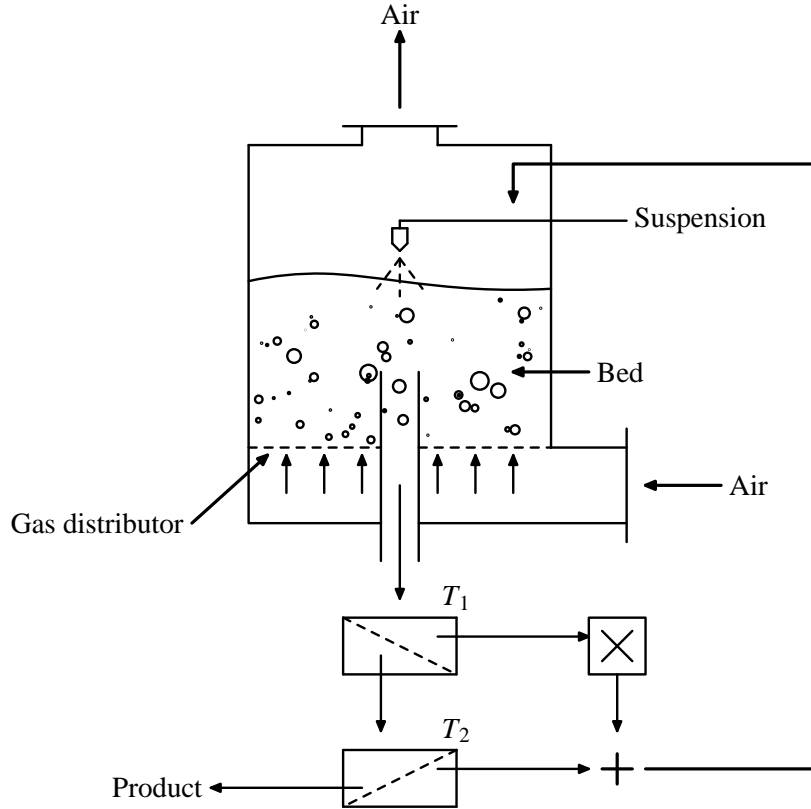


Figure 2.7: Schematics of a continuous spray granulation process with external classification and particle recycle.

are significantly smaller than the residence time of the particles in the process chamber. This implies that the screens and the mill have to be designed such that they can handle the mass flows of particles swiftly.

- No breakage of particles due to the stress of the screening.
- Constant screening and milling characteristics, i.e. no change in the characteristic behaviour of the screens and the mill due to ageing or heavy use.
- Mass conservation during milling of particles.

Then the mass flows of particles, expressed as number density fluxes, can be written as

$$\dot{n}_{os}(t, \xi) = T(\xi) \dot{n}, \quad (2.26)$$

$$\dot{n}_{us}(t, \xi) = (1 - T(\xi)) \dot{n}, \quad (2.27)$$

where the subscript *os* denotes the over-sized portion of the particle flow \dot{n} , and the subscript *us* denotes the under-sized portion.

The function $T(\xi)$ is called the *separation function* of the screen and determines up to which size particles are classified as under-sized or over-sized, respectively. In the ideal case all particles below the characteristic size of the screen are classified as under-sized, all other sizes are characterised as over-sized. The separation function is in this case described by a Heaviside function. In reality, however, also some particles with a size lower than the characteristic size are classified as over-sized and – vice versa – some particles with a size larger than the characteristic size are

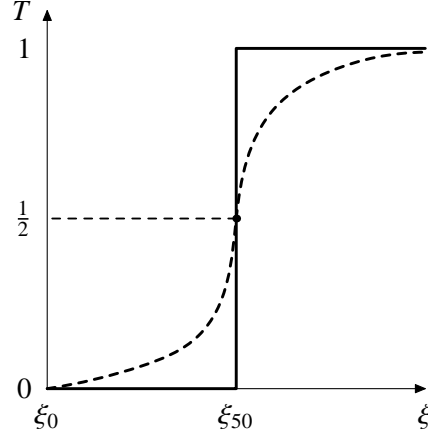


Figure 2.8: Ideal (solid line) and real case (dashed line) of a separation function of a screen. In the figure the characteristic value of the screen is denoted by ξ_{50} . Although the value is the same in both cases the screening results will differ.

classified as under-sized. The amount of particles that are separated erroneously is determined by the shape of the separation function. This situation is depicted in Fig. 2.8, and leads to an error in the screening result.

The modelling of the mill is more difficult: In general, the particles having passed the mill possess a size distribution depending on the characteristics of the mill:

$$\dot{n}_{mill} = B_{mill}(t) q_{0,mill}(\xi). \quad (2.28)$$

In this equation B_{mill} denotes the number flow rate of particles after milling, and $q_{0,mill}$ is a normalised size distribution of the milled particles. The number flow rate of milled particles can be related to the mass flow rate of particles that are put into the mill:

$$B_{mill}(t) = \frac{6 \dot{M}_{mill}(t)}{\rho_s \pi \int_{\xi_0}^{\infty} \xi^3 q_{0,mill}(\xi) d\xi}. \quad (2.29)$$

The practical determination of $q_{0,mill}$ proves to be difficult and depends on many material properties as well as parameters of the mill (e.g. milling velocity), so that even for one mill different distributions are obtained for different materials.

If it is assumed that all particles are milled down to one size ξ_M , then $q_{0,mill} = \delta(\xi - \xi_M)$, a Dirac function, and $B_{mill} = \dot{M}_{mill}/m_{\xi_{mill}}$, where $m_{\xi_{mill}}$ is the mass of one milled particle.

The number density flux of particles re-fed into the process chamber consists of the under-sized particles of the second screen and the milled particles, i.e.

$$\dot{n}_{recycle} = (1 - T_2(\xi))\dot{n}_{us,1} + \dot{n}_{mill} = (1 - T_1(\xi))(1 - T_2(\xi))\dot{n}_{out} + \dot{n}_{mill}. \quad (2.30)$$

The population balance equation can then be written as

$$\frac{\partial n}{\partial t} + \frac{\partial}{\partial \xi}(G_2 n) = -\dot{n}_{out} + \dot{n}_{recycle}, \quad (2.31)$$

with an initial condition $n(0, \xi) = n_0(\xi)$, and a boundary condition $(G_2 n)(t, \xi_0) = B_0(t)$.

A still open problem is the determination of the outlet flux \dot{n}_{out} that leaves the process chamber by the outlet tube. If it is assumed that no particle size is preferred, then the particle outlet can be expressed proportional to the number of particles that possess a certain size:

$$\dot{n}_{out} = K n, \quad (2.32)$$

where K determines the amount of outlet flux. From practical considerations, e.g. product mass flow, hydro- and thermodynamic behaviour, it is desired to have a constant mass $m_{bed,ref}$ of particles in the process chamber. One way to achieve this is given in the article of Heinrich et al. [52]:

$$K = 1 - \min\left(1, \frac{m_{bed,ref}}{m_{bed}}\right). \quad (2.33)$$

This outlet kinetics represents a non-linear, switching feedback controller, that allows for an almost exact control of bed mass for $t \rightarrow \infty$.

A different way to control the bed mass can be derived from the moment model of the process: The third moment μ_3 is proportional to the bed mass (via the total volume of particles). A constant mass requires the time derivative of μ_3 to vanish. From this constraint the following ideal, quasi-static controller can be derived:

$$\begin{aligned} \int_{\xi_0}^{\infty} \xi^3 \left[\frac{\partial n}{\partial t} + \frac{\partial}{\partial \xi}(G_2 n) \right] d\xi &= \int_{\xi_0}^{\infty} \xi^3 [-\dot{n}_{out} + \dot{n}_{recycle}] d\xi \quad (2.34) \\ &= \int_{\xi_0}^{\infty} \xi^3 [-\dot{n}_{out} + (1 - T_1(\xi))(1 - T_2(\xi))\dot{n}_{out} + \dot{n}_{mill}] d\xi. \quad (2.35) \end{aligned}$$

Using the assumption that the total mass flow of particles entering the mill is conserved, this equation can be further simplified:

$$\begin{aligned} \int_{\xi_0}^{\infty} \xi^3 \left[\frac{\partial n}{\partial t} + \frac{\partial}{\partial \xi}(G_2 n) \right] d\xi &= \int_{\xi_0}^{\infty} \xi^3 [-1 + (1 - T_1(\xi))(1 - T_2(\xi)) + T_1(\xi)] \dot{n}_{out} d\xi \quad (2.36) \\ &= \int_{\xi_0}^{\infty} \xi^3 [-T_2(\xi)(1 - T_1(\xi))] Kn d\xi. \quad (2.37) \end{aligned}$$

The left-hand side evaluates to

$$\int_{\xi_0}^{\infty} \xi^3 \left[\frac{\partial n}{\partial t} + \frac{\partial}{\partial \xi}(G_2 n) \right] d\xi = \frac{d\mu_3}{dt} - B_0 \xi_0^3 - 3 \int_{\xi_0}^{\infty} \xi^2 G_2 n d\xi, \quad (2.38)$$

making use of partial integration, the posed boundary condition and the assumption that for $\xi \rightarrow \infty$ the number density function tends sufficiently fast to zero.

Posing the condition $d\mu_3/dt = 0$, the open-loop controller for the particle outlet can be obtained

$$K = \frac{B_0 \xi_0^3 + 3 \int_{\xi_0}^{\infty} \xi^2 G_2 n d\xi}{\int_{\xi_0}^{\infty} \xi^3 [T_2(\xi)(1 - T_1(\xi))] n d\xi}. \quad (2.39)$$

which is for $B_0 = 0$ the result reported by Radichkov et al. [113]. Although this quasi-static controller guarantees a constant bed mass for all times, it is more complex than the one proposed by Heinrich et al. [52]: It requires the knowledge of the size distribution n in order to calculate the value of K . Furthermore, it is only an open-loop controller due to the missing comparison of the actual bed mass and the reference value.

As the process is a continuous one it does possess a steady-state. This is calculated in the following section.

2.6 Derivation of the steady-state distribution in continuous spray granulation

In this section the *steady-state number density function* is derived before in the next one the dynamics of the two process configurations are analysed.

The population balance equation for the number density function $n(t, \xi)$ can be written more explicitly as:

$$\frac{\partial n}{\partial t} + \frac{\partial}{\partial \xi}(G_2 n) = [(1 - T_1(\xi))(1 - T_2(\xi)) - 1] K n + p(\xi, n), \quad (2.40)$$

with the separation functions of the two screens T_1 and T_2 , respectively. The number flow of milled particles is written as $p(\xi, n)$, e.g. $p = B_{mill}(t) q_{0,mill}(\xi)$. The boundary condition is formulated as $(G_2 n)(t, \xi_0) = B_0(t)$.

At steady-state the variables G_2 , K , B_0 and B_{mill} attain constant values: G_s , K_s , $B_{0,s}$ and $B_{mill,s}$. Furthermore, the steady-state number density function is denoted by n_s . Observing that at steady-state $\partial n / \partial t = 0$, the population balance equation at steady-state can be written as

$$G_s \frac{dn_s}{d\xi} = [(1 - T_1(\xi))(1 - T_2(\xi)) - 1] K_s n_s + p_s(\xi, n_s). \quad (2.41)$$

To simplify the notation in the following calculations the following abbreviation is introduced:

$$\Gamma(\xi) = [(1 - T_1(\xi))(1 - T_2(\xi)) - 1]. \quad (2.42)$$

This yields

$$G_s \frac{dn_s}{d\xi} = \Gamma(\xi) K_s n_s + p_s(\xi, n_s). \quad (2.43)$$

From a mathematical point of view, this is an inhomogeneous first-order linear ordinary differential equation with a variable coefficient $\Gamma(\xi)$. This type of equation can be solved by a combination of separation of variables and variation of constants [61].

The homogeneous solution $n_{s,h}$, i.e. the solution to the equation for $p_s \equiv 0$ can be obtained by separation of variables:

$$n_{s,h}(\xi) = C \exp\left(\frac{K_s}{G_s} \int_{\xi_0}^{\xi} \Gamma(y) dy\right). \quad (2.44)$$

The constant of integration can be calculated from the boundary condition, i.e. $C = B_{0,s}/G_s$. The homogeneous solution then reads

$$n_{s,h}(\xi) = \frac{B_{0,s}}{G_s} \exp\left(\frac{K_s}{G_s} \int_{\xi_0}^{\xi} \Gamma(y) dy\right) = \frac{B_{0,s}}{G_s} \exp(F(\xi)), \quad (2.45)$$

where the function F has been introduced to simplify the notation in the following steps.

Following the theory of linear ordinary differential equations the general solution to the inhomogeneous problem can be found by adding one particular solution of the inhomogeneous problem $n_{s,i}$ to the solution of the homogeneous one, i.e. $n_s(\xi) = n_{s,h}(\xi) + n_{s,i}(\xi)$. To that purpose *variation of constants* is used: Using the ansatz $n_{s,i}(\xi) = C(\xi) \exp(F(\xi))$ and inserting into the steady-state population balance equation yields:

$$\frac{dC}{d\xi} \exp(F(\xi)) + C(\xi) \frac{d}{d\xi} [\exp(F(\xi))] = \Gamma(\xi) \frac{K_s}{G_s} C(\xi) \exp(F(\xi)) + \frac{1}{G_s} p_s(\xi), \quad (2.46)$$

$$\frac{dC}{d\xi} \exp(F(\xi)) = \frac{1}{G_s} p_s(\xi). \quad (2.47)$$

The last equation is obtained by application of the differentiation rules for parameter integrals to the function $F(\xi)$. The unknown function $C(\xi)$ can then be calculated:

$$C(\xi) = \int_{\xi_0}^{\xi} \exp(-F(z)) \frac{1}{G_s} p_s(z) dz. \quad (2.48)$$

Here the constant of integration is omitted because only one solution is needed. The inhomogeneous solution then reads:

$$n_{s,i}(\xi) = \exp(F(\xi)) \left[\int_{\xi_0}^{\xi} \exp(-F(z)) \frac{1}{G_s} p_s(z) dz \right]. \quad (2.49)$$

The steady-state number density function for continuous fluidised bed spray drying with external classification and particle re-cycle for *arbitrary* separation and milling functions T_1 , T_2 , and $q_{0,mill}$ can then be written as

$$n_s(\xi) = \frac{B_{0,s}}{G_s} \exp(F(\xi)) + \exp(F(\xi)) \left[\int_{\xi_0}^{\xi} \exp(-F(z)) \frac{1}{G_s} p_s(z) dz \right]. \quad (2.50)$$

with

$$F(\bullet) = \frac{K_s}{G_s} \int_{\xi_0}^{\bullet} \Gamma(y) dy, \quad \Gamma(\bullet) = [(1 - T_1(\bullet))(1 - T_2(\bullet)) - 1]. \quad (2.51)$$

Given the separation functions T_1 and T_2 , and the milling function $q_{0,mill}$ the qualitative shape of the steady-state number density function can be determined. For the general case, this has to be done numerically due to the evaluation of the integrals, but for ideal functions the shape of the steady-state number density function can be constructed quite easily.

For the case of ideal separation functions (with ξ_1 and ξ_2 denoting the separation diameters), i.e.

$$T_1(\xi) = \begin{cases} 0 & \xi < \xi_1, \\ 1 & \xi \geq \xi_1 \end{cases}, \quad T_2(\xi) = \begin{cases} 0 & \xi < \xi_2, \\ 1 & \xi \geq \xi_2 \end{cases}, \quad (2.52)$$

in connection with the ideal milling function $q_{0,mill} = \delta(\xi - \xi_M)$, the shape of the steady-state distribution can be further specified.

An evaluation of the integral defined in function $F(\xi)$ yields

$$F(\xi) = \begin{cases} 0, & \xi < \xi_2, \\ -\frac{K_s}{G_s}(\xi - \xi_2), & \xi \geq \xi_2 \end{cases}; \quad (2.53)$$

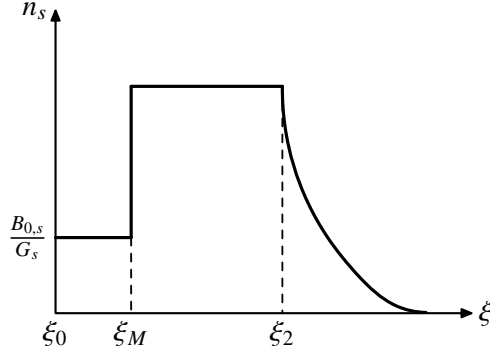


Figure 2.9: Qualitative shape of the steady-state number density distribution in continuous fluidised bed spray granulation with external classification and particle re-cycle for the case of ideal screening and milling.

furthermore, using the ideal milling function

$$\int_{\xi_0}^{\xi} \exp(-F(z)) \frac{1}{G_s} p_s(z) dz = \begin{cases} 0, & \xi < \xi_M, \\ \exp(-F(\xi_M)) p_s(\xi_M) \frac{1}{G_s}, & \xi \geq \xi_M \end{cases} \quad (2.54)$$

The steady-state number density function can then be written as a piece-wise function:

$$n_s(\xi) = \begin{cases} B_{0,s}/G_s, & \xi < \xi_M, \\ B_{0,s}/G_s + \exp(-F(\xi_M)) p_s(\xi_M)/G_s, & \xi_M \leq \xi < \xi_2, \\ B_{0,s}/G_s \exp(F(\xi)) + \exp(F(\xi)) \exp(-F(\xi_M)) p_s(\xi_M)/G_s, & \xi \geq \xi_2 \end{cases} \quad (2.55)$$

The range $\xi < \xi_M$ is completely defined by the boundary flow of nuclei; the middle range $\xi_M \leq \xi < \xi_2$ is defined by the superposition of the nuclei flow and the flux of milled particles. In the range $\xi \geq \xi_2$ the steady-state number density function is determined by the superposition of two decaying exponential functions, because $F(\xi) < 0, \forall \xi > \xi_2$. An example of a steady-state distribution for the ideal case is shown in Fig. 2.9.

For real, smooth, separation and milling functions a smoothing at the boundaries of the three ranges will occur. The widths of the ranges are determined by the choice of ξ_0 , ξ_M , and ξ_2 . Additionally, the following tendencies can be identified: (a) An increase in $B_{0,s}$ will increase the magnitude of the number density function; (b) an increase in G_s will yield a decrease in the magnitude; and (c) an increase in K_s will yield a faster decay of the number density function in the third range ($\xi \geq \xi_2$).

In order to determine the quantitative shape of the steady-state distribution the values of $B_{0,s}$, $B_{mill,s}$, G_s and K_s have to be calculated. The only additional information available are the process parameters, e.g. the mass flow rate of external nuclei, and the reference value for the bed mass $m_{bed,ref}$.

The value of $B_{0,s}$ can be calculated directly from the steady-state mass flow rate of nuclei $\dot{M}_{nuc,s}$:

$$B_{0,s} = \frac{\dot{M}_{nuc,s}}{\pi Q_s \xi_0^3}. \quad (2.56)$$

The calculation of G_s , K_s and $B_{mill,s}$ cannot be carried out in that way due to the occurrence of these values in the steady-state distribution. They can be calculated as the solution of a nonlinear

system of equations given by:

$$0 = K_s - \left[1 - \min \left(1, \frac{m_{bed,ref}}{m_{bed,s}} \right) \right], \quad m_{bed,s} = \frac{\pi}{6} \varrho_s \int_{\xi_0}^{\infty} \xi^3 n_s(\xi) d\xi \quad (2.57)$$

$$0 = G_s - \left[\frac{2\dot{M}_{solid,s}}{\varrho_s \pi \mu_{2,s}} \right], \quad \mu_{2,s} = \int_{\xi_0}^{\infty} \xi^2 n_s(\xi) d\xi, \quad (2.58)$$

$$0 = B_{mill,s} - \left[\frac{\int_{\xi_0}^{\infty} \xi^3 T_1(\xi) K_s n_s(\xi) d\xi}{\int_{\xi_0}^{\infty} \xi^3 q_{0,mill}(\xi) d\xi} \right]. \quad (2.59)$$

This non-linear root-finding problem can be solved iteratively, for instance by a Newton-Raphson algorithm. The number of iterations necessary and the convergence of the algorithm to a solution depends on the initial guesses for G_s , K_s and $B_{mill,s}$.

In principle, the steady-state number density distribution can be obtained in the way shown in this section, and will prove a valuable tool in the forthcoming chapters.

In the next section it will be investigated what kind of dynamic behaviour can be expected in batch spray granulation and continuous spray granulation with external classification and particle recycle.

2.7 Mathematical analysis of particle dynamics

In this section basic results for the process dynamics of the two fluidised batch processes considered in this thesis are summarised. After a discussion of batch spray granulation the analysis is devoted to the continuous case.

2.7.1 Batch spray granulation

From a mathematical point of view the population balance equation for the number density function in a batch spray granulation process

$$\frac{\partial n}{\partial t} + \frac{\partial}{\partial \xi}(G_2 n) = 0 \quad (2.60)$$

is a non-linear (quasi-linear) partial integro-differential equation, due to the occurrence of the sought function n in the growth rate G_2 defined in Eq. (2.22). An initial condition is given by $n(0, \xi) = n_0(\xi)$, and a boundary condition can be formulated as $(G_2 n)(t, \xi_0) = B_0(t)$.

A qualitative discussion of the process dynamics can be obtained by an application of the *method of characteristics*. The fundamentals are presented in Appendix C; a straight-forward application to the initial value problem yields the characteristic system

$$\frac{dt}{d\theta} = 1, \quad t(0, s) = 0, \quad (2.61)$$

$$\frac{d\xi}{d\theta} = G_2, \quad \xi(0, s) = s, \quad (2.62)$$

$$\frac{dn}{d\theta} = 0, \quad n(0, s) = n_0(s). \quad (2.63)$$

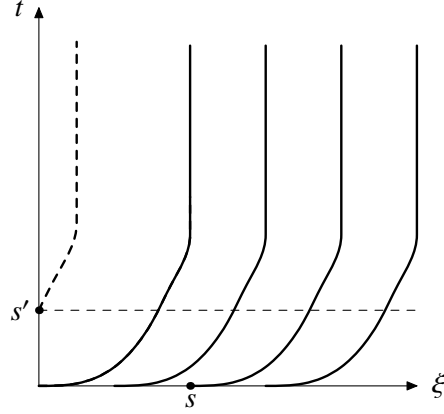


Figure 2.10: Characteristic curves in the $(t - \xi)$ -plane obtained by the method of characteristics.

The growth velocity is a strictly monotonically decreasing function $G_2(\mu_2) \sim \mu_2^{-1}$ and will therefore in the case of $\dot{M}_{sus} \neq 0$ attain a limit for $t \rightarrow \infty$: $\lim_{t \rightarrow \infty} G_2(\mu_2(t)) = 0$.

The slope of the characteristic curves in the $(t - \xi)$ -plane is given by

$$\frac{dt}{d\xi} = \frac{1}{G_2}, \quad (2.64)$$

i.e. the slope will tend to infinity. The characteristic curves for the batch process are depicted in Fig. 2.10.

As the local slope is identical for all characteristic curves starting from the initial condition, which follows from the fact that all sizes are transported with the same velocity G_2 , no intersection of characteristic curves can occur. This means that no shock-formation in the solution is to be expected. The characteristic curves originating from the boundary condition can be obtained by re-parametrising the solution domain. They also have a slope of $dt/d\xi = 1/G_2$. This means the characteristic curves are parallel to each other at each point in time and an intersection, i.e. the formation of a shock is in general not possible. Care has to be taken at the point (t_0, ξ_0) : Here two characteristics originate, and the values of the initial and the boundary condition at this point have to be consistent, in order to avoid a shock in the solution. In the batch case, i.e. $B_0(t) = 0$, this requires $\lim_{\xi \rightarrow \xi_0^+} n(0, \xi) = 0$.

Using the definition of a moment μ_j of a number density function (cf. Eq. (2.13)), two important results can be derived via the dynamic moment equations:

$$\frac{d\mu_0}{dt} = B_0(t), \quad (2.65)$$

$$\frac{d\mu_3}{dt} = B_0(t)\xi_0^3 + 3G_2\mu_2 \quad (2.66)$$

$$= B_0(t)\xi_0^3 + \frac{6\dot{M}_{solid}}{\rho_s \pi}. \quad (2.67)$$

From the first equation follows that in case of $B_0 = 0$ the total number of particles in the system is conserved. From the second equation follows that the third moment, which is proportional to the total mass of particles, is decoupled from all other moments, i.e. the equation describes solely the change in mass due to solid spray and nuclei feed. This will have important ramifications in the design of model-based measurement systems and feedback controllers for this process.

Table 2.1: Process parameters for the continuous spray granulation process

Initial bed mass [kg]	m_{bed}	10.0
Reference bed mass [kg]	$m_{bed,set}$	10.0
Mass flow of nuclei [kg s^{-1}]	\dot{M}_{nuc}	5.55×10^{-5}
Mass flow of solid [kg s^{-1}]	\dot{M}_{solid}	1.38×10^{-2}
Solid density [kg m^{-3}]	ρ_s	1440.0
Size of nuclei [m]	ξ_0	0.1×10^{-3}
Screen size upper screen [m]	ξ_u	0.5×10^{-3}
Screen size lower screen [m]	ξ_l	0.4×10^{-3}
Milling diameter [m]	ξ_M	0.35×10^{-3}
Milling diameter (osc.) [m]	ξ_M	0.2×10^{-3}

2.7.2 Continuous spray granulation with particle recycle

The continuous process utilises the same growth model as the batch process, so new dynamic behaviour can only be introduced by the outlet and the particle re-cycle. The process configuration of a continuous spray granulation with external classification and particle re-cycle was extensively investigated by Heinrich et al. [52] and Radichkov et al. [113] concerning the dynamic behaviour. As was shown in Radichkov et al. the process exhibits different dynamic behaviour depending, amongst others, on the value of the milling size ξ_M : For a certain range a stable steady-state distribution is attained, but for a large parameter range the system exhibits sustained oscillations in the number density function.

This qualitative change in behaviour (a *bifurcation*) is exemplified in Fig. 2.11 and Fig. 2.13 (for the process conditions given in Tab. 2.1), where by a change in the milling diameter ξ_M sustained oscillations result. Also shown is in Fig. 2.12 and Fig. 2.14 that the moments μ_j ($j = 0, 1, 2, 3$), representing total number of particles, total length, total surface area, and total mass also exhibit the non-linear oscillations.

The explanation for the occurrence of sustained oscillation can be found in the re-cycle of milled particles: At some times a large number of very small particles with a large specific surface area is re-fed into the process chamber. As the growth of particles depends on the total surface area, the growth velocity will decrease dramatically, i.e. at some times almost no growth of particles takes place. This leads to the situation that the mass flow of over-sized particles from the first screen to the mill vanishes, i.e. no new particles are re-cycled into the process. As pointed out in Drechsler et al. [35], the constant re-cycle of milled particles to the screen is a fundamental condition for a stable process. With the oscillating flow of particles this condition is not satisfied and an unstable steady-state behaviour is obtained, that Radichkov et al. [113] later identified as a limit-cycle.

The destabilising effect of re-cycle loops has been reported in other particulate systems as well, for instance in crystallisation [141].

The oscillations in the number density function for certain milling size lead to an undesired oscillation in the product mass flow. If a process is to be run at such a milling size because the corresponding steady-state number density function is required in the process specification, then feedback controllers have to be applied to stabilise the open-loop unstable steady-state.

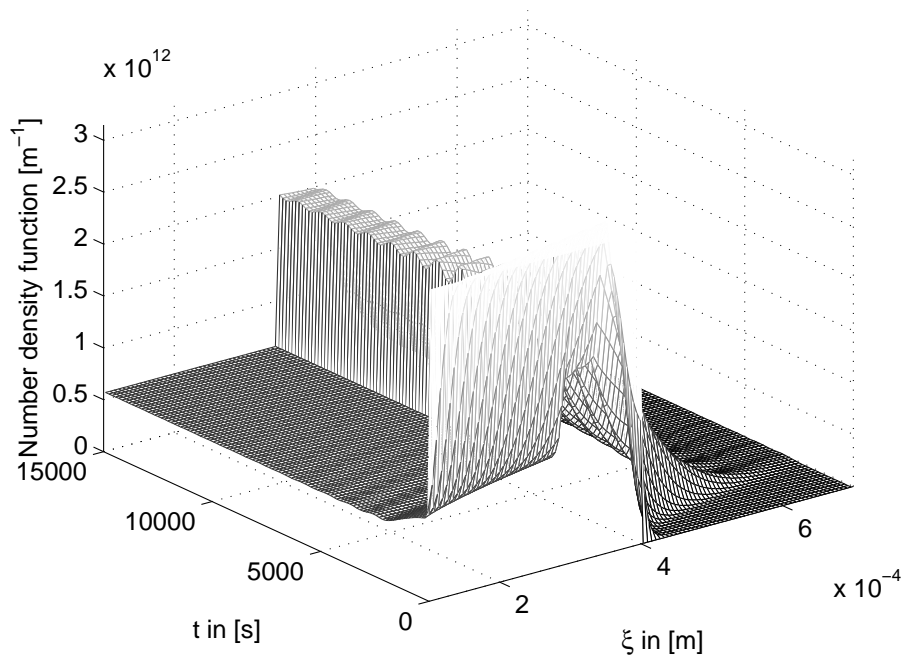


Figure 2.11: Exemplary behaviour of the number density function for a milling size ξ_M that yields a stable steady-state distribution.

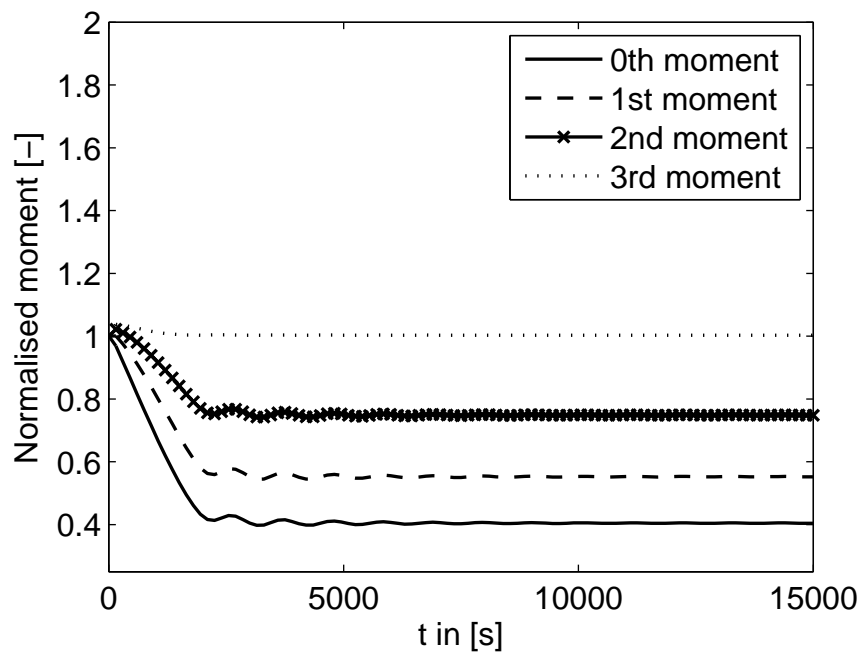


Figure 2.12: Exemplary behaviour of the first four moments, normalised with respect to the initial value $\mu_j(0)$, in case of a stable steady-state.

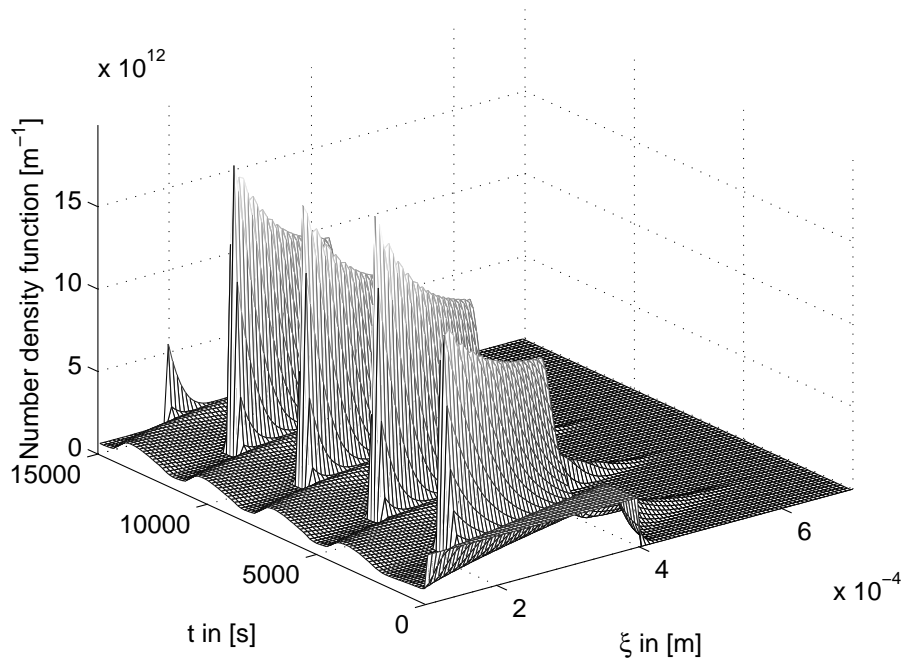


Figure 2.13: Exemplary behaviour of the number density function for a milling diameter ξ_M that yields sustained oscillations.

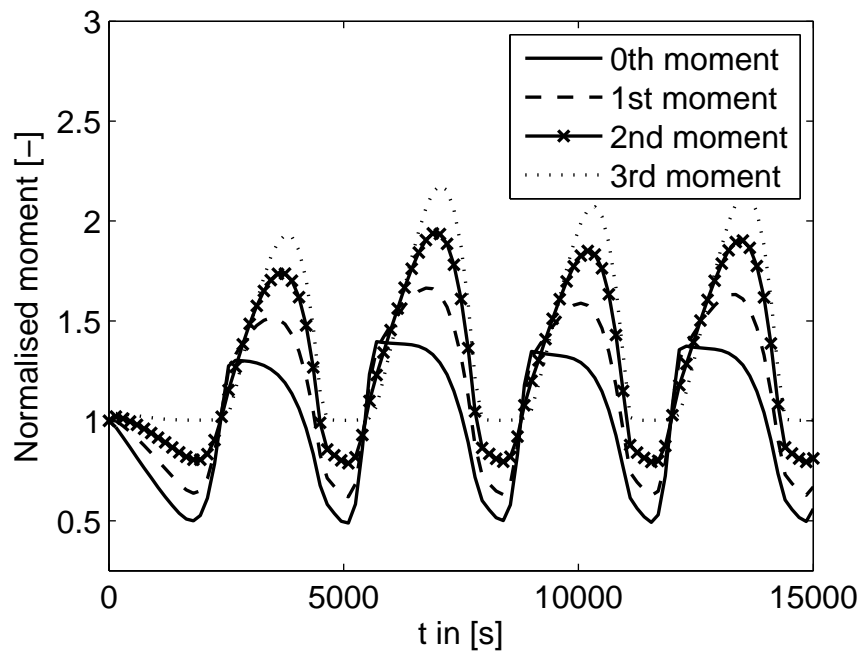


Figure 2.14: Exemplary behaviour of the first four moments, normalised with respect to the initial value $\mu_j(0)$, in case of a unstable steady-state. Here, also in the moments oscillations can be observed.

2.8 Modelling of heat and mass transfer

So far only the number density function, i.e. the size distribution of the particles in the bed has been considered. As was mentioned in the Introduction, the drying conditions have great influence on the product characteristics, for example on the storage stability of the produced particles, or the dissolution characteristic of a pharmaceutical. Additionally, the particle moisture is of importance: It may determine the structure and taste of product, or the susceptibility of the product to germ infections which will lead to a spoilage of the product. The danger of spoilage is increased if the particles are not only moist but also warm, here germs are known to reproduce exponentially, i.e. the product (e.g. a food material) can only be used for a very short time before it becomes hazardous.

The particle temperature is of further importance: It determines the necessary post-processing of a particulate product, for instance the cooling necessary before the product can be packed and shipped. Heating is a cost-intensive sub-process, so the total production cost will increase significantly if the particles are heated unnecessarily. However, it is necessary as the evaporation is thermally driven, and not enough heating (i.e. not enough evaporation of liquid) will lead to agglutination of the bed, transforming the fluidised bed into a fixed bed.

In order to be able to predict and control the temperature and moisture content of the particles, the heat and mass transfer during spray granulation have to be modelled.

The drying process, which lies at the core of the spray granulation process, has been theoretically and experimentally investigated many times, see for instance [51, 1, 14, 145, 108, 140] in varying detail. One of the most advanced drying models is the one of Burgschweiger and Tsotsas [14], considering the distributions of the particle number, particle moisture, and particle enthalpy with respect to the residence time of the particles in the apparatus. Furthermore, the distribution of these distributions with respect to the spatial position in the apparatus is considered. Although this model is known to give excellent results, it is too complex for controller design in the context of this thesis.

Therefore, in view of the aim to derive a dynamic model for controller design, i.e. to control the particle moisture and particle temperature, a simplified model is derived. Its main assumption is that there are no moisture or temperature distributions in the apparatus, i.e. all particles have the same *mean moisture* and *mean temperature*. This assumption can be justified by the strong mixing in the fluidised bed that will lead to an equalisation of the moisture and temperature distributions.

For the simplified heat and mass transfer model for controller design the following assumptions are made:

- The system is ideally mixed.
- The formation of bubbles and its influence on the heat and mass transfer is neglected.
- The moisture in the system is not considered as a phase. It is always considered as part of the solid phase (in its liquid form), or as part of the gas phase (in its vapour form).
- All temperatures are mixing temperatures, i.e. the temperature of the combination of solid and liquid, and gas and vapour, respectively.

From the balances of the mass of dry solid, the mass of liquid on the solid, the mass of dry gas, the mass of vapour in the gas, the enthalpy of the particle (i.e. solid and liquid), and the temperature of the gas (i.e. gas and vapour), dynamic equations for the states of the heat and mass transfer model are derived.

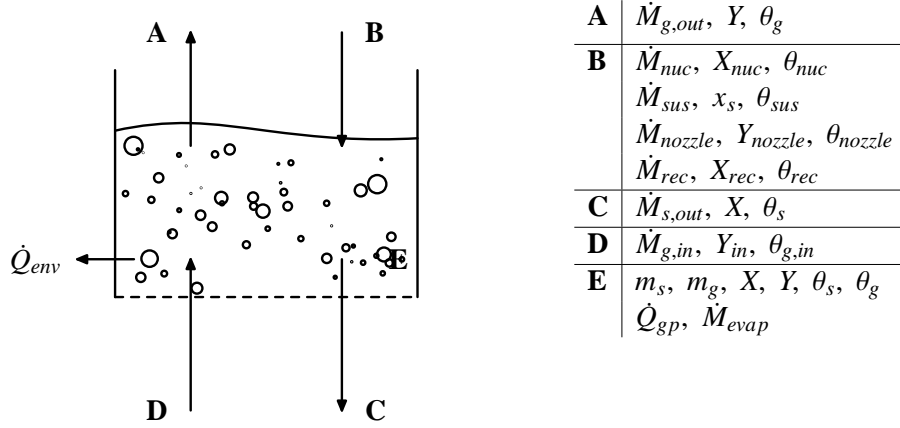


Figure 2.15: Schematics of the heat and mass flows considered in the heat and mass transfer model.

Starting with the total mass of particles m_s , consisting of the mass of dry solid $m_{s,dry}$ and the mass of moisture $m_{s,m}$, i.e. $m_s = m_{s,dry} + m_{s,m}$, the *moisture content* of the particles can be defined by $m_{s,m} = X m_{s,dry}$, $[X] = \text{kg}_{liquid} \text{kg}_{s,dry}^{-1}$, i.e. $m_s = m_{s,dry} (1 + X)$. In an analogous way, a moisture content of gas Y can be introduced, and the mass of gas can be written as $m_g = m_{g,dry} (1 + Y)$.

For all calculations, the reference temperature is set to $\theta_{ref} = 0^\circ\text{C}$. The evaporation enthalpy, i.e. the necessary energy to transform a liquid into vapour at a given pressure without changing its temperature, is evaluated at this reference. The total enthalpy of the particle and the gas phase can be written as:

$$H_{s,total} = m_{s,dry} (c_{p,s} + c_{p,l} X) \theta_s, \quad (2.68)$$

$$H_{g,total} = m_{g,dry} \left((c_{p,g} + c_{p,v} Y) \theta_g + Y \Delta h_{evap} \right) \quad (2.69)$$

with the temperatures θ_s and θ_g ($[\theta] = ^\circ\text{C}$). The total enthalpy of gas consists of the enthalpy of dry air at temperature θ_g and the evaporation enthalpy at θ_{ref} and the enthalpy needed to heat the vapour up to the temperature θ_g .

The state variables derived from these equations are: the mass of dry solid $m_{s,dry}$, the mass of dry gas $m_{g,dry}$, the moisture content of solid X , the moisture content of gas Y , and the two temperatures θ_s and θ_g for the solid and the gas, respectively.

For the balance volume only the fluidised bed is considered, see Fig. 2.15; external apparatuses (e.g. screens and mills) are neglected due to the very short residence times of particles and gas compared to the fluidised bed, i.e. it is assumed that no significant drying occurs in these apparatuses.

With the nomenclature introduced in Fig. 2.15 the following mass balances can be derived:

$$\frac{dm_{s,dry}}{dt} = x_s \dot{M}_{sus} + \dot{M}_{rec} + \dot{M}_{nuc} - \dot{M}_{s,out}, \quad (2.70)$$

$$\frac{dm_{g,dry}}{dt} = \dot{M}_{g,in} + \dot{M}_{nozzle} - \dot{M}_{g,out}, \quad (2.71)$$

$$\frac{dm_{s,m}}{dt} = (1 - x_s) \dot{M}_{sus} + X_{nuc} \dot{M}_{rec} + X_{rec} \dot{M}_{nuc} - X \dot{M}_{s,out} - \dot{M}_{evap}, \quad (2.72)$$

$$\frac{dm_{g,v}}{dt} = Y_{in} \dot{M}_{g,in} + Y_{nozzle} \dot{M}_{nozzle} - Y \dot{M}_{g,out} + \dot{M}_{evap}. \quad (2.73)$$

In this equation \dot{M}_{evap} denotes the mass flow of evaporated liquid from the particulate to the gas

phase. The *solid mass fraction* x_s determines the mass of solid in the total total mass flow \dot{M}_{sus} of suspension (or solution). In lieu with former derivations, the following equality is defined: $\dot{M}_{solid} = x_s \dot{M}_{sus}$.

The temporal evolution of the mass of dry solid can be determined directly from the population balance equation via the third moment of the number density function, i.e.

$$m_{s,dry} = \frac{\pi}{6} \varrho_s \int_{\xi_0}^{\infty} \xi^3 n(t, \xi) d\xi = \frac{\pi}{6} \varrho_s \mu_3. \quad (2.74)$$

It can be further assumed that the gas mass flow of the nozzle, \dot{M}_{nozzle} , is significantly smaller than the inlet mass flow of gas. Therefore, this mass flow is neglected. Another assumption is constant hold-up of gas in the apparatus, i.e. $\dot{M}_{g,in} = \dot{M}_{g,out}$. The moisture content of particles in the re-cycle is assumed to be identical to the moisture content of particles in the bed, i.e. $X_{rec} = X$, due to the small residence time of the particles in the re-cycle loop.

From the mass balances of the liquid and vapour in the solid and the gas phase, dynamic equations for the moisture content can be derived by an application of the product rule to $m_{s,m} = m_{s,dry}X$ and $m_{g,v} = m_{g,dry}Y$:

$$\frac{dm_{s,m}}{dt} = \frac{dm_{s,dry}}{dt} X + \frac{dX}{dt} m_{s,dry}, \quad (2.75)$$

$$\frac{dm_{g,v}}{dt} = \frac{dm_{g,dry}}{dt} Y + \frac{dY}{dt} m_{g,dry}, \quad (2.76)$$

For the enthalpies the following equations are derived:

$$\frac{dH_{s,total}}{dt} = \dot{H}_{sus} + \dot{H}_{rec} + \dot{H}_{nuc} - \dot{H}_{s,out} + \dot{Q}_{gp} - \dot{Q}_{env,s} - \dot{H}_{evap}, \quad (2.77)$$

$$\frac{dH_{g,total}}{dt} = \dot{H}_{g,in} + \dot{H}_{nozzle} - \dot{H}_{g,out} - \dot{Q}_{gp} + \dot{Q}_{env,g} + \dot{H}_{evap}. \quad (2.78)$$

Here it is assumed that the temperatures of the solid particles will not change due to re-cycle, i.e. $\theta_{rec} = \theta_s$.

By evaluation of the product rule, dynamic equations can be derived for the temperatures of the solid and the gas:

$$\frac{dH_{s,total}}{dt} = \frac{dm_{s,dry}}{dt} (c_{p,s} + c_{p,l}X) \theta_s + m_{s,dry} c_{p,l} \frac{dX}{dt} \theta_s + m_{s,dry} (c_{p,s} + c_{p,l}X) \frac{d\theta_s}{dt}, \quad (2.79)$$

$$\frac{dH_{g,total}}{dt} = \frac{dm_{g,dry}}{dt} (c_{p,g} + c_{p,v}Y) \theta_g + m_{g,dry} c_{p,v} \frac{dY}{dt} \theta_g + m_{g,dry} (c_{p,g} + c_{p,v}Y) \frac{d\theta_g}{dt}. \quad (2.80)$$

The dynamic equations can then be obtained from these results by substitution of the balance equations for $dH_{s,total}/dt$ and $dH_{g,total}/dt$, and re-arranging the resulting equation for $d\theta_s/dt$ and $d\theta_g/dt$.

In order to be able to solve this system of equations, correlations are needed that link the mass and enthalpy flows to the balanced quantities.

Heat and mass transfer in fluidised beds is an extensively investigated field, see for instance the works cited earlier in this section. Due to its complexity, stemming from the coupling of the hydro- and thermodynamics, no general solution for all process conditions and materials exist. In most cases empirical or semi-empirical relations are used to describe the heat and mass transport in

some region of operation. A different approach that is used quite successfully is the modelling of heat and mass transfer coefficients and relations for a single sphere and then calculating the flows for the fluidised bed by scaling with the number of particles in the bed [50].

Here, mean quantities of the particle size distribution are used to determine the transfer coefficients, and it is assumed that the liquid droplet spreads uniformly on the particle surface, i.e. the particle surface area is also the heat and mass transfer surface area.

In the following, the focus lies on the mass and heat flows, the major equations for the heat and mass transfer coefficients are presented in Appendix A.

The mass flow of evaporated liquid can be calculated by $\dot{M}_{evap} = \eta (Y_{sat} - Y_{in}) \dot{M}_{g,in}$ [107]. Here η is an efficiency of mass transfer. The saturation moisture content Y_{sat} determines how much moisture can be taken up by the gas phase. It is the theoretical maximum and depends on the saturation temperature which has to be computed from Mollier diagrams.

The efficiency is calculated from $\eta = 1 - \exp(-\dot{\nu} NTU)$ (assuming a plug-flow of gas), or $\eta = NTU \dot{\nu} / (1 + NTU)$ (assuming an ideally mixed gas flow). The value of NTU depends on the mass transfer coefficient β_{gp} :

$$NTU = \frac{\rho_g \beta_{gp} A_{particles}}{\dot{M}_{g,in}} \quad (2.81)$$

with $A_{particles}$ being the total surface area of all particles in the bed: $A_{particles} = \pi \mu_2$.

During drying two stages can be observed: In the first drying stage the free liquid on the surface of the particle is evaporated. In the second drying stage the liquid in the interior of the particle evaporates and the resulting vapour has to be transported to the surface. This transport is limited by material-dependent diffusion – in general a slow-down in drying in this stage can be observed. The change in drying velocity can be modelled by the *normalised drying curve* $\dot{\nu}$ and depends mostly on the particle material. For the first stage of drying $\dot{\nu}$ is constant, and $\dot{\nu} = 1$. In this thesis the first drying stage is considered only.

The evaporation enthalpy is calculated by $\dot{H}_{evap} = \dot{M}_{evap} (c_{p,v} \theta_s + \Delta h_{evap})$. The energy needed for the phase transition of the liquid from its liquid to vaporous state is called the specific evaporation enthalpy. It can be obtained from tables or empirical relations.

The heat flow between particles and the gas $\dot{Q}_{gp} = \alpha_{gp} (\theta_g - \theta_s) A_{particles}$ is modelled as a convective heat transport, i.e. radiative heat transfer is neglected. A correlation for the calculation of α_{gp} , as well as for the heat transfer coefficients for the heat transfer from particles to the wall of the apparatus, α_{pw} , from the gas to the wall of the apparatus, α_{gw} , and from the wall to the environment, α_{we} , are given in Appendix A. These flows are also calculated as convective heat flows. The required temperature of the wall θ_w is obtained from a steady-state energy balance, neglecting the heat transfer by conduction inside the wall:

$$\theta_w = \frac{\alpha_{gw} A_w \theta_g + \alpha_{pw} A_{pw} \theta_s + \alpha_{we} A_w \theta_{env}}{\alpha_{gw} A_w + \alpha_{pw} A_{pw} + \alpha_{we} A_w} \quad (2.82)$$

In this equation A_w denotes the surface area of the wall, and $A_{pw} = 2\pi r_{app} h_{bed}$ the heat transfer surface between the particles in the bed and the wall of the apparatus. The height of the fluidised bed, h_{bed} , is calculated from the mass of dry particles and the porosity of the bed: $h_{bed} = m_{bed} / (\rho_s (1 - \psi) A_{app})$; r_{app} denotes the radius of the process chamber and A_{app} the corresponding cross-sectional area.

The remaining enthalpies are calculated as follows:

$$\dot{H}_{g,in} = \dot{M}_{g,in} (c_{p,g} + c_{p,v} Y_{in}) \theta_{g,in} + \dot{M}_{g,in} Y_{in} \Delta h_{evap} \quad (2.83)$$

$$\dot{H}_{g,out} = \dot{M}_{g,out} (c_{p,g} + c_{p,v}Y) \theta_g + \dot{M}_{g,in} Y \Delta h_{evap} \quad (2.84)$$

$$\dot{H}_{sus} = \dot{M}_{sus} (x_s c_{p,s} + (1 - x_s) c_{p,l}) \theta_{sus} \quad (2.85)$$

$$\dot{H}_{nuc} = \dot{M}_{nuc} (c_{p,s} + c_{p,l}X_{nuc}) \theta_{nuc} \quad (2.86)$$

$$\dot{H}_{rec} = \dot{M}_{rec} (c_{p,s} + c_{p,l}X_{rec}) \theta_{rec} \quad (2.87)$$

$$\dot{H}_{s,out} = \dot{M}_{s,out} (c_{p,s} + c_{p,l}X_{out}) \theta_s \quad (2.88)$$

These are the major equations for the dynamic simulation of the moisture contents and temperatures of the gas and the particles in fluidised bed spray granulation. Minor (help) variables needed for the simulation are listed in the Appendix A or are calculated after Peglow and Cunäus [107]. The most time-consuming part in the evaluation of the dynamic equations is the calculation of the heat and mass transfer coefficients, and the saturation temperature.

If the heat transfer model is used in a continuous spray granulation process, also a steady-state can be calculated, for instance by dynamic simulation.

One important observation is that the states of the heat and mass transfer model are influenced by the population balance equation via the mass of dry particles in the system. The dynamics of the growth of particles is, however, not influenced by these states. This is reasonable under the assumptions made as the population balance equation only considers dry particulate material, but the heat and mass transfer model considers the transition of liquid to vapour.

Although experimental results suggest that heat and mass transfer, in terms of the drying conditions, have an influence on the formation of the layer, for instance influencing the porosity of the layer and thereby the particle size, the direct relationship between drying conditions and particle growth is not well known and subject to investigations. For that reason, *it is assumed* that the heat and mass transfer does not influence the particle growth, i.e. a decoupling of moisture content and temperature from the particle size is assumed. One way to realise this setup is to run the process at different time-scales, i.e. the drying conditions are set such that heat and mass transfer is significantly faster than particle growth. The assumption will have an important influence on the controller design.

Chapter 3

Model-based measurement of particle property distributions

3.1 Introduction

Many properties of a particulate product can be derived directly from the properties of the particles. Up to now, in many industrial applications, the measurement of mean or integral values of the property distributions, for example the mean diameter of particles or the total mass, was deemed sufficient for process monitoring. But with increasing strictness of product specifications and the need to guarantee more than just the compliance of a mean or integral value to the specifications, the interest in additional information on the property distribution in a particulate process increases. From the knowledge of the particle property distribution, in principle, a complete monitoring of the process state is possible, and thus the opportunity to influence the process conditions in order to create a desired product if this information is used in a feedback control scheme.

Most modern control schemes use as much process information as is available, this includes the property distribution. The problem that arises in process monitoring and control is that the measurement of the property distribution must be conducted on-line, i.e. while the process is running, and the measurement result must be made available with as less as possible delay to realise an effective monitoring and control of the process.

In this section the measurement of the characteristic size of particles in a particulate process, for instance fluidised bed spray granulation, is considered. The problems arising in this task are similar to the problems arising in the measurement of other property distributions, e.g. moisture distributions, or temperature distributions. Hence, the ideas presented in this section and illustrated for the size of the particles can be applied, after suitable modifications, to the measurement of other quantities as well.

Methods for measuring the size of particles can be roughly classified into two groups: in-line (or on-line) methods, and off-line methods:

- *off-line methods*: In these methods a sample is taken from the process plant and then transported to a laboratory for analysis, i.e. there is a significant spatial distance between the location where the sample is taken and the location where the sample is analysed, also a significant time-lag can occur. Additionally, the sample material is not re-fed into the process.
- *in-line methods*: Here, the sample is taken in the plant and also analysed inside the plant, i.e. there is no significant spatial distance between the plant and the location of analysis.

Also, the sample is re-fed into the process after analysis.

Important *off-line* methods for analysis are

- Sieving (screening): The sizes of particles are determined by applying the particle sample to a cascade of sieves. The size distribution is then calculated from the mass fraction of the sample that remains on the different sieves. This method is the traditional way of characterising the size distribution of a particulate system. Due to its standardisation, it is the reference for all other measurement and analysis techniques [99].
- Image-based methods: Here the sample is dispersed into a thin veil of particles that falls in front of a camera-system. In discrete time steps pictures of the measurement volume are taken. The particles on these two-dimensional pictures and their sizes are identified and calculated by image-processing algorithms. Due to the simplicity in handling and the wealth and accuracy of the information that is gathered by these measurement systems, they are becoming increasingly popular in industries for particle characterisation. Examples of image-based measurement devices are the Camsizer by Retsch GmbH (Germany), and the PICTOS system by Sympatec GmbH (Germany).

Off-line methods have the important advantage that, apart from particle changes due to the measurement principle, with one sample as many analyses as needed can be performed. By re-analysing a sample the influence of random measurement errors on the final result can be decreased by averaging over the total number of analyses performed on the sample.

But, severe disadvantages can be identified in almost all off-line methods:

- Minimum amount of the sample mass: This can be a critical issue in processes where in total only a very small amount of product is produced, for instance a highly potent pharmaceutical ingredient. The removal of a sample for analysis then further decreases the amount of product.
- Based on the size of the sample the analysis can take a long time, for instance in image-based methods where the sample has to be dispersed into a thin veil. Taking a large sample then takes a long time before the sample has been processed completely.
- The measurement devices are often very sensitive to the environmental conditions, e.g. the optics of the cameras are sensitive to dust. For that reason the devices are situated in external laboratories. The transport of a sample from the plant to the analysis introduces a delay.
- In most cases there is no way of direct communication between the measurement device and the process plant, i.e. analysis results cannot be sent back instantaneously, introducing another delay.

In total, the transport delays and the time needed for the analysis lead to a significant time-lag of the measurement result in comparison to the actual process state. This is a major obstacle for using the results of off-line methods in process monitoring and control.

In order to remedy the disadvantages of off-line methods, in-line measurement and analysis devices have been designed in recent years [99]. Two principles that have become popular in industries are:

- *Focused beam reflectance, laser diffraction*: A focused laser beam sent out from the probe that hits a particle entering the measurement volume is back-scattered. The back-scattered

light is detected by optical fibres and from the time difference between the out-sent ray and the back-scattered light a chord length of the particle is calculated, i.e. the time difference results from the additional path the light travels on the surface of the particle. Further details on the measurement principle and applications can be found in [124, 66]. A realisation of this principle can be found in the FBRM-probe manufactured by Malvern Instruments Ltd. (United Kingdom).

- *Spatial filter velocimetry*: Here a particle entering the measurement volume falls through an array of optical fibres that are illuminated by laser light. The particle creates shadows on the fibres while passing and thus creates pulse signals in each fibre with a frequency proportional to the velocity. One additional fibre is used to detect the time of such a shadowing event. From this information, i.e. velocity of particle and time needed to pass an optical fibre (which has a known diameter), a chord-length of the particle is calculated [40]. This principle is depicted in Fig. 3.1 and is used for instance in the product series IPP of Parsum GmbH (Germany).

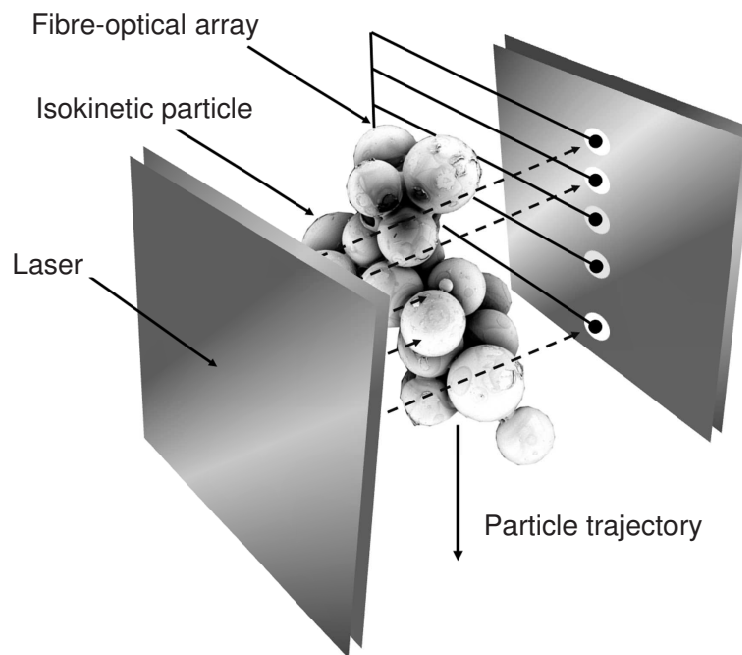


Figure 3.1: Depiction of the general idea of particle size detection by shadowing events created by a particle passing an array of optical fibres (after [40]).

The most important advantages of these in-line probes are that the sample is taken and analysed inside the process plant and the analysis results are available with almost no time delay apart from the time necessary for analysis. This renders in-line probes suitable for the implementation of process monitoring and control schemes.

But, also for this class of measurement devices important limitations can be identified:

- An analysis for one sample cannot be repeated. After a particle has left the measurement volume it enters the process chamber and there is no possibility to fetch it back for further analysis.

- The particles entering the probe must represent statistically the total particle population in the process in order to obtain reliable results for the size distribution. This is a crucial issue in processes where segregation of particles takes place. There, depending on the location where the probe is installed, different distributions are measured, e.g. mainly smaller particles or mainly larger particles.
- The detected chord-length depends on the orientation of the particle with which it passes the optical fibres or is hit by the laser ray. In contrast to image-based off-line methods, where two-dimensional information can be used to determine a size of the particle, here only one dimension is available. This effect is important in agglomeration processes where particles possess a distinct three-dimensional structure that will give a different chord-length depending on the orientation.
- A chord-length is detected instead of the particle size, e.g. the particle diameter. This necessitates a transformation of chord-length information into particle sizes.

By a suitable calibration and placement of the probe in the process, which may require extensive tests of the in-line probe at the plant and some off-line reference device, most of the disadvantages can be mitigated. Only the last point, the transformation of chord-lengths into particle sizes, cannot be handled in a general way.

The transformation of chord-length information into particle sizes is a complex and still open problem for general particle shapes; for special cases that arise quite often in practice solutions have been found in the last decade, see for instance [124, 150, 66, 40, 87].

The general idea for the transformation approaches will now be exemplified for the case of a spherical particle, following the lines of Wynn [150] and Fischer et al. [40]: A spherical particle of diameter ξ can create chord-lengths in the interval $[0, \xi]$, depending on the location where the laser ray hits or the portion that creates the shadow on the optical fibres. From a statistical point of view a function signalling the probability with which a particle of diameter ξ is detected by a chord of size s can be defined: $P(z = s, \xi)$.

On the basis of this probability a static transformation can be defined that allows the calculation of the diameter from the chord-length: The probability of a spherical particle with diameter ξ creating a chord s^* in $[0, \xi]$ can be written as

$$P(0 < s^* < s) = \frac{\xi - 2y(s)}{\xi} = 1 - \sqrt{1 - \left(\frac{s}{\xi}\right)^2} = Q(s), \quad 0 \leq s < \xi \quad (3.1)$$

$$\Delta Q(s_1, s_2) = \sqrt{1 - \left(\frac{s_1}{\xi}\right)^2} - \sqrt{1 - \left(\frac{s_2}{\xi}\right)^2}, \quad 0 < s_1 < s_2 < \xi, \quad s^* \in [s_1, s_2]. \quad (3.2)$$

The chord-length distribution for mono-disperse particles $q(s)$ can be derived by differentiation of $Q(s)$ with respect to s :

$$q_{CLD}(s) = \frac{dQ}{ds} = \frac{s}{\xi \sqrt{\xi^2 - s^2}}, \quad 0 < s < \xi. \quad (3.3)$$

The chord-length distribution of an arbitrary sample can be obtained by weighting these results for all possible particle sizes. The measured chord-length distribution of the sample can then be written as

$$q_{CLD}(s) = \int_0^{\infty} q_{real}(\xi) q_{weight}(\xi, s) d\xi. \quad (3.4)$$

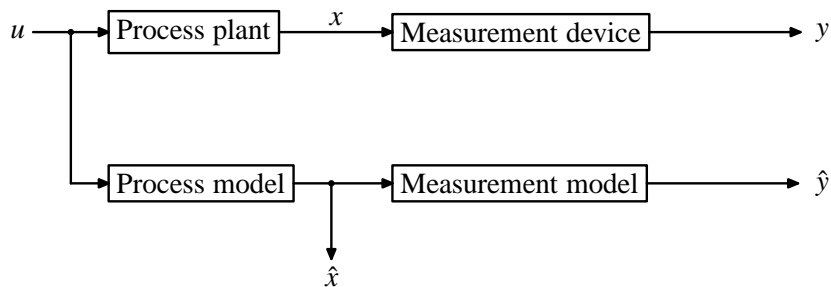


Figure 3.2: Parallel structure of process plant and mathematical process model.

By inversion of this equation with respect to q_{real} , the particle size ξ can be determined from the measured chord-length signal q_{CLD} and the chord-length-dependent weighting q_{weight} . In practical application the inversion is performed by first discretising the equation and then inverting the approximate system of nonlinear equations.

In practice one severe problem arises in the inversion: Small changes in the measured data yield large changes in the calculated size distribution of particles. Mathematically, such problems are called ill-conditioned problems. This effect becomes more dramatic if the discretisation is refined. As process measurements are inevitably subject to measurement noise, the results from static inversion may be unreliable. For a detailed discussion of the influence of noise on the reconstructed size, see for instance [40].

Another source of error is the deviation of particles from the assumed geometric model, for instance if chord-length measurements of non-spherical particles (agglomerates) are reconstructed using the assumption of spherical particles. In that case no further correction of the result can be performed as the reconstruction is static.

One way to circumvent the solution of the inverse problem, the main source of problem in the transformation of chord-length measurements to particle sizes, are *model-based measurement systems*, also known as *state observers* or *state estimators*.

3.2 Fundamentals of model-based measurement systems

The main idea of model-based measurement systems is the use of dynamic mathematical process models, for instance on the basis of population balance equations, to reconstruct process information that is hard to measure directly from measurements more easily obtainable. Under certain conditions these measurements can be limited or be corrupted by noise.

The concept was first conceived in the works of Luenberger [80, 81, 82], and Kalman [68] for linear processes. In the following decades the idea was extended to nonlinear processes, see for instance [136, 71, 53, 11].

The idea behind model-based measurement schemes and the practical implementation is best explained in two steps: First, consider the structure shown in Fig. 3.2, where in parallel to the process plant a dynamic mathematical model of the process is simulated. The input signals u to the plant are also applied to the mathematical model. From the plant, measurements y are obtained by some kind of probe: This device relates the state variables x of the process to the measurement signals. Using the knowledge of the relation between process states and measurements, measurement signals for the mathematical model \hat{y} are calculated from the model states \hat{x} .

In the absence of any model error and process disturbances, and if the initial state of the process

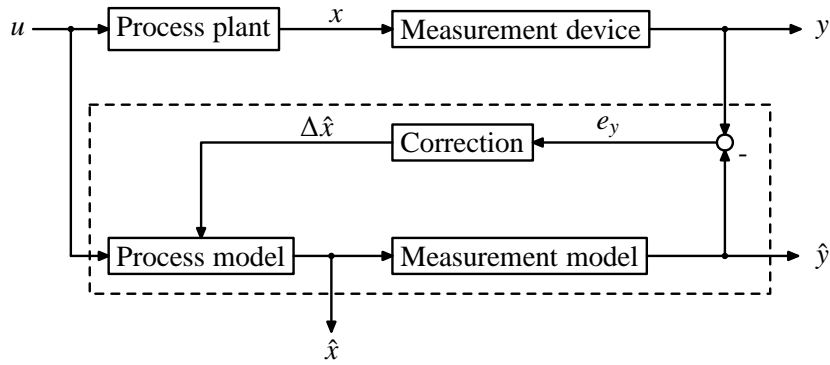


Figure 3.3: Principal structure of a model-based measurement system introduced by Luenberger [80]. The dashed box indicates the components of a model-based measurement system.

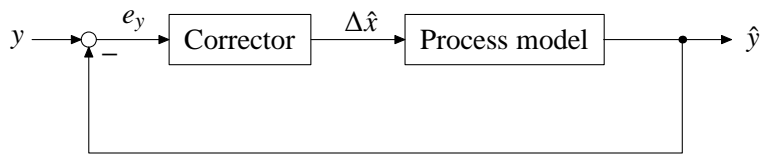


Figure 3.4: Re-interpretation of the state correction as a control-loop for the measurement error.

model is equal to the initial state of the plant, i.e. $\hat{x}_0 = x_0$, the temporal evolution of the states, i.e. $x(t)$ and $\hat{x}(t)$ will be identical. This means that instead of $x(t)$ which can only be accessed in form of the measurements y , the model state $\hat{x}(t)$, which is completely known at all times, can be used.

In practical application, however, the initial state of the process plant x_0 is often not known exactly. Also errors in the mathematical models, due to e.g. simplification and un-modelled disturbances, are often inevitable. Using the structure presented in Fig. 3.2 will yield erroneous results, i.e. $x(t) \neq \hat{x}(t)$, and the model states cannot be used for monitoring or control purposes.

In a second step, in order to account for the differences introduced by deviations in the initial conditions and uncertainties, Luenberger extended the parallel model by a system that calculates a correction of the model state \hat{x} based on the difference in the measurements signals y and \hat{y} (Fig. 3.3). This approach was motivated by the observation that the states of the process model and the plant cannot be identical if the corresponding measurements do not coincide. The important point is that the correction of the state is solely calculated from the available plant measurements, i.e. the error in measurement of the two systems drives the state $\hat{x}(t)$.

If the process plant and the measurements taken therefrom fulfil certain criteria, which will be presented in detail in the next subsection, and the corrector is suitably designed, then the model state $\hat{x}(t)$ will tend to the state of the process plant $x(t)$ despite of uncertainties, model errors, and process disturbances. This result can be stressed by redrawing the correction loop, as done in Fig. 3.4: If the error e_y does not vanish, then a non-vanishing correction of the model state is calculated. This can be seen as a control-loop for the measurement error e_y . In any case the correction is designed such that for vanishing error no further state correction is performed. The observer model is then a pure simulation model of the process plant.

Model-based measurement schemes are applied in diverse industrial fields, for instance mechanical systems (robotics), chemical engineering, and biochemical processes (e.g. [151, 69, 16, 154, 58]).

With respect to the measurement of particle size distributions model-based measurement schemes have one important advantage: From the knowledge of the process model state \hat{x} all possible measured quantities can be calculated. If the number density function is part of the model state then from this information a corresponding chord-length distribution can be calculated as presented in the last section. Taking this calculated chord-length distribution as part of the measurement signals \hat{y} then allows to detect differences in the size distributions by comparison of this data with chord-length measurements taken from the process plant. Based on the error in this measurement, the state, i.e. the number density function, is corrected accordingly. After some time, which depends on the design of the model-based measurement scheme, the particle size distribution in the process model will approach the particle size distribution in the process.

In all calculations no inversion of the measurement map, i.e. the transformation of particle sizes into chord-lengths and vice versa is necessary, which was identified as the foremost problem in reconstructing particle size distributions from chord-length measurements obtained from in-line measurement devices. The disadvantages of model-based measurement schemes are that the reconstruction is now a dynamic problem that has to be solved in parallel with the process, and the need for models of the process and the measurement device. This, however, poses no severe problem as for many interesting applications mathematical process models are available.

In applications chord-length measurements may not be available at all process sub-steps, for instance due to the still high cost of the equipment, or for safety reasons. But certain integral or mean values may be available. The task of the model-based measurement system then is to reconstruct the size distribution from this integral value.

The answer to the question under which circumstances a model-based measurement system can reconstruct the process plant state from the available measurement information leads to the concept of *observability*.

Observability. A dynamical system in state-space representation

$$\begin{aligned} \frac{dx}{dt} &= f(x(t), u(t)), & (3.5) \\ y(t) &= h(x(t), u(t)), & (3.6) \end{aligned}$$

where $x \in \mathbb{R}^N$ denotes the state of the system, $u \in \mathbb{R}^U$ are the inputs to the system, and $y \in \mathbb{R}^M$ represent the measurement information, is said to be observable if the state $x(t)$ at a given time t is completely determined by the knowledge of the inputs $u(\tau)$ and the outputs $y(\tau)$ over a finite time segment $t_0 < \tau \leq t$ [149]. For general nonlinear systems this is only true for a certain set of initial conditions x_0 and inputs $u(t)$. These systems are called locally observable [101].

Practically this definition means, that for a system to be observable all process states x must have a unique influence on the measured variables, i.e. a change in the state must be uniquely detectable in the measured quantity. Furthermore, it must be guaranteed that the error $y - \hat{y}$ vanishes only if the process state and the model state are equal, i.e. $x - \hat{x} = 0$. Then a correction based on the output error e_y will yield a successful reconstruction of the unmeasurable state x from the measurement y in form of \hat{x} .

A formal test for observability is called *observability analysis*. For finite-dimensional, nonlinear systems the following criterion can be derived using concepts from differential geometry [101]: Given a mathematical model $dx/dt = f(x, u)$ of the process and a model of the measurement map $y = h(x)$, calculate successively the Lie derivatives $L_f^i h = L_f(L_f^{i-1} h)$ with $L_f^0 h = h$ and

$L_f h = (\text{grad}_x h)f$, and construct the observability map

$$\begin{bmatrix} y \\ y' \\ \vdots \\ y^i \end{bmatrix} = O(x) = \begin{bmatrix} h(x) \\ L_f h(x) \\ \vdots \\ L_f^i h(x) \end{bmatrix}, \quad i \geq N. \quad (3.7)$$

If O can be uniquely (locally) inverted, $x = O^{-1}(y, y', \dots, y^i)$, then the system is (locally) observable. For infinite-dimensional systems a similar definition, involving operators instead of functions, can be given.

Unfortunately, even in the finite-dimensional case, this problem is equivalent to the proof of existence of (locally) unique solutions of systems of nonlinear equations, and as such only answerable in general for very small systems, i.e. N is a small integer, or for systems with a special structure.

If the process is linear, i.e. $f(x, u) = Ax + Bu$ and $h(x) = Cx$, with constant matrices A, B, C of appropriate dimensions, then the test for observability reduces to the problem of determining the rank of a matrix, the Kalman criterion for observability:

$$O = \begin{bmatrix} C \\ CA \\ CA^2 \\ \vdots \\ CA^{N-1} \end{bmatrix}. \quad (3.8)$$

If the rank of this matrix equals the number of states, i.e. $\text{rank}(O) = N$ then the linear system is observable. From the Cayley-Hamilton theorem [149], which states that any power of a quadratic matrix higher than the number of columns in it can be expressed by a linear combination of lower-order powers, i.e. $A^{n+1} = g(A, A^2, \dots, A^n)$, it follows that if the matrix O is not invertible, taking higher-order powers will not be able to change this situation, i.e. the system is unobservable.

In the practical test for observability the matrix products are not calculated, but an alternative version of the Kalman criterion introduced by Popov, Belevitch and Hautus [149] is used: Let λ_j be the eigenvalues of the matrix A , i.e. non-trivial solutions of $Av_j = \lambda_j v_j$, then a linear system is observable if and only if

$$\text{rank} \begin{bmatrix} \lambda_j I - A \\ C \end{bmatrix} = N$$

is fulfilled for every eigenvalue $j = 1, \dots, N$, where I denotes the identity matrix.

If the elements of A span many orders of magnitudes then the determination of the rank of the observability matrix, or the exact calculation of the eigenvalues of A becomes non-trivial and special numerical methods have to be applied in order to test for (numerical) observability.

A necessary, always exactly evaluable criterion, is given by *structural observability* [119, 148, 33]. Here, only structural information of a linear system, i.e. obtained by linearisation of a non-linear process model in the vicinity of a steady-state, is used to determine observability: Given linear model

$$\frac{dx}{dt} = Ax + Bu, \quad (3.9)$$

$$y = Cx, \quad (3.10)$$

from the matrices A and C the so-called structural matrices A_s and C_s are constructed:

$$A_{i,j,s} = \begin{cases} 1, & A_{ij} \neq 0 \\ 0, & \text{otherwise} \end{cases}, \quad C_{i,j,s} = \begin{cases} 1, & C_{ij} \neq 0 \\ 0, & \text{otherwise} \end{cases}.$$

The matrix A_s can then be interpreted as the adjacency matrix of a graph with the model states as its nodes. The matrix C_s contains the information which states influence the measurements directly.

The question of structural observability is then answered using concepts from graph theory; the main concepts and their connection to the structural matrices are presented in Appendix B.

Structural observability. For structural observability A_s and C_s must meet two criteria: (1) *output-connectedness*, that is each state must in some way (either directly or through other states) have influence on the measurements, and (2) *non-contraction*. This means that given a measurement the influence of all states on this measurement can be uniquely determined. In mathematical terms these criteria can be formulated as follows (T denotes a transposition):

the associated graph to (A_s, C_s) is output-connected, and

$$\text{s-rank}[A_s^T, C_s^T] = N, \quad (3.11)$$

where the structural rank (s-rank) is defined to be the maximum rank a matrix M with the structure given by M_s can attain:

$$\text{s-rank}M_s = \max_{M \in M_s} \text{rank } M. \quad (3.12)$$

In contrast to the former criteria, these can be checked easily using graph-theoretic algorithms.

Structural observability then means, that there exists at least one system (A, B, C) with the structure (A_s, B_s, C_s) that is observable. Although the test does not provide specific information about the system at hand, it gives the information that the structure itself is not unobservable and therefore the task of designing a model-based measurement scheme can be undertaken.

The design steps necessary depend on the method used in the measurement scheme, i.e. there are several possibilities to design appropriate correction terms. Some of them that will later be applied to spray granulation processes are presented in the next section.

3.3 Design methods for model-based measurement systems

In the field of control engineering model-based measurement systems are known as and classified in state observers and state estimators, respectively. Both classes share the same principal idea of using a mathematical process model to obtain estimates for the unknown plant state from available measurements. They differ in the formulation of the mathematical process models: Whereas in a state observer purely deterministic models are used for the process model and the model of the measurement device, state estimators are formulated in a stochastic framework. This means that stochastic influences, for instance measurement noise or unmodelled process dynamics, are accounted for explicitly in the design process. In state observers these influences are not considered explicitly but are handled as general disturbances that are attenuated by the structure of the observer. In the following the term *state observer* is used throughout for state observers and estimators if the concepts and explanations are valid for both classes of model-based measurement systems.

Similar to the classification of dynamic systems into finite-dimensional and infinite-dimensional systems, state observers can be finite- or infinite-dimensional.

Infinite-dimensional state observers possess the structure presented in Fig. 3.3, the main difference is that the process and measurement models are infinite-dimensional functional operators, i.e. operators that map functions into other functions. The observability analysis of these systems

is greatly hindered by their distributed character, i.e. in the general case no specific results can be obtained. Only in case of special structures, for instance linear infinite-dimensional systems, evaluable criteria are known, see for instance [27].

The correction, in the general case, is also an infinite-dimensional operator. For the case of non-linear distributed systems standard design methods are not available, and the success and the performance depends heavily on the process knowledge, experience and creativity of the design engineer. In the literature some successful applications to nonlinear distributed parameter systems are known, for instance in chemical reaction engineering [151, 69, 16, 90, 58]. There, for spatially-distributed systems using discrete measurements of temperatures and concentrations in the spatial directions, physically motivated corrections are designed. The parametrisation of the dynamics is performed by considering the temporal evolution of the (spatially-distributed) measurement error e_y . In summary, the design of non-linear infinite-dimensional observers is an intricate task, the success of which depends strongly on the experience of the designer.

Due to the problems in the design of infinite-dimensional observers, commonly finite-dimensional observers are designed on the basis of a finite-dimensional approximation of the infinite-dimensional process model. Approximations can be obtained for instance by discretisation of the partial differential balance equations, for instance by application of the methods presented in Appendix D. Using finite-dimensional approximations on one hand simplifies the design, because standardised tests for observability and design methods can be used, on the other hand the use of finite-dimensional system instead of infinite-dimensional systems leads to a loss of performance, and in the worst case to instability of the model-based measurement system, due to the loss of information in the approximation step. However, as motivated in Appendix D, this loss and the danger of instability can be reduced by using a sufficiently accurate approximation.

As mentioned before, in the *finite-dimensional* case for the test of observability and for the design of state observers standard methods are available. But, the availability does not imply that the actual design is trivial; if the structure of the dynamic process model is arbitrary then difficulties can arise, for instance in the calculation of the Lie derivatives that are needed for observability analysis and in many design methods.

3.3.1 Design methods for state observers

In the following important design methods for state observers and state estimators, which will later be applied to the fluidised bed spray granulation processes and design methods needed for subsequent derivations are presented. Other important design methods that are not applied to the task of reconstructing the particle size distribution are only mentioned and references are given.

Luenberger observer for linear systems

The classical Luenberger observer for linear systems [82] uses for a linear time-invariant system

$$\frac{dx}{dt} = Ax(t) + Bu(t), \quad x(0) = x_0, \quad y(t) = Cx(t) \quad (3.13)$$

the following structure for the state observer

$$\frac{d\hat{x}}{dt} = A\hat{x}(t) + Bu(t) + K(y(t) - \hat{y}(t)), \quad \hat{x}(0) = \hat{x}_0, \quad \hat{y}(t) = C\hat{x}(t). \quad (3.14)$$

In both systems the matrices A , B , C and K are constant. The matrix K denotes the gain of the state correction. In case of vanishing measurement error $e_y(t) = y(t) - \hat{y}(t)$, the correction vanishes, too.

In that case the observer model is identical to the process, i.e. the simulation condition is fulfilled. The task is then to design the gain K such that the error in the states, $x - \hat{x}$, tends to zero. If the system is observable, which is assumed in the following, then the rate of decay in error can be specified arbitrarily by the choice of K .

One way to obtain a suitable matrix K is the following: Defining the error in the states of the process and the observer, $e = x - \hat{x}$, a dynamic equation for the error can be derived:

$$\frac{de}{dt} = Ax + Bu - A\hat{x} - Bu - K(y - \hat{y}), \quad (3.15)$$

$$= Ae - K(y - \hat{y}), \quad (3.16)$$

$$\frac{de}{dt} = (A - KC)e, \quad e(0) = x_0 - \hat{x}_0. \quad (3.17)$$

From the theory of linear ordinary differential equations follows that the solution $e(t)$ tends to zero exponentially, if all the eigenvalues of the matrix $(A - KC)$ lie in the open left complex half-plane, i.e. the real part of all eigenvalues has to be strictly negative. From a control engineering point of view the gain K is designed by pole placement of the eigenvalues for the state error e . In general, a high gain will yield a fast decay of the error for perfect measurements, that is, no noise is present in the measurement signal y . If there is noise, i.e. $y(t) = y_{nf}(t) + \eta(t)$, where y_{nf} is the noise-free signal and η a noise signal, then an error proportional to K is introduced, as can be seen by substitution into the dynamic equation for the state error. The equation is then no longer homogeneous and the error will not tend to zero, but to a non-zero steady-state. A linear estimator that is able to cope with measurement noise, the Kalman filter, will be presented later.

For non-linear systems a variety of design methods is available. Due to the peculiarities of non-linear systems, these are often limited to dynamic systems with a special structure, for instance normal form observers, high-gain observers, extended Luenberger observers, or sliding-mode observers. The assumed special structures allow at some point in the design process to reduce the calculation of the gain for the non-linear system to the calculation of a gain for a linear error system, which reduces the effort considerably. However, non-linear transformations have to be constructed in order to arrive at the linear error system. These can only be calculated if the system possesses the assumed special structure. If this is not the case, then the transformations cannot be calculated, i.e. the observers cannot be designed for the system.

In the following a state observation method is presented that does not require a special structure of the dynamic process model. In addition, it has the virtues that it provides an optimal estimate \hat{x} of the state x in some sense, and the convergence of the method for general non-linear systems can be proved.

State observation by on-line minimisation

The idea of obtaining an estimate \hat{x} of an unmeasurable process state x by solving an on-line optimisation problem in a deterministic setting was used by Zimmer [154] to derive a very elegant method that is presented in this section.

Given a non-linear dynamic process

$$\frac{dx}{dt} = f(x(t), u(t)), \quad x(0) = x_0, \quad y(t) = h(x(t)) \quad (3.18)$$

the state and output trajectories can be written formally as $x(t; t_0, x_0)$ and $y(t; t_0, x_0)$, i.e. the state at time t depends on the initial time t_0 (to determine how long the process is running), and the initial state at t_0 given by x_0 . The output trajectory can be interpreted in a analogous way.

The observer model is chosen to be

$$\frac{d\hat{x}}{dt} = f(\hat{x}(t), u(t)), \quad \hat{x}(0) = \hat{x}_0, \quad \hat{y}(t) = h(\hat{x}(t)), \quad (3.19)$$

with the corresponding trajectories $\hat{x}(t; t_0, \hat{x}_0)$ and $\hat{y}(t; t_0, \hat{x}_0)$.

If the process time span is sub-divided into intervals of length T , i.e. $[t_0, t_0 + T]$, $[t_0 + T, t_0 + 2T]$, \dots , that is, into non-overlapping time *horizons*, then the following functional over each one of these horizons can be defined:

$$\mathcal{N} = \frac{1}{2} \int_{t_0+kT}^{t_0+(k+1)T} (\hat{y} - y)^\top (\hat{y} - y) dt, \quad k = 0, 1, \dots \quad (3.20)$$

This functional can be interpreted as measuring the square of the distance in the measurement signals \hat{y} and y over the horizon. As the measurement signal \hat{y} over a time horizon depends only on the initial state of the observer model at the beginning of the interval, i.e. \hat{x}_0 , and given the measurement $y(t; t_0, x_0)$ obtained from the process during $t \in [t_0 + kT, t_0 + (k + 1)T]$ the functional depends on the initial state of the observer model \hat{x}_0 and the measurements y , i.e. $\mathcal{N}(\hat{x}_0, y)$, over a time horizon.

Observability of a dynamic system states that if the error in the measurements e_y vanishes, then the state of the observer is equal to the unmeasurable process state. In terms of the defined functional this means that it has to be minimised, i.e. the measurement sequence \hat{y} has to be chosen such that $\hat{y} - y$ vanishes. As was pointed out, the measurement sequence depends on the initial state of the observer model, so the minimisation problem can be written as

$$\min_{\hat{x}_0} \mathcal{N}(\hat{x}_0, y) = \min_{\hat{x}_0} \frac{1}{2} \int_{t_0+kT}^{t_0+(k+1)T} (\hat{y} - y)^\top (\hat{y} - y) dt, \quad k = 0, 1, \dots, \quad (3.21)$$

i.e. the task is to determine the initial condition of the observer model at the beginning of the time horizon such that the error in measurements is minimised. The optimisation problem is constrained by the nonlinear observer state equations that have to be fulfilled over the time horizon, i.e. it is a nonlinear, constrained optimisation problem.

Zimmer [154] then reduced the optimisation problem further by using the fact that for \hat{x}_0 to be an extremal of $\mathcal{N}(\hat{x}_0, y)$ the following necessary condition has to be fulfilled:

$$\frac{\partial}{\partial \hat{x}_0} \mathcal{N}(\hat{x}_0, y) = 0. \quad (3.22)$$

So, instead of solving the optimisation problem, the value \hat{x}_0 has to be found such that the non-linear system of algebraic equations $\partial \mathcal{N} / \partial \hat{x}_0 = 0$ is fulfilled, i.e. the nonlinear, constrained optimisation problem is reduced to a root-finding problem.

One standard method that can be used to find the roots of non-linear algebraic equations is the Newton-Raphson method [54]. It is an iterative method that refines a given initial guess of the root by evaluation of the system of equations and the gradient of the equation. In case of the system at hand, using the short-cut notation $\mathcal{N}' = \partial \mathcal{N} / \partial \hat{x}_0$ (the gradient of the cost functional), and $\mathcal{N}'' = \partial^2 \mathcal{N} / \partial \hat{x}_0^2$ (the Hessian of the cost functional, and the gradient of the necessary condition), one step of the iteration can be written as:

$$\hat{x}_0^+ = \hat{x}_0^- - [\mathcal{N}''(\hat{x}_0^-, y)]^{-1} [\mathcal{N}'(\hat{x}_0^-, y)]^\top, \quad (3.23)$$

where \hat{x}_0^- is the guess for the root, and \hat{x}_0^+ is the corrected value based on the information contained in \mathcal{N}' and \mathcal{N}'' .

In order to be able to calculate the new estimate \hat{x}_0^+ based on the measurement information, the gradient and the Hessian of the cost functional \mathcal{N} are required. An evaluation for the gradient yields

$$\mathcal{N}'(\hat{x}_0, y) = \int_{t_0+kT}^{t_0+(k+1)T} (\hat{y} - y)^\top \frac{\partial \hat{y}}{\partial \hat{x}_0} dt = \int_{t_0+kT}^{t_0+(k+1)T} (\hat{y} - y)^\top \left. \frac{\partial h}{\partial x} \right|_{\hat{x}} \left(\frac{\partial \hat{x}}{\partial \hat{x}_0} \right) dt. \quad (3.24)$$

In this equation $\partial h/\partial x$ denotes the linearisation of the output function h along the observer state trajectory \hat{x} and $\partial \hat{x}/\partial \hat{x}_0$ denotes the sensitivity of the state trajectory \hat{x} with respect to a change in the initial condition \hat{x}_0 .

Taking derivatives with respect to time, a dynamic equation for the gradient can be derived:

$$\frac{d\mathcal{N}'}{dt} = (\hat{y} - y)^\top \left. \frac{\partial h}{\partial x} \right|_{\hat{x}} \left(\frac{\partial \hat{x}}{\partial \hat{x}_0} \right), \quad \mathcal{N}'(t_0) = 0^\top. \quad (3.25)$$

The initial condition for the gradient can be obtained from the fact that the estimate of the state at the end of the last observation horizon (which is the initial state of current horizon) was optimal with respect to the cost functional.

In a similar way the Hessian of \mathcal{N} can be evaluated:

$$\mathcal{N}''(\hat{x}_0, y) = \int_{t_0+kT}^{t_0+(k+1)T} \left(\frac{\partial \hat{y}}{\partial \hat{x}_0} \right)^\top \left(\frac{\partial \hat{y}}{\partial \hat{x}_0} \right) dt + \int_{t_0+kT}^{t_0+(k+1)T} (\hat{y} - y)^\top \left(\frac{\partial^2 \hat{y}}{\partial \hat{x}_0^2} \right) dt \quad (3.26)$$

$$\approx \int_{t_0+kT}^{t_0+(k+1)T} \left(\frac{\partial \hat{x}}{\partial \hat{x}_0} \right)^\top \left. \frac{\partial h}{\partial x} \right|_{\hat{x}}^\top \left. \frac{\partial h}{\partial x} \right|_{\hat{x}} \left(\frac{\partial \hat{x}}{\partial \hat{x}_0} \right) dt. \quad (3.27)$$

Here the exact Hessian is approximated only by neglecting higher-order derivatives of the observer measurements. This approximation is justified if \hat{x} does not deviate too much from x over the time horizon.

The corresponding dynamic equation reads:

$$\frac{d\mathcal{N}''}{dt} = \left(\frac{\partial \hat{x}}{\partial \hat{x}_0} \right)^\top \left. \frac{\partial h}{\partial x} \right|_{\hat{x}}^\top \left. \frac{\partial h}{\partial x} \right|_{\hat{x}} \left(\frac{\partial \hat{x}}{\partial \hat{x}_0} \right), \quad \mathcal{N}''(t_0) = 0. \quad (3.28)$$

The required gradient and Hessian of the functional \mathcal{N} can be evaluated if the sensitivity matrix $\partial \hat{x}/\partial \hat{x}_0$ is known over the horizon $[t_0 + kT, t_0 + (k + 1)T]$. A suitable dynamic equation can be derived as follows:

$$\frac{d}{dt} \left(\frac{\partial \hat{x}}{\partial \hat{x}_0} \right) = \frac{\partial}{\partial \hat{x}_0} \left(\frac{\partial \hat{x}}{\partial t} \right) = \frac{\partial}{\partial \hat{x}_0} (f(\hat{x}(t); t_0, \hat{x}_0)) = \left(\frac{\partial f}{\partial \hat{x}_0} \right) \left(\frac{\partial \hat{x}}{\partial \hat{x}_0} \right), \quad \left. \left(\frac{\partial \hat{x}}{\partial \hat{x}_0} \right) \right|_{t_0} = \left(\frac{\partial \hat{x}_0}{\partial \hat{x}_0} \right) = I. \quad (3.29)$$

Using these equations an algorithm for state observation by on-line minimisation can be given: For $t \in [t_0, t_0 + T]$, given the process measurements $y(t)$:

1. Solve the dynamic equations for \hat{x} , \mathcal{N}' , \mathcal{N}'' and $\left(\frac{\partial \hat{x}}{\partial \hat{x}_0} \right)$, starting from the respective initial conditions, i.e. $\hat{x}(t_0) = \hat{x}_0 = \hat{x}_0^-$, $\mathcal{N}'(t_0) = 0^\top$, $\mathcal{N}''(t_0) = 0$, and the identity matrix as initial condition for the sensitivity equation.

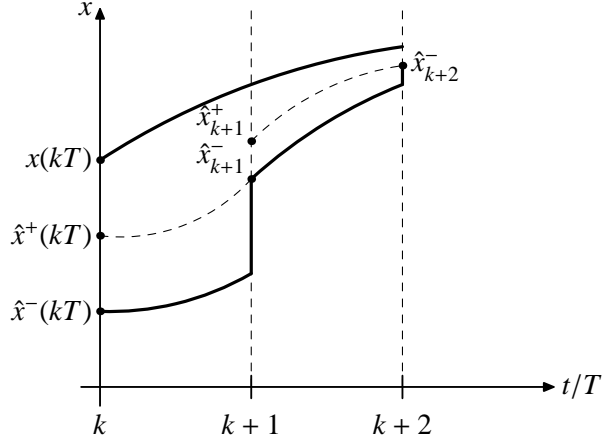


Figure 3.5: Idea of state observation by on-line minimisation after Zimmer [154].

2. Correct the initial guess \hat{x}_0^- by one iteration of the Newton-Raphson method:

$$\hat{x}_0^+ = \hat{x}_0^- - [\mathcal{N}''(\hat{x}_0^-, y)]^{-1} [\mathcal{N}'(\hat{x}_0^-, y)]^T, \quad (3.30)$$

3. Re-solve the observer model equation for the initial condition \hat{x}_0^+ obtaining the corrected state trajectory $\hat{x}^+(t; t_0, \hat{x}_0^+)$.
4. For the next observation horizon, set $\hat{x}_0^- = \hat{x}^+(T; t_0, \hat{x}_0^+)$ and $t_0 = t_0 + T$. Repeat with step 1.

Using this algorithm a sequence of state corrections is obtained. The idea of the algorithm, and the resulting observer state trajectories are depicted in Fig. 3.5.

In a practical implementation the initial guess \hat{x}_0^- and the resulting state trajectory $\hat{x}^-(t; t_0, \hat{x}_0^-)$ is used for process monitoring and control purposes on the time horizon $[t_0, t_0 + T]$. Meanwhile, the process measurement trajectory $y(t; t_0, x_0)$ is recorded. At the end of the time horizon the presented algorithm is executed yielding the corrected observer state trajectory $\hat{x}^+(t; t_0, \hat{x}_0^+)$. The observer state at $\hat{x}^+(t_0 + T; t_0, \hat{x}_0^+)$ is then taken as the initial guess \hat{x}_0^- , see step 4 of the algorithm. This requires that the dynamic equations in the algorithm can be simulated much faster than real-time as the corrected estimate of $\hat{x}^+(t_0 + T; t_0, \hat{x}_0^+)$ should be available with as less time delay as possible to give a reliable estimate of the state of the process plant.

From the formulation of the algorithm it can be derived that one approximation step, i.e. $\hat{x}^+(t_0 + T) \rightarrow \hat{x}^+(t_0 + 2T)$ requires the solution of $2N^2 + 3N$ ordinary differential equations, where N is the dimension of the state x . This proves to be a high computational burden, especially if the dimension of x is large. However, special algorithms are available to reduce the effort in computation, see for instance Cao et al. [17].

Zimmer [154] proves under quite general conditions that the Newton-Raphson iteration converges to a new estimate of the observer state, provided that the initial deviation $x - \hat{x}$ is sufficiently small. Due to the high convergence order of the Newton-Raphson method (quadratic), a very fast convergence within a few iterations can be expected.

This idea of calculating estimates for the observer state can be generalised and extended into a stochastic framework, yielding *state estimators*.

3.3.2 Design methods for state estimators

In many practical applications the process measurement is biased, i.e. instead of the true value y a value of $y + \eta$ is measured, where η denotes the bias. This may be a systematic measurement error, e.g. a measurement offset, or a time-varying, stochastic quantity, e.g. measurement noise. Whereas constant offsets can often be identified and eliminated by careful re-calibration of the measurement device, stochastic influences are harder to compensate: Here often only some information on the probability distribution, for instance the mean and the variance, is available. State estimation algorithms use this available information in the design process to counter the influence of stochastic processes, e.g. noise or unmodelled process dynamics, on the estimation result. Because of the fact that these algorithms filter out the stochastic components in the signals, they are also called *filters*. In order to do so, in addition to the process model and the model of the measurement device, a model of the stochastic disturbances is needed in the design process.

In the following important finite-dimensional state estimators (state filters) are presented, starting with an extension of the concept of state observation by on-line minimisation: the moving-horizon estimator. Subsequently, an introduction to Bayesian filtering is given, which allows for the design of state estimators in a purely statistical setting. Afterwards Kalman filtering and Unscented Kalman filtering are presented (as approximations of Bayesian filters), allowing for state estimation in (non-)linear dynamic systems subject to stochastic disturbances.

Moving-horizon estimators

Like state observation by on-line minimisation, moving-horizon estimators [123] calculate an estimate of the observer state by solving on-line an appropriate optimisation problem. The main differences to the aforementioned algorithm are that stochastic disturbances on the process and on the measurements are accounted for explicitly, and that now the time horizons can overlap.

The idea of a moving-horizon estimator is motivated as follows: Given a process model

$$\frac{dx}{dt} = f(x, u) + \omega \quad y_k = h(x_k) + \eta_k, \quad (3.31)$$

where x is the process state, y_k is the measurement at *sampling time* t_k , i.e. measurements are only taken at discrete points in time, and ω and η are additive stochastic influences with not necessarily known statistics. Assuming that the sampling interval Δt , i.e. the temporal distance between two measurements, is constant, the process states at time t_k , denoted by x_k , can be calculated formally by integrating the state equation for one sampling interval:

$$x_k = x_{k-1} + \int_{(k-1)\Delta t}^{k\Delta t} f(x(t), u_{k-1}) dt + \int_{(k-1)\Delta t}^{k\Delta t} \omega dt \quad (3.32)$$

$$= F(x_{k-1}, u_{k-1}) + w_{k-1}. \quad (3.33)$$

Using this equation over time a sequence of state and measurement values can be generated: $\{(x_k, y_k)\}$, $k = 0, 1, \dots$

The measurement information can then be used to determine an estimate of the process state: Given an initial estimate \hat{x}_0^- , the sequence of measurements $\{y_0, \dots, y_k\}$ and a model of the process, find the initial state \hat{x}_0^+ and a sequence of process disturbances $\{w_0, \dots, w_{k-1}\}$ such that a given functional is minimised, for instance a least-squares criterion:

$$\min_{\hat{x}_0^-, \{w\}} \sum_{l=1}^k \eta_l^T R^{-1} \eta_l + \sum_{l=1}^{k-1} w_l^T Q^{-1} w_l, \quad (3.34)$$

subject to the constraints $\eta_l = y_l - h(\hat{x}_l)$ and $\hat{x}_l = F(\hat{x}_l, u_{l-1}) + w_{l-1}$ with $\hat{x}_0 = \hat{x}_0^-$. In this formulation the statistics of the stochastic sequences w_l and η_l are incorporated in the functional by the *covariances* R and Q .

The solution of this optimisation problem then gives an optimal estimate of the initial value, \hat{x}_0^+ , and the process noise sequence $\{w_0, \dots, w_{k-1}\}$. Using this data an estimate at time t_k can be generated by solving the dynamic state equation using the optimal initial value and the sequence of stochastic disturbances.

In this formulation all measurement information up to time t_k is used in obtaining an estimate of the process state \hat{x}_k . The major problem here is that with increasing time the number of optimisation variables increases as for each additional step an additional process disturbance has to be estimated, so the number of variables in the optimisation problem is unbounded. As time necessary to solve an optimisation problem depends on the number of optimisation variables, this time will also increase rendering the approach infeasible for large amounts of measurement information.

In order to circumvent this problem, a moving-horizon strategy is used [123]: Instead of considering all available measurement information up to time t_k only a fixed number m of past measurements and the measurement available at t_k are used in the estimation process. This results in an optimisation problem with a maximum number of optimisation variables proportional to the number of measurements considered. The time span $[t_{k-m+1}, t_k]$ then is the horizon of the estimation problem. The cost functional is rewritten, yielding:

$$\min_{\hat{x}_{k-m+1}^-, \{w\}} \sum_{l=k-m+1}^k \eta_l^T R^{-1} \eta_l + \sum_{l=k-m+1}^{k-1} w_l^T Q^{-1} w_l + \hat{x}_{k-m+1}^{-,T} P_{k-m+1}^{-1} \hat{x}_{k-m+1}^- \quad (3.35)$$

The new term involving the state covariance P accounts for the confidence in the initial estimate \hat{x}_{k-m+1}^- at the beginning of the estimation horizon. It incorporates all information about how the process evolved from its initial state at t_0 to the state t_k and may be crucial to the performance of the estimator [116].

If time advances from t_k to t_{k+1} , the first measurement is discarded from the optimisation problem. Instead, the measurement value at t_{k+1} is added to the formulation and the optimisation problem is re-solved to obtain an optimal estimate $\hat{x}_{(k+1)-m+1}$. This recursive property necessitates that the optimisation problem is re-solved every time a new measurement becomes available, i.e. the estimation problem has to be solved on-line in parallel to the process.

Moving-horizon estimation offers two main advantages to state observation by on-line minimisation: First is the possibility to directly use knowledge on stochastic influences on the process and the measurements in the estimation algorithm. The second advantage is that additional constraints on the estimates and the process disturbances can be posed: If it is known before-hand that certain states can only attain non-negative values, for instance due to physical reasons, this can be formulated explicitly as an inequality constraint in the optimisation problem. However, care has to be taken in the formulation of constraints to not render the problem infeasible, see for instance Rao and Rawlings [116].

The type of the optimisation problem depends on the type of the state and measurement equations and the functional to be minimised. In the most general case, in moving-horizon estimation non-linear constrained optimisation problems have to be solved. General convergence results for this class of problems are not available due to the non-linearity and the possibility of multiple local optima. For special classes of problems, e.g. linear process models and quadratic functionals, convergence results for the unconstrained and the constrained case are available [123].

Instead of using a deterministic approach and modifying it to incorporate the available knowledge about the stochastic influences, state estimators and filters can be derived using purely statistical

arguments and mathematical probability theory. This approach, known as *Bayesian filtering*, is presented next.

Bayesian filtering

Bayesian filtering is a powerful tool for the design of state estimators for arbitrary non-linear systems with stochastic influences with arbitrary statistics. It draws heavily from the theory of conditional probabilities, especially the theorem of Bayes.

In the following a Bayes filter for the non-linear process model

$$x_k = f(x_{k-1}, u_{k-1}, \omega_k), \quad y_k = h(x_k, \eta_k), \quad (3.36)$$

where ω and η are arbitrary stochastic influences, will be derived, following Arulampalam et al. [7]. The properties of the filter are then shortly discussed.

For this task Bayes' theorem can be stated as

$$p(x_k|y_k) = \frac{p(y_k|x_k)}{p(y_k)} \times \text{a priori estimate}. \quad (3.37)$$

The notation $p(A|B)$ denotes the conditional probability distribution for an event A to occur given the occurrence of event B . In terms of state estimation, the *a posteriori estimate* $p(x_k|y_k)$ denotes the probability that x_k is the process state given the measurement y_k . Analogously, $p(y_k|x_k)$ denotes the probability that y_k is the measurement if x_k is the current process state. The probability that y_k is measured is denoted by $p(y_k)$.

The *a priori estimate* denotes the best estimate of the probability of x_k before the measurement y_k becomes available, i.e.

$$\text{a priori estimate} = p(x_k|y_{k-1}, y_{k-2}, \dots), \quad (3.38)$$

i.e. the best estimate using all available measurement information.

In total the calculation of an a posteriori estimate can be written as

$$p(x_k|y_k) = \frac{p(y_k|x_k)}{p(y_k)} \times p(x_k|y_{k-1}, y_{k-2}, \dots). \quad (3.39)$$

This equation can be solved if the a priori probability is known.

From mathematical statistics the following is known:

$$p(x_k|y_{k-1}, \dots) = \int p(x_k, x_{k-1}|y_{k-1}, y_{k-2}, \dots) dx_{k-1}. \quad (3.40)$$

The probability on the left-hand side denotes the marginal distribution of the probability on the right-hand side of the equation. $p(x_k, x_{k-1}|y_{k-1}, y_{k-2}, \dots)$ is called the joint probability distribution of x_k and x_{k-1} conditioned to the measurement data y_{k-1}, y_{k-2}, \dots .

Using the equality $p(A, B|C) = p(A|B, C)p(B|C)$, the marginal distribution can be written as

$$p(x_k|y_{k-1}, \dots) = \int p(x_k|x_{k-1}, y_{k-1}, y_{k-2}, \dots) p(x_{k-1}|y_{k-1}, y_{k-2}, \dots) dx_{k-1}. \quad (3.41)$$

In order to evaluate $p(x_k|x_{k-1}, y_{k-1}, y_{k-2}, \dots)$ no measurement information is needed, as the dynamics for the state transition from x_{k-1} to x_k is known by the state equation, i.e.

$$p(x_k|x_{k-1}, y_{k-1}, y_{k-2}, \dots) = p(x_k|x_{k-1}). \quad (3.42)$$

The probability density $p(x_{k-1}|y_{k-1}, y_{k-2}, \dots)$ is just the a posteriori estimate of x_{k-1} . The equations therefore provide a recursion for obtaining a state estimate at time t_k given the estimate at time t_{k-1} . This formal recursive Bayes filter can be decomposed into two steps: a prediction step, calculating the a priori estimate of x_k

$$p(x_k|y_{k-1}, \dots) = \int p(x_k|x_{k-1}, y_{k-1}, y_{k-2}, \dots) p(x_{k-1}|y_{k-1}, y_{k-2}, \dots) dx_{k-1} \quad (3.43)$$

and a correction of the a priori estimate given the measurement information at t_k , i.e. y_k :

$$p(x_k|y_k) = \frac{p(y_k|x_k)}{p(y_k)} \times p(x_k|y_{k-1}, y_{k-2}, \dots). \quad (3.44)$$

In this general form the recursive Bayes filter is an important tool in theoretical reasoning but it is only of limited practical use. The main problem is the evaluation of the integral, i.e. the calculation of the marginal distribution. This is in general a multidimensional integral, depending on the dimension of the state vector x . The sampling of the probability densities, i.e. the evaluation of the probability for the occurrence of a specific event, is a difficult task in its own right due to the possibly arbitrary shape of the probability densities.

In order to apply the concept of Bayesian filtering practically, approximations have to be made. In most cases assumptions on the type of the state equation (linear, non-linear) or the statistics of the stochastic disturbances are made. The most commonly known approximations are

- Monte-Carlo filtering, or particle filtering,
- Unscented Kalman filtering,
- Extended Kalman filtering, and
- Kalman filtering.

Monte-Carlo, particle filtering

Monte-Carlo filtering (or particle filtering (PF), bootstrap filtering) [131] is an approximation approach that gained popularity in recent years with the increasing availability of computational resources.

Given a dynamic estimator model of a process

$$\hat{x}_k = f(\hat{x}_{k-1}, \omega_{k-1}), \quad \hat{x}_0 = \hat{x}_0^+, \quad \hat{y}_k = h(\hat{x}_k, \eta_k), \quad (3.45)$$

where ω and η are stochastic sequences, an a posteriori estimate can be obtained using the following procedure:

At $k = 0$ a fixed number N of realisations of the initial state \hat{x}_0^+ is created using the knowledge of the a posteriori probability distribution of \hat{x}_0^+ : $\hat{x}_{0,i}^+$, ($i = 1, \dots, N$). The realisations are called *particles*, thus the name particle filtering.

For every time step $k = 1, 2, \dots$, a priori estimates are calculated by

$$\hat{x}_{k,i}^- = f(\hat{x}_{k-1,i}^+, \omega_{k-1,i}). \quad (3.46)$$

Using the knowledge of h and the statistics of η_k the probability $p(\hat{y}_k|\hat{x}_{k,i}^-)$ can be evaluated. This is used in the correction step, called *re-sampling*, where the a posteriori estimates are chosen such from the $\hat{x}_{k,i}^-$ such that for $N \rightarrow \infty$ the probabilities

$$p(\hat{x}_{k,i}^+|y_k) = p(x_k|y_k) \quad (3.47)$$

are equal, i.e. the probability density of the estimated state is equal to the probability density of the (unmeasurable) process state given the measurement information at time t_k . All necessary statistics of the a posteriori estimated state can then be calculated from the set of $\hat{x}_{k,i}^+$, for example the mean.

The Monte-Carlo approach to Bayesian filtering is a brute-force method with several disadvantages: The most important is that the calculation is very time-consuming due to the re-sampling step [7, 131]. Additionally, convergence of the filter is only guaranteed for $N \rightarrow \infty$. Its main advantage is that it is applicable to general non-linear systems with arbitrary stochastic input sequences. The idea of using special realisations of the state to calculate recursively the state estimates will be re-used in the Unscented Kalman filter.

The family of Kalman filters uses assumptions about the type of model equations and the stochastic sequences to make the actual computation of state estimates tractable. Filters based on the idea of Kalman are estimation algorithms most often found in practical applications.

Kalman filtering of linear systems

Historically, one of the first applications of Bayesian filtering to linear process models subject to Gaussian random variables was given by Kalman [68]. For this case Kalman was able to derive an analytical, optimal solution to the filtering problem: the Kalman filter (KF). In the following decades this result was extended to other classes, i.e. non-linear systems, resulting in a family of filtering algorithms, for instance the Unscented Kalman filter.

Kalman considered the time-discrete linear time-invariant state space model

$$x_k = Ax_{k-1} + Bu_{k-1} + w_{k-1}, \quad y_k = Cx_k + \eta_k, \quad (3.48)$$

where w and η are zero-mean, normally distributed, non-correlated random sequences, i.e.

$$\begin{aligned} w &\sim N(0, Q), & E\{w(t)\eta^T(\tilde{t})\} &= 0, \\ \eta &\sim N(0, R), \end{aligned} \quad (3.49)$$

with constant covariance matrices Q and R .

Let \hat{x}_k^- be the a priori estimate of x_k and \hat{x}_k^+ the a posteriori estimate using the measurement information y_k . Then the covariances of the a priori estimation error $e_k^- = x_k - \hat{x}_k^-$ and the a posteriori estimation error $e_k^+ = x_k - \hat{x}_k^+$ are given by

$$P_k^- := E\{e_k^- e_k^{-T}\}, \quad P_k^+ := E\{e_k^+ e_k^{+T}\}. \quad (3.50)$$

Kalman then derived an equation for \hat{x}_k^+ such that the a posteriori error covariance matrix P_k^+ is minimised [68], i.e. the squared error $x_k - \hat{x}_k^+$ is minimised. It turns out to be a linear equation incorporating the a priori estimate of the state \hat{x}_k^- and the measurement information y_k :

$$\hat{x}_k^+ = \hat{x}_k^- + K_k(y_k - C\hat{x}_k^-). \quad (3.51)$$

The correction gain K_k is calculated based on the a priori estimate of the error covariance matrix P_k^- and the covariance matrix of the measurement noise R :

$$K_k = P_k^- C^T (C P_k^- C^T + R)^{-1}. \quad (3.52)$$

Because of the changes in the estimation errors e_k^- and e_k^+ an update equation for the error covariances is needed [68, 43]:

$$P_k^- = A P_{k-1}^+ A^T + Q. \quad (3.53)$$

Here the knowledge of the statistics of the process noise in form of the covariance matrix Q is incorporated into the estimator design.

The filtering algorithm can then also be stated in two steps: In the prediction step the a priori estimate of the state and the error covariance matrix at time t_k are calculated using the a posteriori values at time t_{k-1} :

$$\begin{aligned} \hat{x}_k^- &= A \hat{x}_{k-1}^+ + B u_{k-1}, \\ P_k^- &= A P_{k-1}^+ A^T + Q. \end{aligned} \quad (3.54)$$

Using the measurement information y_k , the correction gain and the corrected, a posteriori values of the state and error covariance matrix are calculated:

$$\begin{aligned} K_k &= P_k^- C^T (C P_k^- C^T + R)^{-1}, \\ \hat{x}_k^+ &= \hat{x}_k^- + K_k (y_k - C \hat{x}_k^-), \\ P_k^+ &= (I - K_k C) P_k^-. \end{aligned} \quad (3.55)$$

In many applications the values of K_k and P_k^+ tend within a few iterations to a steady state: The steady state values only need to be computed once off-line and can then be used in the in-line application of the estimator. The possibility to compute the gain off-line is of great importance in the application of the filter algorithm to high-dimensional dynamic systems.

The algorithm gives a stable state estimator if given Q and R at each time t_k a symmetric, positive definite solution for the error covariance matrices can be calculated: This requires the system to be observable and poses some restrictions on the choice of covariance matrices Q and R , see for instance [68, 43].

Kalman proved that a correction gain calculated in this way provides an optimal estimate of the state in a linear time-discrete process with Gaussian input sequences [68]. For other types of random input sequences the Kalman filter will also provide an estimate but it is not necessarily an optimum.

Although linear systems are an important class of processes, most processes are non-linear. In this case the Kalman filter is not able to provide a stable estimation of the process state. But the idea can be transported to non-linear systems, resulting in the *extended Kalman filter* (EKF): Here the non-linear process

$$\left. \begin{aligned} x_k &= f(x_{k-1}, u_{k-1}, w_{k-1}) \\ y_k &= h(x_k, \eta_k) \end{aligned} \right\} \quad (3.56)$$

is linearised at each time t_k at the current state x_k . This reduces the non-linear process to a linear time-varying process to which the Kalman filtering algorithm can be applied: The prediction steps for the a priori estimates \hat{x}_k^- and P_k^- read

$$\begin{aligned} \hat{x}_k^- &= f(\hat{x}_{k-1}, u_{k-1}, w_{k-1}), \\ P_k^- &= A_k P_{k-1} A_k^T + W_k Q_{k-1} W_k^T. \end{aligned} \quad (3.57)$$

The correction step reads

$$\begin{aligned} K_k &= P_k^- C_k^T (C_k P_k^- C_k^T + V_k R V_k^T)^{-1}, \\ \hat{x}_k &= \hat{x}_k^- + K_k (y_k - h(\hat{x}_k^-, \eta_k)) \\ P_k &= (I - K_k C_k) P_k^- \end{aligned} \quad (3.58)$$

The matrices A_k, B_k, C_k, W_k and V_k are obtained from linearisation of the state equations at the a priori estimate \hat{x}_k^- :

$$\begin{aligned} A_k &= \frac{\partial f}{\partial x}(\hat{x}_k^-, u_k, w_k), & W_k &= \frac{\partial f}{\partial w}(\hat{x}_k^-, u_k, w_k), \\ C_k &= \frac{\partial h}{\partial x}(\hat{x}_k^-, w_k), & V_k &= \frac{\partial h}{\partial \eta}(\hat{x}_k^-, \eta_k). \end{aligned} \quad (3.59)$$

In summary the EKF obtains an estimate of the process state in a non-linear system by first approximating the state distribution by a Gaussian probability distribution and then propagating this distribution using a linearised model of the process. Due to the approximations, the estimates obtained by an EKF are not optimal for the non-linear process but a first-order approximation. For strongly non-linear systems, or systems where the dynamics cannot be modelled sufficiently by the linear approximation, the EKF is known to diverge due to the approximation error. In general, convergence of the EKF is hard to prove explicitly, i.e. a successful design strongly depends on the design engineer and an extensive test of a designed algorithm.

One obstacle in the implementation of the EKF algorithm is the evaluation of the matrices A_k, B_k, C_k, W_k and V_k : Either the partial derivatives of the functions f and h with respect to the state and random inputs are calculated analytically and are implemented explicitly in the algorithm or some kind of numerical linearisation algorithm is used. Whereas the former possibility is often only tractable for non-linear systems with a small number of states, the latter approach will introduce additional errors into the algorithm that will increase the danger of divergence of the filter.

These disadvantages motivated the design of other non-linear filtering algorithms, for instance the Unscented Kalman filter, that combines ideas from particle and Kalman filtering to design an algorithm for non-linear systems.

Unscented Kalman filtering of non-linear systems

The unscented Kalman filter (UKF) is a descendant of the Kalman filter that allows the estimation of states in non-linear systems from noisy measurements. While the Kalman filter provides an optimal estimate of the mean and the variance of the states, as motivated in the last section, this is no longer true for non-linear systems. The extended Kalman filter (EKF) uses a linearisation of the nonlinear process to calculate the state correction term and can only give a first-order approximation of the variance of the states. In case of highly non-linear processes, which are only poorly described by their linearisations, the filter is known to diverge, becoming unusable for process monitoring and control purposes.

The UKF draws from the idea of particle filtering and uses a technique known as *unscented transform* introduced by Julier et al. [64] to gain higher-order approximations of the estimates and to reduce the possibility of divergence of the filter due to non-linear effects.

Using the notation of Julier and Uhlmann [65], given a nonlinear time-invariant dynamic system

$$\frac{dx}{dt} = f(x, u) + v, \quad (3.60)$$

$$y_k = h(x_k, u_k) + w_k, \quad (3.61)$$

where $x \in \mathbb{R}^N$ denotes the state of the system, $y_k \in \mathbb{R}^M$ is the measurement at consecutive times t_k , ($k \geq 0$), $v \sim N(0, R_v)$ denotes white process noise with zero mean and spectral density matrix R_v , and the normally distributed measurement noise $w \sim N(0, R_w)$ with zero mean and covariance R_w . It is assumed that the random variables v and w are uncorrelated.

Due to the influence of the noise terms v and w on the states, these are no longer deterministic but also random variables with a certain mean and (co)variance. The main idea of the unscented transform is to propagate the distribution through the process non-linearity f and then calculate an approximation of the new mean and covariance. This is in contrast to the EKF which approximates the non-linearity and then propagates the mean and covariance by this approximation.

According to the work of Julier and co-workers [65, 64] a state estimate \hat{x} of the unknown state x can be reconstructed by a predictor-corrector approach. In the following a special modification of the UKF that has better numerical properties will be presented: the square-root unscented Kalman filter (SRUKF) by van der Merwe and Wan [139].

In an initialisation step the observer state \hat{x}_0 is set to the initially guessed value. From this the matrix square root of the state covariance matrix, S_0 , is calculated by a Cholesky decomposition:

$$\hat{x}_0 = E\{x_0\}, \quad S_0 = \text{cholesky}(P_0). \quad (3.62)$$

Given the positive-definite matrix P_0 , the Cholesky decomposition calculates the unique lower-triangular matrix S_0 such that $P_0 = S_0 S_0^\top$.

Then for every measurement time step $k = 1, 2, \dots$ the following predictor-corrector algorithm is executed to obtain an estimate of the process state:

In the *prediction step* a finite number of *sigma points* X_k are chosen. These are then transformed by the nonlinear process model. As in particle filtering, a set of sigma points is selected in the state space. In contrast to particle filtering, these sigma points are not generated randomly from the probability distribution but chosen deterministically such that the mean and the variance of the statistically distributed variables are captured. This allows to drastically reduce the number of particles necessary in order to obtain reliable estimates: Julier and Uhlmann [65] show that for the practically important case of Gaussian distributions of the noise sequences v and w_k only $2N + 1$ sigma points are needed to capture the probability distribution of the state variables accurately.

A predicted state \hat{x}_k^- is calculated from the transformed sigma points as a weighted mean. Also the new covariance matrix root S_k^- is predicted. Afterwards new sigma points are generated to incorporate the potential process noise and a predicted measurement \hat{y}_k^- is calculated from the measurements generated by these sigma points:

$$X_{k-1} = [\hat{x}_{k-1}, \eta S_{k-1} + \hat{x}_{k-1}, -\eta S_{k-1} + \hat{x}_{k-1}] \quad (3.63)$$

$$X_{k|k-1} = f(X_{k-1}, u_{k-1}) \quad (3.64)$$

$$\hat{x}_k^- = \sum_{j=0}^{2N} w_j^{(m)} X_{j,k|k-1} \quad (3.65)$$

$$S_k^- = \text{qr} \left[\sqrt{w_1^{(c)}} (X_{1:2N,k|k-1} - \hat{x}_k^-), \sqrt{R_v} \right] \quad (3.66)$$

$$S_k^- = \text{cholupdate} \{S_k^-, X_{0,k|k-1} - \hat{x}_k^-, w_0^{(c)}\} \quad (3.67)$$

$$X_{k|k-1}^* = [\hat{x}_k^-, \eta S_k^- + \hat{x}_k^-, -\eta S_k^- + \hat{x}_k^-] \quad (3.68)$$

$$Y_{k|k-1} = h(X_{k|k-1}^*) \quad (3.69)$$

$$\hat{y}_k^- = \sum_{j=0}^{2N} w_j^{(m)} Y_{j,k|k-1} \quad (3.70)$$

In these equations, $\eta = \sqrt{N + \lambda}$ where $\lambda = N(\alpha^2 - 1)$, the weights $w_0^{(m)} = \lambda/(N + \lambda)$, $w_0^{(c)} = \lambda/(N + \lambda) + (1 - \alpha^2 + \beta)$, and $w_j^{(m)} = w_j^{(c)} = 1/(2(N + \lambda))$. All matrix-vector operations in this algorithm are performed column-wise.

The operator *qr* denotes the QR-decomposition of a matrix: A given matrix A is decomposed by this operation into a orthogonal matrix Q and a upper triangular matrix R , i.e. $A = QR$. In the calculation above, S_k^- denotes this upper triangular matrix.

The operator *cholupdate* realises a efficient update of the Cholesky factor L of a given positive-definite matrix $A = LL^T$, if it is modified by a rank-1-matrix zz^T (z being a column vector), i.e. $A \pm zz^T$. In general, it is possible to calculate this modified Cholesky factor by first creating A from L , then performing the modification of A into $A \pm zz^T$, and then to calculate the modified Cholesky factor by decomposing the modified matrix. The operator *cholupdate* updates the Cholesky factor L , given z , without explicitly calculating the modified matrix $A + zz^T$. Care has to be taken if the matrix A is down-dated, i.e. the modified matrix is given by $A - zz^T$. In this case it may happen that the modified matrix is no longer positive-definite and a Cholesky decomposition is not possible.

For the calculation of the correction gain K_k at first the covariances from the predicted measurements and the covariance of the transformed sigma points and the generated measurements are calculated to incorporate the measurement noise. Using this information the gain is calculated and the predicted state \hat{x}_k^- and the predicted covariance matrix root S_k^- are updated using the available process measurement y_k :

$$S_{y_k}^- = \text{qr} \left[\sqrt{w_1^{(c)}} (Y_{1:2N, k|k-1} - \hat{y}_k^-), \sqrt{R_n} \right] \quad (3.71)$$

$$S_{y_k}^- = \text{cholupdate} \left\{ S_{y_k}, Y_{0, k|k-1} - \hat{y}_k^-, w_0^{(c)} \right\} \quad (3.72)$$

$$P_{x_k, y_k} = \sum_{j=0}^{2N} w_j^{(c)} [X_{j, k|k-1} - \hat{x}_k^-] [Y_{j, k|k-1} - \hat{y}_k^-]^T \quad (3.73)$$

$$K_k = (P_{x_k, y_k} / S_{y_k}^-) / S_{y_k} \quad (3.74)$$

$$\hat{x}_k = \hat{x}_k^- + K_k (y_k - \hat{y}_k) \quad (3.75)$$

$$S_k = \text{cholupdate} \left\{ S_k^-, K_k S_{y_k}, -1 \right\} \quad (3.76)$$

In this algorithm $\alpha \in [10^{-4}, 1)$ is a design parameter that influences the dynamics of the estimator. As will be pointed out later the choice of α is not arbitrary. The parameter β incorporates some a priori knowledge about the noise distributions, for Gaussian noise $\beta = 2$ is found to be optimal [64]. Specific noise models for v and w can be incorporated quite easily by augmenting the state vector. The covariances of the noise variables need not be constant but can vary in time or can be state-dependent. The idea of the algorithm is summarised in Fig. 3.6.

The SRUKF has various advantages over the EKF and other estimation algorithms:

- It does not need analytical derivatives of the model equations which are often very difficult to obtain.
- It also does not require a special structure of the model equations.
- It can be shown that the estimates obtained by the unscented transform are of at least second order (EKF: first order), and are in case of Gaussian noise at least third order accurate.
- The state covariance matrix is guaranteed to be positive definite, and
- the computational cost of the SRUKF is comparable to that of the EKF.

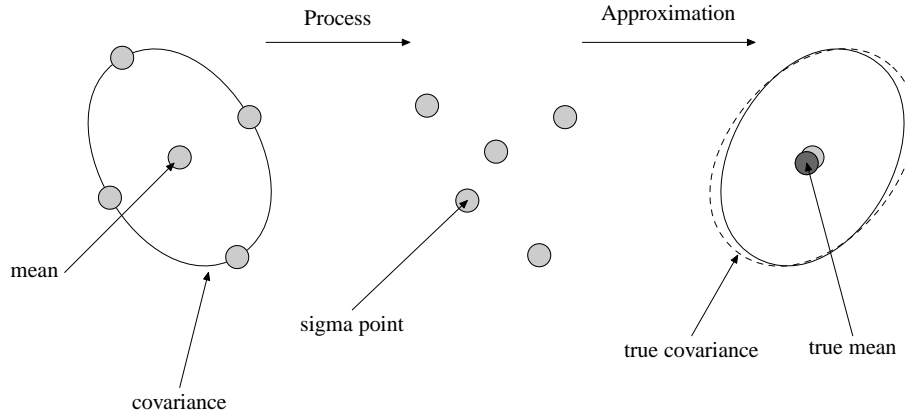


Figure 3.6: General idea of the unscented transform as introduced by Julier et al. [64].

In order to design a working state estimator as much a priori knowledge about the process should be used as possible, for instance to choose a suitable measurement rate it is of great help to know the dominant time constant of the process. The choice of the initial covariance matrix (which determines the trust in the initial estimate \hat{x}_0) is crucial to the performance of the estimator. Too small values lead to small corrections and therefore slow down the convergence of the estimate to the process state.

The parameter α must be chosen such that the Cholesky down-date of the covariance matrix root in the correction step is always possible. A measurement interval that is too large for the process dynamics can lead to a large correction (e.g. in case of very steep gradients in the state during this time interval) which may result in a down-dated covariance matrix that is no longer positive definite. In this case the algorithm breaks down. The correct choice of the parameter α therefore has to be determined off-line, for instance by estimator simulations using different noise levels and measurement intervals.

The main computational load of this algorithm lies in the propagation of the sigma points by the non-linear process, i.e. the solution of (at least) $2N+1$ state equations over a measurement interval. If the state dimension is very high and the measurement interval is short, the simulation step may violate the condition that the filtering algorithm must be faster than real-time as otherwise the estimates are only of limited use. However, the propagation of the sigma points can be executed in parallel because the propagation of one sigma point does not depend on the other sigma points, i.e. the calculation can be distributed independently to different computers. This simple observation can yield a considerable speed-up in computation as was demonstrated in Mangold et al. [89].

A comparison of the different estimation algorithms with respect to the accuracy and the computational effort in a non-linear process is given in Fig. 3.7. It can be seen there that the effort increases with the required accuracy starting with the original Kalman filter that on the one hand is the computationally cheapest but also gives the poorest estimate. At the other end, Monte-Carlo filters provide most accurate estimates but at the cost of a high computational effort. The EKF and the UKF lie between these two extrema: The practical choice of the algorithm depends on the process model, e.g. are analytical expressions for the linearisation available, or are the noise sequences non-Gaussian, and the experience of the design engineer.

After the presentation of various design methods for state observers and state estimators these are applied in the next section to the task of calculating an estimate of the particle size distribution in fluidised bed spray granulation processes.

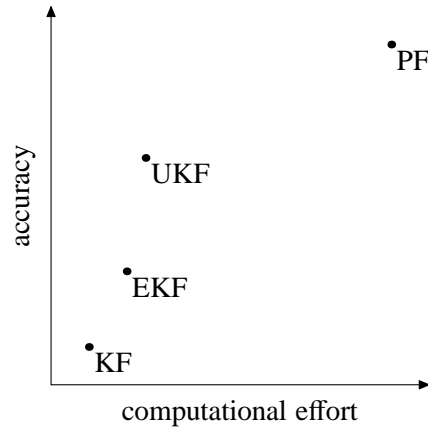


Figure 3.7: Comparison of the different state estimators based on Bayesian filtering with respect to accuracy of the estimate and required computational effort (after Simon [131]).

3.4 Model-based measurement of size distributions

In this section model-based measurement schemes are applied to the batch and continuous fluidised bed processes modelled in Chapter 2. The task is to reconstruct the particle size distribution from noisy or limited measurement information. Before the design of an estimator or observer is undertaken, the observability of the process with respect to available measurements has to be checked.

Observability of the processes is motivated by a structural analysis of finite-dimensional approximations of the process models. These can be obtained from the population balance equations for example by application of one of the discretisation methods presented in Appendix D.

From a practical point of view, the following measurement classes are of interest:

- *total moments*: for instance the total mass of particles in the process which is proportional to μ_3 ;
- *normalised moments*: in particular $\xi_{50} = \mu_1/\mu_0$ which denotes an average particle size obtainable from most in-line particle probes;
- *chord length distributions*: the main measurement results obtained from in-line probes such as FBRM or IPP-70 (Parsum GmbH, Germany);
- *(normalised) number density functions*: Although this case seems trivial at first, this is not true, as even the (normalised) number density function may be corrupted by measurement noise.

These measurement classes are now investigated to find out whether they possess the necessary properties for structural observability of the processes under consideration, or not.

3.4.1 Structural observability of the spray granulation process

At first the distributed measurements, i.e. number density functions and chord-length distributions, are tested for structural observability: The notions of output-connectedness and non-contraction were introduced in Section 3.2 – summarising, a process is structural observable if every state of the model has a unique influence on the process measurement.

Trivially, if the number density function $n(t, \xi)$ can be measured, or its finite-dimensional approximation, then the process model (or its finite-dimensional approximation) is observable, as every state is measured directly and uniquely.

The chord-length distribution can be written as $y = Sn = Cn$, where y is the process measurement (the chord-length distribution in this case) and S is a triangular matrix relating the sizes to all possible chord-lengths. The matrix S is triangular due to the fact that the maximum chord-length that can be generated is equal to the particle size, i.e. size greater than this cannot be generated. The important point for structural analysis is that the structural matrix $S_s = C_s$ obtained from S has a diagonal of ones, i.e. the structural rank of S_s is equal to the number of states, provided that at least this number of chords are considered. In general, S is a rectangular matrix, with the number of rows depending on the discretisation grid of the number density function and the chord lengths, respectively. In most cases the discretisation of the chord length is much finer than the discretisation of the number density function, see for instance Mangold [87]. The diagonal of ones means that the states of the model are output-connected. The condition for non-contraction is also fulfilled by this result, as the structural matrix S_s provides the required structural rank. From this it is clear that the processes are structurally observable by this measurement.

In the following, structural observability is investigated for two families of scalar measurements: $y_k = \mu_k$, the k th unnormalised moment of the number density function, and $\tilde{y}_k = \mu_k/\mu_0$, the normalised or averaged k th moment.

Using the notation

$$\langle w_k, n \rangle = w_k^T n = \sum_{i=1}^N \xi_i^k n(t, \xi_i) \Delta \xi_i, \quad (3.77)$$

for the finite-dimensional approximation of the unnormalised k th moment of the number density function, these measurements can be expressed as

$$y_k = \langle w_k, n \rangle, \quad \tilde{y}_k = \frac{\langle w_k, n \rangle}{\langle w_0, n \rangle}. \quad (3.78)$$

The population balance equation is rewritten in the form

$$\frac{dn}{dt} = -G\mathcal{D}_N n + p(n), \quad (3.79)$$

$$G = 2 \frac{\dot{M}_{solid}}{Q_s \pi \langle w_2, n \rangle}, \quad (3.80)$$

where the regular matrix $\mathcal{D}_N \in \mathbb{R}^{N \times N}$ is a finite dimensional approximation of the derivative operator $\partial/\partial \xi$ and $p(n)$ is a the net-production of particles in the process. In case of the batch process $p(n) = 0$ holds for all times.

The structural observability analysis for both processes and both measurement families can be performed simultaneously:

- **Output-connectedness:** In case of $y_k = \langle w_k, n \rangle$ the measurement is linear with respect to the approximated size distribution n , therefore the structural matrix $C_{s,k}$ (in this case just a row vector) can be obtained by inspection. As all weights $w_{k,i} \neq 0$ it follows $C_{s,k} = [1, \dots, 1]$, i.e. all model states have direct influence on the measurement and the process is output-connected. As this property does not depend on the dynamics of the model, it holds for both processes.

In case of $\tilde{y}_k = \langle w_k, n \rangle / \langle w_0, n \rangle$ – which is nonlinear in n – at first the linear approximation has to be obtained:

$$\tilde{y}_k \approx \frac{1}{\langle w_0, n \rangle^2} \left[w_k^T \langle w_0, n \rangle - \langle w_k, n \rangle w_0^T \right]. \quad (3.81)$$

An evaluation of the scalar products shows that under the assumption that n is not identically zero for all times every entry of the row vector is not identically zero. Therefore the structural matrix $\tilde{C}_{s,k}$ has the form $\tilde{C}_{s,k} = [1, \dots, 1]$, and output-connectedness for both processes under this family of measurements follows immediately.

- **Non-contraction:** From equation (3.80) it can be seen that the growth rate G is non-zero for all relevant applications. G vanishes only in case of an infinite bed surface which is never attained in practical application or in case of $\dot{M}_{solid} = 0$ which is contradictory to the aim of the process.

The linearisation of the convective term in equation (3.79) can be obtained by application of the product rule:

$$A = \frac{\partial}{\partial n} [-(\mathcal{D}_N n)G] = - \left[\frac{\partial}{\partial n} (\mathcal{D}_N n)G + (\mathcal{D}_N n) \frac{\partial G}{\partial n} \right]. \quad (3.82)$$

A similar computation using the definition of the growth rate yields

$$\frac{\partial G}{\partial n} = -\omega^T G, \quad (3.83)$$

where the entries of ω are given by $\omega_i = w_{2,i} / \langle w_2, n \rangle \neq 0$.

Using standard results of multivariable calculus this leads to

$$A = -\mathcal{D}_N \left[I_N - n \omega^T \right] G, \quad (3.84)$$

where I_N denotes the $N \times N$ identity matrix.

From this follows immediately that the structural matrix A_s has a diagonal of ones as a result of the regularity of \mathcal{D}_N , in fact – due to the structure of G – it can be shown by evaluation of the expression above that there are no zero entries in the structural matrix. The s-rank of such a square matrix is by definition equal to the number of columns N .

As both processes contain this convective term and the additional term $p(n)$ of the continuous process does not eradicate non-zero entries from the structural matrix A_s , both processes possess the property of non-contraction under these measurements. As they are also output-connected they are both structurally observable.

Two remarks on the validity of the results have to be given: (1) The analysis neither depends on a certain number of grid nodes used in the discretisation nor on a special discretisation scheme as long as the form (3.79) is obtained. (2) The analysis does not point out which measurements are practically useful as it depends on the sensitivity to changes in the size distribution. This has to be checked additionally, e.g. in simulations, or can be inferred from the process conditions. For instance in both processes the third moment μ_3 , which is proportional to the total mass of particles in the process, is not a suitable measurement: In case of the batch process it is decoupled from the dynamics of all other moments, depending only on the amount of sprayed liquid (as shown in Section 2.7); examples of number density functions that are completely different but give the same total mass can be generated quite easily. In case of the continuous process the bed mass is controlled to be constant, i.e. a change in the number density function is not detectable in the measurement of the third moment.

In case of the continuous process the structural result can be made more precise: An observability analysis using the steady-state number density function can be performed: Linearising the process model gives a high-dimensional linear state space model. By the Hautus-Belevitch-Popov criterion the observability of the process given the measurements can be checked, giving a result that is valid for the linear process and also for the non-linear process as long as the state is in the vicinity of the steady-state.

3.4.2 Application to batch fluidised bed spray granulation

Infinite-dimensional Luenberger observer

Although the design of infinite-dimensional observers for infinite-dimensional systems is in general difficult, for spatially-distributed systems some results are reported in the literature, see for instance [151, 69, 16, 90, 58] for applications in reaction engineering and separation processes. In these cases the distributed quantity of interest, e.g. the temperature in a tubular reactor, is measured at discrete points in the reactor. The state profile between two measurement locations is then interpolated. The state correction is then motivated by the physics of the process and calculated using the interpolated profiles.

The problem in measuring the size distribution is that discrete measurements, i.e. the measurement of some distinct sizes, is practically not realisable and the approach presented cannot be used.

In the case of a scalar, lumped measurement, e.g. the mean particle size ξ_{50} , a dynamic infinite-dimensional equation for the error in the number density function is obtained, the problem being the calculation of an infinite-dimensional state correction given the scalar measurement.

First, an infinite-dimensional observer for the number density function $n(t, \xi)$ given the scalar, lumped measurement $y = \xi_{50}(t) = \mu_1(t)/\mu_0(t)$ is designed. Afterwards, using the idea introduced in the first case an observer for the normalised number density function $y = q_0(t, \xi) = n(t, \xi)/\mu_0(t)$ is designed. The suitability of the observers is tested in simulations by varying the process conditions.

Case 1: Mean particle size. Given are the population balance equation for the number density function in the batch fluidised bed spray granulation process

$$\frac{\partial n}{\partial t} = -G \frac{\partial n}{\partial \xi}, \quad (3.85)$$

and the measurement $y = \xi_{50}(t) = \mu_1(t)/\mu_0(t)$. Observing that the total number of particles is constant in a batch process, the number density function can be scaled by $\mu_0(t = 0)$, giving the normalised number density functions $q_0(t, \xi) = n(t, \xi)/\mu_0(t = 0)$. The population balance equation then reads

$$\frac{\partial q_0}{\partial t} = -G^* \frac{\partial q_0}{\partial \xi}, \quad (3.86)$$

where G^* denotes that the growth rate, evaluated using q_0 and μ_0 .

The Luenberger observer is set up as

$$\frac{\partial \hat{q}_0}{\partial t} = -\hat{G}^* \frac{\partial \hat{q}_0}{\partial \xi} + k(\xi, y, \hat{y}), \quad (3.87)$$

with the corresponding measurement $\hat{y} = \hat{\mu}_1(t)/\hat{\mu}_0(t)$, that can also be calculated directly from a given normalised number density function.

The initial normalised number density functions of the process and the observer model are represented by $q_0(0, \xi) = q_{0,0}$ and $\hat{q}_0(0, \xi) = \hat{q}_{0,0}$, respectively. Introducing the state observation error

$$e(t, \xi) := q_0(t, \xi) - \hat{q}_0(t, \xi) \quad (3.88)$$

the dynamic equation for the error can be written as

$$\frac{\partial e}{\partial t} = - \left(G^* \frac{\partial q_0}{\partial \xi} - \hat{G}^* \frac{\partial \hat{q}_0}{\partial \xi} \right) - k(\xi, y, \hat{y}), \quad e_y(0, \xi) = q_{0,0} - \hat{q}_{0,0}. \quad (3.89)$$

The task of designing the correction $k(\xi, y, \hat{y})$ requires that from the scalar, lumped measurement an infinite-dimensional state profile correction is calculated. This is not possible in general. However, under the assumptions listed a suitable correction can be designed:

(A1) The growth rates are sufficiently close to each other, i.e. $G^* \approx \hat{G}^*$.

(A2) The (normalised) number density function is mono-modal and can be represented as a Gaussian function, i.e.

$$q_0(t, \xi) \sim \frac{1}{\sqrt{2\pi}\sigma} \exp \left[-\frac{1}{2} \left(\frac{\xi - \xi_{50}}{\sigma} \right)^2 \right], \quad (3.90)$$

$$\hat{q}_0(t, \xi) \sim \frac{1}{\sqrt{2\pi}\hat{\sigma}} \exp \left[-\frac{1}{2} \left(\frac{\xi - \hat{\xi}_{50}}{\hat{\sigma}} \right)^2 \right], \quad (3.91)$$

where $\xi_{50}, \hat{\xi}_{50}$ denote the mean values of the Gaussian functions and $\sigma, \hat{\sigma}$ the variances, respectively.

(A3) The variances are assumed to be equal, i.e. $\sigma = \hat{\sigma}$.

Assumption (A2) is natural in many practical applications, (A3) can be satisfied by measuring the initial normalised number density function in a off-line measurement device from which a suitable value for the variance can be extracted. Assumption (A1) depends on the number density function n . Given an estimate of the initial normalised number density distribution and an estimate of the total mass of particles in the bed, an estimate of the total number of particles can be calculated yielding an initial estimate of the growth rate.

Using assumption (A1) the error equation simplifies to

$$\frac{\partial e}{\partial t} = -\hat{G}^* \left(\frac{\partial e}{\partial \xi} \right) - k(\xi, y, \hat{y}). \quad (3.92)$$

In order to derive an equation for the error e that can be interpreted with respect to the dynamic behaviour, the state correction $k(\xi, y, \hat{y})$ is designed such that

$$k(\xi, y, \hat{y}) = \alpha e(t, \xi) = \alpha(q_0 - \hat{q}_0), \quad (3.93)$$

with α being a *tuning parameter*.

Using the definition of e and assumptions (A2) and (A3) yields

$$e = q_0(t, \xi) - \hat{q}_0(t, \xi) \quad (3.94)$$

$$= C \exp \left[-\frac{1}{2} \left(\frac{\xi - \xi_{50}}{\sigma} \right)^2 \right] - C \exp \left[-\frac{1}{2} \left(\frac{\xi - \hat{\xi}_{50}}{\sigma} \right)^2 \right] \quad (3.95)$$

$$\approx C \frac{\partial}{\partial \hat{\xi}_{50}} \left\{ \exp \left[-\frac{1}{2} \left(\frac{\xi - \hat{\xi}_{50}}{\sigma} \right)^2 \right] \right\} \Big|_{\hat{\xi}_{50}(t) = \xi_{50}(t)} (\hat{\xi}_{50} - \xi_{50}) \quad (3.96)$$

$$\approx \left\{ C \left(\frac{\xi - \xi_{50}}{\sigma^2} \right) \exp \left[-\frac{1}{2} \left(\frac{\xi - \xi_{50}}{\sigma} \right)^2 \right] \right\} (\xi_{50} - \hat{\xi}_{50}) \quad (3.97)$$

$$=: \varphi(\xi, y(t))(y - \hat{y}) =: k(\xi, y, \hat{y}) \times \alpha^{-1}. \quad (3.98)$$

where the substitution $C = 1/(\sqrt{2\pi}\sigma)$ is used and α is the aforementioned tuning parameter. What is done in the state correction design is that a global distribution function $\varphi(\xi, y(t))$ based on the current measurement is calculated by linearising the error in the assumed shape around the current estimated measurement value.

The dynamic equation for the error e can thus be written approximately as

$$\frac{\partial e}{\partial t} \approx -\hat{G}^* \left(\frac{\partial e}{\partial \xi} \right) - \alpha e, \quad e(0, \xi) = q_{0,0} - \hat{q}_{0,0}. \quad (3.99)$$

The designed observer is functional, if the observation error e is converging to $e(t, \xi) = 0$. That this is indeed the case if assumptions (A1)–(A4) are fulfilled will now be motivated: An application of the method of characteristics to the error equation yields the following system of characteristic equations:

$$\frac{dt}{d\theta} = 1, \quad (3.100)$$

$$\frac{d\xi}{d\theta} = \hat{G}^*, \quad (3.101)$$

$$\frac{de}{d\theta} \approx -\alpha e. \quad (3.102)$$

Whereas the first two equations give the characteristic curves, the third describes the development of the error on these curves. From this it is immediately obtained that $e \sim \exp(-\alpha t)$, i.e. the error decays approximately exponentially on the characteristic curves originating from all possible values ξ . The decay can be manipulated by choice of the design parameter $\alpha > 0$. This means that over time the observation error tends point-wise to zero, given that the assumptions are satisfied.

This result can be further motivated by considering the evolution of the square of the L_2 -norm of the distributed error. It is defined by

$$E_2(t) = \|e(t, \xi)\|_{L_2}^2 = \int_{\xi_0}^{\infty} e(t, \xi)^2 d\xi, \quad (3.103)$$

and measures the total quadratic distance of the error profile e to the zero profile. From the definition it follows that $E_2 \geq 0$ and $E_2 = 0$ if $e = 0$.

Introducing the function $V(t) = 1/2 E_2(t)$ the following result on the evolution of E_2 can be obtained:

$$\frac{dV}{dt} = \int_{\xi_0}^{\infty} e(t, \xi) \frac{\partial e}{\partial t} d\xi = \int_{\xi_0}^{\infty} e(t, \xi) \left(-\hat{G}^* \frac{\partial e}{\partial \xi} \right) d\xi - \alpha \int_{\xi_0}^{\infty} e(t, \xi)^2 d\xi \quad (3.104)$$

$$= \int_{\xi_0}^{\infty} e(t, \xi) \left(-\hat{G}^* \frac{\partial e}{\partial \xi} \right) d\xi - 2\alpha V \quad (3.105)$$

Table 3.1: Process parameters for the batch spray granulation process.

Initial bed mass [kg]	m_{bed}	10.0
Mass flow of solid [kg s ⁻¹]	\dot{M}_{solid}	1.38×10^{-2}
Solid density [kg m ⁻³]	ρ_s	1440.0

$$= -\frac{\hat{G}^*}{2} \int_{\xi_0}^{\infty} \frac{\partial e^2}{\partial \xi} d\xi - 2\alpha V \quad (3.106)$$

$$= \frac{1}{2} (G^* e)(t, \xi_0) e(t, \xi_0) - 2\alpha V \quad (3.107)$$

$$= -2\alpha V \leq 0. \quad (3.108)$$

In these calculations the vanishing boundary conditions, i.e. $(G^* e)|_{\xi_0} = (G^* n - G^* \hat{n})|_{\xi_0} = 0$, and the fact that the growth rate is independent of the particle size ξ are used.

From the last line it can be obtained that

$$V(t) \sim \exp(-2\alpha t), \quad (3.109)$$

i.e. the L_2 -norm of the error decreases exponentially to zero under the stated assumptions. It has to be noted that for non-zero error profiles $e(t, \xi)$ with vanishing L_2 -norm the convergence result yields an erroneous result, as here the time derivative of the function V also vanishes, although the state observation error does not do so. However, these theoretical limit cases do not appear in general application and are neglected.

Exponential convergence of the error implies that the designed observer possesses a certain robustness against modelling errors and stochastic influences, e.g. measurement noise, as these are smoothed out. Robustness against modelling errors is important because it is likely for a given batch fluidised bed process to violate assumptions (A1)–(A3). The violation is then counteracted up to a certain degree by the exponential convergence and limits the error in the estimated state profile, the number density distribution.

In the following simulation results for two cases are presented, taking into account modelling errors and parameter uncertainties. For the implementation in the simulation environment Matlab the infinite-dimensional observer is discretised using a finite volume method (cf. Appendix D). The process parameters are listed in Tab. 3.1.

Scenario 1. Given the initial profiles shown in Fig. 3.8 for the process and the observer model, respectively, after a process simulation of 10000 seconds the results shown in Fig. 3.9 are obtained. A tuning factor $\alpha = 0.05$ is used which was determined by test simulations.

Compared to a pure parallel simulation of the process model (denoted by ‘‘Simulator’’ in the figure), i.e. without correction of the state estimate based on the available measurement information, the position of the number density function in the process is estimated better. However, a slight deviation in the magnitude is observed. This leads to a non-vanishing state observation error which can also be identified in the plot of the L_2 -norm of the error shown in Fig. 3.10. Additionally, it can be observed that the error decreases very rapidly in the beginning. This is due to the initially large deviation of the number density functions which is also present in the normalised number density functions that are used to calculate the state correction. After this initial phase, which corrects mainly the position of the estimate, the differences in the magnitudes are corrected. These are, however, not easily represented by *normalised* number density functions, thus the convergence speed is decreased almost to zero. This is also true for the approximation of the growth rate which is shown in Fig. 3.11.

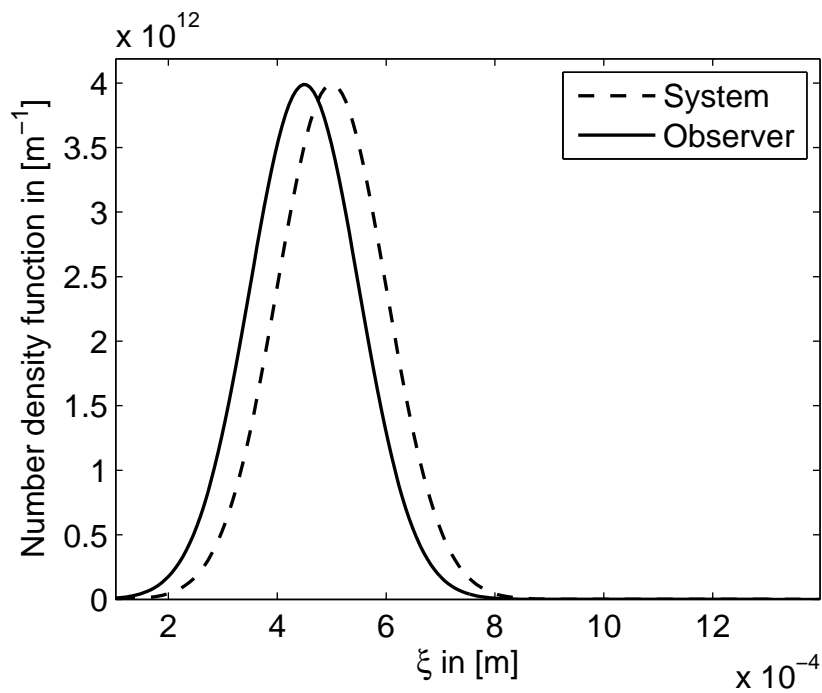


Figure 3.8: Initial conditions used in Scenario 1 for the process and the observer model. Besides a deviation in the mean particle size the number density functions are identical. (Infinite-dimensional Luenberger observer, Case 1, Scenario 1)

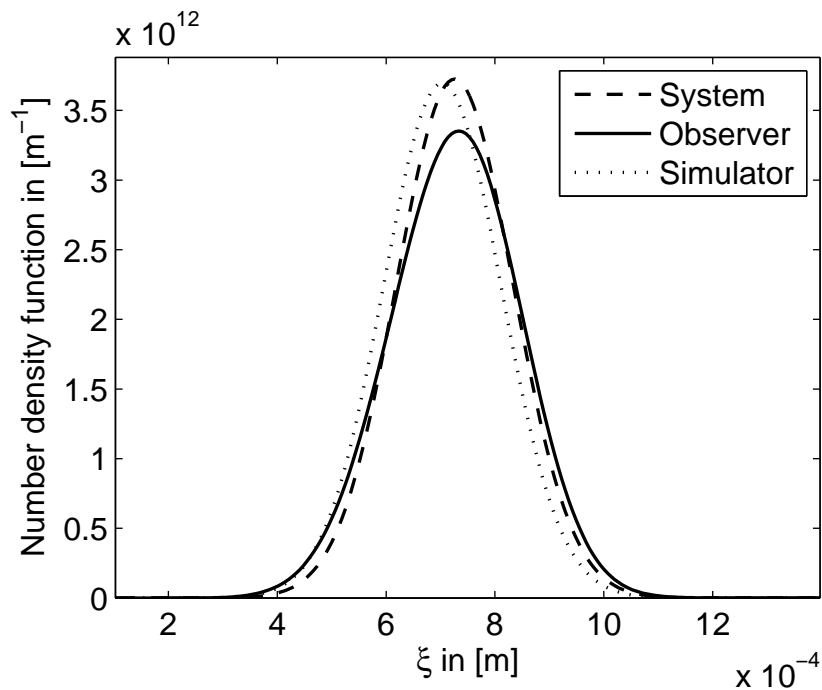


Figure 3.9: Results obtained from the infinite-dimensional Luenberger observer after 10000 s. It can be seen that the shape and the position of the number density function are approximated well, but a deviation in the magnitude is observed. (Infinite-dimensional Luenberger observer, Case 1, Scenario 1)

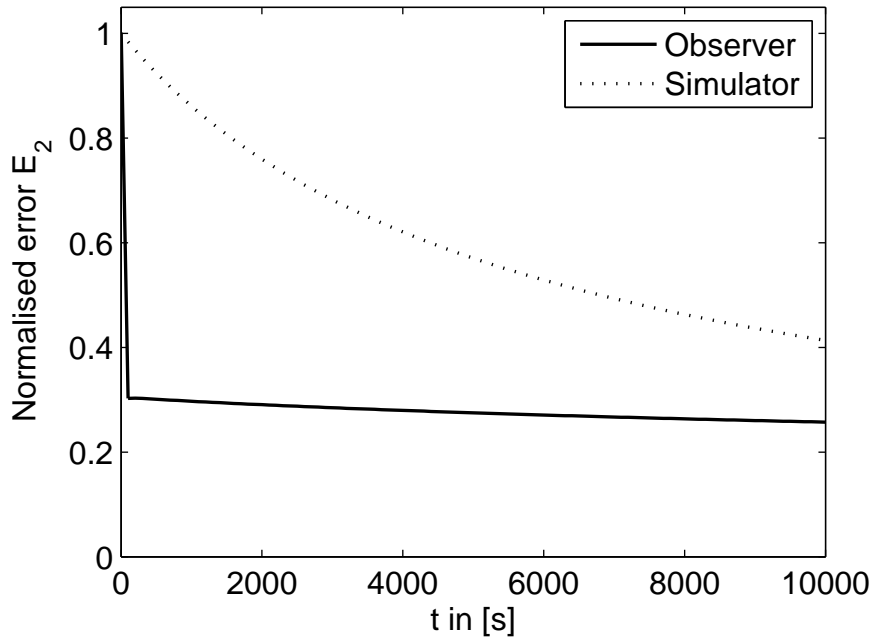


Figure 3.10: Evolution of the normalised state observation error E_2 . After an initial sharp decrease the error tends to a steady-state value, signalling the error in the observed magnitude of the number density function. (Infinite-dimensional Luenberger observer, Case 1, Scenario 1)

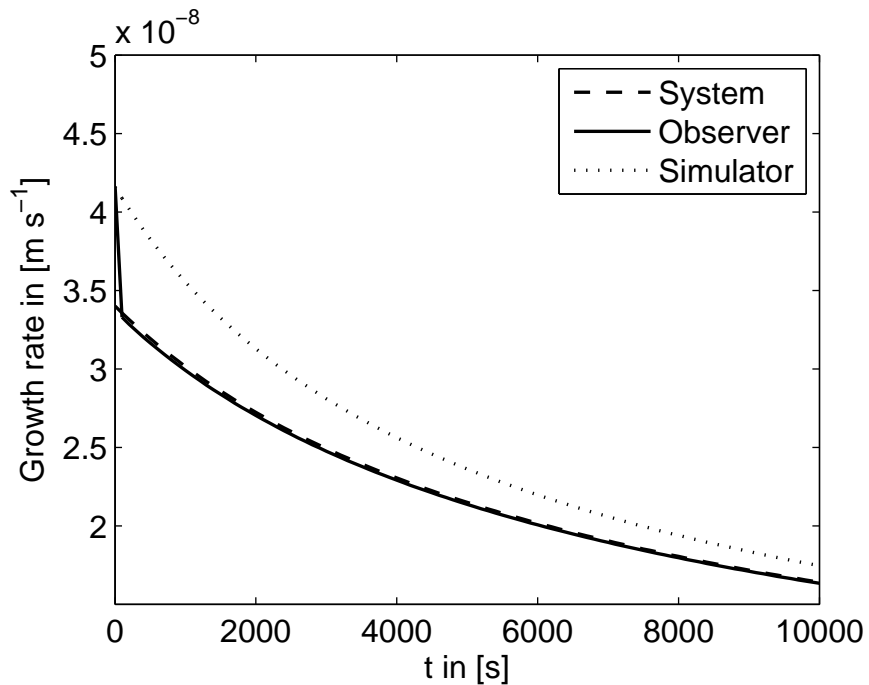


Figure 3.11: Observation results for the particle growth rate. Although a non-vanishing error in the observed number density function remains, the growth rate is estimated almost exactly. (Infinite-dimensional Luenberger observer, Case 1, Scenario 1)

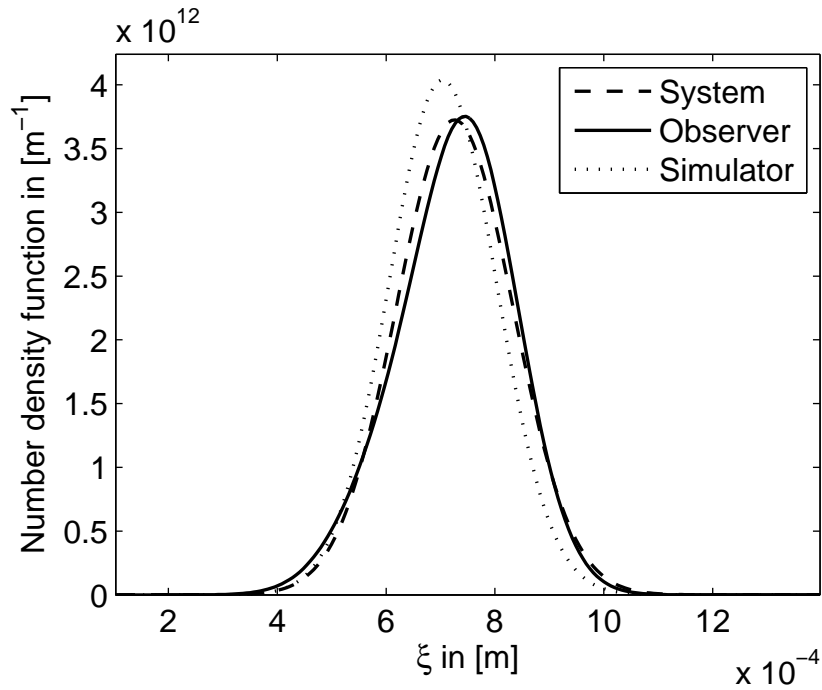


Figure 3.12: Results obtained from the infinite-dimensional Luenberger observer in Scenario 2 after 10000 s. Although a constant error in the shape of the correction profile is present, the shape and the position of the number density function are approximated well. (Infinite-dimensional Luenberger observer, Case 1, Scenario 2)

As can be seen in Fig. 3.11 even for a simple choice of initial profile error a violation of assumption (A1) is likely. However, the observer is able to compensate for this error, so that it can be stated that it is functional for this scenario.

Deviations from the motivated convergence results can be ascribed to the non-linearity of the process and the resulting non-linearity of the observation error, as well as the initial violation of assumption (A1).

Scenario 2. Under the same conditions as in Scenario 1 an initial distribution of the observer similar to the one shown in Fig. 3.8 is used, but with the modification that the estimated variance $\hat{\sigma}$ is erroneous: $\hat{\sigma} = 0.9\sigma$, i.e. assumption (A3) is constantly violated. As is shown in Fig. 3.12, the observer is able to compensate for this bias. However, it has to be pointed out that for large deviations the observer will not be able to compensate the error and will diverge as the approximations used in the derivation of the state correction, especially the calculation of the global shape function φ , are no longer valid.

The state observation error E_2 and the approximation of the growth rate are qualitatively similar to Scenario 1. This means that even for a persistent violation of an assumption the designed observer is functional.

Scenario 3. In this scenario the observer is tested for parametric uncertainties ($\alpha = 0.05$). Starting with the initial profiles shown in Fig. 3.8, in the calculation of the growth rate of the observer an erroneous value for the solid density $\hat{\rho}_s$ is used: $\hat{\rho}_s = 1.1\rho_s$. This error influences the growth rate and by this all states of the observer model.

Even in this case a good approximation of the number density function in the process is calculated by the observer (Fig. 3.13). However, a widening of the estimated distribution and an

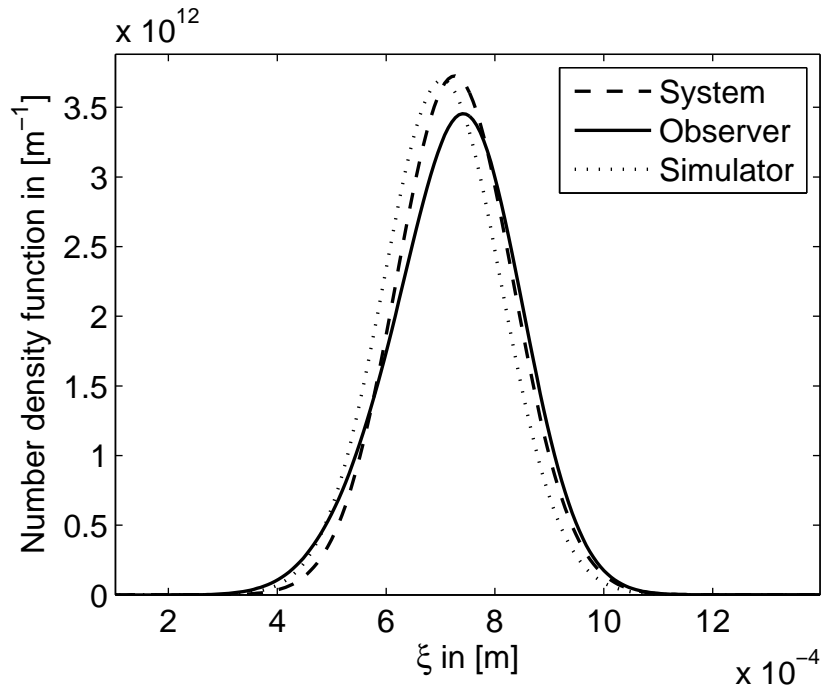


Figure 3.13: Reconstructed number density function for a parametric uncertainty in the infinite-dimensional Luenberger observer (Infinite-dimensional Luenberger observer, Case 1, Scenario 3, after 10000 s).

under-estimation of the magnitude can be seen, but the result is still sufficiently useful for process monitoring purposes.

The state observation error tends to a non-vanishing steady-state error, and the growth rate is also approximated well. In both cases the temporal evolution is comparable to the ones obtained in Scenario 1.

Based on these results it can be stated that the designed infinite-dimensional Luenberger state observer is able to reconstruct a number density function in a batch spray granulation process given only scalar measurements of the mean diameter of the particles in the process. A further improvement of the results presented may be obtained by using higher-order approximations of the error profiles in the derivation of the correction gain $k(\xi, y, \hat{y})$.

In-line measurement devices are often able to provide a normalised number density function of the particles in the process. Using the idea presented here, a corresponding state observer for this kind of measurement can be designed.

Case 2: Normalised number density function. Given a normalised number density function $y(t, \xi) = q_0(t, \xi)$ a state observer can be designed using assumption (A1), i.e. $G \approx \hat{G}$. An analogous derivation of the dynamic error equation yields $k(\xi, y, \hat{y}) = -\alpha(y - \hat{y}) = -\alpha e$, giving exponential convergence of the estimation error. The assumptions made in Case 1 can be relaxed, as $q_0(t, \xi)$ contains all qualitative information on the profile. This also means that the observer is able to reconstruct the number density functions in a process even if they are not close to each other, initially.

This result is exemplified by the following scenario: Initially, in the fluidised bed a bi-modal distribution is present as shown in Fig. 3.14. The observer is only given information on the first mode on the far left-hand side. This information is not perfect as an error in the magnitude of this

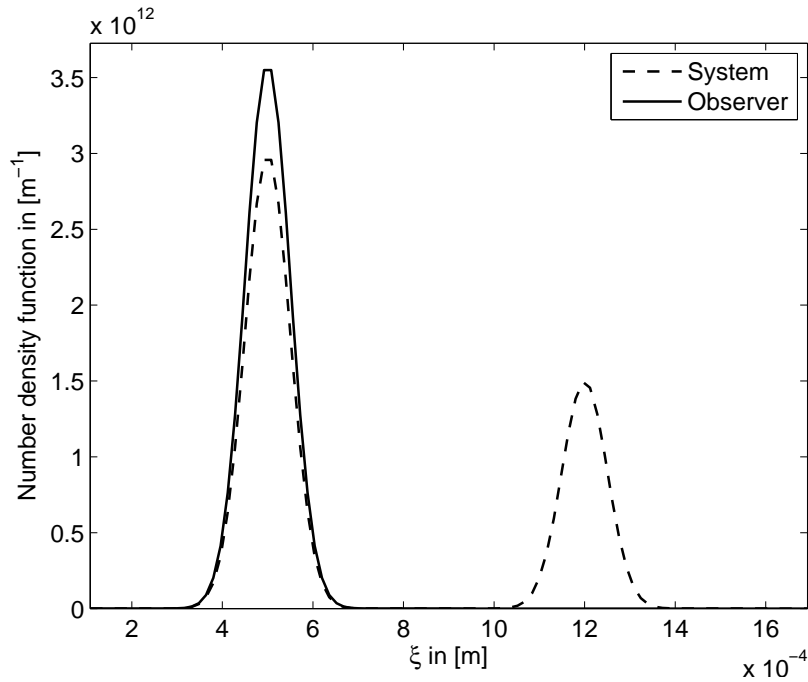


Figure 3.14: Initial conditions used in Scenario 1 for the process and the observer model. Besides a deviation in the mean particle size the number density functions are identical. (Infinite-dimensional Luenberger observer, Case 2)

mode is present.

The results obtained from the observer after 10000 seconds of process time are shown in Fig. 3.15. There it can be seen that the initially unknown mode is reconstructed successfully by the state observer. A deviation in the magnitudes of both modes is observed, signalling that the observer is not fully able to compensate the error in the total number of particles in the observer model $\hat{\mu}_0$. It can clearly be seen that the observer structure outperforms the parallel simulator that only propagates the initially known mode over time, yielding a result that deviates strongly from the process.

In the plot of the normalised error E_2 shown in Fig. 3.16 it can be seen that a good approximation is already obtained by the observer after a short time (compared to the total process time). This time can be further reduced by increasing the tuning factor (design parameter) α in the observer model. However, care has to be taken if the measurement information is biased by noise. In this case the noise is amplified by the tuning factor yielding errors in the calculated state correction.

In every case the time necessary to compute the state correction given the measurement is negligible compared to the time constant of the process, as only the shape function has to be evaluated which is then multiplied by the tuning factor.

State observation by on-line minimisation

In a first case a state observer using the approach of Zimmer [154] is designed for the measurement of the number density function, i.e. $y = n(t, \xi)$. Although this measurement is trivial with respect to the reconstruction of the number density function, it allows to evaluate the performance of the state observer under measurements biased by noise and model uncertainties. In the following cases results for the measurements of normalised number density functions and mean particle size

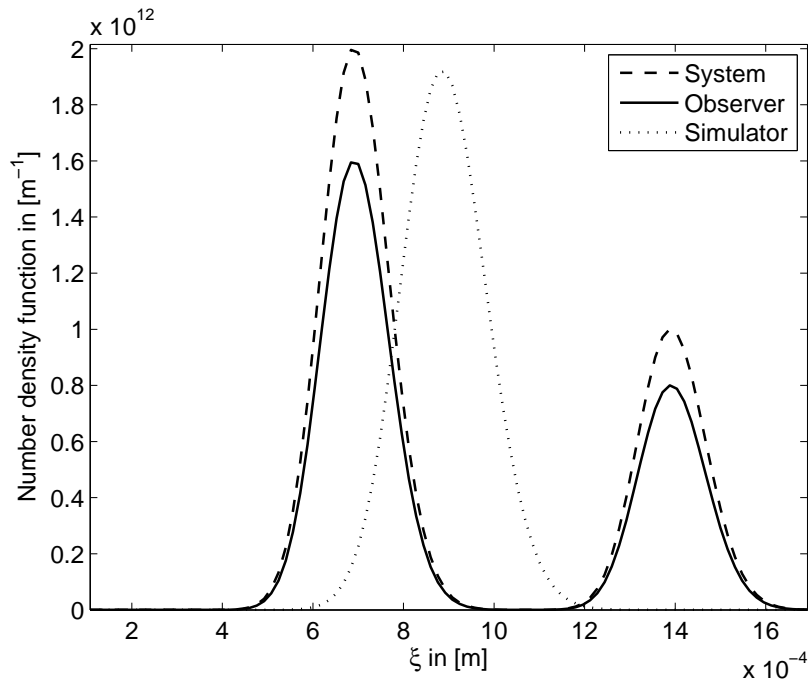


Figure 3.15: Reconstructed number density function after 10000 s. This example shows the shortcomings of the simulator approach, which only propagates the initially known mode. (Infinite-dimensional Luenberger observer, Case 2)

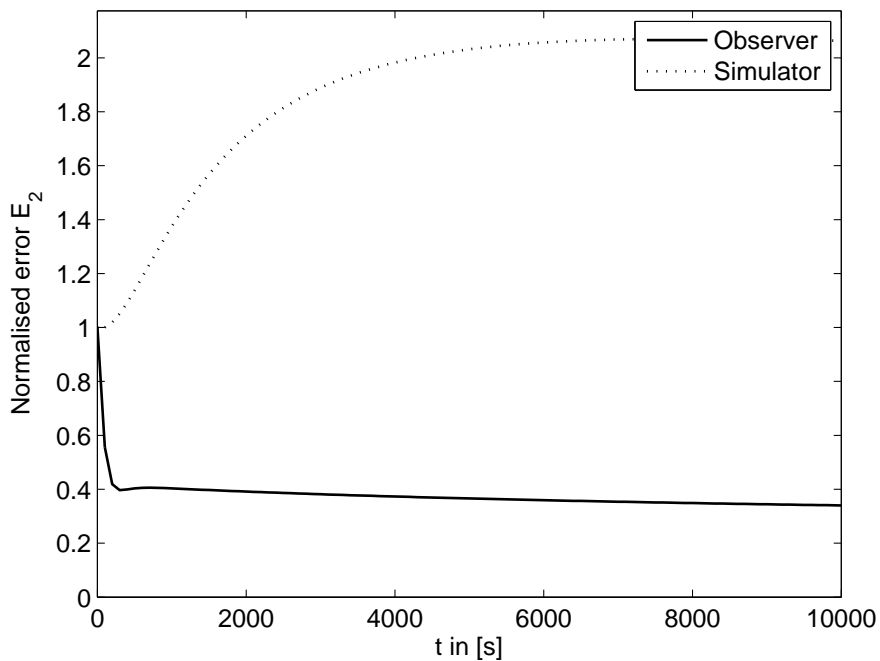


Figure 3.16: Evolution of the state observation error (normalised to its initial value). It can be seen that the observation error decreases over time, i.e. it is lower than the initial value, signalling a convergence of the observer state to the process state. In contrast, the error in the simulator model, i.e. without correction based on measurements, increases, signalling a non-convergence. (Infinite-dimensional Luenberger observer, Case 2)

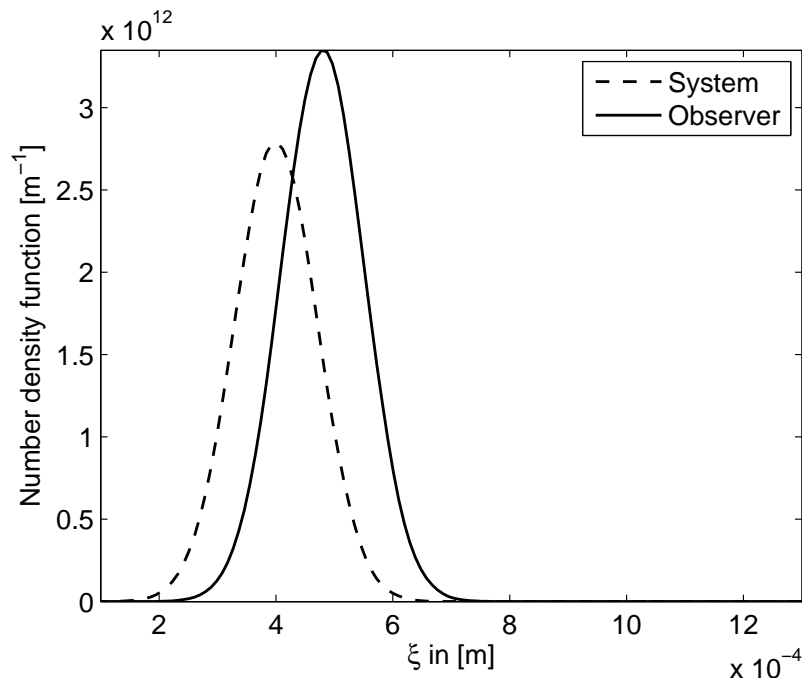


Figure 3.17: Initial conditions used in for the process and the observer model for the test of a state observer designed after Zimmer [154]. (Zimmer, Case 1)

are presented and discussed. In order to solve the process and observer equations the population balances are discretised by a pseudo-spectral method (cf. Appendix D), as it allows in this case to significantly reduce the number of grid nodes necessary to represent the number density functions sufficiently. As the number of differential equations to be solved in the observer algorithm depends quadratically on the number of grid nodes, a considerable speed-up compared to traditional finite volume methods is achieved.

Case 1: Number density function. Choosing an observation horizon of $T = 500$ seconds and the initial conditions for the process and the observer model shown in Fig. 3.17, the process is simulated for a process time of 10000 seconds. In each observation horizon the process measurement is subjected to additive noise that is normally distributed, i.e. $\eta_i \sim N(0, 10^{10})$, ($i = 1, \dots$) and assumed to be constant over the observation horizon. The value of 10^{10} is chosen based on the maximum magnitude of the initial number density function.

As is shown in Fig. 3.18, the state observer reconstructs the number density function in the process almost perfectly, i.e. it is able to compensate the random errors introduced in the measurement.

In the evolution of the normalised error E_2 , shown in Fig. 3.19 the convergence behaviour of the algorithm can be identified: After a few iterations the error is almost decreased to zero owing to the high convergence speed of the Newton-Raphson algorithm used in calculation of the state correction.

Similar results are obtained if a parametric error is present in the observer model. For a test an error of ten percent in the growth velocity is introduced by setting $\hat{\varrho}_s = 1.1\varrho_s$. For the same initial condition it is shown in Fig. 3.20 that the number density function in the process is almost perfectly reconstructed, too. However, the error is not decreasing as smoothly as in the case of a perfect observer model, due to the persistent error in growth velocity which leads to a persistent deviation of the observer state from the process state.

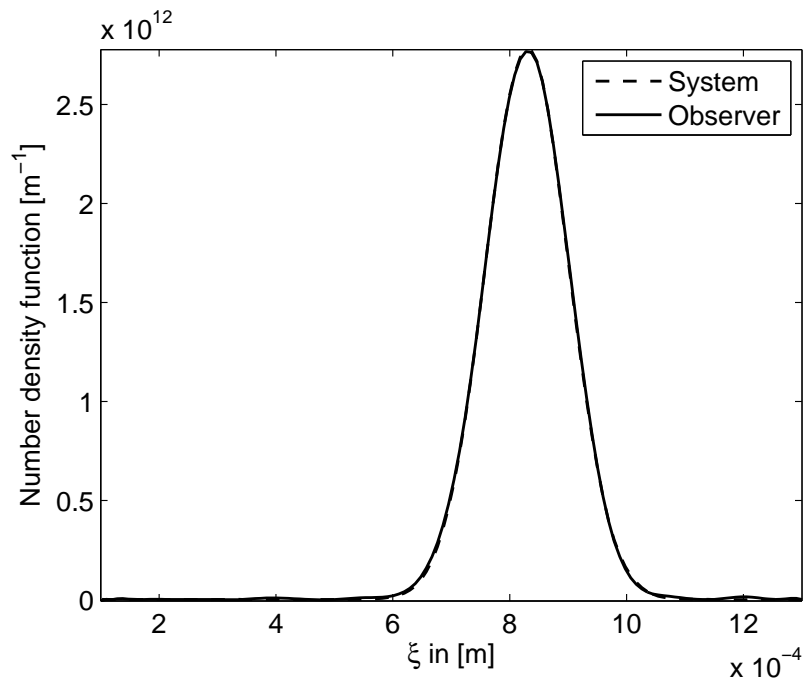


Figure 3.18: Reconstructed profile by on-line minimisation. The reconstruction is almost perfect, indicating that the observer is able to attenuate measurement errors. (Zimmer, Case 1, after 10000 s)

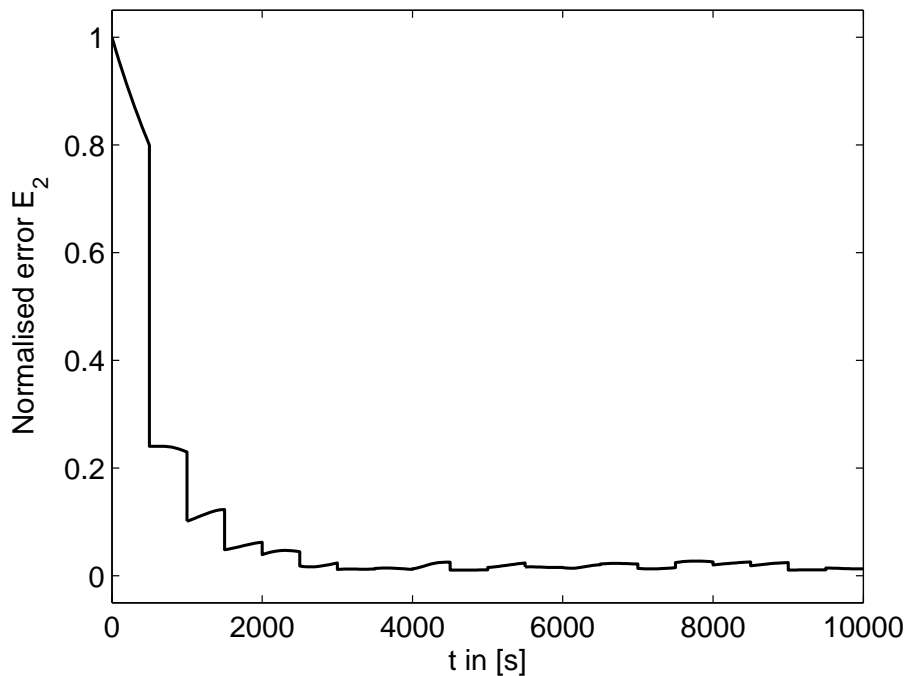


Figure 3.19: Temporal evolution of state observation error. Owing to the convergence order of the Newton-Raphson algorithm used in the method the profile is approximated quite well after a few iterations. The remaining error is due to the time-varying noise influence between two observation horizons. (Zimmer, Case 1)

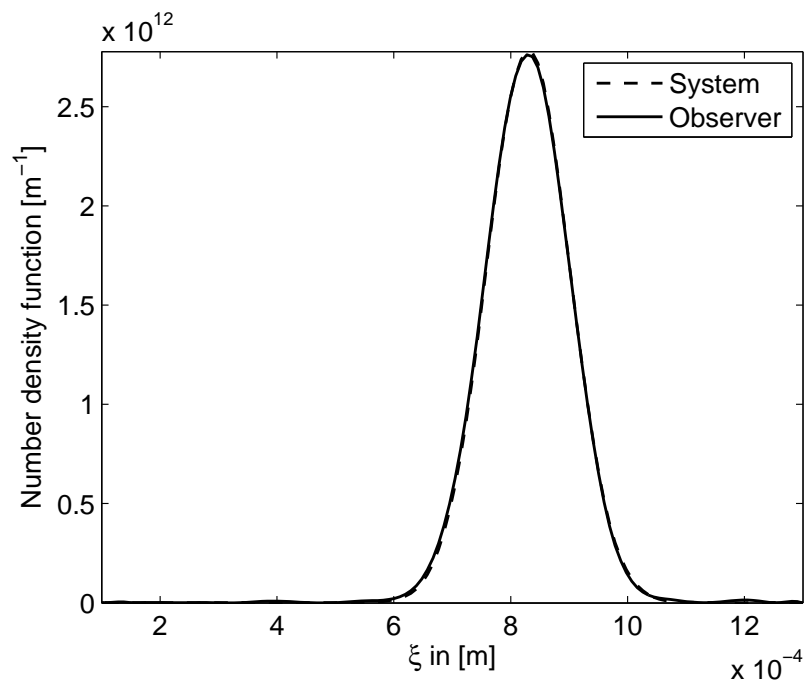


Figure 3.20: Reconstructed profile by on-line minimisation. The reconstruction is almost perfect, signalling that the observer is able to attenuate, in addition to measurement errors, parametric uncertainties, i.e. a the algorithm possesses robustness properties. (Zimmer, Case 1, parametric uncertainty, after 10000 s)

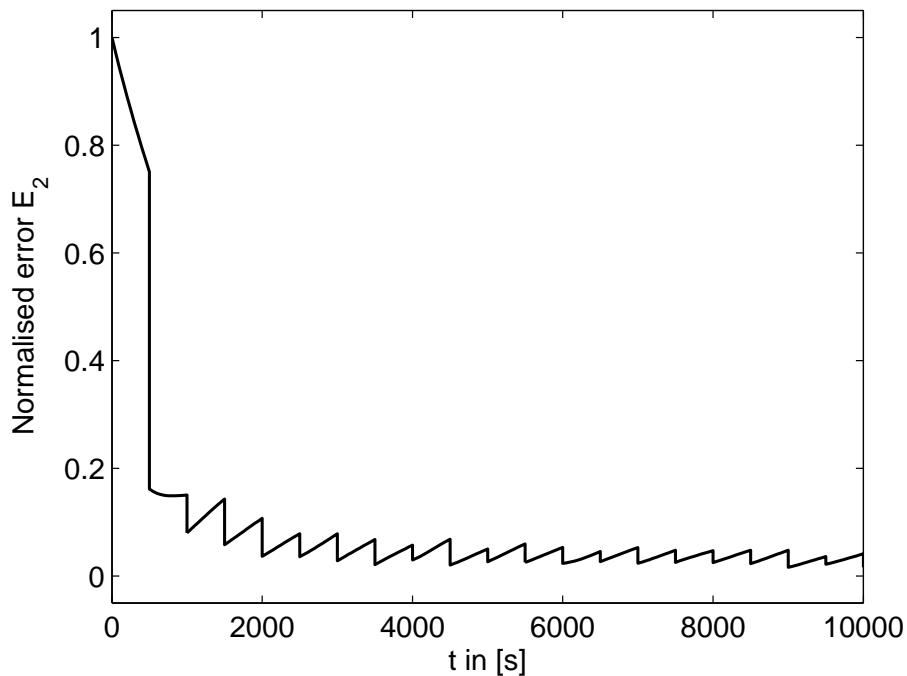


Figure 3.21: Temporal evolution of state observation error. Due to the error in the growth rate, the observer state deviates from the process state during each observation horizon. The deviation is compensated at the end of the horizon leading to the zigzag appearance of the error plot. (Zimmer, Case 1, parametric uncertainty)

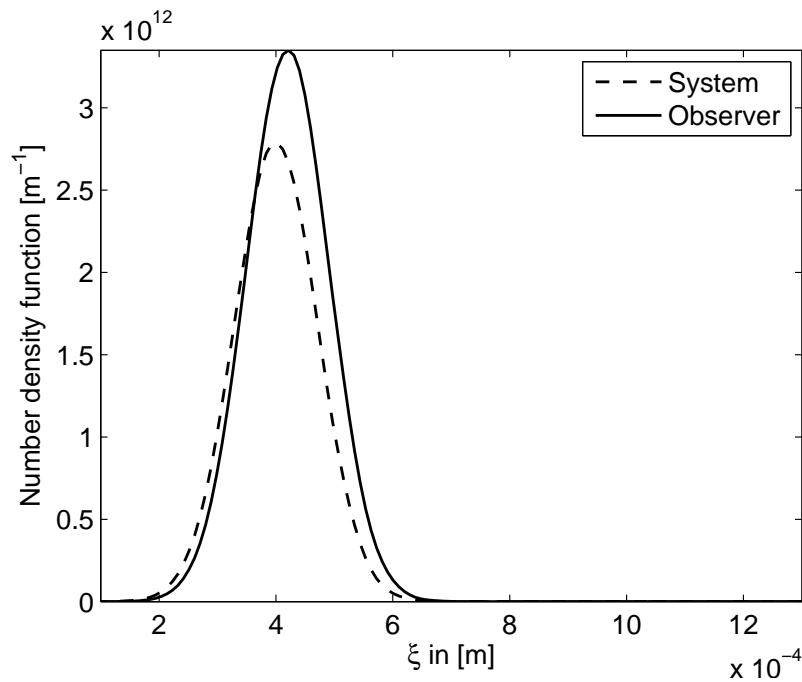


Figure 3.22: Initial condition used in state observation by on-line minimisation given normalised number density function measurements. (Zimmer, Case 2)

Case 2: Normalised number density function. Switching to the normalised number density function as a process measurement, i.e. $y = q_0(t, \xi)$, leads to a significant change in the performance of the observation algorithm. As can be seen in Fig. 3.23 the algorithm is not able to provide a reliable estimate of the number density function although the initial deviation is small (cf. Fig. 3.22). This result does not change when the initial error is decreased further.

The reason for the inefficiency of the algorithm can be found in the computation of the Hessian \mathcal{N}'' of the functional \mathcal{N} which is used to calculate the state correction. It turns out that by removing the quantitative information on the number density function from the measurements, i.e. normalising the measurement with respect to the total number of particles μ_0 , the Hessian becomes ill-conditioned leading to numerical problems in the calculation of the state correction. Based on this it has to be concluded that state observation by on-line minimisation using measurements of the normalised number density function is not likely to yield a successful model-based measurement system.

Case 3: Mean particle size. The problem pointed out in Case 2 becomes more severe in case of a lumped, scalar measurement, e.g. the mean particle size. Here the Hessian, due to scaling issues, is almost identical to a zero matrix, prohibiting the necessary inversion of \mathcal{N}'' in the calculation of the state correction. Although successful applications for this kind of measurement are known in crystallisation processes [89], in the present formulation it does not yield a working model-based measurement system. The problem might be remedied by using a different formulation, for instance the one proposed by Cao et al. [17].

Square-root unscented Kalman filter

In the following simulations results for an SRUKF applied to a batch fluidised bed spray granulation process are presented using the *mean particle size* as the available process measurement.

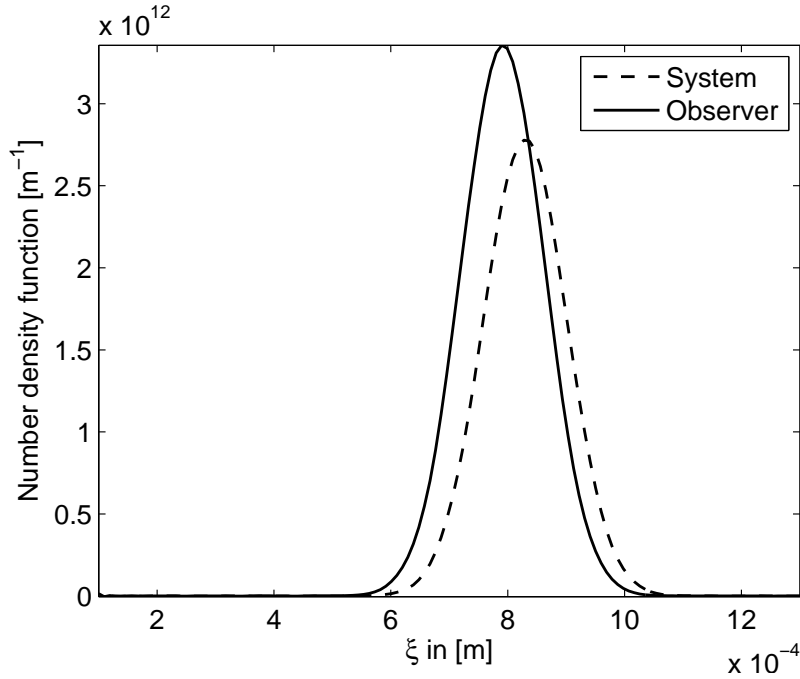


Figure 3.23: Result of the state observation algorithm using on-line minimisation given the normalised number density function as process measurements. The estimated profile is rather poor compared to the initial deviation in the observer model, shown in Fig. 3.22. (Zimmer, Case 2, after 10000 s)

Table 3.2: Simulation and design parameters UKF for the batch process.

Number of discretised states	N	100
Simulation time interval [s]	t_{end}	20000.0
Measurement time interval [s]	Δt	50.0
Variance of measurement [m^2]	R_n	10^{-10}
Process noise covariance [$m^{-1} s^{-1}$]	R_v	$10^{-40} I_N$
Design parameter SRUKF	α	0.7

For the tests the balance equations were discretised by a finite volume method using 100 equally spaced grid nodes in the size interval $[\xi_0, \xi_{max}]$, where the maximum size was determined by process simulations. Following the design procedure for unscented Kalman filters this yields a deterministic choice of 201 sigma points.

Scenario 1. In this scenario normally distributed measurement noise in the order of ten percent of the measurement is added to the simulated plant measurement to create a noisy measurement which is then used in the estimation algorithm. The sampling time of the estimator is chosen to be $\Delta t = 60$ s. As initial condition a bi-modal distribution was chosen for the plant, where the initial guess provided for the estimator considers only a mono-modal distribution which is overestimated in magnitude by thirty percent, see Fig. 3.24. This choice leads to a difference in the growth velocity of the estimator model that influences all states of the model. Other necessary parameters are listed in Tab. 3.2.

It can be seen in Fig. 3.25 that the estimation of the number density function is quite good. The known but overestimated mode is reconstructed almost exactly, only a slight deviation in position

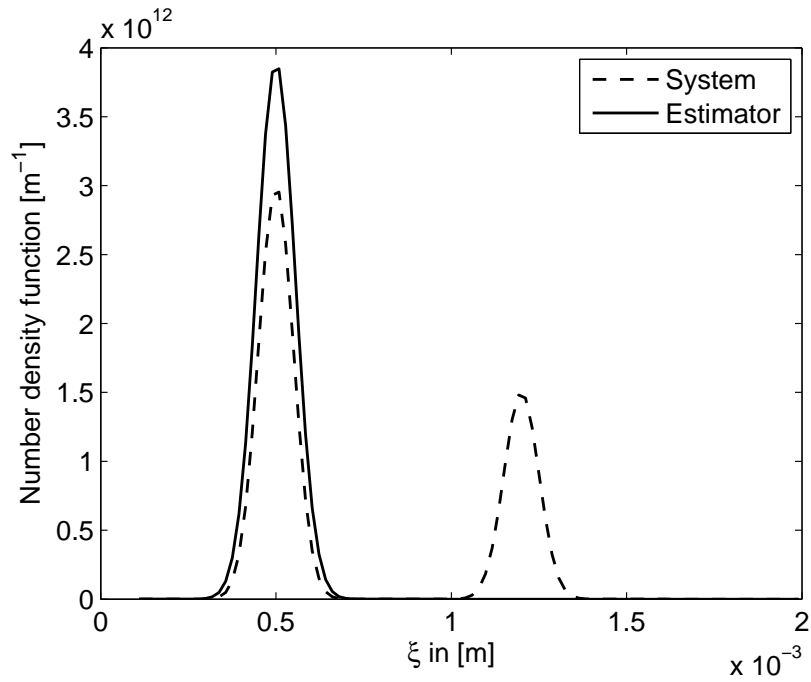


Figure 3.24: Initial condition used for the process and the estimator model. Note that in the observer model initially only a rough estimate of one of the modes of the bi-model process distribution is known. (UKF, Scenario 1)

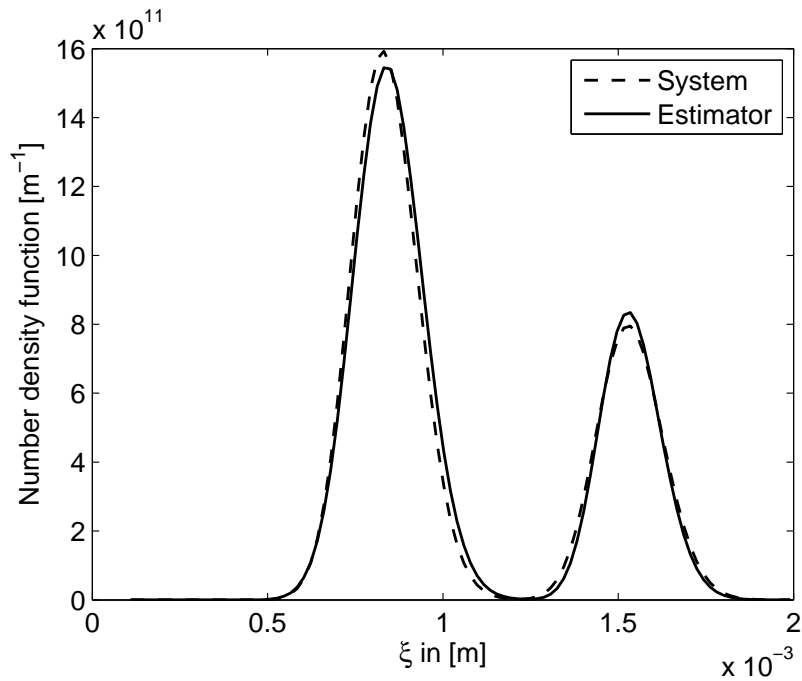


Figure 3.25: Profiles for the number density functions at the end of the process simulation ($t = 20000$ s). (UKF, Scenario 1)

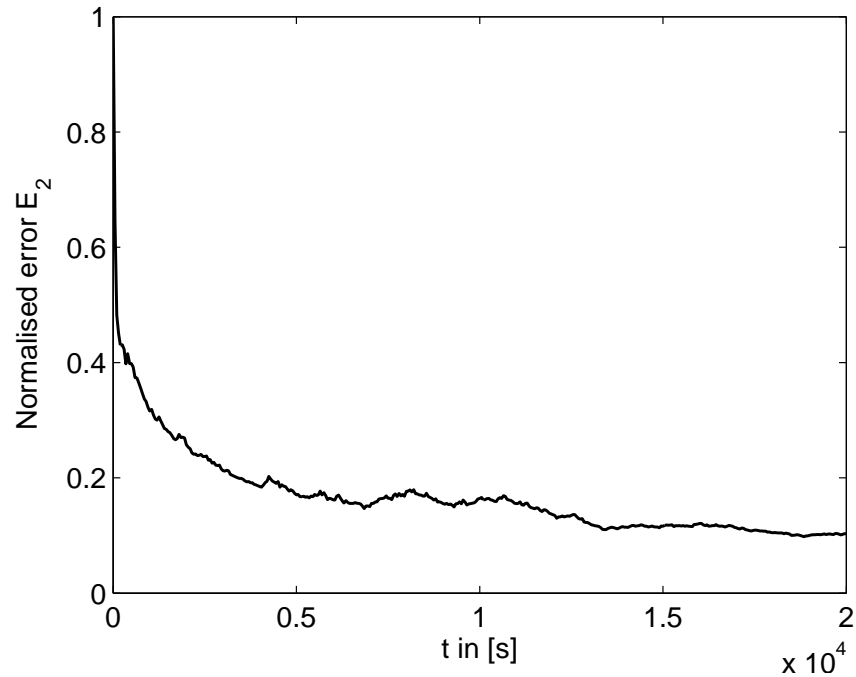


Figure 3.26: Evolution of the state observation error E_2 : After an initial fast decrease it converges to a non-zero value. (UKF, Scenario 1)

of the mean and a slightly too large variance can be noticed. The position of the second mode, which is initially unknown, is estimated with a very small offset, and the magnitude of the peak is overestimated. The time evolution of the estimation error E_2 is shown in Fig. 3.26. There it can be seen that the error decreases almost monotonically over time. The error at the end of the simulation interval can be further decreased by decreasing the time interval of measurements, which yields more measurements and thus more state corrections.

The rather large deviation in the initial number density functions is chosen to highlight that even large initial errors can be corrected using this non-linear estimation algorithm. The time necessary to compensate the error depends on the initial deviation, so in practical application the best possible guess should be used to increase the convergence. It should also be noted that the error E_2 does not converge to zero but to a non-zero steady-state. This is due to the measurement noise present and the approximation of the non-linear probability distribution of the estimator states in the calculation of the state correction.

Scenario 2. In practice not all process parameters are known exactly, or errors might occur in the setup of the estimator parameters. For application the estimation algorithm therefore has to possess a certain robustness to parametric errors. In case of the batch granulation process under noisy measurements this robustness is tested by applying a mass flow rate of suspension that is ten percent larger than the actually supplied rate. As this parameter is part of the growth rate, this error affects all states of the estimator.

In Fig. 3.27 it can be seen that even in this case the estimation error decreases. It can also be seen that at end of the process simulation the error is larger than in the other scenario. The estimated profile (Fig. 3.28) also shows a larger deviation in the position and the magnitude of the peaks. The variance for both modes is also overestimated, but still a useful estimate of the number density function is obtained.

The parametric error, if its source is known, can be compensated if it is estimated as well, but in

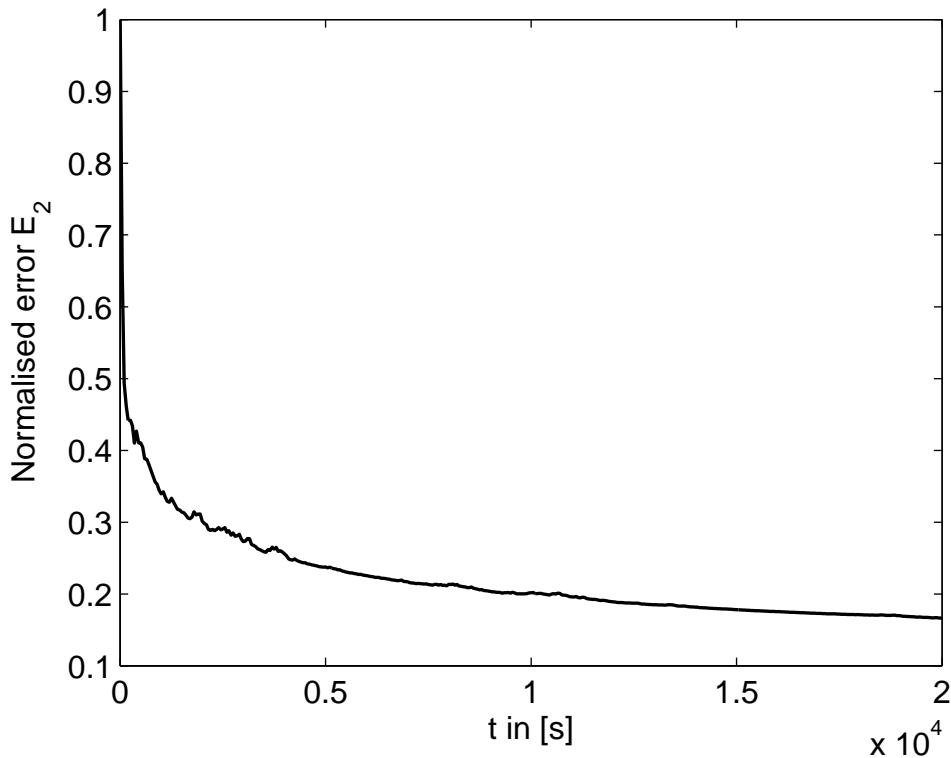


Figure 3.27: In case of parametric errors the estimator error also decreases. This decrease is slower than in the other scenarios and tends to a fixed value. (UKF, Scenario 2)

general there will be no perfect estimator model and a non-zero estimation error has to be accepted.

This result shows that in case of a batch granulation process the estimator is able to compensate up to a certain degree parametric errors, but in order to get most precise estimates it is necessary to supply precise parameter values. By a suitable choice of measurement interval and number of sigma points (which follows from the number of grid nodes used in the discretisation of the observer model), a balance between the accuracy of the estimation and the computational load can be achieved, as motivated in Bück et al. [13]. As was mentioned in the description of the algorithm, a further speed-up can be achieved by using parallelisation in the sigma point propagation step.

Based on these results it can be stated that the application of the UKF algorithm to batch spray granulation processes given the mean particle size yields a functional model-based measurement system for the number density function.

3.4.3 Application to continuous spray granulation with particle recycle

As was motivated in Chapter 2.7 the continuous process with external classification and particle recycle does possess different dynamic behaviour depending on the mean diameter of the milled and recycled particles: Either a stable steady-state distribution is obtained, or a stable limit cycle occurs in the system. The corresponding steady-state number density function is unstable – small deviations will lead to a drift of the process dynamics towards a limit cycle, i.e. sustained oscillations in the number density function.

In case of a stable steady-state and given a perfect process model initial errors in the process and the observer model are attenuated automatically as the steady-state does not depend on the initial

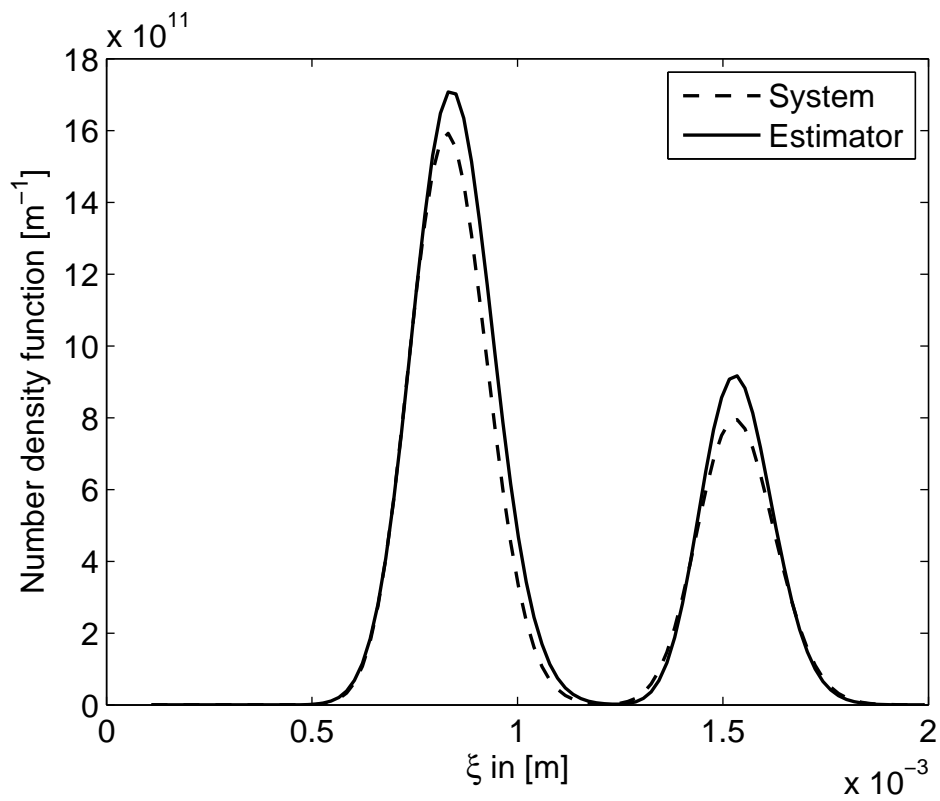


Figure 3.28: Reconstructed number density function in the presence of parametric model errors. The parametric errors are only compensated up to a certain degree. (UKF, Scenario 2, $t = 20000$ s)

Table 3.3: Process parameters for the continuous spray granulation process

Initial bed mass [kg]	m_{bed}	10.0
Reference bed mass [kg]	$m_{bed,set}$	10.0
Mass flow of nuclei [kg s^{-1}]	\dot{M}_{nuc}	5.55×10^{-5}
Mass flow of solid [kg s^{-1}]	\dot{M}_{solid}	1.38×10^{-2}
Solid density [kg m^{-3}]	ρ_s	1440.0
Size of nuclei [m]	ξ_0	0.1×10^{-3}
Screen size upper screen [m]	ξ_u	0.5×10^{-3}
Screen size lower screen [m]	ξ_l	0.4×10^{-3}
Milling diameter [m]	ξ_M	0.35×10^{-3}
Milling diameter (osc.) [m]	ξ_M	0.2×10^{-3}

conditions, i.e. the observer model will converge to the steady-state number density function. The use of the observer then lies with the compensation of modelling and measurement errors, as will be demonstrated by the Unscented Kalman filter.

Also presented are results for the application of selected state observation and estimation algorithms to the continuous process with an unstable steady-state behaviour. The availability of information on the number density function then provides means to stabilise the unstable steady-state number density function by feedback control.

Based on the results in the batch fluidised bed spray granulation, the state observation by on-line minimisation is not applied to the continuous process.

For all simulations the process parameters listed in Tab. 3.3 are used.

Infinite-dimensional Luenberger observer

The idea for calculation of the state correction in batch spray granulation processes is re-used to design an observer for the continuous spray granulation process. As was done before, the correction is designed such that the state observation error decreases over time.

Given the measurement of the normalised number density function $y = q_0(t, \xi)$, the equation for the state observation error $e = n - \hat{n}$ reads

$$\frac{\partial e}{\partial t} = - \left(G \frac{\partial n}{\partial \xi} - \hat{G} \frac{\partial \hat{n}}{\partial \xi} \right) + P(n) - P(\hat{n}) - k(\xi, y, \hat{y}). \quad (3.110)$$

The correction term is then designed such that $k(\xi, y, \hat{y}) \approx \alpha e$ with a tuning factor α under the assumption that $n \approx \hat{n}$.

The problem here lies in the calculation of e given the measurement y : The measurement contains only qualitative information on the number density function, i.e. the shape, because it is normalised with respect to the total number of particles. But the error also contains quantitative information, i.e. the magnitudes: $e = \mu_0 y - \hat{\mu}_0 \hat{y}$. This means that the information of the magnitudes must somehow be obtained. One possible solution is to use the total number of particles in the observer model also as an estimate of the total number of particles in the process: $e = \hat{\mu}_0 (y - \hat{y})$. By this approximation the use of the observer is limited to processes where $\mu_0 \approx \hat{\mu}_0$. A fairly accurate estimate of the total number of particles at the beginning of the process can be obtained by taking a representative sample of the bed material and scaling the normalised number density function, obtained for instance from an off-line measurement device, by the available information on the

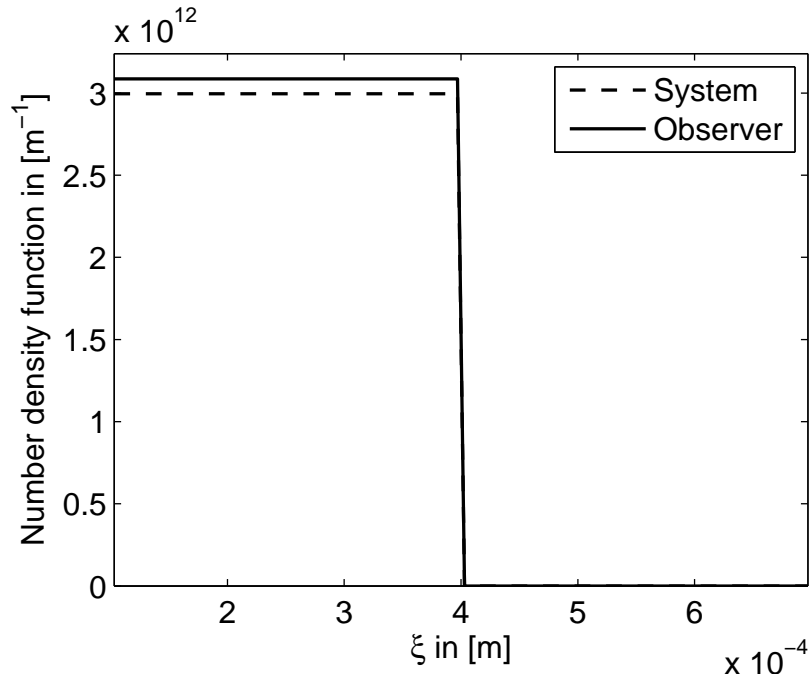


Figure 3.29: Initial condition of process and observer model. (Infinite-dimensional Luenberger observer, continuous process)

total amount of bed material. However, over the process time a drift in the quantitative result is to be expected due to uncertainties in the modelling of the observer, e.g. the characteristic milling function.

The performance of this setup (for $\alpha = 0.025$) is presented in Fig. 3.29 – Fig. 3.31: Given the initial conditions shown in Fig. 3.29 the results at the end of the process time are shown in Fig. 3.30. There it can be seen that the position of the number density function n is approximated quite well, however, a large error in the magnitude is present. Taking a look at the normalised number density functions q_0 in Fig. 3.31 reveals that the normalised number density function is estimated almost perfectly, i.e. qualitatively the observer works well. The error in the magnitude is therefore introduced by the sole use of $\hat{\mu}_0$ as a scaling in the calculation of the state correction. Instead of using $\hat{\mu}_0$, an estimate of the total number of particles can be obtained in each measurement instant by additionally measuring the total mass of particles in the fluidised bed:

$$m_{bed} = \frac{\pi}{6} \rho_s \int_{\xi_0}^{\infty} \xi^3 \mu_0(t) q_0(t, \xi) d\xi, \quad (3.111)$$

and then using this estimate in the calculation of the state correction. By this modification also quantitative results on the number density function can be obtained, otherwise the results of the observer are only qualitative.

The use of a lumped measurement, for instance the mean particle size, to reconstruct the number density function does not prove to be successful. The main problem again is the determination of a suitable relation that calculates a distributed state correction based on the scalar measurement. Whereas in the batch process the knowledge on the principal shape of the number density function in many industrial application could be used to motivate such a correction, this is not possible in the unstable continuous case, as here the shape varies significantly and a fixed shape for the state correction will not be able to calculate a suitable correction.

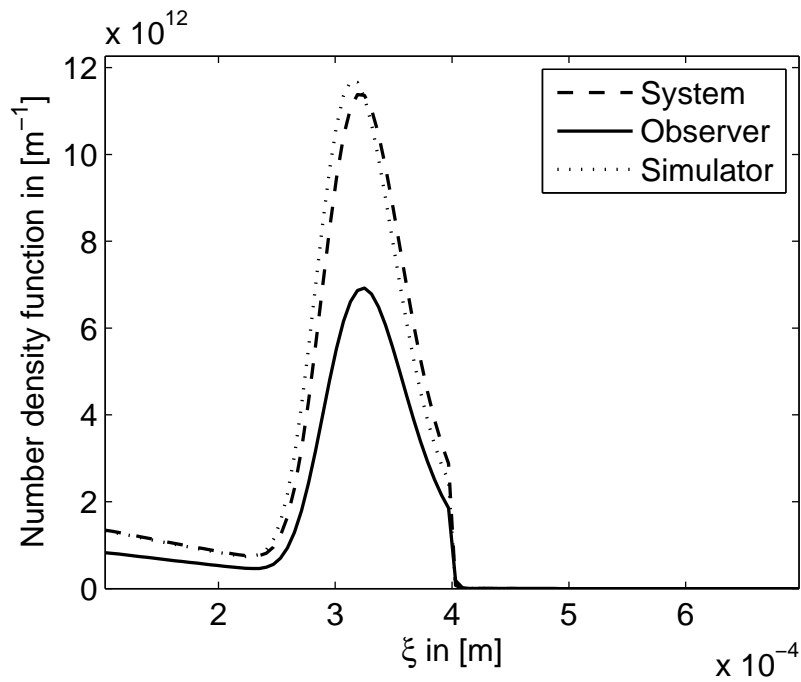


Figure 3.30: Reconstructed number density function using the infinite-dimensional state observer after 10000 s. (Infinite-dimensional Luenberger observer, continuous process)

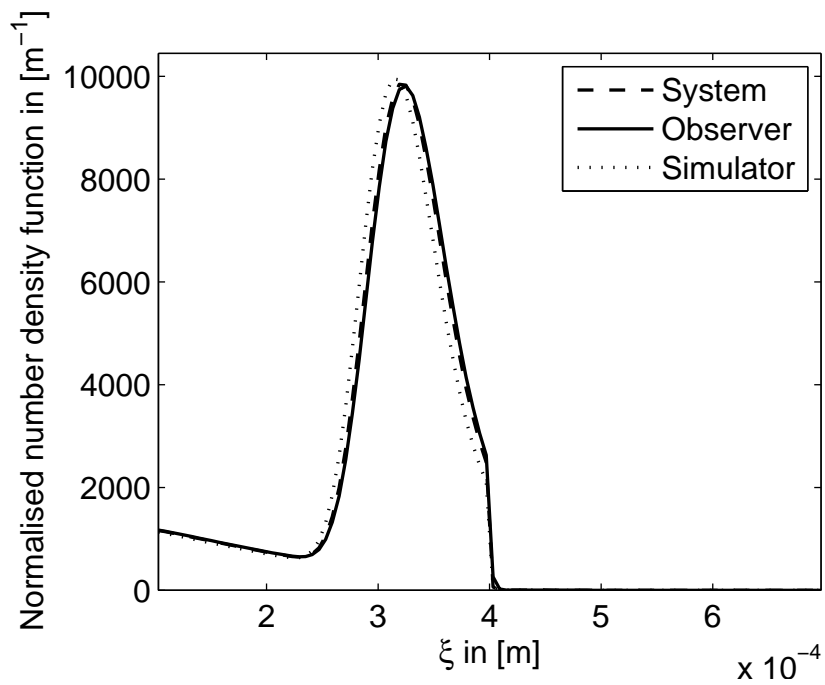


Figure 3.31: Reconstructed normalised number density function used to calculate the state correction. As the profiles are nearly identical the state is not further corrected, although a large error in the magnitude is present. (Infinite-dimensional Luenberger observer, continuous process, after 10000 s)

Finite-dimensional steady-state observer

Using the analytically derived steady-state number density function a steady-state observer for the continuous process can be designed. Restricting the focus on a discretised balance model results in the design of a linear Luenberger observer or Kalman filter. The observer is designed in a standard way as a simulator with an additive state correction based on the difference in the measurements

$$\frac{d\hat{n}}{dt} = -GD\hat{n} + P(\hat{n}) + K(y - \hat{y}), \quad (3.112)$$

where $y = h(n)$ is the measurement obtained from the (non-linear) plant and $\hat{y} = h(\hat{n})$ is the measurement calculated from the non-linear observer model. The state correction K is calculated using the linear approximations of the non-linear models in the vicinity of the steady-state solution. The design problem then reduces to the calculation of the coefficients of the observer gain matrix that can be achieved by placing the poles of the error equations at specified positions in the complex plane. For a sufficiently accurate approximation of the process model by discretisation the number of states in the observer model is quite high, so an explicit calculation of the coefficients is cumbersome. Fortunately, in many simulation packages, e.g. Matlab, algorithms are available that calculate the required coefficients automatically from the specified pole positions.

In the present formulation, the poles were not placed explicitly due to numerical issues. A suitable observer gain matrix was determined by considering the Luenberger observer a limit case of the Kalman filter, i.e. almost vanishing noise influence, and calculating the gain matrix by solving an optimisation programme. This is done by available Matlab routines and the designed linear observer is applied to the non-linear process.

In the following presentation the results were obtained using the approach to reconstruct the number density function from the measurement of the mean particle size.

Starting from the initial conditions shown in Fig. 3.32 for a milling diameter that gives sustained oscillations in the number density function the observer is able to compensate the rather large initial error as evidenced by Fig. 3.33. In order to show that the correction is necessary to obtain a correct estimate of the number density function in the process, the result of using the parallel simulator only is also depicted. The evolution of the error E_2 is depicted in Fig. 3.34 and shows almost monotone convergence towards zero. This result is somewhat surprising, given that only a linear approximation of the process is used to calculate the state correction.

Given these results, the question arises whether other estimation algorithms are needed to reconstruct the number density function from measurements of the mean particle diameter. The answer is positive for the following reasons: The steady-state observer uses a quasi-continuous measurement of the mean particle size, i.e. the sampling interval of measurements is negligible compared to the dominant time constant of the process, whereas in many practical application measurements are taken only at discrete points in time, i.e. a time-discrete sampling is performed. Additionally, the steady-state observer will be susceptible to model uncertainties and noise influences. It also requires the knowledge of the exact steady-state number density function, an assumption that might not hold in many applications as there the exact characteristics of the screens and the mill are not known. Thus it has to be expected that the performance of the steady-state observer will decrease if it is implemented in a time-discrete setting.

That the performance does indeed decrease is shown in Fig. 3.35 and Fig. 3.36. There the observer is implemented with a sampling time of $\Delta t = 60$ s, i.e. only every minute a new measurement is made available to the observer algorithm. At each sampling instant the plant measurement is biased by normally distributed measurement noise in the order of ten percent of the measured value. As can be seen in the error plot (Fig. 3.35), the normalised error E_2 lies for a significant

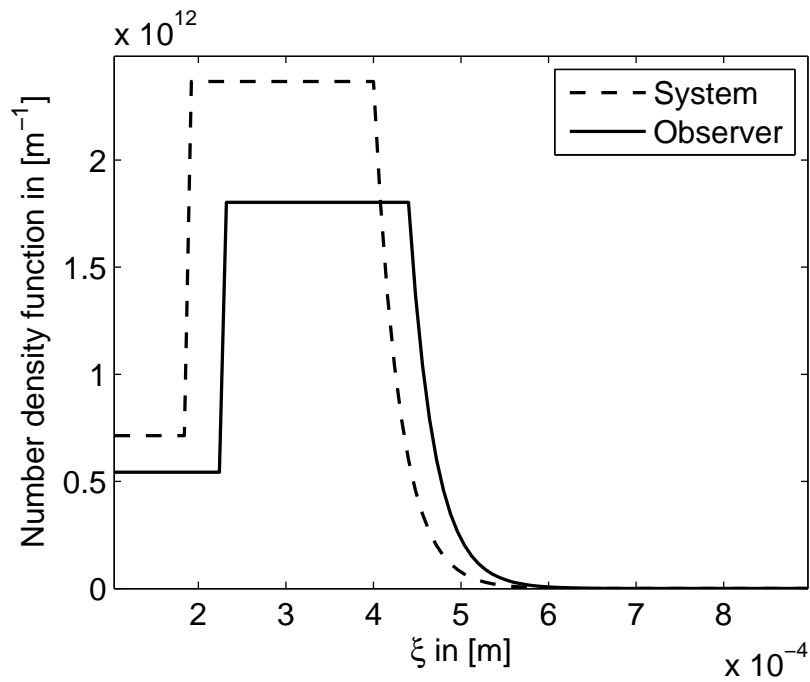


Figure 3.32: Initial condition of the process and the observer model used in the test of the Luenberger steady-state observer. (Luenberger steady-state observer)

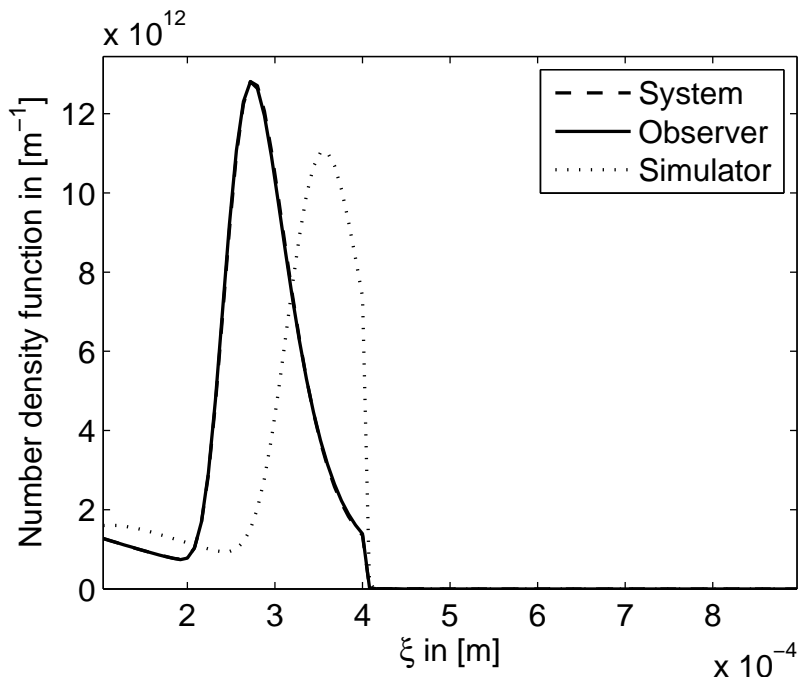


Figure 3.33: Number densities in the process and the observer model. Although only a linear approximation of the process dynamics is used to correct the number density function in the observer model based on mean particle size measurements, the estimation of the density function in the process is almost perfect. (Luenberger steady-state observer, after 5000 s)

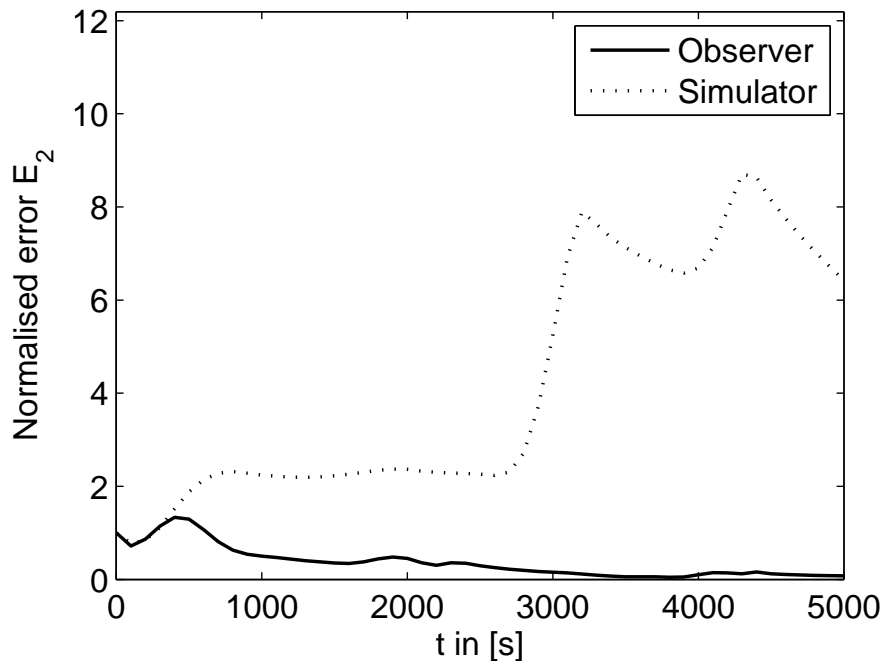


Figure 3.34: Evolution of the state observation error. The observer error decreases almost monotonically over time, whereas the error in the estimate provided by parallel simulation strongly increases. (Luenberger steady-state observer)

fraction of the process simulation above the initial value of one, i.e. in the integral measure the quality of the estimate decreases. In Fig. 3.36 it can be seen that the position of the number density function is corrected, however, the magnitude is not reconstructed correctly, contributing to the large error. Nonetheless, the time-discrete observer can be applied if the initial estimate is close enough to the number density function in the process.

If this is not the case, a non-linear state estimation algorithm such as the Unscented Kalman filter can give more reliable reconstructions of the number density function as it uses on one hand the full non-linear process information and on the other hand provides means to counteract stochastic influences, for instance measurement noise, by offering the possibility to include mathematical models of the stochastic processes, which results in more appropriate state corrections. In the next section an unscented Kalman filter is applied to the continuous fluidised bed spray granulation process with particle recycle.

Unscented Kalman filtering

One of the main advantages of the Unscented Kalman filter is that it does not require specific information on the structure of the process to be estimated. This means that the algorithm can be applied without any changes (apart from a change in the design parameter α) to the continuous process. This also allows to use one estimator implementation for both dynamic regimes, i.e. stable and oscillatory, as long as there is the possibility to change the milling diameter in the estimator model.

In Scenarios 1 and 2 the performance of the estimator for the stable regime is evaluated, followed by an evaluation of the estimator in the oscillatory regime (Scenario 3 and 4). In all cases the available process measurement is the *mean particle size* which is biased by Gaussian noise. In all

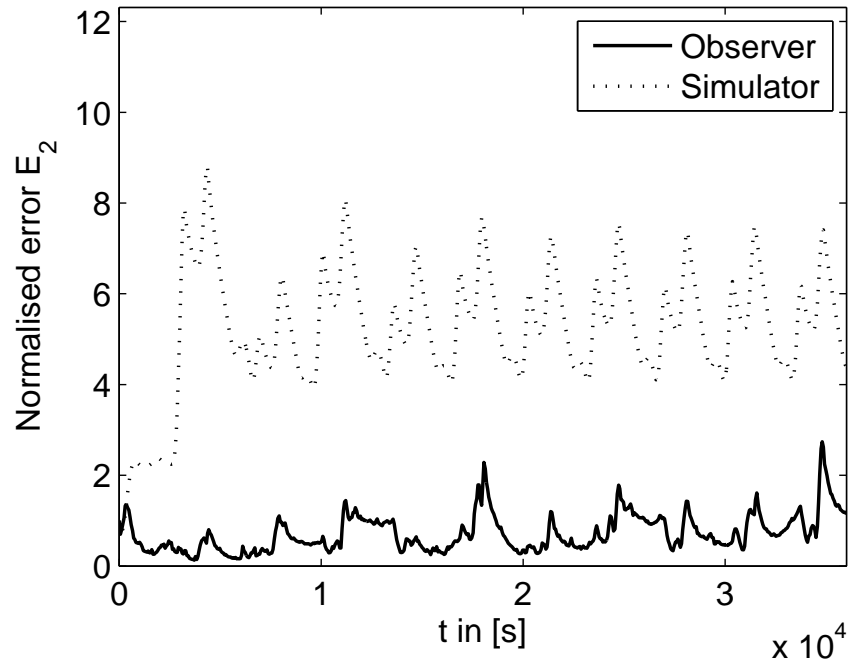


Figure 3.35: Evolution of the state observation error. In a time-discrete setting the observer error increases with respect to the initial error, but does not grow without bounds. This signals an error in the magnitude of the reconstructed number density function. (Luenberger observer, time-discrete)

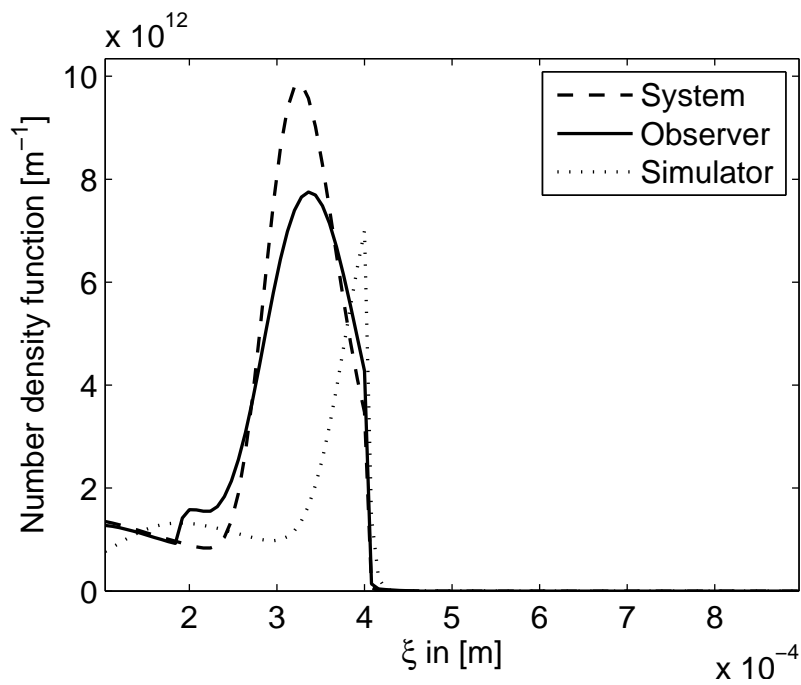


Figure 3.36: Number density functions in the plant and the observer model. In contrast to the quasi-continuous measurement case, a difference in the density functions is present if a time-discrete setting is used ($\Delta t = 60$ s). (Luenberger observer, time-discrete, after 36000 s)

Table 3.4: Simulation and design parameters UKF.

Number of discretised states	N	100
Simulation time interval [s]	t_{end}	10000.0
Measurement time interval [s]	Δt	50.0
Measurement time interval (osc.) [s]	Δt	10.0
Variance of measurement [m ²]	R_n	10^{-10}
Process noise covariance [m ⁻¹ s ⁻¹]	R_v	$10^{-40} I_N$
Design parameter SRUKF	α	0.6

cases the simulated measurement from the plant model is disturbed in the order of ten percent of the measured value to create a noisy measurement for the estimator. The estimator parameters are given in Tab. 3.4.

Scenario 1. In this first scenario only measurement noise is taken into account. As an initial condition a uniform number density function mass is chosen for the plant. The estimator model is initialised with a distribution that is off by approximately thirty percent. Similar to the batch process this large initial error will slow down the convergence but show that even large errors in the profiles can be corrected. In most practical applications the initial error will be smaller and the convergence will be achieved much faster.

The measurements used in the estimation algorithm and the estimator measurements (calculated from the estimated number density function) are depicted in Fig. 3.37. It can be observed that after an initial period the plant and the observer measurements converge to each other, despite the noise in the measurement signal. This behaviour can be attributed to the inclusion of a noise model in the estimation algorithm. The plot of the corresponding error E_2 (Fig. 3.38) in the number density functions of the plant and the observer shows damped oscillatory convergence of the error. The reasons for this are similar to the batch process, but as in that configuration, the estimation is excellent: The profiles are almost indistinguishable, as is shown in Fig. 3.39.

Scenario 2. In order to test the robustness of the estimator for the continuous process with respect to parametric errors the mean diameter of the mill that crushes the over-sized particles from the first screen is set to a two-and-a-half percent larger value in the estimator than in the plant. This influences the number of particles that is re-cycled to the fluidised bed and by this the growth rate in the estimator model, and thereby all particles are influenced.

The result for the error E_2 shows that although it still decreases, a higher steady-state error is attained (Fig. 3.40). This can also be seen in the estimated profile that shows errors in the position and the magnitude (Fig. 3.41). Nonetheless, the estimation result is quite good and could be used for process monitoring or control purposes. Additionally, it can be concluded that the milling diameter has a strong influence on the functionality of the estimator. This influence will be weaker for smooth milling and separation functions due to the superposition of the characteristic ranges. However, this is only true as long as the dynamic behaviour of the process model used in the estimator is similar to the process. If the process and the process model work in different dynamic regimes, the estimator will not be able to reconstruct the number density function correctly [13].

Scenario 3. In this scenario it is tested how the estimator performs in case of an oscillatory process behaviour. Therefore a milling parameter is chosen that leads to sustained oscillations in the number density function. The same initial condition as in the stable steady-state case is used, as it provides oscillations with a reasonable amplitude and period. The reconstruction also works for other initial distributions in the process as long as the initial profile of the estimator is close enough to this one.

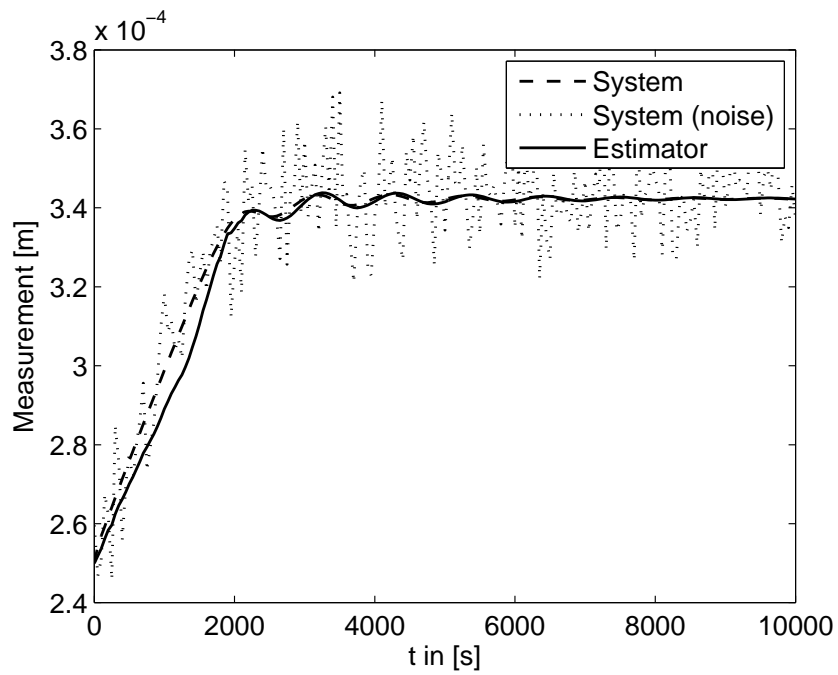


Figure 3.37: Depiction of the measurements used in the estimation algorithm (with noise) and the measurement information generated from the estimated number density function. (UKF, Scenario 1)

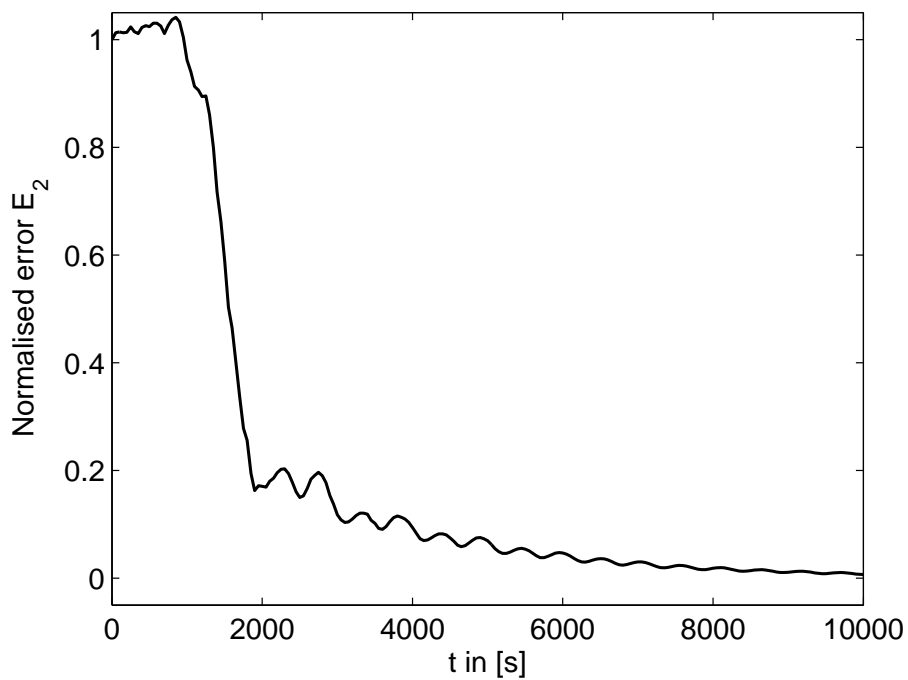


Figure 3.38: Evolution of the state observation error E_2 showing a damped oscillatory convergence of the error to a non-zero steady-state. (UKF, Scenario 1)

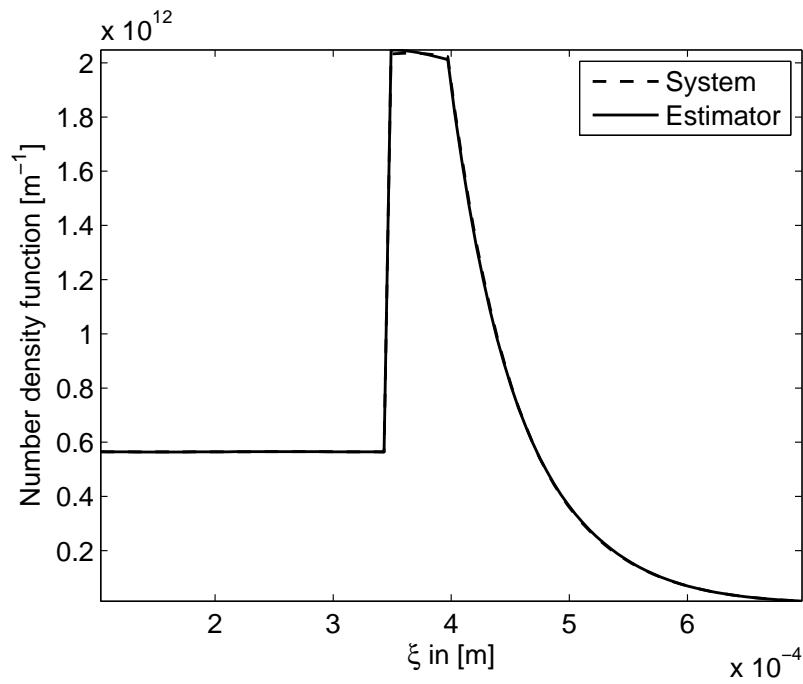


Figure 3.39: Number density functions in the estimator and plant at the end of the process simulation ($t = 10000$ s). The estimated profile is almost indistinguishable from the plant profile. (UKF, Scenario 1)

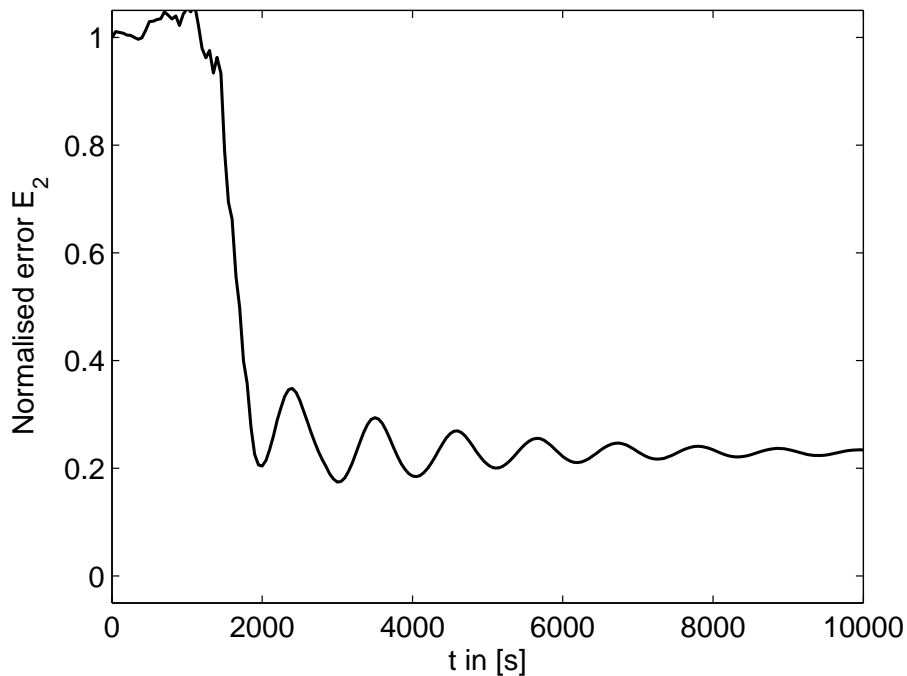


Figure 3.40: Evolution of the state observation error E_2 showing a damped oscillatory convergence of the error to a non-zero steady-state. Due to the parametric uncertainty in the estimator model the steady-state error is larger than in Scenario 1. (UKF, Scenario 2)

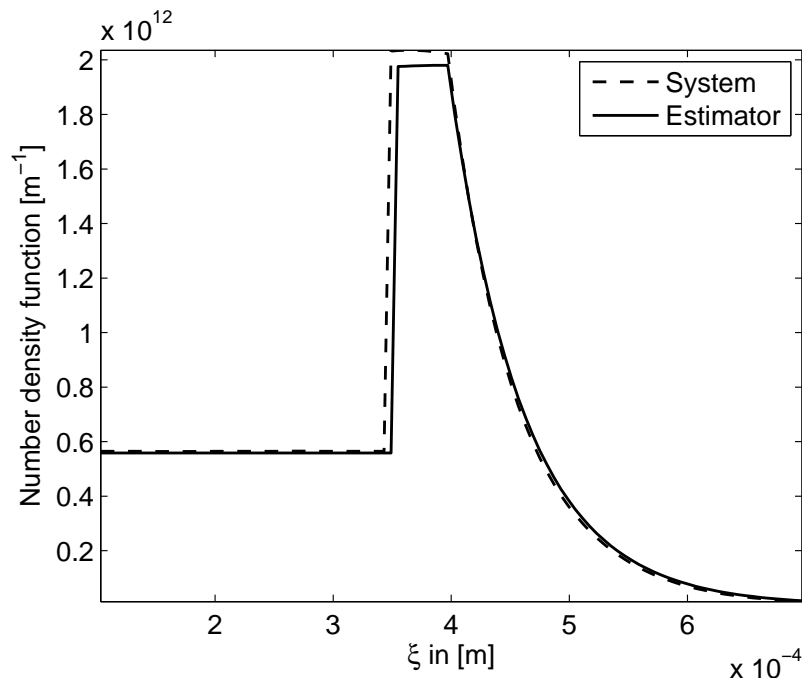


Figure 3.41: Number density functions in the estimator and plant at the end of the process simulation. The estimated profile shows a deviation in the position and the magnitude compared to the plant profile. (UKF, Scenario 2, after 10000 s)

An illustration of the measurement information used in the estimation is given in Fig. 3.42. There the noise-free process measurement, the measurement information with added noise that is used in the estimation, and the measurement information calculated from the reconstructed number density function are depicted.

In order to fulfil the requirements of the estimation algorithm, i.e. the positive-definiteness of the down-dated matrices constructed in the algorithm (see the remark on the operator *cholupdate*), the measurement time interval has to be decreased. As can be seen in the plot in Fig. 3.43 the error decreases only very slowly and non-uniformly. The error peaks correspond to the peaks in the size distribution and are due to the fact that the initial error in the profiles of process and estimator model introduces an error in the growth rate that leads to a deviation in the (temporal) position of the peaks. But as is shown in Fig. 3.44, even in a case for which the error E_2 is large, the estimation of the number density function is quite good, only a slight deviation in the position and the magnitude can be observed.

The magnitude of the error peaks is decreasing over time, so with a further increase of the number of measurements (and therefore state corrections) the convergence of the error to zero can be accelerated. The price that has to be paid for this is the increase in computation time that scales with the number of measurements. A too short measurement interval may lead to difficulties in use of the estimator in feedback control schemes that require some time to calculate the appropriate control inputs to the process.

Scenario 4. To test the robustness of the estimation algorithm an error in the milling diameter of the estimator model is introduced in such a way that the process and the estimator model still operate in the oscillatory regime (+2.5% of the nominal value). As in Scenario 3, the error decreases non-uniformly with intermediate increases, but a good estimation of the profile is achieved with a slight deviation in position and magnitude of the peaks as shown in Fig. 3.45. This means that

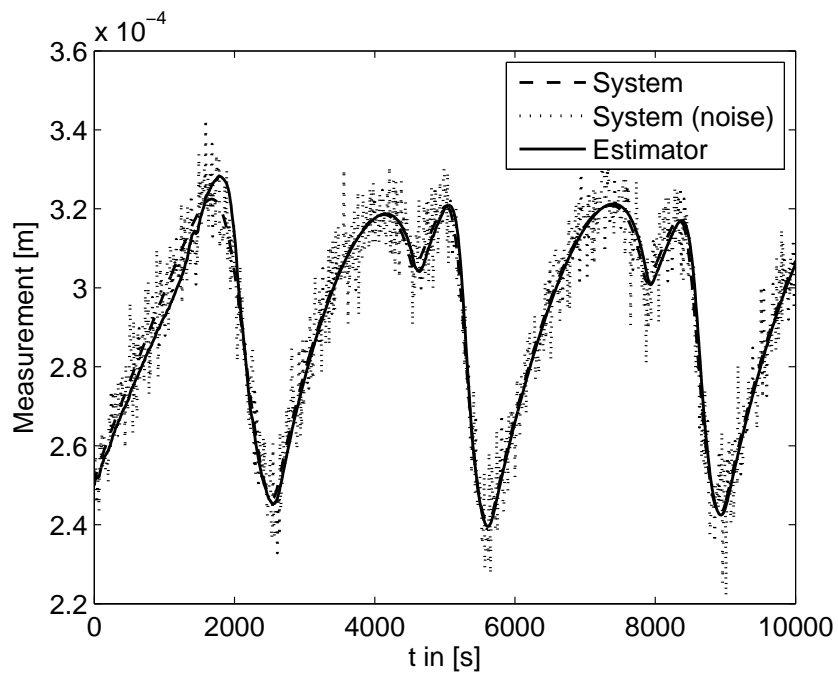


Figure 3.42: Depiction of the measurements used in the estimation algorithm (with noise) and the measurement information generated from the estimated number density. (UKF, Scenario 3)

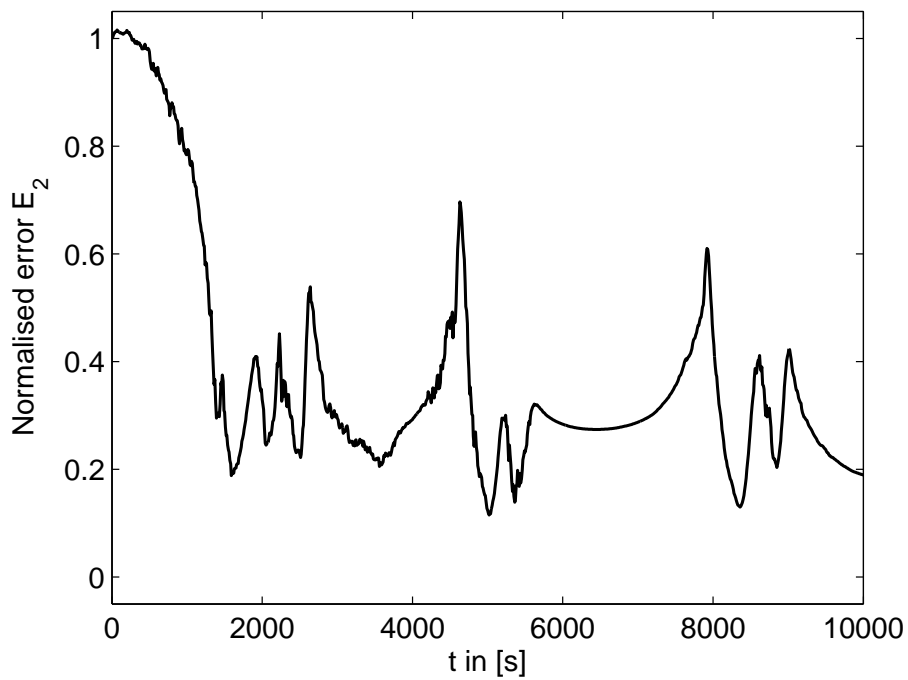


Figure 3.43: Evolution of the normalised state estimation error E_2 . (UKF, Scenario 3)

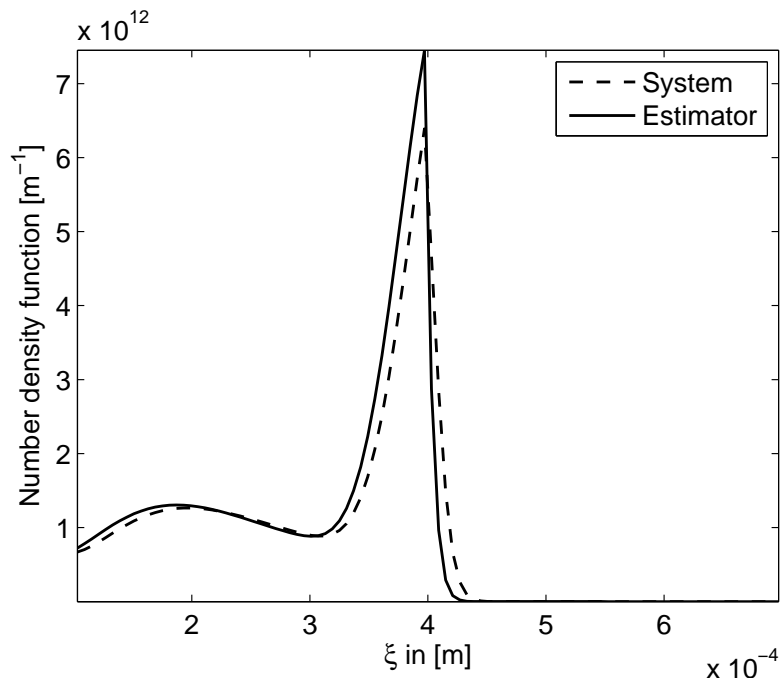


Figure 3.44: Reconstructed number density function. The profile corresponds to the peak in the E_2 -plot at approximately $t = 4300$ s. (UKF, Scenario 3)

for a milling diameter (which has great influence on the dynamic behaviour of the process) that is close to the nominal value, reliable estimates of the number density function can be obtained. However, if the error in the milling diameter is such that the process and the estimator model operate in different dynamic regimes the estimator algorithm is not able to calculate an estimate of the number density function in the process [13].

The results presented in this chapter show that for fluidised bed spray granulation processes model-based measurement systems can be designed that allow the reconstruction of the number density function from several classes of measurements. The reconstructed number density function can then be used for on-line process monitoring and, as will be shown in the next chapter, for feedback control of the spray granulation process.

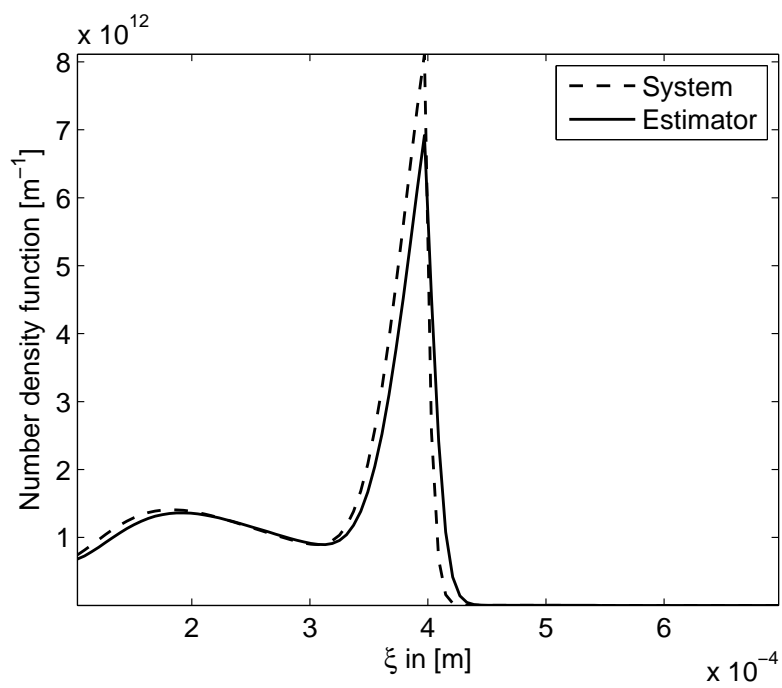


Figure 3.45: Reconstructed number density function in case of a parametric error in the milling diameter. (UKF, Scenario 4, after 10000 s)

Chapter 4

Model-based feedback control of fluidised bed spray granulation processes

4.1 Introduction

Whenever the result of a process, in case of a fluidised bed spray granulation process for instance the particle size distribution or the particle moisture, does not comply to the required specifications the process conditions have to be modified such that the specifications are fulfilled. The important tasks are the identification of suitable process inputs, *manipulated variables*, and the determination of a relation that modifies the inputs corresponding to the current error in the process with respect to the specification. The error is hereby determined with the help of certain process outputs, that will later be called *controlled variables*. They specify the product properties of interest, for instance the moisture content of a particle.

In an abstract setting any process under consideration can be represented as

$$y = \mathcal{P} \circ u + d, \quad (4.1)$$

where y denotes the controlled variables, i.e. the product quantities of interest, \mathcal{P} is an abstract representation of the process; the manipulated variables, i.e. external inputs to the process, are transformed by the process into the controlled variables subject to the output disturbances subsumed in d . The task therefore is to determine a relation that generates a sequence of process inputs u such that a required result y is obtained from the process \mathcal{P} even if disturbances d are present.

One way to modify the manipulated variables such that specified process results are obtained is the use of control mechanisms. They are in general separated into two groups: *open-loop* control and *feedback control* (also: closed-loop control).

In open-loop control the process inputs u are determined by the control law

$$u = C \circ r, \quad (4.2)$$

where C is an abstract representation of the open-loop controller, and r is the desired process result (*reference*). This setup is depicted in Fig. 4.1.

Ideally, under the assumption that $d = 0$ the controller C could be chosen as the inverse of the

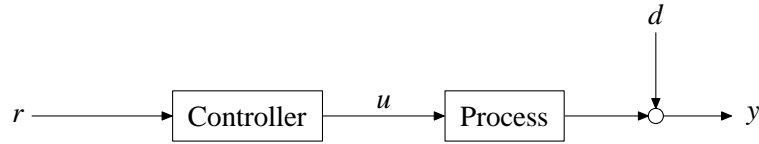


Figure 4.1: Open-loop control configuration: The inputs u to the process are calculated solely on the basis of the reference signal r .

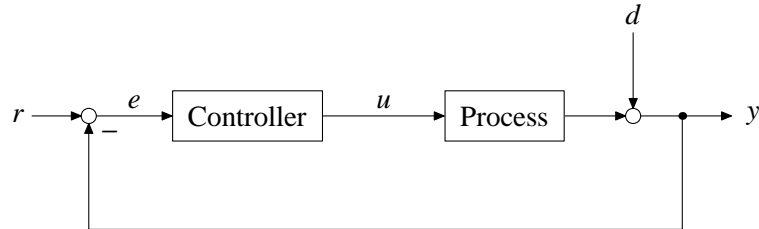


Figure 4.2: Closed-loop control configuration: The inputs u to the process are calculated on the basis of the deviation between the controlled output y and the reference signal r . This allows for the detection of drift in the controlled variables for instance due to disturbances.

process, i.e. $C = \mathcal{P}^{-1}$:

$$y = \mathcal{P} \circ \mathcal{P}^{-1} \circ r = r \quad (4.3)$$

yielding perfect control of the process.

However, in practice the disturbance signal d is not equal to zero and thus a control error remains: $y = r + d \neq r$. As the offset in the controlled variable is not detected by the controller, this configuration may lead to unsatisfying results. Additionally, the process \mathcal{P} , and therefore \mathcal{P}^{-1} , is not known exactly, only a sufficiently accurate approximation is available. This further introduces errors in the control that are not compensated. Even if the influence of errors can be neglected, the controller C may not be realisable practically, depending on the properties of the process \mathcal{P} .

In order to remedy these problems the controlled variables y can be measured and be fed back to the controller in order to calculate the necessary manipulated inputs. This configuration is depicted in Fig. 4.2. As can be seen there the input to the controller now is no longer the reference signal but the error $e = r - y$, i.e. the manipulated variables are calculated on the basis of the deviation of the current process state from the desired process state. In an abstract setting (with $d = 0$):

$$y = \mathcal{P} \circ C \circ e. \quad (4.4)$$

Using this configuration offset in the controlled variables, for instance due to disturbances, is detected by the controller and the process inputs are modified accordingly, i.e. feedback control possesses an intrinsic capability of compensating disturbances.

A major assumption in the use of control mechanisms is that the controlled variables y are directly measurable in order to be able to implement the control law. If only a subset of y can be measured directly and all other information can only be obtained in the form of a measurement z , then the missing information on the process has to be reconstructed from z , for instance by a model-based measurement system.

The remaining task is the design of a suitable controller C , which is in general a dynamic system, that will yield the desired process result. Based on the prospect of the superior properties of feedback control, this configuration will be treated almost exclusively in the following.

The basis for all subsequent steps is a dynamic model of the process. The controller is then designed using the information on the process and is thus a model-based controller. This term becomes more explicit if the process model is used directly in the calculation of the manipulated variables. Implementing the designed controller then leads to a closed control loop.

The main requirements on the control loop are (in descending order of importance) [83]:

- *Stability*: For the concept of stability several definitions exist, which will be discussed subsequently. The general task is to guarantee that finite exogenous signals (e.g. references, disturbances) only yield finite changes in all internal and external signals, for example the measured and controlled variables.
- *Disturbance attenuation*: For disturbance classes of interest d the steady-state error e should vanish, i.e.

$$\lim_{t \rightarrow \infty} e(t) = \lim_{t \rightarrow \infty} r(t) - y(t) = 0, \quad (4.5)$$

i.e. there is no persistent error in the control result. This requirement can be fulfilled by a suitable choice of the controller structure depending on the process structure.

- *Dynamics*: The transition of the process between two states, for instance the return into its initial state after the occurrence of a disturbance, should be sufficiently fast without too much perturbations in the measured and controlled variables.
- *Robustness*: The three requirements should be fulfilled even if the process model used in the design of the controller contains errors in comparison with the real process, for instance due to unknown process kinetics or the simplification of a complex but accurate process model.

Based on the nature of the reference signal, i.e. constant or time-varying, two types of control tasks can be defined: First is stabilisation or disturbance attenuation: There the reference signal is constant and the controller is required to keep this reference by counteracting disturbances. This task can often be found in steady-state operation of a plant where the aim is to keep the plant in the steady-state despite the occurrence of disturbances. The second task is called model-following: There a reference trajectory is generated by a dynamic process and the task of the controller is to determine the necessary inputs to the process such that it follows the reference as closely as possible. This task has to be performed for instance if the process has to be moved from one steady-state to another. Here the reference is generated such that the process does not attain states in between the two steady-states that may violate safety requirements.

The most important requirement for a control loop is *stability*, especially if the process itself is unstable. Two established definitions help to make the intuitive concept of stability more precise: *input-output stability* and *state stability*.

Input-output stability. A dynamic process $y = \mathcal{P} \circ u$ is called input-output stable if finite input signals u only create finite output signals y , i.e. bounded inputs yield bounded outputs.

This definition, although it is useful for many classes of processes, does not give information on the stability of internal signals, i.e. signals in the process P that are not measured. Instability in terms of unbounded, unmeasured signals in the process is not detected.

The concept of input-output stability is therefore extended to the concept of state stability.

State stability. A process in state space representation is given by

$$\frac{dx}{dt} = f(x), \quad y = h(x), \quad (4.6)$$

with x denoting the state variables of the process. A steady-state solution of the process is assumed to be x_s . The steady-state solution is called stable in the sense of Lyapunov [101] if there exists for a given $\delta > 0$ an $\varepsilon > 0$ such that

$$\|x(0) - x_s\| < \delta \quad \Rightarrow \quad \|x(t) - x_s\| < \varepsilon \quad \forall t. \quad (4.7)$$

This means that the state remains within a bounded distance ε from the equilibrium x_s for all times provided that the initial distance is smaller than the given δ . The equilibrium is called asymptotically stable if the state $x(t)$ returns to the equilibrium:

$$\lim_{t \rightarrow \infty} \|x(t) - x_s\| = 0. \quad (4.8)$$

Practically, stability in the sense of Lyapunov can be proved if a function V with the following properties:

$$V \geq 0, \quad V = 0 \Leftrightarrow x = x_s, \quad (4.9)$$

$$\frac{dV}{dt} \leq 0, \quad \frac{dV}{dt} = 0 \Leftrightarrow x = x_s, \quad (4.10)$$

called a *Lyapunov function* can be found. Then V can be interpreted as a generalised energy of the system and the condition $\dot{V} \leq 0$ means that this energy is decreasing over time until the minimum $V = 0$ is attained, i.e. $x = x_s$. This means that starting from a state $x \neq x_s$ the equilibrium x_s is reached. The construction of a suitable Lyapunov function for an arbitrary process is non-trivial, only for certain classes direct approaches are known. Further, the construction of a Lyapunov function is only a sufficient criterion for the stability of an equilibrium.

For linear time-invariant systems

$$\frac{dx}{dt} = Ax, \quad (4.11)$$

with the trivial equilibrium $x_s = 0$ state stability can be tested by considering the eigenvalues of the constant matrix A : If all eigenvalues lie in \mathbb{C}^- , i.e. the real-part of all eigenvalues is negative, then the system is asymptotically stable. If at least one eigenvalue lies in \mathbb{C}^+ then the system is unstable. Eigenvalues with zero real-part require special treatment, and the stability depends on the geometric multiplicity of the eigenvalue [83].

In case that the complete process state is measured, i.e. $y = x$, the definitions of input-output stability and state stability are equivalent.

Having determined the stability behaviour of the process the next question to be answered is which process states can be reached by the available manipulated variables.

State controllability [149]. A system in state-space representation

$$\frac{dx}{dt} = f(x, u), \quad y = h(x), \quad (4.12)$$

is called *completely controllable*, if it can be transferred from any initial state $x(t_0)$ into any final state $x(T)$ by a finite input function $u(t)$, $t \in [t_0, T]$ in a finite time T . If controllability depends on the initial time t_0 the system is called *controllable at t_0* .

Controllability can be tested by methods similar to the test for observability, i.e. a controllability map is constructed from the knowledge of $f(x, u)$. If this map can be uniquely inverted then the non-linear state-space system is controllable [101]. The actual computation and inversion of the controllability map is hindered by the same obstacles as is the computation of the observability map: Only if special structures can be exploited global results can be obtained.

In case of linear time-invariant systems

$$\frac{dx}{dt} = Ax + Bu, \quad y = Cx, \quad (4.13)$$

Kalman provided a simple rank criterion for the test of controllability: If

$$\text{rank} [B, AB, A^2B, \dots, A^{n-1}B] = n, \quad (4.14)$$

where n is the state dimension, then the linear time-invariant system is controllable. An evaluation of this criterion beyond $n - 1$ does not provide further information as all powers of A starting from A^n can be expressed as a linear combination of the lower-order powers by the theorem of Cayleigh and Hamilton. A criterion that does not require the evaluation of the matrix powers was provided by Popov, Belevitch and Hautus: If for all eigenvalues λ of the matrix A the condition

$$\text{rank} [\lambda I - A, B] = n \quad (4.15)$$

is fulfilled then the system is controllable.

Similar to observability, *structural controllability* can be defined: A linear system in state-space representation is structural controllable if

the associated graph to (A_s, B_s) is input-connected, i.e. every state can be influenced by at least one manipulated variable, and

$$\text{s-rank}[A_s, B_s] = n, \quad (4.16)$$

where the structural rank (s-rank) is again defined to be the maximum rank a matrix M with the structure given by M_s can attain:

$$\text{s-rank} M_s = \max_{M \in M_s} \text{rank} M. \quad (4.17)$$

This criterion also gives just necessary conditions for the controllability of the linear system (A, B) .

From a practical point of view restrictions in the controllability of a process always have to be expected due to limitations in the realisation of the manipulated variables. If possible these limitations should be incorporated into the controller design.

In the rest of the chapter, design of feedback controllers for fluidised bed spray granulation processes is presented. In the continuous process with particle recycle, the focus lies on the stabilisation of the unstable steady-state behaviour in the number density function; in the batch process a controller is designed to guarantee a desired number density function at a given final time. Additionally controllers are designed to keep the product moisture and temperature within given limits, i.e. feedback control of the heat and mass transfer during spray granulation is designed.

4.2 Stabilisation of the continuous process with particle recycle

A result of the investigation of the process dynamics of the continuous process with external screening, milling, and particle recycle in Chapter 2.7 was that for certain milling diameters a stable steady-state number density function was obtained whereas for others sustained oscillations appeared in the process. A direct consequence, if the number density distribution is used to characterise the product properties, is a variation in the product quality, as well as a variation in the

product mass flow. For practical application this is undesired: The plant is expected to work in a steady-state giving a constant product quality at a constant mass flow rate.

If, however, the desired steady-state distribution is unstable then a feedback controller can be applied to stabilise the unstable steady-state. For the number density function this means that the occurring oscillations have to be damped out, i.e. the limit cycle has to be eliminated.

As the stability of the continuous process is significantly influenced by the milling diameter, a controlled variation can be used to damp out the oscillations in the number density function, and thus establishing a stable steady-state. The mean diameter of the milled particles is therefore selected as the manipulated variable for the stabilisation task. The milling diameter can be changed by increasing or decreasing the rotation velocity of the mill.

From simulation it is obtained that the total surface area of particles in the bed is a suitable measured output to characterise the dynamic process behaviour. As the surface area of all particles in the bed cannot be measured *in situ* it has to be reconstructed from other measurements by a model-based measurement system.

In the following various feedback controllers for the stabilisation of a given unstable steady-state number density function of the continuous fluidised bed spray granulation process with particle recycle are designed. The principal approach is the following:

1. Given the process parameters and a milling diameter the corresponding steady-state number density function is calculated.
2. The process model is linearised in the vicinity of the steady-state. The dynamics of the non-linear process are approximated correctly in a sufficiently small region of the state-space around the (hyperbolic) steady-state as a consequence of the Hartman-Grobmann theorem [125].
3. Based on the linear process model a feedback controller is designed.
4. The feedback controller is evaluated for different scenarios by application to the non-linear process.

The first step was already described in Chapter 2.6 and is not repeated here. Therefore the design proceeds with step 2, the linearisation of the model equations.

4.2.1 Linearisation of the model equations

A non-linear mathematical process model is given in state-space representation

$$\frac{dx}{dt} = f(x, u), \quad y = h(x), \quad (4.18)$$

that can be obtained for instance from a first-principles modelling and, like in the present case, a subsequent finite-dimensional approximation. An equilibrium, a steady-state, of the process (x_s, u_s) is assumed to be known.

Then the dynamics in the vicinity of the steady-state can be described by the linear approximation of the process model. Introducing the deviation variables $\Delta x = x - x_s$ and $\Delta u = u - u_s$ the following dynamic equation for Δx can be derived:

$$\frac{d\Delta x}{dt} = \frac{dx}{dt} - \frac{dx_s}{dt} \quad (4.19)$$

$$= f(x_s + \Delta x, u_s + \Delta u_s) - f(x_s, u_s) \quad (4.20)$$

$$\approx f(x_s, u_s) + \left. \frac{\partial f}{\partial x} \right|_{x_s, u_s} \Delta x + \left. \frac{\partial f}{\partial u} \right|_{x_s, u_s} \Delta u - f(x_s, u_s) \quad (4.21)$$

$$\frac{d\Delta x}{dt} = A \Delta x + B \Delta u, \quad (4.22)$$

where in the last line the matrices A and B are defined by

$$A = \left. \frac{\partial f}{\partial x} \right|_{x_s, u_s}, \quad B = \left. \frac{\partial f}{\partial u} \right|_{x_s, u_s}. \quad (4.23)$$

Applying the same procedure to the output equation $y = h(x)$ yields

$$\Delta y = C \Delta x, \quad C = \left. \frac{\partial h}{\partial x} \right|_{x_s, u_s}. \quad (4.24)$$

In total a linear time-invariant state-space system is obtained:

$$\frac{d\Delta x}{dt} = A \Delta x + B \Delta u, \quad \Delta y = C \Delta x. \quad (4.25)$$

An equivalent representation of the linearised process model can be obtained by considering the input-output behaviour only. Using the Laplace transform the input-output behaviour can be written as

$$\Delta Y(s) = P(s) \Delta U(s), \quad (4.26)$$

where ΔY and ΔU are the Laplace transforms of Δy and Δu , respectively, and the initial condition $x(0) = 0$ is assumed. The complex variable s describes the behaviour of the system in the Laplace domain. The transfer function $P(s)$ describes the transformation of the input ΔU into the outputs ΔY . It is given by

$$P(s) = C (sI - A)^{-1} B. \quad (4.27)$$

In practical application the analytical calculation of the partial derivatives necessary to construct the matrices A , B and C is complex and time-consuming. Often the partial derivatives are therefore numerically approximated, for instance by finite differences [133]. The accuracy of the approximation then depends on the order of the method.

The stability analysis can be performed by investigation of the eigenvalues of the matrix A , or equivalently by investigating the poles of $P(s) = N(s)/D(s)$, i.e. solutions s^* of $D(s^*) = 0$. If there exists at least one eigenvalue with a positive real part then the steady-state is unstable and has to be stabilised by a feedback controller.

In the following it is assumed that the steady-state number density function is unstable. Feedback controllers are designed on the basis of the linear process model and are applied to the non-linear process in order to stabilise the steady-state.

4.2.2 Proportional-integral feedback control

Linear proportional-integral feedback controllers are one of the most applied types of feedback controllers. The design process is straight-forward and due to its sufficient performance in many applications it is industrially accepted.

Considering the single-input single-output closed control loop reproduced in Fig. 4.3 the closed-loop *transfer function* from the reference r to the controlled output y , denoted by G_{ry} is

$$G_{ry}(s) = (1 + P(s)C(s))^{-1} P(s)C(s), \quad (4.28)$$

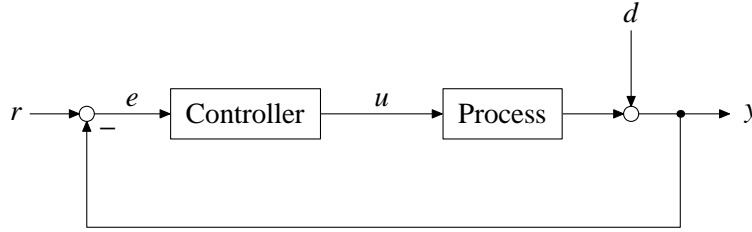


Figure 4.3: Standard closed-loop control configuration used for the design of proportional-integral feedback controllers.

where P is the transfer function of the linear time-invariant plant to be controlled and $C(s)$ is the transfer function of the controller to be designed. The closed-loop relation between the Laplace transforms of the reference signal R and the controlled output Y can then be written as

$$Y(s) = G_{ry}(s)R(s). \quad (4.29)$$

The closed-loop stability depends on the location of the poles of the transfer function G_{ry} in the complex plane. For asymptotic stability, all poles have to lie in the open left half plane. The poles of G_{ry} can be calculated as the roots of $(1 + P(s)C(s))^{-1} = 0$. This equation is also known as the *characteristic equation*.

The aim of the controller is thus by a suitable choice of a controller structure and controller parameters to place the poles of the transfer function at the desired location in the complex plane. Depending on the choice of the controller structure a different number of poles can be positioned.

The idea of the proportional-integral feedback controller is to calculate the manipulated variable $U(s)$ from the control error $E(s) = R(s) - Y(s)$ by considering two parallel influences: The proportional part calculates the manipulated variable based solely on the current control error whereas the integral part sums up the total error over a predefined time horizon and calculates the manipulated variable based on this information. The proportional part attributes to the dynamics of the controller; the integral part attributes to the accuracy of the controller as the integral of the error only vanishes if the error over the time horizon vanishes. Both parts are connected in parallel to calculate the manipulated variable U from the control error E .

In standard Laplace transform notation the proportional-integral (PI) feedback controller takes the following form

$$C(s) = K \left(1 + \frac{1}{T_N s} \right) = K \left(\frac{T_N s + 1}{T_N s} \right). \quad (4.30)$$

Here K is the controller gain and T_N is the integrator time constant, i.e. the PI controller provides two degrees-of-freedom to influence the position of the closed-loop poles. One important observation is that the controller only uses the information provided by the controlled output Y . This type of controller is therefor called *output-feedback controller*.

For the determination of the controller parameters K and T_N various standard methods exist, for instance loop-shaping in Bode plots or the root-locus method, that is presented briefly in Appendix E, or by solving an appropriate optimisation problem, for instance the minimisation of the integral squared control error (ISE)

$$\text{ISE} = \int_0^{\infty} e(t)^2 dt. \quad (4.31)$$

These standard calculations can be performed with the help of software packages for instance the Matlab SISO toolbox. The result is a practical standard controller that – despite its simple

structure – possesses a robustness against model uncertainties. It also provides in many cases satisfying disturbance attenuation [83].

4.2.3 LQ-optimal feedback control

Instead of an output-feedback controller $u = k(y)$ where the manipulated variable is calculated solely based on the knowledge of the measured (controlled) outputs y , state-feedback controllers can be utilised. They calculate the manipulated variable based on the knowledge of the whole state information available at the current process time, i.e. $u = k(x)$, where x denotes the state of the system.

Apart from only requiring that the closed-loop system is stable it can be furthermore required that from all possible solutions that stabilise the system one is chosen such that a given cost functional is minimised, i.e. an optimal control law is sought.

For linear time-invariant systems in deviation coordinates

$$\frac{d\Delta x}{dt} = A \Delta x + B \Delta u, \quad \Delta y = C \Delta x, \quad (4.32)$$

a large class of cost functionals can be expressed as quadratic forms in Δx and Δu :

$$J(\Delta u) = \int_0^T (\Delta x)^T Q (\Delta x) + (\Delta u)^T R (\Delta u) dt. \quad (4.33)$$

over the time horizon $[0, T]$. The functional only depends on Δu because the evolution of the state Δx is restricted by the process model that is in turn driven by Δu . The matrices Q and R are weights that influence the dynamics of the closed-loop system by punishing deviations of the state from its steady-state value and weighting the use of the manipulated variables. From a technical point of view the matrix Q must be positive semi-definite, i.e. $(\Delta x)^T Q (\Delta x) \geq 0$, the matrix R must be positive definite, i.e. $(\Delta u)^T R (\Delta u) > 0$.

An optimal control law for the linear process model and the quadratic cost functional, LQ-optimal control, can be derived analytically for arbitrary horizons $[0, T]$ resulting in a dynamic control law $\Delta u = -K(t)\Delta x$, where K is the controller gain matrix, see for instance Anderson and Moore [5]. In case of an infinite time horizon $T \rightarrow \infty$ a static proportional controller $\Delta u = -K \Delta x$ can be derived as

$$\Delta u = -(R^{-1}B^T P)\Delta x = -K \Delta x, \quad (4.34)$$

where P is the symmetric, positive-definite solution of the algebraic Riccati equation (ARE):

$$PA + A^T P - PBR^{-1}B^T P + Q = 0. \quad (4.35)$$

The advantage of the static controller is that it can be computed offline once given the matrices A, B, Q and R , whereas the dynamic controller gain has to be computed on-line.

If the given linear time-invariant system is observable and controllable and for the given weighting matrices Q and R a symmetric, positive-definite solution P of the algebraic Riccati equation can be calculated then the control law $\Delta u = -K \Delta x$ yields a stable closed loop system and is optimal with respect to the cost functional (Eq. (4.33)) [5]. If for a given Q and R , no solution P with the required properties can be found, the weights have to be modified by the control engineer until a solution can be found.

For the practical implementation the process state Δx has to be known, either directly or by a model-based measurement system. In order to use the controlled variables Δy in the cost functional

the weighting matrix Q can be chosen as $Q = C^T C$. The LQ-controller is known to possess a certain robustness against modelling errors but compared to PI controllers it is reduced as more system information (in form of the matrices A and B) is used directly in the controller design.

4.2.4 Model predictive control

Although the advantages of linear-quadratic optimal control methods were acknowledged in industries they were not often applied. The reasons for this can be found in the theory behind the methods that was considered elaborate, difficulties in formulating practical cost functionals in the required quadratic form and most important the framework does not provide the possibility to formulate constraints on the manipulated or controlled variables that are often encountered in practical application.

Based on the idea of calculating the manipulated variable as the solution of an optimisation problem in the 1970s new methods were developed in chemical industries, for instance Dynamic Matrix Control (DMC) [111] or predictive functional control [121].

All these methods, which were later subsumed under the label *model predictive control* (MPC), work after the following general scheme:

1. Based on the current process state $x(t_0)$ and a predefined trajectory for the manipulated $u(t)$ over a finite time horizon $[t_0, t_0 + T]$ the evolution of the process state is predicted with the help of a mathematical process model, i.e. the solution $x(t; t_0, x(t_0))$ over the horizon $[t_0, t_0 + T]$ is calculated.
2. A given cost functional is evaluated over the prediction horizon using the predicted state trajectory $x(t; t_0, x(t_0))$ and the input trajectory $u(t)$, $t \in [t_0, t_0 + T]$.
3. In an optimisation step the input trajectory is modified such that an optimum of the cost functional over the prediction horizon is achieved. The optimum input $u_{opt}(t)$ is directly given as the solution of the optimisation problem.
4. The optimum input $u_{opt}(t)$ is applied to the process until the next measurement of the process state becomes available. Then the scheme restarts at step 1.

The main ingredients of model predictive control schemes can be identified from this general description as

- dynamic process model: for the prediction of the evolution of the process state,
- cost functional: measuring the deviation of the process states from a desired process state,
- optimisation algorithm: calculation of the optimal input u_{opt} based on the predicted states and the cost functional.

The main advantages of model predictive control over linear-quadratic optimal control are that arbitrary dynamic models are possible, i.e. the type and structure of the model is not restricted to certain classes; the structure of the cost functional is also arbitrary, i.e. it does not have to be quadratic; the solution of the optimisation algorithm can be performed with respect to constraints, for instance in the manipulated variable.

The main disadvantage of model predictive control in this general formulation is that often no offline solution can be obtained, i.e. the optimum input trajectory has to be calculated on-line

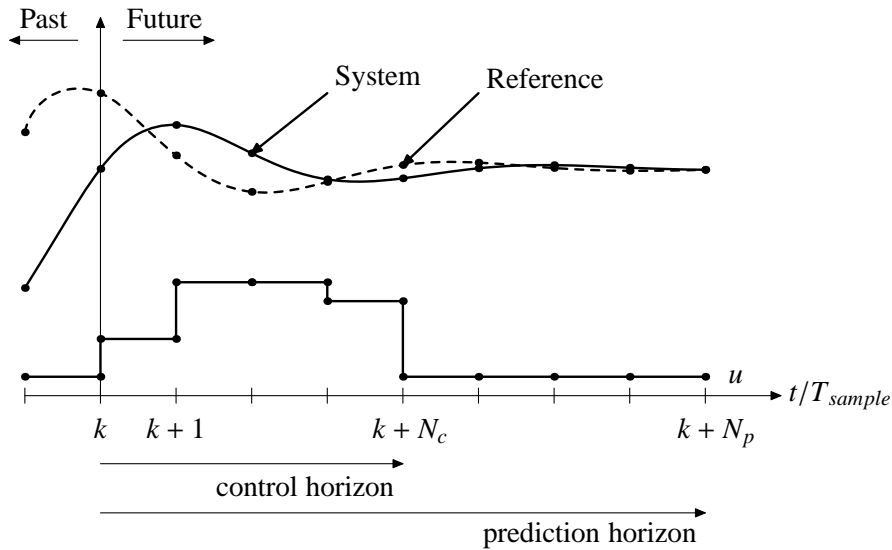


Figure 4.4: Representation of the general idea of model predictive control.

while the process is running. The computational effort stems from two sources: The prediction of the state over the prediction horizon, i.e. the solution of the dynamic process equations. The prediction horizon is chosen such that all time-scales in the process are sufficiently resolved. The second source is the solution of the optimisation problem which is often the crucial part.

In the present formulation the determination of model predictive control schemes necessitates the calculation of the optimum input trajectory u_{opt} for all times $t \in [t_0, t_0 + T]$, which poses an optimisation problem with an infinite number of decision variables. In order to reduce the computational effort a control horizon shorter or equal to the prediction horizon is chosen and assumptions on the input trajectory are posed to limit the number of decision variables in the optimisation.

In almost all practical implementation a time-discrete formulation of the model predictive control scheme is used: Here, time is discretised by a sampling time T_{sample} . The prediction horizon and the control horizon are chosen as integer multiples of the sampling time, for instance a prediction horizon of $N_p T_{sample}$, and a control horizon of $N_c T_{sample}$ with $N_c \leq N_p$ and $N_c, N_p \in \mathbb{N}_+$.

An often used assumption for the input trajectory is that it is piecewise constant over a sampling interval in the control horizon, i.e. $u(t) = u_k(t)$, $t \in [t_k, t_k + T_{sample}]$. If time progresses outside the control horizon, but is within the prediction horizon, then it is assumed that $u(t) = u_{N_c}$, for all $t \in [t_{k+N_c T_{sample}}, t_{k+N_p T_{sample}}]$. Thereby the dimension of the optimisation problem is reduced to N_c decision variables. This setup is depicted in Fig. 4.4. The calculated optimal input trajectory is then implemented to the process for exactly one sampling interval before the algorithm is restarted with the remaining input trajectory as initial guess.

Although in the steps 1–3 of a model predictive control scheme only an open-loop control problem is solved, i.e. no further information of the plant state is used in the calculation of u_{opt} , the complete scheme gives a feedback control system by only applying a portion of the input trajectory and recalculating the input based on the process measurement available at the next sampling time, i.e. the control scheme reacts on changes in the process states.

Formulation for linear time-invariant systems

In the following a linear time-invariant state-space system is considered in a time-discrete setting [15, 146]:

$$x(k+1) = A_m x(k) + B_m u(k), \quad y(k) = C_m x(k). \quad (4.36)$$

Introducing the *increments*

$$\Delta x(k) = x(k) - x(k-1), \quad (4.37)$$

$$\Delta x(k+1) = x(k+1) - x(k), \quad (4.38)$$

$$\Delta u(k) = u(k) - u(k-1), \quad (4.39)$$

$$\Delta y(k+1) = y(k+1) - y(k), \quad (4.40)$$

the following system of equations in *incremental form* can be derived

$$\Delta x(k+1) = A_m \Delta x(k) + B_m \Delta u(k), \quad \Delta y(k+1) = C_m A_m \Delta x(k) + C_m B_m \Delta u(k). \quad (4.41)$$

Solving the output equation for $y(k+1)$ and rearranging the terms an *extended model* can be derived:

$$\begin{bmatrix} \Delta x \\ y \end{bmatrix} (k+1) = \begin{bmatrix} A_m & 0 \\ C_m A_m & I \end{bmatrix} \begin{bmatrix} \Delta x \\ y \end{bmatrix} (k) + \begin{bmatrix} B_m \\ C_m B_m \end{bmatrix} \Delta u(k) \quad (4.42)$$

$$y(k) = \begin{bmatrix} 0 & I \end{bmatrix} \begin{bmatrix} \Delta x \\ y \end{bmatrix} (k). \quad (4.43)$$

Using the incremental model, it can be seen that integrators for the controlled (and measured) outputs are present in the model formulation. In formulating the extended model it has to be verified that it is observable and controllable, otherwise the following steps cannot be performed.

Introducing a new state $z^T = [(\Delta x)^T, y^T]$ the augmented state model can be written in standard form:

$$z(k+1) = A z(k) + B \Delta u(k), \quad y(k) = C z(k), \quad (4.44)$$

where the matrices are obtained by simple substitution.

Choosing the prediction and control horizon as integer multiples of the sampling time T_{sample} , i.e. N_p and N_c , respectively, a state sequence and an output sequence can be defined:

$$z(k|k) = z(k), \quad z(k+1|k), \quad z(k+2|k), \quad \dots, \quad z(k+N_p|k), \quad (4.45)$$

$$y(k|k) = y(k), \quad y(k+1|k), \quad y(k+2|k), \quad \dots, \quad y(k+N_p|k). \quad (4.46)$$

Here the notation $z(k+1|k)$ denotes the state at sampling time $k+1$ given the state information at sampling time k . The notation $y(k+1|k)$ is to be interpreted analogously.

The state sequence, i.e. the state prediction based on the knowledge of the state at sampling time k , can be calculated using the augmented process model:

$$z(k+1|k) = A z(k) + B \Delta u(k) \quad (4.47)$$

$$z(k+2|k) = A z(k+1|k) + B \Delta u(k+1) \quad (4.48)$$

$$= A^2 z(k|k) + A B \Delta u(k) + B \Delta u(k+1) \quad (4.49)$$

$$\vdots$$

$$\begin{aligned} z(k+N_p|k) &= A^{N_p} z(k|k) + A^{N_p-1} B \Delta u(k) + A^{N_p-2} B \Delta u(k+1) \\ &\quad + \dots + A^{N_p-N_c} B \Delta u(k+N_c-1). \end{aligned} \quad (4.50)$$

Similarly, the predicted output sequence can be calculated using the output equation of the augmented model:

$$y(k+1|k) = CAz(k|k) + CB\Delta u(k) \quad (4.51)$$

$$\begin{aligned} & \vdots \\ & \vdots \\ y(k+N_p|k) &= CA^{N_p}z(k|k) + CA^{N_p-1}B\Delta u(k) + CA^{N_p-2}B\Delta u(k+1) \\ & \quad + \dots + CA^{N_p-N_c}B\Delta u(k+N_c-1). \end{aligned} \quad (4.52)$$

The important point is that both sequences can be calculated solely based on the knowledge of the state $z(k|k)$ and the input sequence $\Delta u(k), \dots, \Delta u(k+N_c-1)$. The output sequence over one prediction horizon can be written more concisely as

$$Y = Fz(k|k) + \Phi\Delta U, \quad (4.53)$$

where the vectors Y and ΔU as well as the matrices F and Φ are created by stacking the equations for all sampling times, i.e.

$$Y = \begin{bmatrix} y(k+1|k) \\ \vdots \\ y(k+N_p|k) \end{bmatrix} \quad \Delta U = \begin{bmatrix} \Delta u(k) \\ \vdots \\ \Delta u(k+N_c-1) \end{bmatrix}, \quad (4.54)$$

$$F = \begin{bmatrix} CA \\ CA^2 \\ \vdots \\ CA^{N_p} \end{bmatrix} \quad \Phi = \begin{bmatrix} CB & 0 & & 0 \\ CAB & CB & & 0 \\ \vdots & \vdots & \ddots & \vdots \\ CA^{N_p-1}B & CA^{N_p-2}B & & CA^{N_p-N_c}B \end{bmatrix}. \quad (4.55)$$

These results can be used to calculate the optimum input sequence ΔU given a cost functional. The actual solution of the optimisation problem depends on whether constraints are formulated or not.

Unconstrained linear model predictive control

Suppose that the model equations are linear and the cost functional is quadratic, for instance

$$J(\Delta U) = (R - Y)^T(R - Y) + (\Delta U)^T W(\Delta U), \quad (4.56)$$

where W is an input weighting matrix, and R a scaling vector for the reference step trajectory over the prediction horizon, i.e. $r = R\bar{r}$, where \bar{r} is a unit-step signal. If no further constraints apart from the dynamic state equation are present then an analytic solution for the optimum input sequence $(\Delta U)_{opt}$ for each prediction horizon can be obtained.

In most cases it is required that the optimum input sequence $(\Delta U)_{opt}$ minimises the cost functional, i.e.

$$(\Delta U)_{opt} = \arg \min_{\Delta U} J(\Delta U). \quad (4.57)$$

The necessary condition for $(\Delta U)_{opt}$ to be a minimiser of $J(\Delta U)$ is that the partial derivatives of J with respect to ΔU vanish at $\Delta U = (\Delta U)_{opt}$, i.e.

$$\left. \frac{\partial J}{\partial \Delta U} \right|_{(\Delta U)_{opt}} = 0. \quad (4.58)$$

Evaluating the given cost functional $J(\Delta U) = (R - Y)^T(R - Y) + (\Delta U)^T W(\Delta U)$ and using the output equation $Y = Fz(k|k) + \Phi \Delta U$ yields for the optimum input sequence

$$(\Delta U)_{opt} = (\Phi^T \Phi + W)^{-1} \Phi^T (R - Fz(k|k)). \quad (4.59)$$

This expression can be split up into two parts giving:

$$(\Delta U)_{opt} = (\Phi^T \Phi + W)^{-1} \Phi^T R - (\Phi^T \Phi + W)^{-1} \Phi^T Fz(k|k). \quad (4.60)$$

Here the second part of the right-hand side of the equation can be interpreted as state feedback, the first part is a pre-filter that will guarantee a zero steady-state control error. This becomes more explicit if only $(\Delta u)_{opt}(k)$, the actually implemented input, is considered. It can be written as

$$(\Delta u)_{opt}(k) = K_y \bar{r} - K_{MPC} z(k|k), \quad (4.61)$$

and reveals the classical structure of a state feedback controller with a pre-filter for reference tracking. The matrices K_y and K_{MPC} can be obtained from the complete solution over the prediction horizon by taking the first row of the matrices $(\Phi^T \Phi + W)^{-1} \Phi^T R$ and $(\Phi^T \Phi + W)^{-1} \Phi^T F$, respectively.

It can be shown, see for instance Wang [146], that the optimal solution to the linear unconstrained model predictive control problem is equivalent to the LQ-optimal solution over the same finite time-horizon. The advantage of the MPC formulation lies in the decreased mathematical effort that is needed to arrive at this results, for instance no Riccati equation has to be solved. However, special care has to be taken to guarantee the stability of the closed-loop system and will be discussed later.

Constrained linear model predictive control

In many practical applications constraints are present, for instance

- *input constraints*, e.g. $u_{min} \leq u(k) \leq u_{max}$
- *slope constraints*, e.g. $(\Delta u)_{min} \leq \Delta u(k) \leq (\Delta u)_{max}$,
- *output constraints*, e.g. $y_{min} \leq y(k) \leq y_{max}$, or
- *bandwidth constraints*, e.g. $y_{min}(k) \leq y \leq y_{max}(k)$.

It is also possible to formulate *state constraints*, e.g. $z(k) \in \mathbb{Z}, \forall k$, where \mathbb{Z} is a suitably defined portion of the state space, for instance the region in state space where all states are non-negative.

The constraints are incorporated into the optimisation problem as equality or inequality constraints. If the model equations are linear and

- the cost function is quadratic and no constraints are present, then the optimal solution for the control law can be calculated explicitly offline and is equivalent to linear-quadratic optimal control;
- the cost functional is quadratic and the constraints are linear in ΔU , then the resulting optimisation problem is a quadratic programme;
- the cost functional is expressed as the 1-norm, i.e. $J(\Delta U) = \sum_{k=1}^{N_p} |J_k|$ and linear constraints are present, then a linear programme is obtained.

The linear and the quadratic programme cannot be solved analytically and therefore have to be solved on-line by iterative optimisation algorithms. This raises the question of convergence of these algorithms and the computational time necessary to calculate the optimal solution. For linear and quadratic programmes standard numerical algorithms, for instance conjugate gradient method, interior point method, or the active-set method are available. A quite general treatment of these methods and their convergence behaviour can be found for instance in Nocedal and Wright [102].

In order to be evaluable, the constraints have to be expressed in terms of the decision variables, i.e. the input sequence ΔU .

Slope constraints of the form $(\Delta u)_{min} \leq \Delta u(k) \leq (\Delta u)_{max}$, can be transformed into $(\Delta U)_{min} \leq \Delta U \leq (\Delta U)_{max}$. This inequality can be split up into two equivalent inequalities, i.e. $-\Delta U \leq -(\Delta U)_{min}$ and $\Delta U \leq (\Delta U)_{max}$. Rearrangement of these equations yields

$$\begin{bmatrix} -I \\ I \end{bmatrix} \Delta U \leq \begin{bmatrix} -(\Delta U)_{min} \\ (\Delta U)_{max} \end{bmatrix}. \quad (4.62)$$

Input constraints of the form $u_{min} \leq u(k) \leq u_{max}$ can be expressed in terms of ΔU by observing that

$$u(k) = u(k-1) + \Delta u(k) = Iu(k-1) + I\Delta u(k) \quad (4.63)$$

and therefor

$$\begin{bmatrix} u(k) \\ u(k+1) \\ \vdots \\ u(k+N_c-1) \end{bmatrix} = \begin{bmatrix} I \\ I \\ \vdots \\ I \end{bmatrix} u(k-1) + \begin{bmatrix} I & 0 & \cdots & 0 \\ I & I & & 0 \\ \vdots & & \ddots & 0 \\ I & I & \cdots & I \end{bmatrix} \begin{bmatrix} \Delta u(k) \\ \Delta u(k+1) \\ \vdots \\ \Delta u(k+N_c-1) \end{bmatrix} = C_1 u(k-1) + C_2 \Delta U \quad (4.64)$$

Splitting up this equation as was done for the slope constraints yields the set of linear inequalities

$$\begin{bmatrix} -(C_1 u(k-1) + C_2 \Delta U) \\ C_1 u(k-1) + C_2 \Delta U \end{bmatrix} \leq \begin{bmatrix} -U_{min} \\ U_{max} \end{bmatrix}. \quad (4.65)$$

Output constraints can be transformed analogously using the output equation and yield

$$\begin{bmatrix} -\Phi \\ \Phi \end{bmatrix} \Delta U \leq \begin{bmatrix} -Y_{min} + Fz(k|k) \\ Y_{min} - Fz(k|k) \end{bmatrix}. \quad (4.66)$$

In general the constraints can be written as

$$M\Delta U \leq N, \text{ with } M = \begin{bmatrix} M_1 \\ M_2 \\ M_3 \end{bmatrix}, N = \begin{bmatrix} N_1 \\ N_2 \\ N_3 \end{bmatrix}, \quad (4.67)$$

where the sub-matrices are given by

$$M_1 = \begin{bmatrix} -C_2 \\ C_2 \end{bmatrix}, \quad N_1 = \begin{bmatrix} -U_{min} + C_1 u(k-1) \\ U_{max} - C_1 u(k-1) \end{bmatrix} \quad (4.68)$$

$$M_2 = \begin{bmatrix} -I \\ I \end{bmatrix}, \quad N_2 = \begin{bmatrix} -(\Delta U)_{min} \\ (\Delta U)_{max} \end{bmatrix} \quad (4.69)$$

$$M_3 = \begin{bmatrix} -\Phi \\ \Phi \end{bmatrix}, \quad N_3 = \begin{bmatrix} -Y_{min} + Fz(k|k) \\ Y_{min} - Fz(k|k) \end{bmatrix} \quad (4.70)$$

Due to the occurrence of $u(k-1)$ and $z(k|k)$ the matrices N_1 and N_3 have to be updated at every sampling time k and therefor the optimisation problem requires an on-line solution.

The cost functional can be expressed as

$$J(\Delta U) = (R - Y)^T(R - Y) + (\Delta U)^T W(\Delta U) \quad (4.71)$$

$$\begin{aligned} &= (R - Fz(k|k))^T(R - Fz(k|k)) - 2(\Delta U)^T \Phi^T(R - Fz(k|k)) \\ &\quad + (\Delta U)^T(\Phi^T \Phi + W)(\Delta U), \end{aligned} \quad (4.72)$$

where the output prediction equation $Y = Fz(k|k) + \Phi \Delta U$ has been used. The first term involving $(R - Fz(k|k))$ is independent of ΔU , so it has not to be considered in the optimisation.

The complete optimisation problem, a quadratic programme, can thus be stated as

$$\min_{\Delta U} J(\Delta U) = \min_{\Delta U} (\Delta U)^T(\Phi^T \Phi + W)(\Delta U) - 2(\Delta U)^T \Phi^T(R - Fz(k|k)), \quad (4.73)$$

$$\text{subject to} \quad M\Delta U \leq N(k). \quad (4.74)$$

The solution to this quadratic programme gives the required control law. Due to the constraints the resulting controller is *non-linear*, i.e. the closed-loop system is a non-linear dynamic system.

The question whether this optimal control law calculated over a finite time horizon stabilises the closed-loop system is dealt with next.

Stability of the closed-loop system

Stability analysis of model predictive control systems is a complex task due to possibly non-linear interaction of the dynamic process model, the cost functional and the presence of (non-)linear constraints. In the most general formulation, stability analysis of MPC schemes is still an active field of research.

In the following stability conditions for linear time-invariant time-discrete systems under model predictive control are presented, summarising the ideas and arguments presented in the works of Mayne et al. [96] and Chen and Allgöwer [19].

In the case of *unconstrained* MPC with the dynamic model and the cost functional given by

$$J(\Delta U) = \sum_{k=1}^{N_p} [z(k)^T Qz(k) + (\Delta u(k))^T W(\Delta u(k))], \quad (4.75)$$

$$z(k+1) = Az(k) + B\Delta u, \quad (4.76)$$

$$y(k) = Cz(k), \quad (4.77)$$

and the optimal input trajectory over the prediction horizon given by $(\Delta U)_{opt}$, three equivalent ways exist to investigate the stability of the closed loop:

Closed-loop eigenvalues. As was derived, the control law in the unconstrained case can be expressed explicitly in terms of the reference signal and a state feedback:

$$(\Delta u)_{opt}(k) = -K_{MPC}z(k) + K_y \bar{r}. \quad (4.78)$$

Inserting the control law into the dynamic equation yields the closed-loop dynamic equation:

$$z(k+1) = (A - BK_{MPC})z(k) + BK_y \bar{r}. \quad (4.79)$$

The time-discrete system is stable if all eigenvalues of $(A - BK_{MPC})$ satisfy the condition

$$|\lambda_i(A - BK_{MPC})| < 1, \quad i = 1, \dots, n, \quad (4.80)$$

i.e. all n eigenvalues of the closed-loop system have to lie in the interior of the unit circle in the complex plane. As the controller gain K_{MPC} can be calculated explicitly given the design matrices, this condition can be checked offline. If the condition is not satisfied, then the design matrices have to be modified until the eigenvalues all lie in the interior of the unit circle.

Infinite prediction horizon. Drawing from the equivalence of the unconstrained MPC solution to the linear-quadratic optimal control, by choosing a prediction horizon that is large enough, in the limit $N_p \rightarrow \infty$, a stable closed-loop system is obtained, provided that Q is positive definite and the matrix pair $[A, Q^{1/2}]$ is observable. In a practical computation of $J(\Delta U)$ the requirement of $N_p \rightarrow \infty$ poses the problems that only a finite number of calculations can be carried out in a finite time; additionally an internal overflow can occur in the summation, for instance if the process is unstable, rendering the cost functional useless.

Terminal weight. The introduction of a terminal weight into the cost functional to guarantee closed-loop stability also draws from the similarity of unconstrained linear MPC to LQ-optimal control.

The terminal weight \bar{Q} is introduced as

$$J(\Delta U) = \sum_{k=1}^{N_p-1} \left[z(k)^T Q z(k) + (\Delta u(k))^T W(\Delta u(k)) \right] + z(N_p)^T \bar{Q} z(N_p), \quad (4.81)$$

and is calculated such that the following condition holds:

$$\begin{aligned} \sum_{k=1}^{\infty} \left[z(k)^T Q z(k) + (\Delta u(k))^T W(\Delta u(k)) \right] &= \sum_{k=1}^{N_p-1} \left[z(k)^T Q z(k) + (\Delta u(k))^T W(\Delta u(k)) \right] \\ &+ \sum_{k=N_p}^{\infty} \left[z(k)^T Q z(k) + (\Delta u(k))^T W(\Delta u(k)) \right] \quad (4.82) \\ &= \sum_{k=1}^{N_p-1} \left[z(k)^T Q z(k) + (\Delta u(k))^T W(\Delta u(k)) \right] \\ &+ z(N_p)^T \bar{Q} z(N_p), \quad (4.83) \end{aligned}$$

i.e. the terminal weight accounts for all cost on the infinite time horizon $[N_p, \infty) T_{sample}$ that is not dealt with explicitly in the cost functional and thus avoiding the problem of time restrictions and overflow in the computation of $J(\Delta U)$. For the actual computation of \bar{Q} a Lyapunov equation can be derived, details are given for instance in Mayne et al. [96].

Although all three methods are equivalent, the idea of a terminal weight proves the most useful in stability analysis of *constrained* linear model predictive control. As the controller in general is no longer linear, due to the presence of constraints, the closed-loop system is non-linear, i.e. for stability analysis non-linear methods have to be applied.

The general approach is to consider the optimal cost functional, i.e. $J_{opt} = J((\Delta U)_{opt})$, as a candidate for a Lyapunov function [19, 96]. If J_{opt} is positive definite, which is satisfied if Q is positive definite or $[A, Q^{1/2}]$ is observable, the terminal weight is chosen such that J is equivalent to the infinite-horizon cost, and $(\Delta u)_{opt}(k)$ satisfies the constraints of the optimisation problem at $k + 1$, then J_{opt} is non-increasing along the state trajectory of the closed-loop system, i.e.

$$J_{opt}(k+1) - J_{opt}(k) \leq - \left[z(k)^T Q z(k) + (\Delta u)^T(k) W(\Delta u)(k) \right] \leq 0. \quad (4.84)$$

Table 4.1: Process parameters for the continuous spray granulation process

Initial bed mass [kg]	m_{bed}	10.0
Reference bed mass [kg]	$m_{bed,set}$	10.0
Mass flow of nuclei [kg s ⁻¹]	\dot{M}_{nuc}	5.55×10^{-5}
Mass flow of solid [kg s ⁻¹]	\dot{M}_{solid}	1.38×10^{-2}
Solid mass fraction [-]	x_s	1.0
Solid density [kg m ⁻³]	ρ_s	1440.0
Size of nuclei [m]	ξ_0	0.1×10^{-3}
Screen size upper screen [m]	ξ_u	0.5×10^{-3}
Screen size lower screen [m]	ξ_l	0.4×10^{-3}
Milling diameter [m]	ξ_M	0.35×10^{-3}
Milling diameter (osc.) [m]	ξ_M	0.2×10^{-3}

The particular terminal weight can be chosen as the stabilising solution P of the unconstrained problem on an infinite time horizon, i.e. by LQ-optimal control.

Using this concept, the idea is to choose the prediction horizon large enough that the state is steered into a portion of state space where all constraints are satisfied and remain satisfied. From this time forward the stabilisation task is an unconstrained problem and a stabilising solution exists if the problem is handled as a linear-quadratic optimal control problem for the rest of the time horizon [96]. An important fact used in this reasoning is that the stability of the closed-loop system does not depend on the optimality of the found solution but on the feasibility of the optimisation problem, i.e. whether a solution exists [19].

4.2.5 Feedback control results

In order to stabilise the unstable steady-state number density function in the continuous process the total surface area of all particles, which is proportional to the second total moment μ_2 of the number density function, is used as the controlled output. As the manipulated variable the milling diameter is chosen. For the plant model the population balance derived in Chapter 2.5 with ideal sieves and mill is used. All other process parameters are listed in Tab. 4.1: The milling diameter $\xi_M = 0.35 \times 10^{-3}$ m yields a stable steady-state, the milling diameter $\xi_M = 0.2 \times 10^{-3}$ m corresponds to an unstable steady-state where non-linear oscillations in the number density function can be observed.

Given the analytic expression for the number density function n_s corresponding to the unstable steady-state with a milling diameter $\xi_{M,s}$ and a total second moment $\mu_{2,s}$ the task of the controller is to guarantee $\mu_2 \rightarrow \mu_{2,s}$. That this also implies that $n(t, \xi) \rightarrow n_s(\xi)$ can be motivated as follows: If the process states are observable by the measurement of μ_2 , a result that was shown to hold at least structurally, then to each measurement of μ_2 a unique number density function can be assigned. For $\mu_{2,s}$ this is the steady-state number density function, i.e. by convergence of μ_2 to $\mu_{2,s}$ the number density function in the process comes arbitrarily close to the steady-state distribution.

Although the second moment μ_2 cannot be measured directly, it is assumed in the following that is available and the controllers are evaluated for this ideal measurement. Later this assumption is dropped, and μ_2 is obtained by use of a model-based measurement scheme.

In the following simulations the initial condition shown in Fig. 4.5 is used. It is chosen such that the uncontrolled system yields sustained oscillations in the number density function.

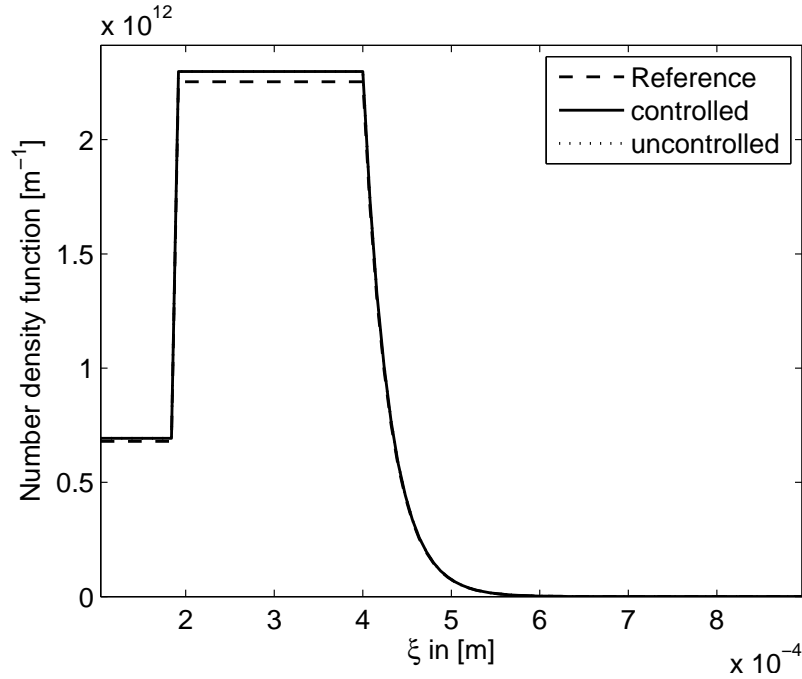


Figure 4.5: Initial condition used in the feedback control simulations. The initial deviation from the unstable steady-state is chosen such that the linear process model is valid.

PI control

The controller transfer function $C(s)$ is calculated on the basis of the transfer function G_{ry} derived from the linearised process model such that the ISE is minimised. The calculation was carried out using the Matlab SISO toolbox and yields

$$C(s) = -1.267 \times 10^{-8} \left(\frac{1 - 2.3 \times 10^3 s}{s} \right). \quad (4.85)$$

This controller is implemented and applied to the non-linear process. In order to calculate the manipulated variable deviation variables have to be used as the inputs to the controller; the result is then a process input expressed as a deviation $\Delta u = \Delta \xi_M$. Adding the corresponding steady-state value $\xi_{M,s}$ yields the control input to the non-linear process.

The results of the application are shown in Fig. 4.6 – Fig. 4.9. There it is immediately observed that the PI controller cannot guarantee $\mu_2 \rightarrow \mu_{2,s}$: The controlled output also oscillates around the steady-state value, albeit with a slightly reduced amplitude. The plot of the manipulated variable reveals sustained oscillations. The snapshots of the number density functions taken at $t_1 = 40$ minutes, $t_2 = 80$ minutes, $t_3 = 120$ minutes, and $t_4 = 160$ minutes show that the errors are due to the large deviations in the milling diameter. However, it is also seen that although the results do not seem satisfactorily they are at least better than in the uncontrolled case. This is exemplified by the plot of the error E_2 (Fig. 4.9) that is defined by

$$E_2(t) = \|n(t, \xi) - n_s(\xi)\|_2 = \left(\int_{\xi_0}^{\infty} (n(t, \xi) - n_s(\xi))^2 d\xi \right)^{\frac{1}{2}}. \quad (4.86)$$

There it can clearly be seen that although the normalised error is quite large it is significantly smaller for most of the time than in the uncontrolled case.

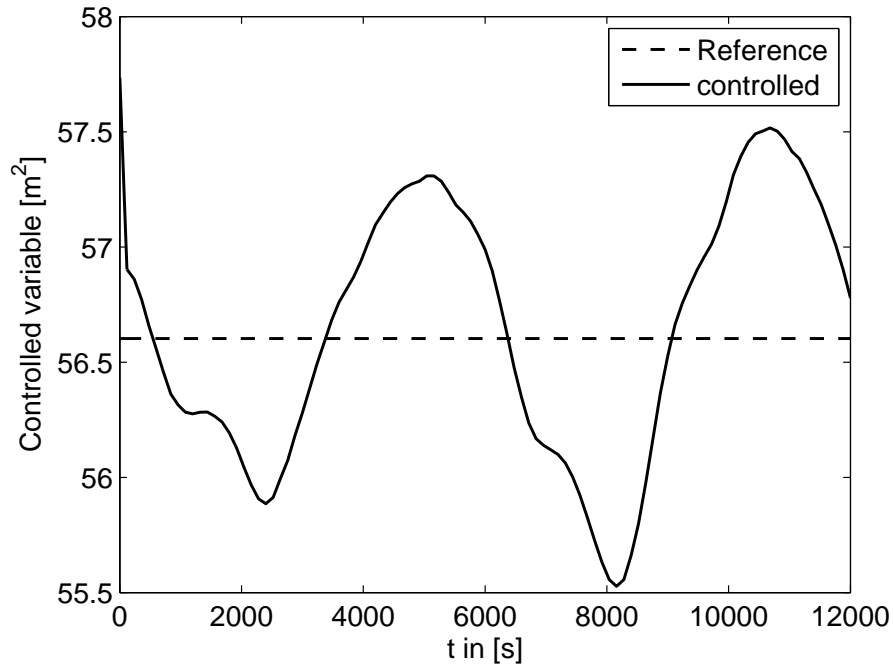


Figure 4.6: Evolution of the controlled output. It can be seen that it oscillates around the required steady-state value and does not converge, i.e. the unstable steady-state number density function is not stabilised. (PI controller)

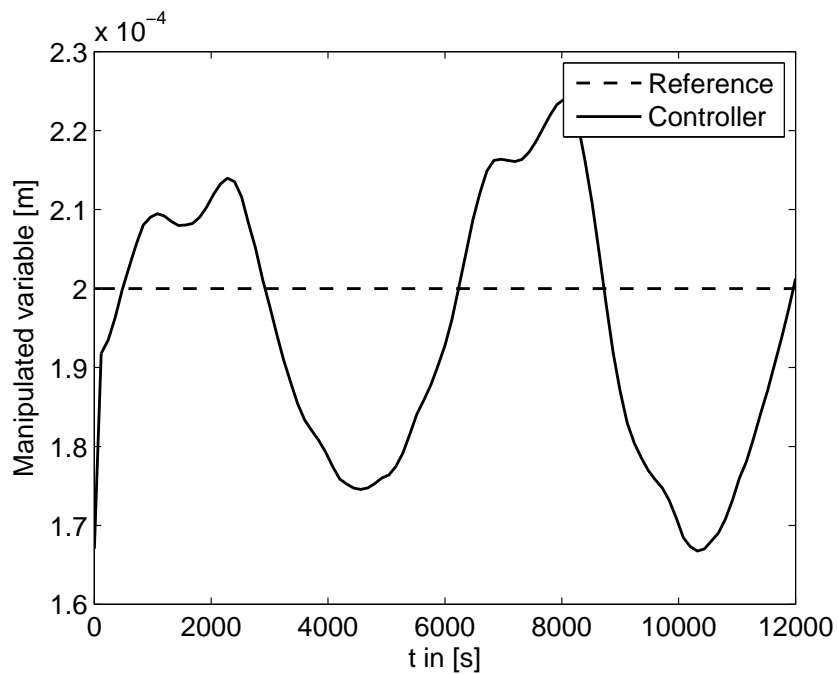


Figure 4.7: Plot of the input to the process calculated by the proportional-integral controller. (PI controller)

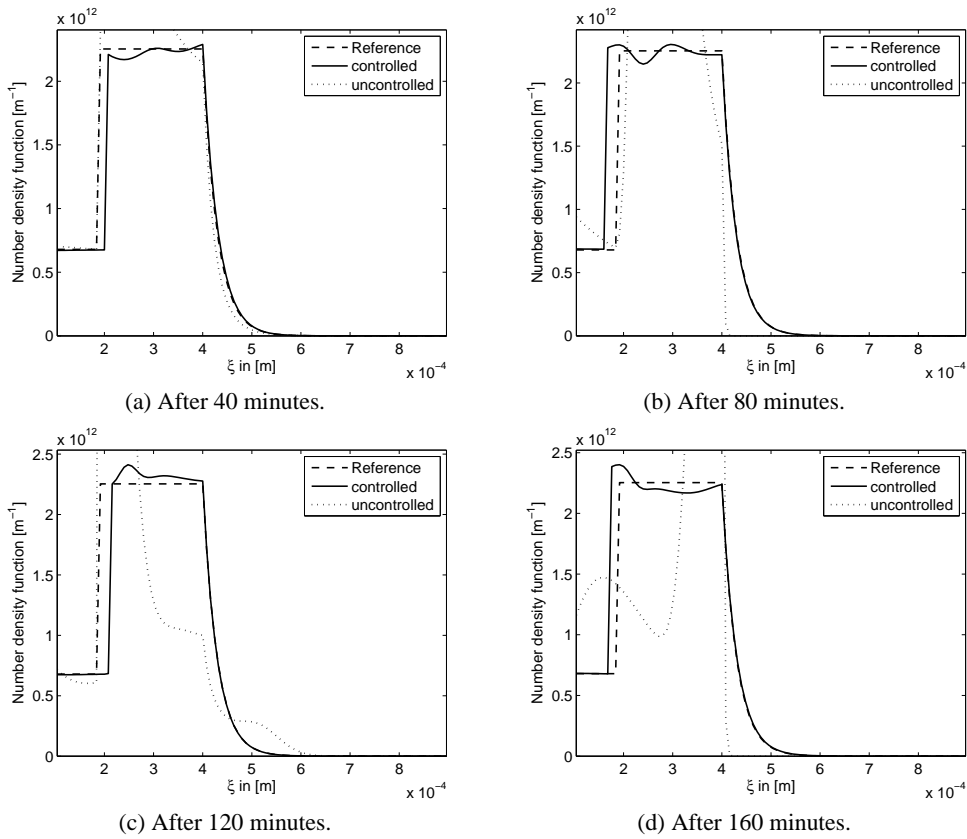


Figure 4.8: Snapshots of the number density function in the fluidised bed under application of proportional-integral control. (PI controller)

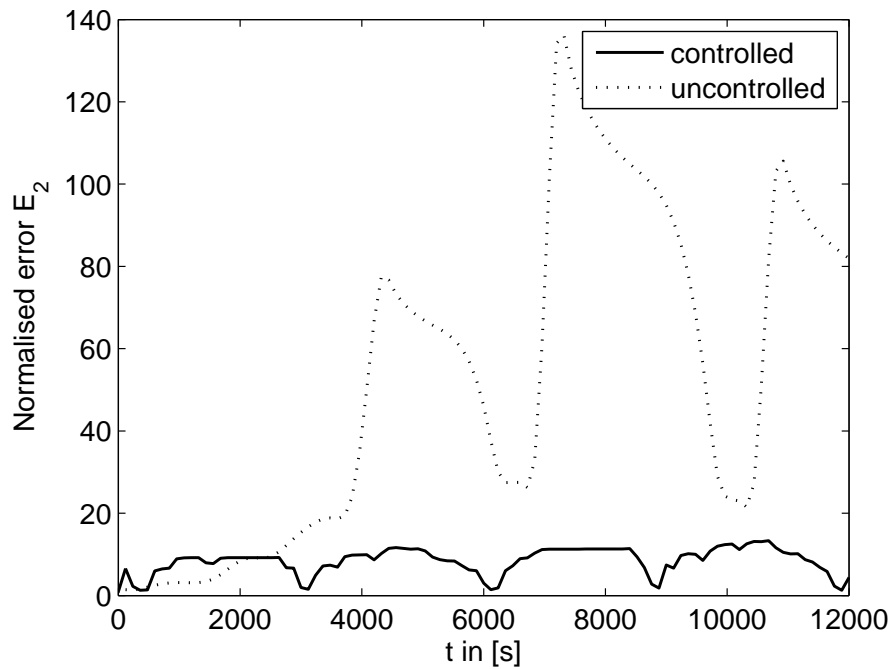


Figure 4.9: Plot of the normalised error of the number density distribution in the process with respect to the desired steady-state distribution. For comparison the open-loop error evolution is also shown. (PI controller)

One possibility to improve the controller performance is to vary the controller gain to speed-up the convergence of the control error to zero. Due to the presence of right-half plane zeros in the plant transfer function, i.e. s^* with $P(s^*) = 0$, this would result in instability of the closed control loop as the poles move for high gains to the locations of the zeros of the transfer function (cf. Appendix E), i.e. some poles of the closed loop will cross the stability boundary, a phenomenon known as *high-gain instability*.

In summary it has to be said that a proportional-integral controller is not able to stabilise unstable steady-states of the continuous fluidised bed granulation process. Instead more advanced output-feedback controller structures, for instance H_∞ -controllers [105] or discrepancy-based controllers [104], or *state feedback controllers* that utilise the complete available information on the process state to calculate the manipulated variables have to be used.

LQ-optimal control

The following linear-quadratic optimal control problem was considered: The cost functional is given by

$$J(u) = \int_0^{\infty} [(Cz(t))^T Q(Cz(t)) + u^T(t)Wu(t)] dt, \quad (4.87)$$

with $Q = 1$ and $W = 10^8$ for scaling of the output magnitude of μ_2 and magnitude of the manipulated variable ξ_M . The state space model derived from the linearisation and a discretisation of the population balance equation was augmented by an output integrator, yielding the augmented state space model

$$\frac{dz}{dt} = Az(t) + B\Delta u(t), \quad y(t) = Cz(t), \quad (4.88)$$

where z and y denote the respective deviation coordinates of the linear model and Δu is the control increment.

The reason why the model is augmented by an integrator for the controlled output is that by the particular choice of the weighting of the states in the cost functional an output feedback is realised. The LQ-controller in its basic form calculates the manipulated variable proportional to the state deviation (measured with respect to zero), i.e there is no integral action that is usually required for a zero steady-state control error. By augmenting the state model integral action is included into the LQ-control formulation. The augmented state model is observable and controllable by the chosen measured output and manipulated output.

From a practical point of view a time-discrete realisation of the controller is of interest, so the model equation and the cost functional were sampled with a sampling time T_{sample} yielding a time-discrete linear dynamic model. The control law

$$\Delta u(k) = -Kz(k) \quad (4.89)$$

was then automatically calculated by the *dlqr* routine (discrete-time linear-quadratic regulator) provided by the Matlab simulation environment and then implemented at the non-linear process.

The results of the application are shown in Fig. 4.10 – Fig. 4.13. There it can be seen that the LQ-controller yields $\mu_2 \rightarrow \mu_{2,s}$: Initially, the system oscillates around the steady-state value but these oscillations are damped out. The snapshots of the number density function in the non-linear process (Fig. 4.12), which are taken at exactly the same times points as in the application of the PI controller, show that the error with respect to the steady-state number density function is decreasing over time, i.e. the unstable steady-state is stabilised by the linear-quadratic optimal

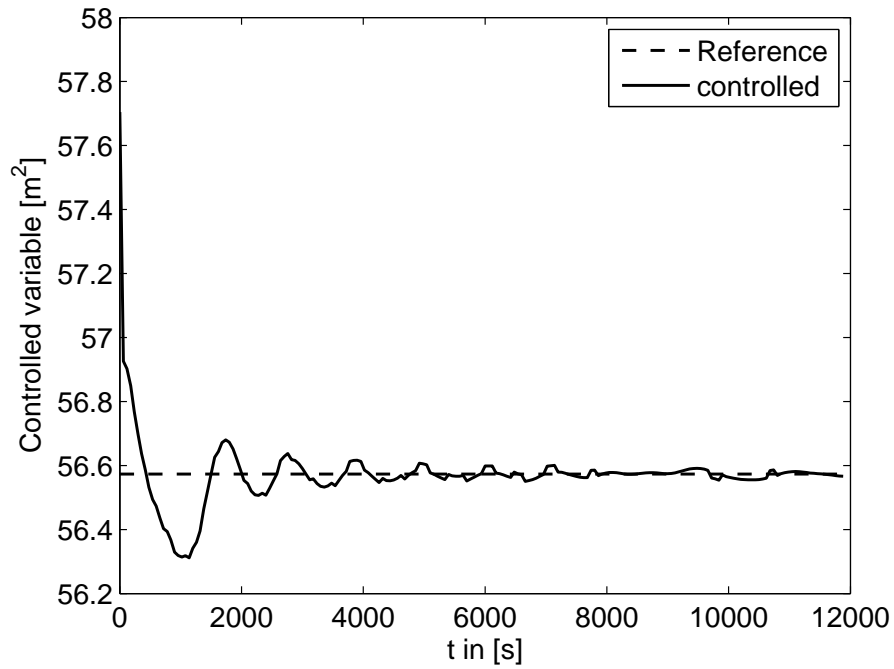


Figure 4.10: Evolution of the controlled output. In contrast to the PI controller the oscillations are damped and the output converges to the reference value. (LQ-controller)

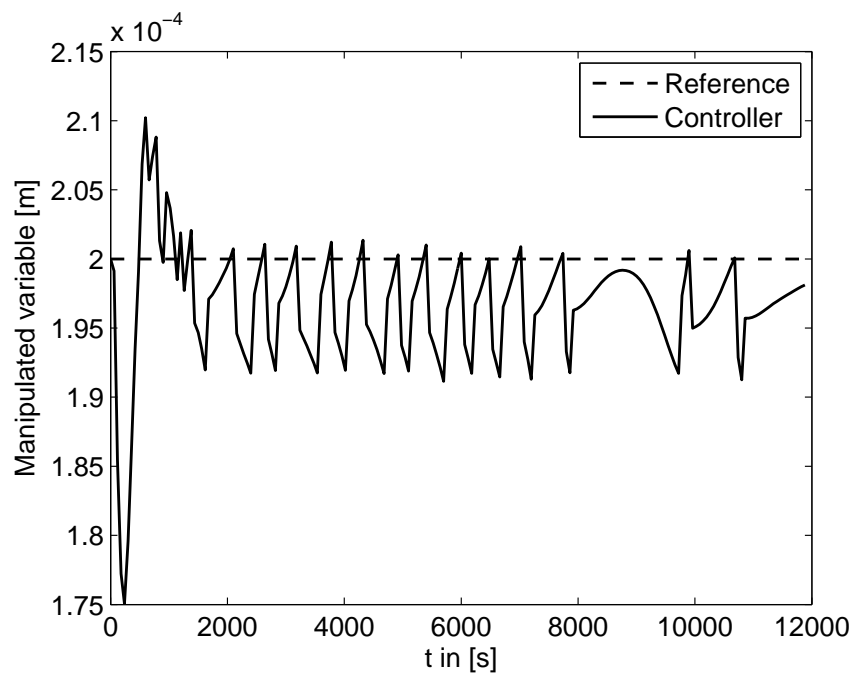


Figure 4.11: Input trajectory calculated by the linear-quadratic optimal control law and implemented in a time-discrete setting. (LQ-controller)

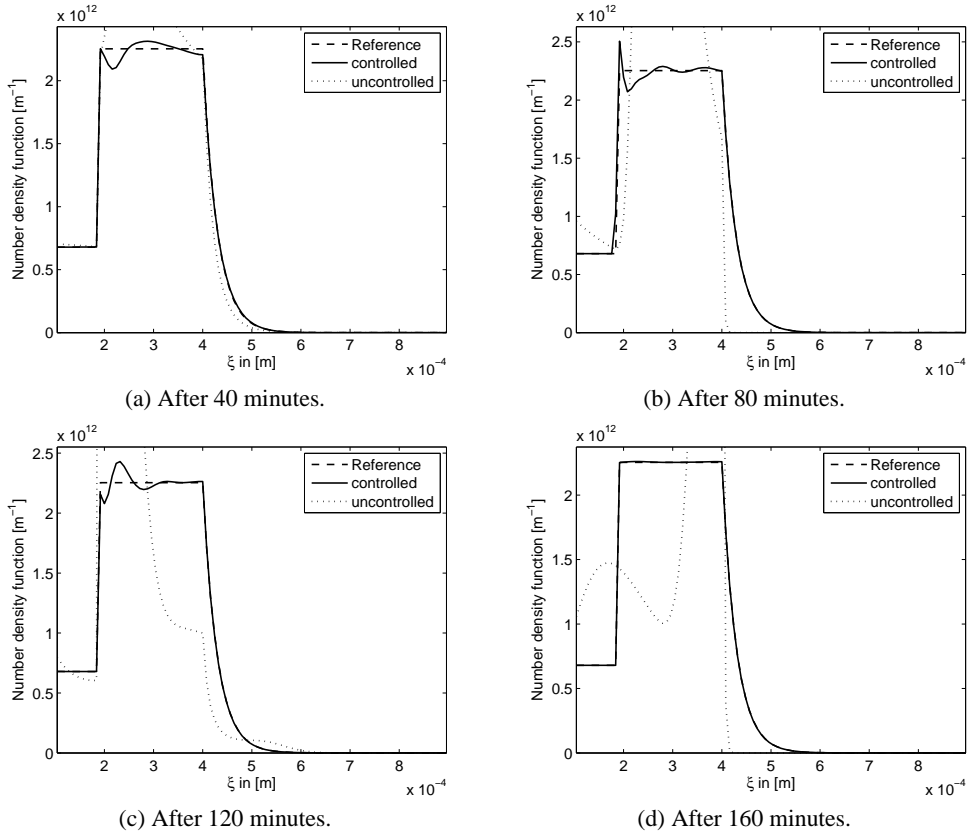


Figure 4.12: Snapshots of the number density function in the fluidised bed under application of LQ-optimal control. (LQ-controller)

controller. This can also be seen in the plot of the error E_2 which decreases over time. The corresponding input trajectory is shown in Fig. 4.11, compared with the PI controller the input oscillates faster but with a much smaller amplitude. The error E_2 (Fig. 4.13) is also significantly smaller, converging almost to zero, i.e. the unstable steady-state can be considered as stabilised.

Model predictive control

For the test of the model predictive controller the augmented time-discrete system is used for controller design. Using the notation introduced in the section on MPC the cost functional is expressed as

$$J(\Delta U) = (R - Y)^T(R - Y) + (\Delta U)^T W(\Delta U), \quad (4.90)$$

Table 4.2: Design parameters of model predictive controller.

Number of discretised states	N	100
Simulation time interval [s]	t_{end}	12000
Sampling time [s]	T_{sample}	60
Prediction horizon	N_p	30
Control horizon	N_c	10
Minimum manipulated variable [m]	u_{min}	0.18×10^{-3}
Maximum manipulated variable [m]	u_{max}	0.22×10^{-3}

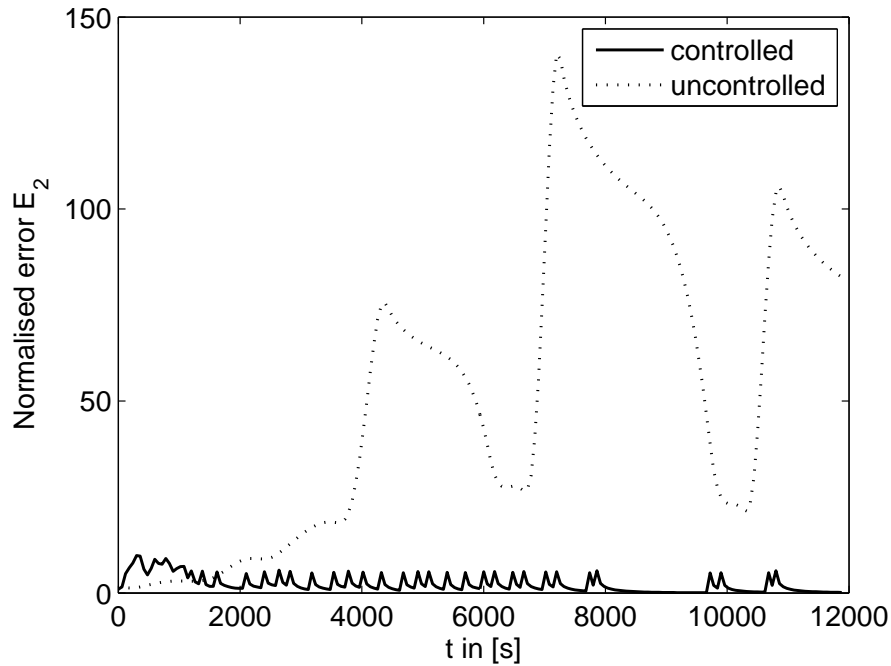


Figure 4.13: Plot of the normalised error of the number density distribution in the process with respect to the desired steady-state distribution. The error converges almost to zero, i.e. a stabilisation of the unstable steady-state is achieved with sufficient accuracy. (LQ-controller)

with W being a diagonal matrix where all diagonal elements are equal to 10^8 . The observability and controllability conditions can be proved to hold structurally as well as numerically at the steady-state. For the calculation of the model predictive controller the prediction horizon and the sampling time have to be chosen. This was done based on the knowledge of the eigenvalues of the matrix A : The prediction horizon was chosen corresponding to the eigenvalue that is nearest to the stability boundary. The control horizon was chosen to be considerably smaller than the prediction horizon in order to keep the dimension of the optimisation problem small (cf. Tab. 4.2).

In case of *unconstrained* model predictive control the optimal control law is calculated as presented in Eq. (4.59). It is then applied to the non-linear process.

As can be seen in the plot of the controlled variable (Fig. 4.14), the total surface area of all particles in the bed, the oscillations in the controlled variable are damped out over time, i.e. $\mu_2 \rightarrow \mu_{2,s}$. The corresponding error in the number density function, represented by the integral measure E_2 (Fig. 4.15), shows that after an initial increase, the error is decreased, i.e. a convergence of the number density function to the required steady-state number density function is achieved. That the error does not vanish totally is due to the fact that only a linear controller is applied to the non-linear process and that this controller only generates new inputs at the beginning of every sampling interval. Errors in the number density function that occur within the sampling interval, where the input is kept constant, are only partially dealt with so that at the end of the sampling interval an increase in the error is possible. However, as can be seen in the snapshots of the number density functions a satisfying control result is achieved. The corresponding input trajectory is shown in Fig. 4.16 and shows a behaviour similar to the linear-quadratic control. The closed-loop poles are shown in Fig. 4.18 where it can be seen that no poles lie outside the stability domain, i.e. the closed-loop system is stable.

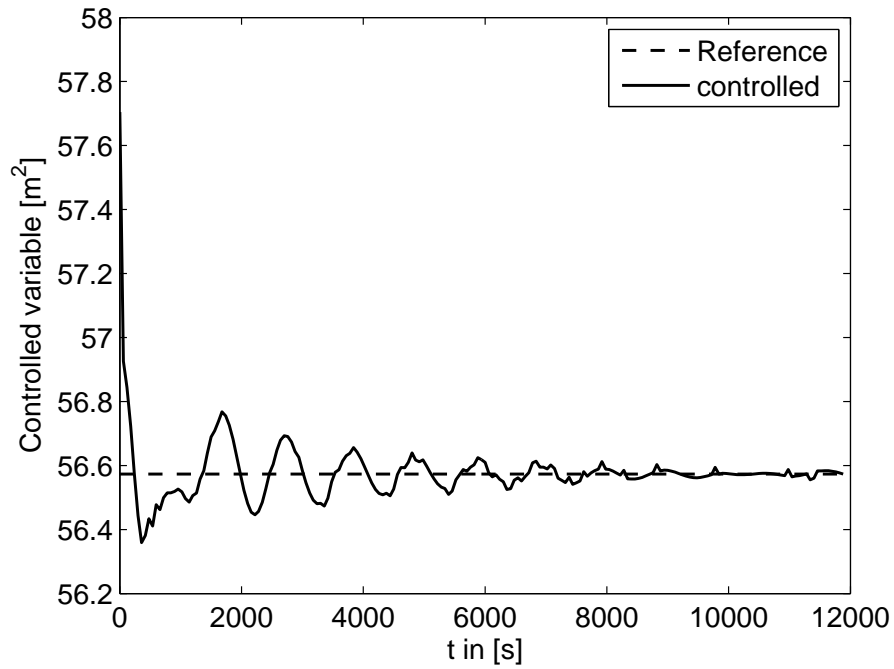


Figure 4.14: Evolution of the controlled output. For the unconstrained model predictive controller a damped response similar to LQ-optimal control is obtained. (MPC, unconstrained)

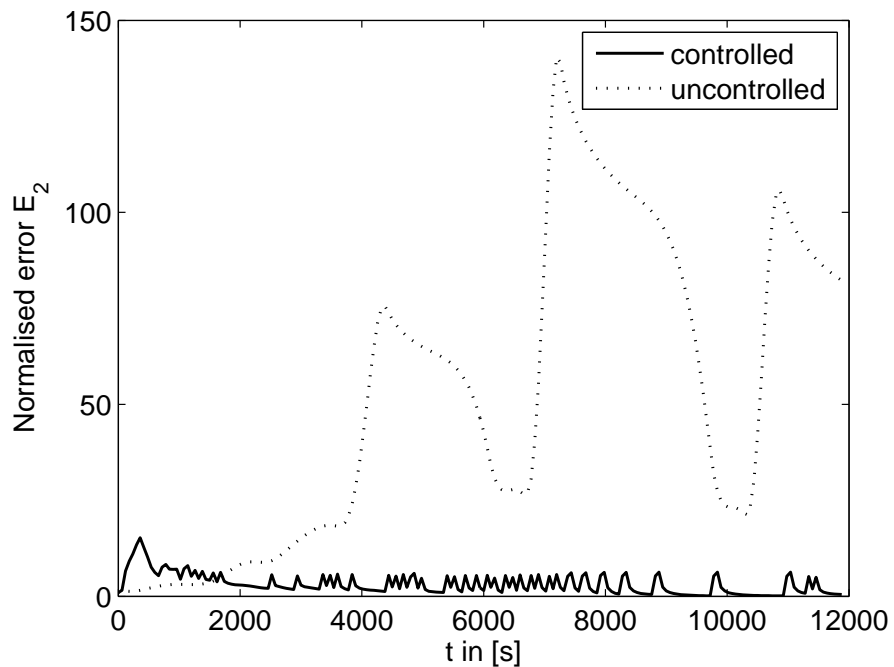


Figure 4.15: Plot of the normalised error E_2 : As it converges to zero, apart from small temporary increases, the steady-state is stabilised by the feedback controller. (MPC, unconstrained)

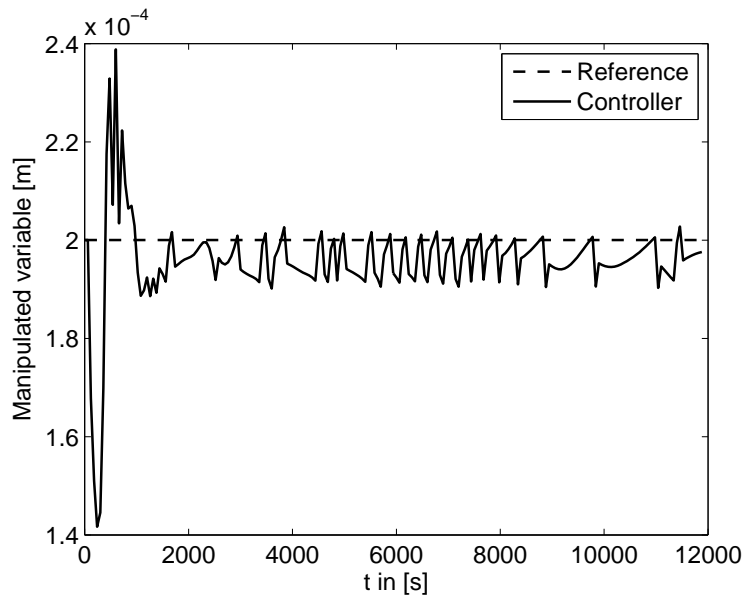


Figure 4.16: Input trajectory calculated by unconstrained model predictive control and implemented in a time-discrete setting. (MPC, unconstrained)

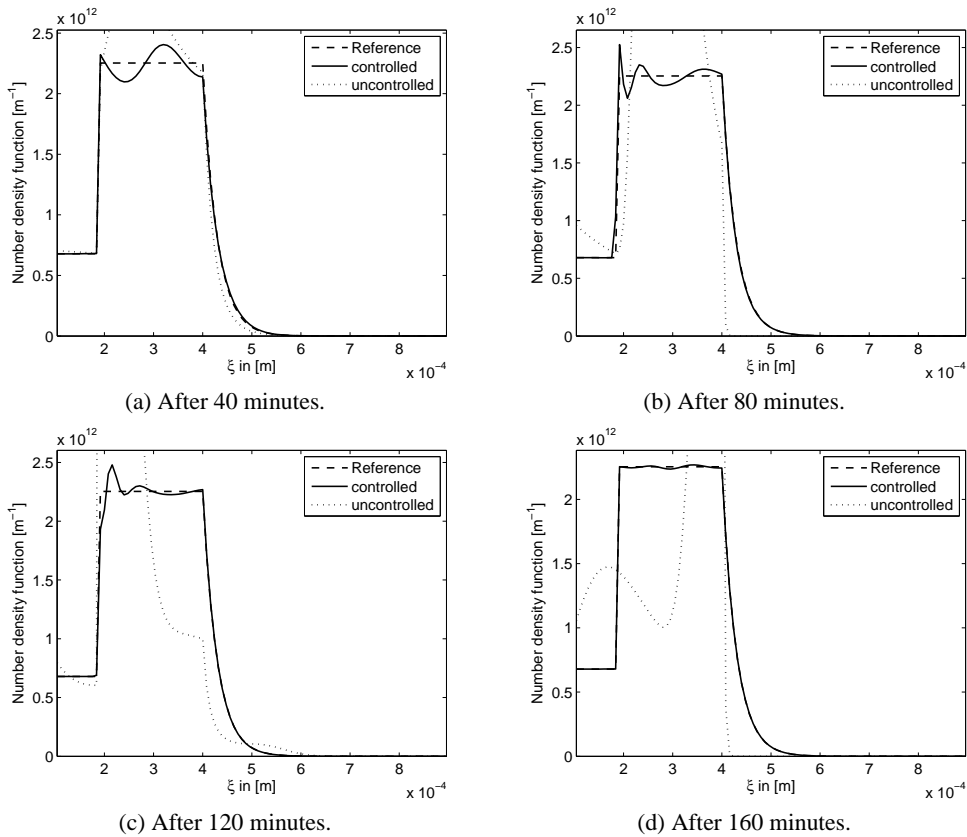


Figure 4.17: Snapshots of the number density function in the fluidised bed under application of unconstrained model predictive control. (MPC, unconstrained)

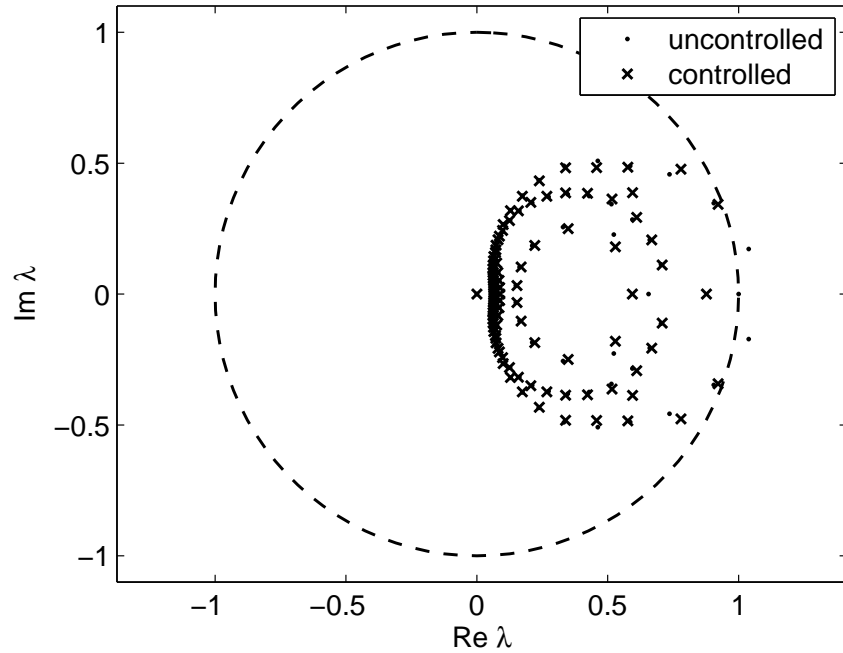


Figure 4.18: Plot of the locations of the open-loop (uncontrolled) process poles and the closed-loop (controlled) poles. The stability domain in a time-discrete setting is given by the interior of the unit circle in the complex plane: All poles of the closed-loop system lie within the stability domain whereas the open-loop poles do not. (MPC, unconstrained)

As an example of *constrained* model predictive control the following scenario is considered: For practical reasons the range of milling diameters is limited, i.e. $\xi_{M,min} \leq \xi_M \leq \xi_{M,max}$, yielding an input constraint for the optimisation problem. All other process conditions are identical to the unconstrained case. Proceeding as described, a quadratic programme with a linear constraint over the prediction horizon is derived. This programme is solved on-line by the Matlab's optimisation algorithm *quadprog* that utilises an active-set strategy [102]. In the formulation of the optimisation programme a terminal weight is used to guarantee closed-loop stability. It is obtained from the solution of the corresponding LQ-optimal control problem presented earlier in this section.

Similar to the unconstrained case, the oscillations in the controlled variable are damped out over time, i.e. $\mu_2 \rightarrow \mu_{2,s}$, as shown in (Fig. 4.19). This observation holds also for the state error E_2 with the limitations highlighted in the unconstrained case (Fig. 4.20).

The corresponding input trajectory is shown in Fig. 4.21; there it can be seen that the manipulated variable stays within the posed minimum and maximum value, in contrast to the unconstrained case.

The snapshots of the number density function show that in the beginning, compared to the unconstrained case, a larger error with respect to the required steady-state is present. This is due to the limitation of the input which becomes active at the beginning of the simulation (cf. Fig. 4.16). If limitations on the input are posed that are too strict, there is the possibility that the steady-state cannot be stabilised. Thus in parallel to the derivation the linear controller has to be extensively evaluated at the non-linear model. The computational effort of the optimisation problem was such that at each sampling time the solution was obtained almost instantaneously, thus no significant delay was introduced into the control loop by the solution of the optimisation problem.

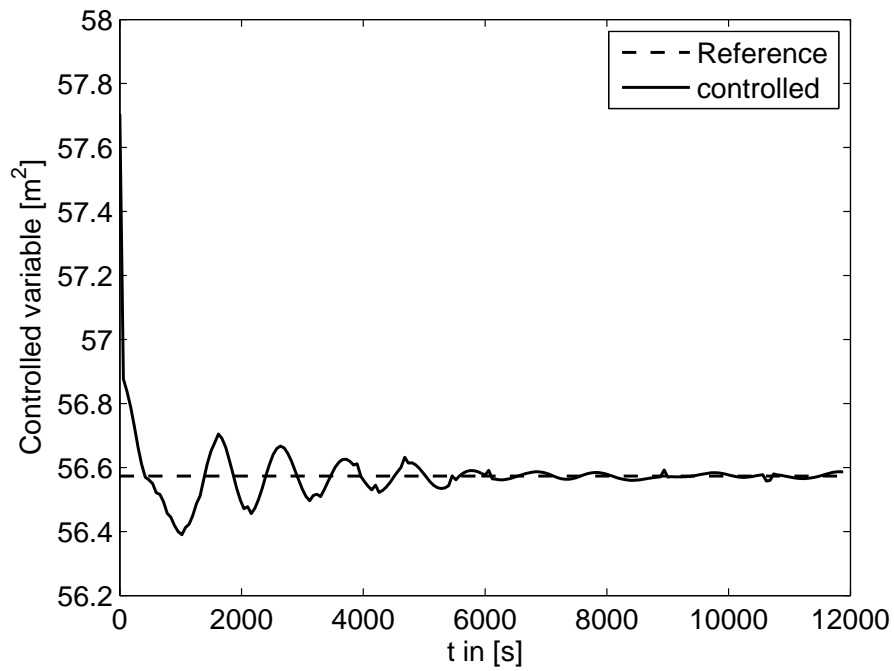


Figure 4.19: Evolution of the controlled output. For the constrained model predictive controller a damped response similar to LQ-optimal control is obtained. (MPC, constrained)

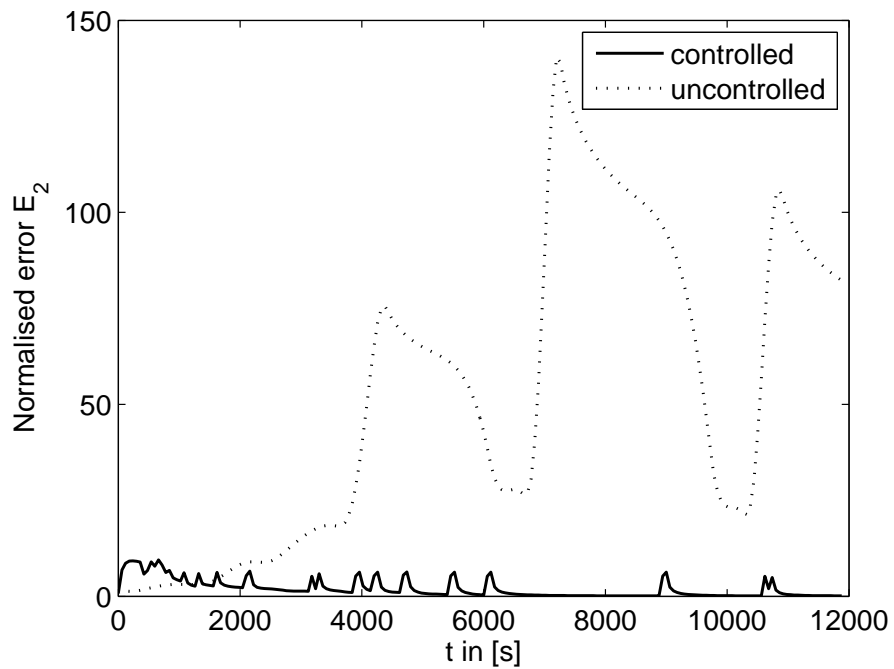


Figure 4.20: Plot of the normalised error E_2 : Despite the input constraints, it also converges to zero, i.e. the steady-state is stabilised by the constrained feedback controller. (MPC, constrained)

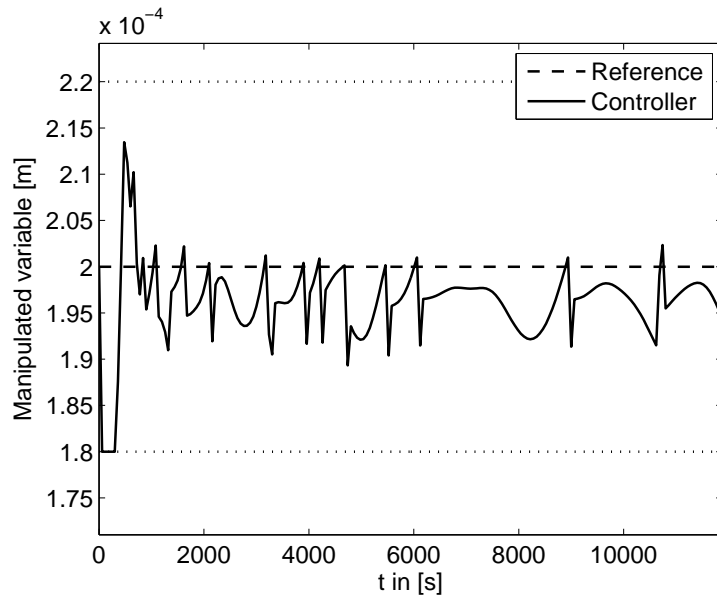


Figure 4.21: Input trajectory calculated by the constrained model predictive controller. The input constraints are shown to be satisfied for all times. (MPC, constrained)

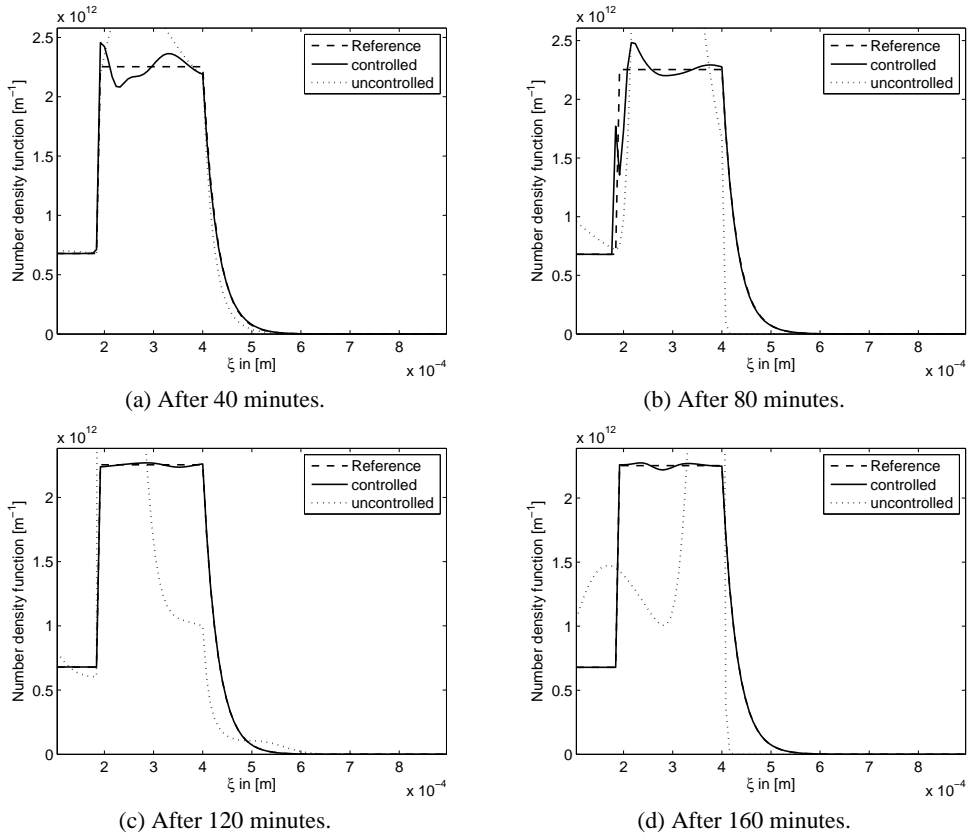


Figure 4.22: Snapshots of the number density function in the fluidised bed under application of constrained model predictive control. (MPC, constrained)

Based on the results presented here the following can be concluded: Although a proportional-integral controller is able to reduce the error in the number density distribution with respect to the uncontrolled case, it is not able to stabilise the unstable steady-state. This can be achieved by application of linear-quadratic optimal or model predictive control. LQ-control and MPC are equivalent in the unconstrained case with respect to the dynamics of the closed-loop system. The advantage of the LQ-controller is that stability of the closed-loop is guaranteed by the design process. The great disadvantage is that no constraints on inputs or outputs can be posed. Model predictive control on the other hand allows for the formulation of constraints that are often present in practical application. But this leads to an optimisation programme that has to be solved on-line in order to obtain the required input trajectory, yielding a non-linear controller. Additionally, the question of closed-loop stability has to be answered separately. Nonetheless, (linear) model predictive control is a powerful tool for the stabilisation of unstable steady-state number density distributions in continuous fluidised bed spray granulation processes with particle re-cycle.

4.3 Feedback control of batch fluidised bed spray granulation

In the previous section the stabilisation of a given unstable steady-state in continuous process has been considered. In this section the control of another important class is investigated: *batch processes*.

In contrast to continuous processes no steady-state can be derived for this task, so the full non-linear behaviour of the process has to be taken into account. Although it is possible to linearise the process dynamics in the vicinity of a given state trajectory, the resulting process dynamics are time-varying and pose a similar complexity.

Using the idea of model predictive control yields, due to the presence of a non-linear process model and a possibly non-linear cost functional and constraints, a non-linear optimisation programme that has to be solved on-line for each sampling interval. The calculation of an optimal control law based on the solution of a non-linear optimisation programme subject to non-linear process dynamics is called *non-linear model predictive control* (NMPC) [4].

Research in NMPC is still active, especially in the fields of stability of the closed-loop system [19], and existence and uniqueness of the calculated solution. These questions are much harder to answer than in the linear case due to the different solution structure of non-linear processes. Another important field of research is the development of new, fast optimisation algorithms for the solution of non-linear programmes. Due to its non-linearity, analytical solution can only be derived in a small number of cases; in all other cases iterative numerical algorithms have to be applied. In order to fulfil the practical constraint that the optimal input must be available at real-time poses a severe requirement on the optimisation algorithms, especially for large-scale systems, i.e. systems with a large number of decision variables or constraints [31, 32].

The scope of this section is limited to an application of non-linear model predictive control to a batch fluidised bed spray granulation process. The process is modelled as described in Chapter 2.4, i.e. a suspension is sprayed onto the fluidised, spherical particles that grow in size (diameter) according to a surface proportional law.

Given an initial number density function at the beginning of the batch, i.e. $t = 0$, the task is to provide a desired distribution at the end of process at time $t = T$ under the influence of process disturbances. Owing to the size-independence of the growth law, it can be derived that arbitrary number density functions cannot be achieved by this process, as the size-independent growth results in a transition of the initial number density function to higher particle sizes. However, this

scenario is of interest, for instance if the initial density function varies from batch to batch. Then the use of the same process parameters will yield different process results at $t = T$.

The main influence on the growth of particles is exercised by the mass flow rate of solid in the spray, $x_s \dot{M}_{sus}$, where \dot{M}_{sus} denotes the total mass flow rate of spray and x_s is the solid mass fraction. The suspension or solution is usually stored in large tanks and is pumped to the process chamber. Due to different effects, for instance partial recrystallisation of the dissolved solid or inhomogeneities in the mixing of the storage tank, the solid content of the spray can vary over process time, or between batches.

The spraying of suspension with a varying solid content will lead to undesired deviations of the number density distribution at the end of the process time $t = T$. For that reason, the solid content is considered as a process disturbance and the task is to control the total mass flow rate in such a way that the desired number density distribution is achieved at the end of the process.

If the solid content is measurable and no error in the position of the initial number density function exists, then the solution to this problem can be given explicitly by

$$\dot{M}_{sus}(t) = \frac{\dot{M}_{sus,des}(t)x_{s,des}(t)}{x_s(t)}, \quad (4.91)$$

where $\dot{M}_{sus,des}(t)x_{s,des}(t)$ defines the necessary solid mass flow rate to achieve the number density function at $t = T$.

However, the disturbance cannot be measured easily, so its deviation from the solid content necessary to reach the desired number density function at $t = T$, $x_{s,des}$, is assumed to be unknown. In order to measure the deviation of the number density function $n(T, \xi)$ from the desired number density function $n_{des}(\xi)$ the following cost functional, a purely terminal weight, is defined:

$$J(u) = \frac{1}{2} \int_{\xi_0}^{\infty} [n(T, \xi) - n_{des}(\xi)]^2 d\xi, \quad (4.92)$$

which is subject to the population balance equation that describes the temporal evolution of the number density function $n(t, \xi)$ under the process input $u = \dot{M}_{sus}$. This input is subject to constraints, i.e. a minimum mass flow rate u_{min} of zero and a maximum mass flow rate u_{max} given by the pump and nozzle used in the plant, i.e. $u_{min} \leq u \leq u_{max}$.

In summary the control task can thus be stated as: Given an initial number density function in the process, a fixed final time T and a desired number density function at that time, an input trajectory is to be calculated such that the defined cost functional is minimised subject to the input constraint and process disturbance.

Due to the unknown character of the process disturbance over process time an open-loop control will not yield sufficient results. For that reason a non-linear feedback control scheme is applied. The principal steps are the same as described in Chapter 4.2.4 with one modification: The fixed time interval $[0, T]$ is divided into N_T horizons of length T_{sample} . Starting with the knowledge or an estimate of the plant state at the beginning of horizon k only the remaining $N_T - k$ horizons are considered in the optimisation programme. This strategy is known as a *shrinking-horizon* and is depicted in Fig. 4.23.

As no further information is available on the process disturbance it is assumed that it remains constant over the remaining time horizon $[k, N_T] T_{sample}$. Thus it is tried by the controller to calculate a one-step optimal control for the remaining process time. This control input is then recalculated for each sub-interval, given the information on the number density function and requires the use of a model-based measurement scheme.

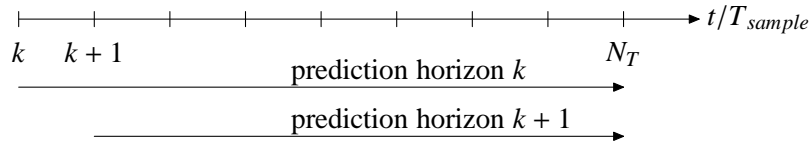


Figure 4.23: Illustration of the shrinking horizon strategy in batch non-linear model predictive control.

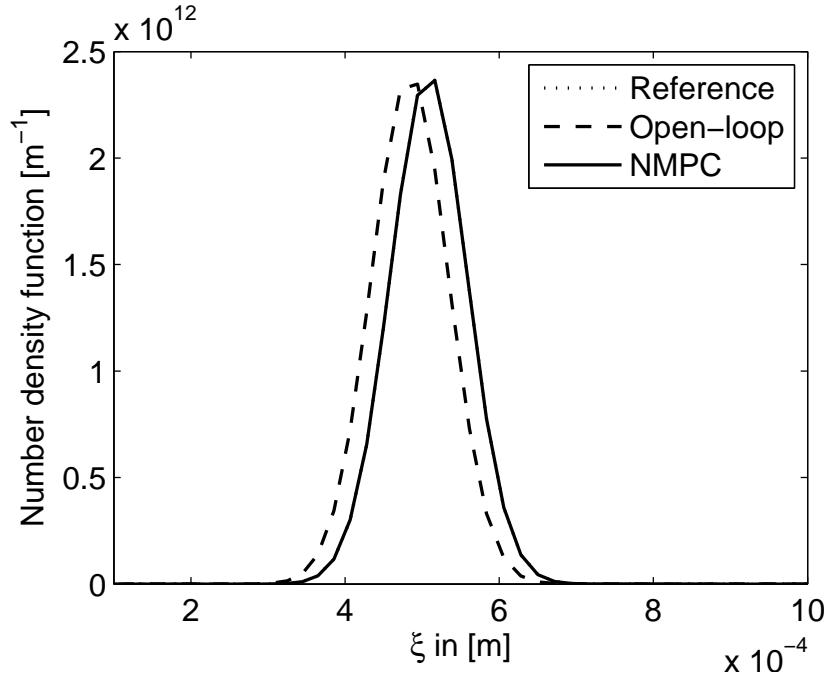


Figure 4.24: Number density functions with and without non-linear model predictive control. The reference is almost indistinguishable from the result obtained by non-linear model predictive control. (Batch, NMPC, after 10000 s)

Assuming that the number density function is exactly measurable, the results in Fig. 4.24 – Fig. 4.26 are obtained: First, starting from a given initial number density function, a final distribution is generated by the population balance model using a constant total mass flow rate and a constant solid content in the suspension. Then for the test of the NMPC scheme, an error in the initial position of the number density function is introduced: The solid content is decreased by ten percent and subjected to stochastic disturbances which are represented by zero-mean Gaussian noise. The optimisation programme is solved using an active-set algorithm provided by the Matlab command *fmincon*.

As can be seen in Fig. 4.24, compared to the open-loop case, a much better process result is achieved, i.e. the use of a non-linear model predictive controller yields an improvement in the process result. Additionally, as can be seen in Fig. 4.25 the input constraint is fulfilled for all times. The calculated input increases gradually towards the end of the process as the time available to compensate for an error is decreasing. This effect depends heavily on the disturbance: If it is too large, a higher total mass flow rate is needed than can be provided; this may then lead to errors in the final number density function, if the missing amount of suspension cannot be balanced over the remaining process horizon.

The total computation time needed to calculate the input trajectory for the remaining process is

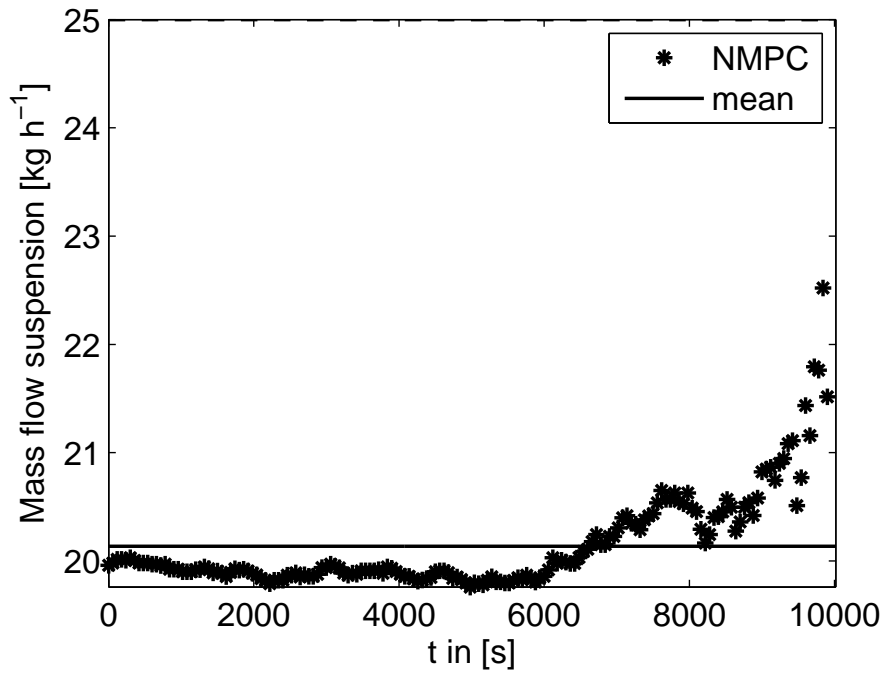


Figure 4.25: Computed optimal control inputs for the batch spray granulation process.

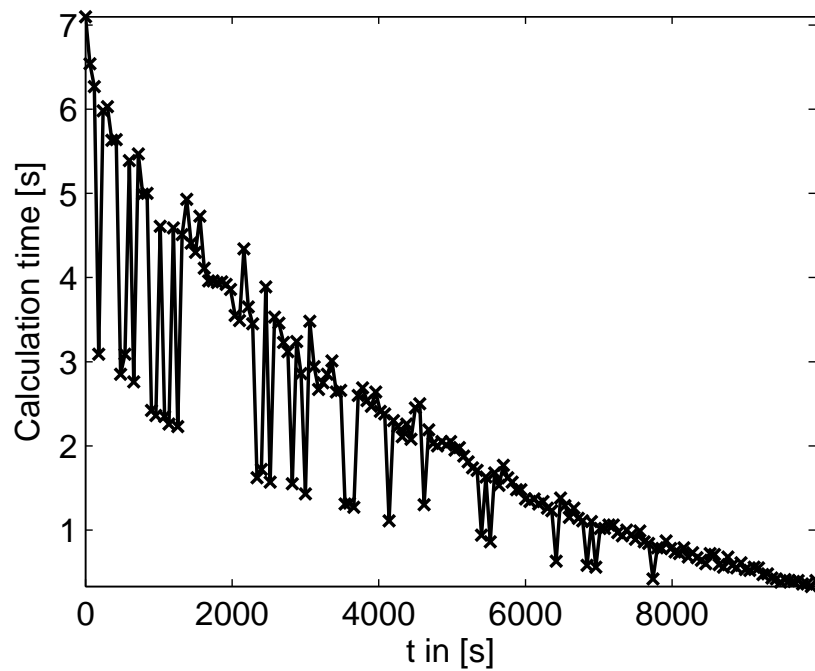


Figure 4.26: Computation time necessary for the calculation of the optimal process input for the remaining batch horizon.

shown in Fig. 4.26. An appropriate choice of sampling time can be derived from this plot: It has to be chosen such that the optimisation programme can be solved well within the sampling interval. The maximum time necessary is often given by the computation time necessary for the whole process horizon, i.e. an appropriate sampling time can be determined iteratively, by solving the optimisation programme for $[0, T]$ and choosing T_{sample} such that the computation time needed for this optimisation is considerably smaller than T_{sample} .

4.4 Feedback control of heat and mass transfer

Up to now only the solid phase of the process has been considered with the focus on the size distribution of the particles. As was motivated in the introduction, other properties, for instance the moisture content and the temperature also have an important influence on the resulting product characteristics. The moisture content and the temperature of the product are determined by the heat and mass transfer processes, i.e. in order to achieve desired product moisture and temperature the heat and mass transfer has to be manipulated, for instance by feedback control.

One way to design a control scheme for the heat and mass transfer could be to use model predictive control. Here, in general it is possible to append the requirements for the states of the heat and mass transfer model to the cost functional and to extend the set of constraints by the corresponding dynamic equations. This approach results in a central controller: One model predictive feedback controller is used for all requirements, i.e. the manipulated inputs for the heat and mass transfer and the particulate phase are computed by one and the same controller.

Although this approach has some appeal due to its simplicity in extending the feedback control, it is in case of the heat and mass transfer only of limited use. The reason for this is that the heat and mass transfer model possesses a much faster dynamics, in the order of seconds, than the particulate phase, in the order of minutes or hours. Also, the mean residence times of the phases vary by several magnitudes. A central MPC controller would thus require a very short sampling time to capture the fast dynamics sufficiently and a long prediction horizon to capture the slow dynamics of the particulate phase.

The control horizon of the central controller then has to be chosen proportional to the fast sampling rate; this necessitates a very often re-solution of the optimisation programme to obtain the input trajectory for all process inputs. Although this is necessary for the states that describe the heat and mass transfer, the large number of input commands is unnecessary – and may be even unrealisable – for the particulate phase. The large number of process inputs over the horizon also increases the complexity of the optimisation programme as each input at a sampling time has to be included as a (vector-valued) decision variable in the optimisation.

This reasoning leads to the use of two decentralised controllers: For instance a model predictive controller for the particulate phase as presented in the last section, and another controller for the heat and mass transfer. Motivated by the differences in the dynamics and the general structure of the model equations, a time-continuous feedback controller is to be designed where the focus lies on practical, linear controller structures.

Using the simplified heat and mass transfer model derived in Chapter 2.8, the following manipulated variables are available: the mass flow rate of spray (with a given solid content), the mass flow rate of fluidisation gas, the mass flow rate of nuclei fed to the system, and the inlet temperature of the gas.

The controlled variables are the mean particle moisture content and the mean temperature of the particles in the fluidised bed process. It will be assumed that these values are measured *in situ*.

The moisture content and the temperature of the fluidisation gas are uncontrolled.

From a process point of view, the mass flow rate of fluidisation gas and the temperature of the gas are suitable process inputs. The mass flow rate of suspension is not suitable as it directly influences the product mass flow which in many applications is required to be constant. The mass flow of nuclei is often hard to realise practically, as it has to be produced separately in an external process.

An analysis of the complete process reveals that it is partially decoupled: The states of the dispersed phase, i.e. the number density function, do influence the states used to describe the heat and mass transfer, i.e. particle moisture content, particle temperature, gas moisture content, and gas temperature. However, in the process model the heat and mass transfer does not influence the growth or other particulate processes in the dispersed phase, i.e. the dispersed phase dynamics is decoupled from the dynamics of heat and mass transfer.

In total, an input-output model for heat and mass transfer can be derived. It is a multiple-input multiple-output (MIMO) model due to the presence of two manipulated inputs (gas flow rate and gas temperature) and two outputs to be controlled (particle moisture content, particle temperature).

As mentioned above, the transition processes of the states of the heat and mass transfer model are fast. In addition to the open-loop stability of the sub-processes it can be assumed that the heat and mass transfer is always in the vicinity of a steady-state, i.e. a linearised model can be used to describe the dynamics sufficiently well.

The linearised model can be represented in Laplace domain by

$$Y(s) = P(s)U(s), \quad (4.93)$$

where Y and U are the Laplace transforms of the process outputs and inputs in deviation variables, respectively, and P is the transfer function matrix relating the two inputs U_1 and U_2 to the outputs Y_1 and Y_2 :

$$\begin{bmatrix} Y_1(s) \\ Y_2(s) \end{bmatrix} = \begin{bmatrix} P_{11}(s) & P_{12}(s) \\ P_{21}(s) & P_{22}(s) \end{bmatrix} \begin{bmatrix} U_1(s) \\ U_2(s) \end{bmatrix}. \quad (4.94)$$

The step responses of the input-output model for a simultaneous step change in the process inputs are shown in Fig. 4.27. There the total responses, i.e. the superposition of both input influences on the individual outputs, are shown. It can be seen that both outputs do not attain the required reference value of one, i.e. the open-loop plant does possess a non-zero steady-state error.

A further analysis shows that a step in the input U_1 also influences the output Y_2 and a step in input U_2 has influence on the output Y_1 , i.e. there is a cross-coupling between the inputs and the outputs. Furthermore, it can be shown that all four transfer functions are stable but the use of feedback control is necessary to attain the required reference values.

In order to devise a control scheme the coupling of the inputs and outputs has to be investigated further. Generally neglecting the coupling in the design process, i.e. setting $P_{12}(s) = 0$ and $P_{21}(s) = 0$, may lead to unsatisfying closed-loop behaviour or even instability of the closed loop. If the coupling is only small then the transfer functions P_{12} and P_{21} may be neglected and controllers designed only for P_{11} and P_{22} may yield acceptable control performance.

For the quantification of input-output coupling in MIMO linear time-invariant models different measures exist: One of them is the *coupling factor* \varkappa [84] which is defined as

$$\varkappa(s) = \frac{P_{12}(s)P_{21}(s)}{P_{11}(s)P_{22}(s)}. \quad (4.95)$$

If the absolute value of this frequency-depending, empirical measure, i.e. $|\varkappa(s)|$, is considerably smaller than one, only a small coupling is present and the plant may be controlled by two separate single-input single-output controllers for the main transfer functions P_{11} and P_{22} .

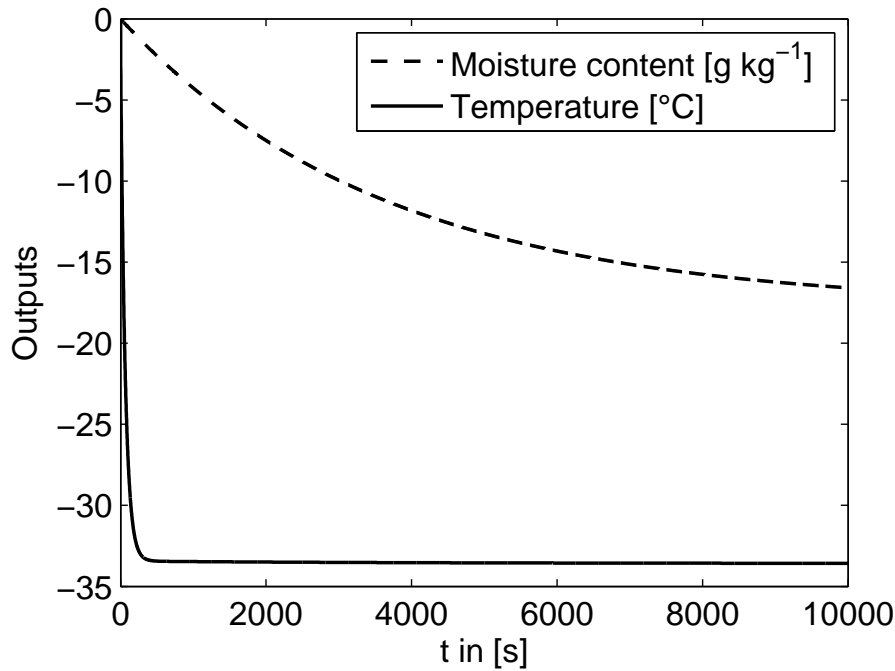


Figure 4.27: Open-loop plant response for a simultaneous positive step change in the mass flow rate of gas and the gas inlet temperature.

For a given linearised model the coupling factor is depicted in Fig. 4.28, showing a value much smaller than one over a very large frequency range, i.e. a controller design neglecting the coupling may yield an acceptable result.

For the design of the single-input single-output controllers the practically accepted proportional-integral controller structure is chosen in order to achieve a zero steady-state error in the closed loop.

The question whether a PI controller structure yields a stable closed-loop behaviour can be answered before the actual design by the so called *Niederlinsky index* K_{SI} :

$$K_{SI} = \frac{\det(P(s=0))}{\prod_i P_{ii}(s=0)}. \quad (4.96)$$

If this index is smaller than zero the use of proportional-integral controllers will yield an unstable closed-loop process regardless of the tuning of the controller parameters. This means that a new combination of manipulated variables has to be found that yields a non-negative value. If the value is positive, then the stability depends on the choice of the controller parameters – the Niederlinsky index is therefore only a sufficient criterion for general MIMO system. However, in case of 2×2 -systems it is also necessary [25].

A calculation of the index for a given transfer function model shows that the use of PI controllers will yield a stable closed feedback control loop.

The PI controllers for the transfer functions P_{11} and P_{22} are denoted by C_{11} and C_{22} , respectively:

$$C_{ii}(s) = K_{p,i} \left(\frac{T_{N,i} s + 1}{T_{N,i} s} \right), \quad i = 1, 2. \quad (4.97)$$

This structure offers two parameters for the design of the closed-loop behaviour, the controller gain K_p and the integral time T_N . The integral time can for instance to be chosen such that the

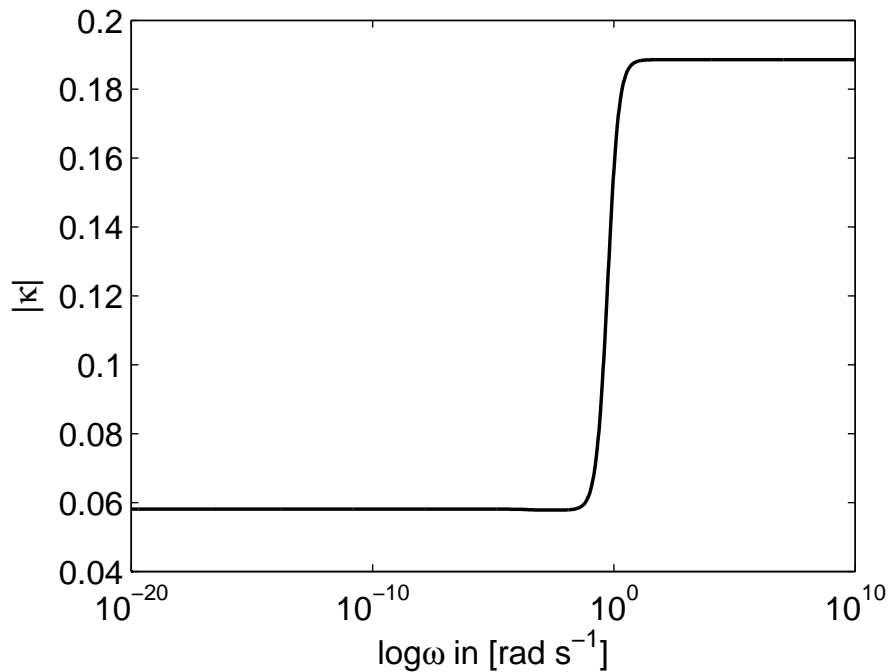


Figure 4.28: Plot of the absolute value of the coupling factor κ , an empirical measure for the coupling of inputs and outputs in multiple-input multiple-output processes.

largest time constant of the plant transfer function is compensated, i.e. the speed of the closed loop is increased, or to give a sufficiently damped step response of the closed loop.

After fixing the integration time constant, the controller possesses one additional degree of freedom: the controller gain. A suitable value can be obtained by use of the root-locus method (see Appendix E).

The designed controllers are then used to build up the overall feedback controller $C(s)$

$$C(s) = \begin{bmatrix} C_{11}(s) & 0 \\ 0 & C_{22}(s) \end{bmatrix} = K_p + K_I \frac{1}{s}, \quad (4.98)$$

with diagonal, constant matrices K_p and K_I . The resulting controller is thus a diagonal proportional integral controller, neglecting the internal coupling of the process inputs and outputs.

Applying this controller to the plant transfer function $P(s)$ yields the closed-loop transfer function

$$Y(s) = \left[(I + P(s)C(s))^{-1} P(s)C(s) \right] R(s) \quad (4.99)$$

For a simultaneous positive step change in both reference values R_1 and R_2 the step responses are depicted in Fig. 4.29. The step changes in the reference inputs are scaled to values that are encountered in practical applications. Whereas the temperature attains the specified reference value fast and smoothly, initially a large undershoot in the step response of the moisture content is observed. This would correspond to a very high drying of particles that are then re-wetted to achieve the reference particle moisture content. Apart from the fact that over-drying of particles is economically inefficient, the re-wetting may also have a significant influence on the consistency of the product. In a worst case a required structure of the product is destroyed by the over-drying and re-wetting, rendering the product useless. It can also be observed that the transition process is rather slow and may be even too slow if the heat and mass transfer is to be controlled in a short-time

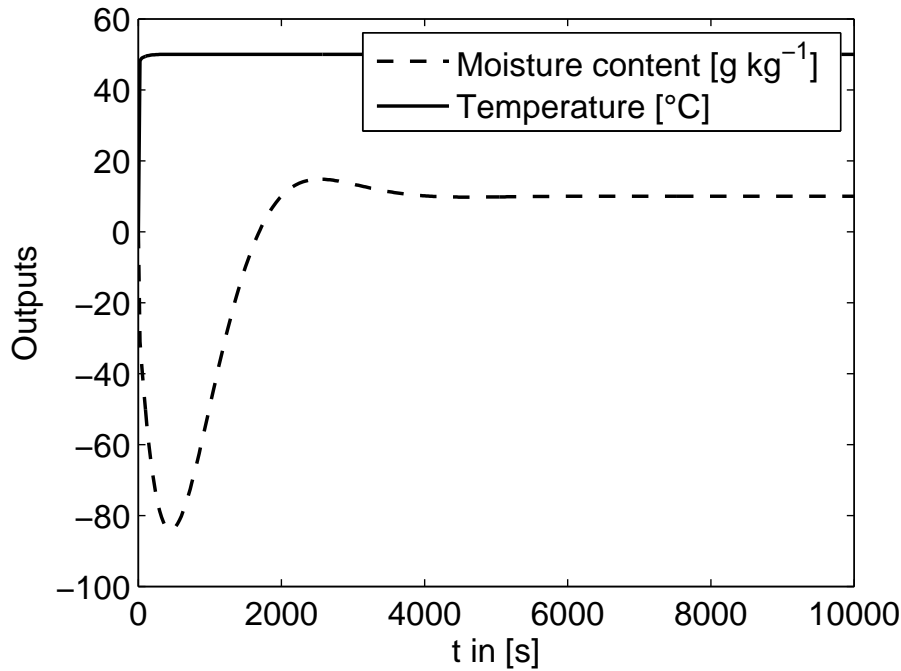


Figure 4.29: Closed-loop response of the process under a diagonal MIMO PI controller, i.e. two separate single-input single-output controllers, for a simultaneous scaled step change in the references.

batch process. Summarising, the designed diagonal proportional-integral controller yields a stable closed-loop system with a zero steady-state error but the transition dynamics are not sufficient.

The consequence of these observations is that the internal coupling of the manipulated variables and the controlled outputs should not be neglected in the design process if a satisfying dynamic behaviour of the closed-loop process is to be achieved.

One approach to improve the performance of the closed-loop is the idea of *decoupling* the multiple-input multiple-output plant, i.e. the plant is augmented by a *decoupling network* $\Xi(s)$ such that the coupling is compensated:

$$P(s)\Xi(s) = \Lambda(s), \quad (4.100)$$

where $\Lambda(s)$ is a diagonal transfer function matrix. To be more precise, instead of ignoring the coupling in the controller design, the input-output behaviour is transformed by the decoupling network in such a way that the new input-output behaviour is equivalent to two decoupled single-input single-output plants.

If the transfer functions of the decoupled plants are denoted by Λ_1 and Λ_2 , two single-input single-output controllers C_i^* , ($i = 1, 2$) can be designed separately. Combining these controllers into a diagonal controller C^* yields for the open-loop:

$$(P(s)\Xi(s))C^*(s) = P(s)(\Xi(s)C^*(s)) = P(s)C(s). \quad (4.101)$$

The new controller C , combining the diagonal controller C^* and the decoupling network Ξ , is a genuine multiple-input multiple-output controller that accounts for the coupling of the inputs and outputs of the process plant.

The practical realisation of this idea is often hindered by the following: In order to compensate the coupling completely, i.e. for all times and input signals, the decoupling network has to be

a dynamic system itself. In combination with the chosen controller structure for the diagonal controller C^* a multiple-input multiple-output controller may result that is not realisable. For that reason the decoupling is often limited to the steady-state, i.e. instead of a dynamic network $\Xi(s)$ a static network $\Xi(s=0) = \Xi_0$ is used throughout.

If the steady-state gain of the plant is given by

$$\lim_{s \rightarrow \infty} P(s) = K_s, \quad (4.102)$$

a suitable choice for a static decoupling network is

$$\Xi_0 = K_s^{-1}, \quad (4.103)$$

yielding at steady-state $s = 0$:

$$P(s=0) \Xi_0 = K_s K_s^{-1} = I = \Lambda, \quad (4.104)$$

i.e. a decoupling of the process inputs and outputs is achieved. For all other times and signals, i.e. $s \neq 0$, the compensation of the coupling will not be perfect, decreasing the performance of the control loop. This has to be accepted if this simple, proportional decoupling network is to be used.

As the decoupling network is only proportional, the resulting multiple-input multiple-output controller C is only a fixed linear combination of the individual controllers C_i^* , i.e. a restriction to standard linear controller structures will yield a MIMO controller that can be practically implemented as a network of standard controllers that are easily available. For example, if the controllers C_i^* are proportional-integral, the MIMO controller C is also proportional-integral.

For feedback control of the heat and mass transfer the steady-state gain K_s is determined for a given steady-state. The static decoupling network is chosen as the inverse of this matrix, yielding a steady-state decoupling of the plant and an approximate decoupling otherwise. For the transfer functions Λ_1 and Λ_2 of the decoupled plant, proportional-integral controllers are designed by the root-locus method, yielding:

$$C_1^*(s) = 120 \left(\frac{3638s + 1}{3638s} \right), \quad (4.105)$$

$$C_2^*(s) = 0.36 \left(\frac{37s + 1}{37s} \right). \quad (4.106)$$

The parameters of the controllers are determined iteratively, starting with the integral time T_N chosen to compensate the largest time constant of the transfer function and a unity controller gain. By iterative refinement of the T_N and the controller gain the root-locus is shaped such that the closed-loop system is stable and a suitable dynamic behaviour is achieved. The diagonal controller C^* can be written as

$$C^*(s) = \begin{bmatrix} 120 & 0 \\ 0 & 0.36 \end{bmatrix} + \begin{bmatrix} 0.033 & 0 \\ 0 & 0.0097 \end{bmatrix} \frac{1}{s} = K_p + K_I \frac{1}{s}. \quad (4.107)$$

The resulting multiple-input multiple-output controller resulting from the combination of this controller with the static decoupling network Ξ_0 can be written as:

$$C(s) = \Xi_0 K_p + \Xi_0 K_I \frac{1}{s}, \quad (4.108)$$

i.e. the structure of the controller is conserved, only the gains of the proportional and the integral part of the controller are modified by the decoupling network.

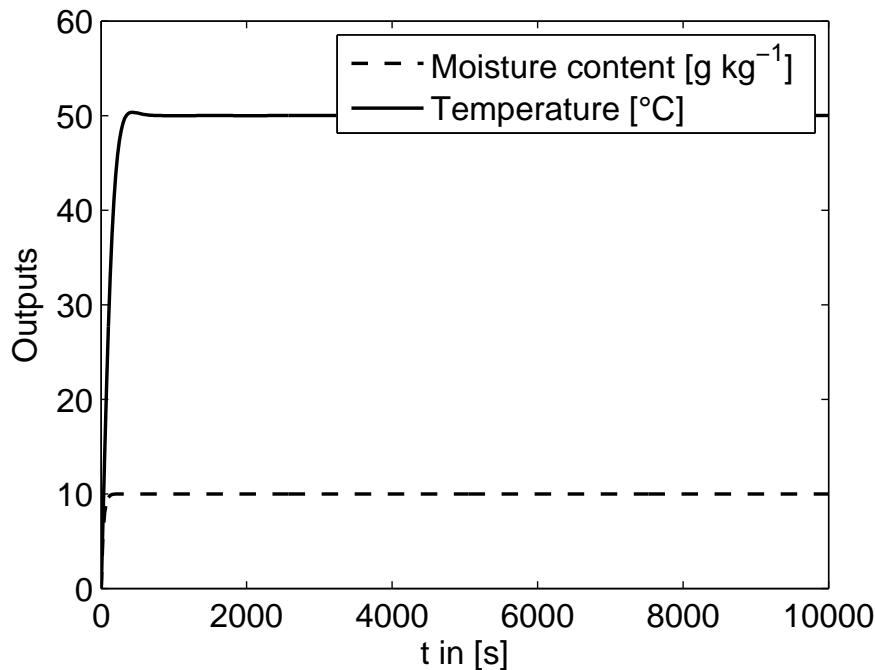


Figure 4.30: Closed-loop response of the process under a MIMO PI controller using a decoupling network for a simultaneous (scaled) step change in the reference values.

The step response of the closed-loop system for a simultaneous positive increase in the references is shown in Fig. 4.30: It can be observed that the temperature reference value is now attained more slowly. The transition is smooth avoiding temperature peaks that may lead to damages in the structure of the particles due to thermal stress induced by a rapid heating of the material. A significant improvement can be observed in the particle moisture content: Using the MIMO controller, no undershoot or overshoot in the moisture content is present. Additionally, the transition period to the reference value is shortened significantly.

The design of the above linear controllers assumes that the manipulated variables can attain any desired value, which is certainly true if the deviation of the process from the steady-state is sufficiently small, i.e. the deviation of the manipulated variables from their corresponding steady-state values is small. In practice, especially if the controllers are applied in processes that are not close to a steady-state, the manipulated variables are subject to actuator constraints, i.e. only a limited range of values for the process inputs can be used or generated.

An application of the linear controllers to the nonlinear heat and mass transfer model, using the parameters listed in Tab. 4.3, is depicted in Fig. 4.31 and Fig. 4.32. There the manipulated variables, the mass flow rate of gas and the gas temperature are restricted: The mass flow rate of gas is limited such that the bed is fluidised, i.e. $u_{mf} < u_g < u_{elu}$. The minimum and maximum gas temperatures are chosen either from practical considerations, for instance the typical power output of an air conditioning device, or safety considerations. The outputs of the controller, i.e. the inputs to the process, are tested for their compliance to the limitations, and are clipped if they do not satisfy the requirements.

Starting with an initially very wet particle and a low particle temperature, obtained from open-loop steady-state simulation, the required particle moisture is set to a significantly lower value whereas the particle temperature is required to be higher. The reason for the specification of a higher particle temperature is given by the thermodynamics of drying: The maximum amount of

Table 4.3: Heat and mass transfer model parameters.

Specific heat capacity water vapour [$\text{J kg}^{-1} \text{K}^{-1}$]	$c_{p,v}$	2000
Specific heat capacity liquid water [$\text{J kg}^{-1} \text{K}^{-1}$]	$c_{p,l}$	4200
Specific heat capacity gas (air) [$\text{J kg}^{-1} \text{K}^{-1}$]	$c_{p,g}$	1000
Specific heat capacity solid [$\text{J kg}^{-1} \text{K}^{-1}$]	$c_{p,s}$	1000
Specific evaporation enthalpy of water [J kg^{-1}]	Δh_{evap}	2.5×10^6
Solid density [kg m^{-3}]	ρ_s	1440
Solid mass fraction suspension [-]	x_s	0.3
Ambient temperature [$^{\circ}\text{C}$]	θ_{env}	20.0
Plant pressure [Pa]	p_{plant}	101300
Reference particle moisture content [(kg water) (kg solid) $^{-1}$]	X_{ref}	0.008
Reference particle temperature [$^{\circ}\text{C}$]	$\theta_{s,ref}$	80

liquid that can be absorbed by the fluidisation gas depends on the temperature of that gas, i.e. at higher gas temperatures more liquid can be absorbed. Requiring a low particle temperature would then require a low gas inlet temperature which would in turn decrease the drying potential. Thus the achievable set of particle moisture contents and temperatures is given by the thermodynamics of the drying process. In order to test the controllers, reference values are chosen that lie within the achievable regions.

In Fig. 4.31 the evolution of the particle moisture contents in the continuous process with external classification and particle recycle under the two designed controllers are shown: Although the diagonal controller acts faster than the controller with decoupling network, it undershoots, i.e. over-dries, the particles and then has to re-wet the material. This is a very slow process as by the inlet gas only a very limited amount of moisture is additionally applied to the process. This results in an almost vanishing steady-state error in the particle moisture content. The feedback controller with decoupling network on the other hand acts more slowly but attains the specified value without over-drying the material.

The discussion also holds for the particle temperatures (Fig. 4.32): Although the purely diagonal controller achieves the reference value faster, it does so by overshooting. Depending on the material in the process the overshoot may induce thermal stress in the structure that may damage the product. Accounting for the coupling of the process inputs and outputs a control result without overshooting is achieved. However, the time necessary to achieve the reference value is increased. This is also linked to the slower, but more accurate control of the particle moisture content. The dynamics of the closed-loop system may be increased by a tuning of the controller gains. But due to the input constraints only a limited improvement may be achieved.

The necessary effort for the design of the two controllers is comparable: In both approaches the task is to design two single-input single-output controllers for two single-loop control plants for instance by the root-locus method. The static decoupling network Ξ_0 can be determined easily from the plant model contributing only a small portion to the design effort.

Focusing on the particle moisture content as the more interesting particle property, the results justify the use of a genuine MIMO controller over simple diagonal controllers that neglect the coupling in the process. If only a fast and accurate control of the particle temperature is needed then the purely diagonal controller, or even just a single-input single-output controller, is sufficient.

In view of the robustness of the controllers, the purely diagonal PI controller is able to compensate for model errors in the main transfer functions for which it is designed. Errors in the coupling terms can only be expected to be compensated partially by feedback as no information on the

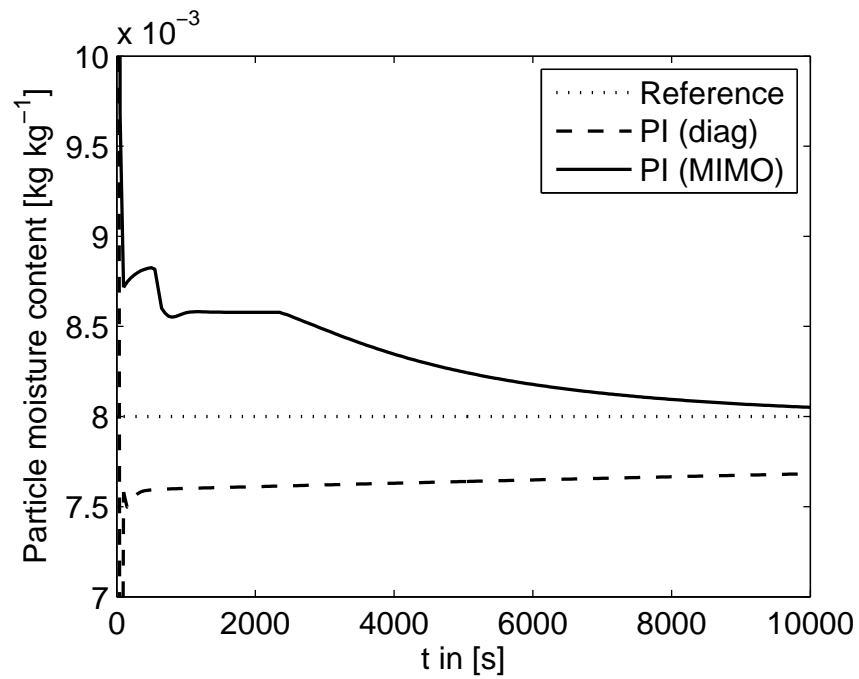


Figure 4.31: Particle moisture content in fluidised bed spray granulation process under two different PI controller structures.

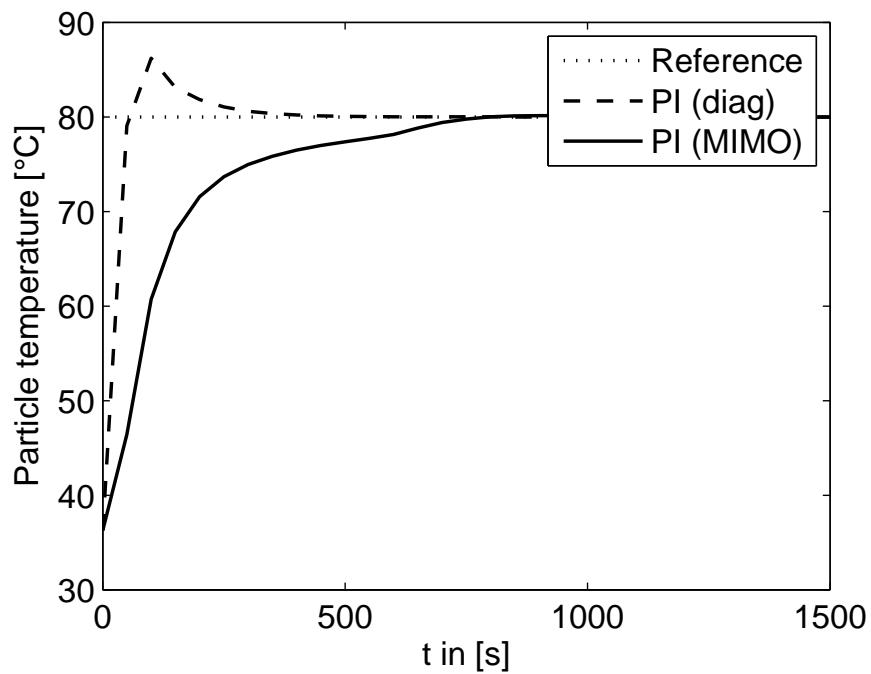


Figure 4.32: Particle temperature in fluidised bed spray granulation using two different PI controller structures.

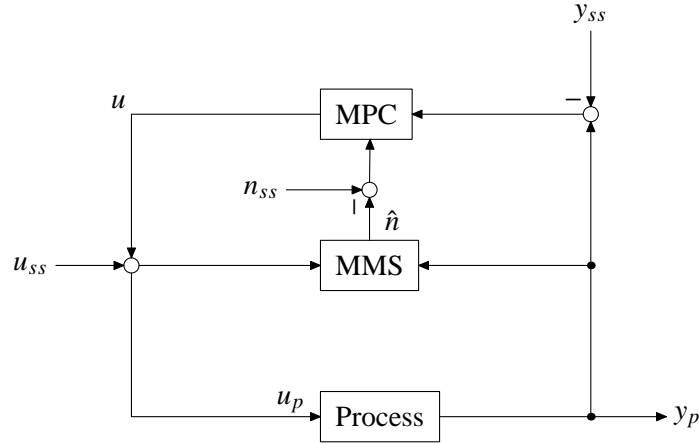


Figure 4.33: Combination of a model-predictive controller and a model-based measurement system to obtain an estimate \hat{n} of the number density function n in the process which is used to calculate the necessary input u_p to the process. The subscript ss denotes steady-state values needed for the application of linear controllers to non-linear processes.

effects is directly available to the controller. The MIMO controller accounts up to a certain degree directly for the coupling in the process and thus an increased robustness with respect to modelling errors can be achieved.

4.5 Model-based control systems for fluidised bed spray granulation processes

In the preceding section feedback controllers for the tasks of controlling the number density functions and the heat and mass transfer in fluidised bed spray granulation processes were designed and tested separately. In this final section both controllers are applied simultaneously to the processes. Furthermore, the number density functions in the processes are reconstructed from practically available process measurements by a model-based measurement scheme. This combination of model-based measurement and feedback control for the number density function is shown in Fig. 4.33 and forms together with the controller for the mean particle moisture and mean temperature a model-based control system for fluidised bed spray granulation processes.

Whereas it is motivated by the structure of the process model that the control of the number density distribution and the heat and mass transfer can be performed almost separately, an open question is whether the combination of the model-based measurement system and the feedback controller yields acceptable results. In general it is difficult to decide whether observers and controllers that are designed separately yield a stable closed-loop system. If the open-loop dynamics of a process is given by

$$\frac{dx}{dt} = f(x, u), \quad (4.109)$$

the error dynamics of a suitably designed model-based measurement system is given by

$$\frac{de}{dt} = \gamma(e, u), \quad (4.110)$$

and the designed controller is implemented using the estimate \hat{x} of the state x , i.e. $u = \varphi(\hat{x})$, the

Table 4.4: Process and design parameters for the batch spray granulation feedback control by non-linear model predictive control.

Initial bed mass [kg]	m_{bed}	10.0
Mass flow of suspension [kg s^{-1}]	\dot{M}_{sus}	1.38×10^{-2}
Solid density [kg m^{-3}]	ρ_s	1440.0
Sampling time [s]	T_{sample}	60

closed-loop dynamics of the model-based control scheme are given by

$$\frac{d}{dt} \begin{bmatrix} x \\ e \end{bmatrix} = \begin{bmatrix} f(x, \varphi(x - e)) \\ \gamma(e, \varphi(x - e)) \end{bmatrix}, \quad (4.111)$$

i.e. a coupled system of non-linear differential equations. General stability results are hard to obtain. The design of a stable model-based control system therefore relies on process knowledge, tuning and the experience of the designer.

In the special case that the process dynamics are linear time-invariant, i.e.

$$\frac{dx}{dt} = Ax + Bu, \quad (4.112)$$

a linear estimator is used with error dynamics given by

$$\frac{de}{dt} = (A - LC)e, \quad (4.113)$$

and a state-feedback controller is given by $u = -K\hat{x}$, the closed-loop dynamics are given by

$$\frac{d}{dt} \begin{bmatrix} x \\ e \end{bmatrix} = \begin{bmatrix} A - BK & BK \\ 0 & A - LC \end{bmatrix} \begin{bmatrix} x \\ e \end{bmatrix}. \quad (4.114)$$

From this equation follows that the closed-loop system is stable if and only if the two sub-systems on the diagonal are stable, i.e. a controller K is designed that stabilises $A - BK$, and an observer L is designed such that the observation error system is stable. A theoretical justification is given by the *separation theorem* [125].

In the following results of the application of the designed model-based control systems, i.e. feedback control of the number density function using a model-based measurement scheme and feedback control of the heat and mass transfer are presented.

4.5.1 Batch fluidised bed spray granulation

For feedback control of batch fluidised bed spray granulation a non-linear model predictive controller is coupled with an infinite-dimensional Luenberger observer that reconstructs quasi-continuously the number density function from measurements of the mean particle size in the spray granulation process (Ch. 3.4, pg. 63). For the control of heat and mass transfer the designed multiple-input multiple-output linear proportional-integral controller using a static decoupling network is used. The process and design parameters are listed in Tab. 4.4 and Tab. 4.3.

The task is as before to steer the number density function towards a given required density function at $t = T$. Additionally, the particles shall have a specified moisture content and temperature at the end of the batch.

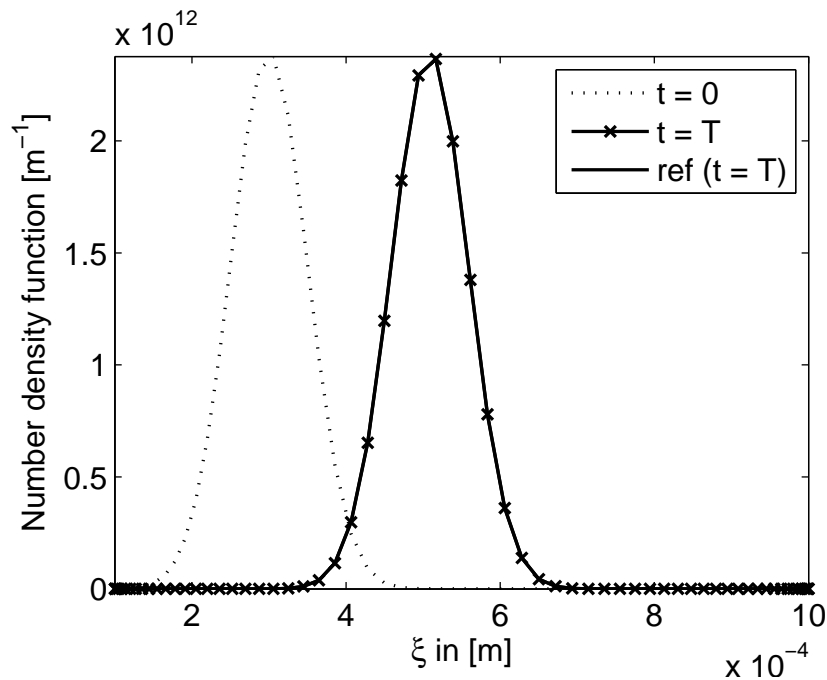


Figure 4.34: Plot of the number density function at the end of the batch process using a model-based control scheme consisting of an infinite-dimensional Luenberger observer, a non-linear model predictive controller for the dispersed phase and a linear MIMO PI controller for heat and mass transfer.

As is shown in Fig. 4.34 the use of the estimated number density function in the calculation of the optimal process input trajectory does not yield a severe degradation of the control result: The desired number density function and the achieved number density function at $t = T$ are almost indistinguishable, although there is an error in the magnitude of the estimated number density function compared to the number density function in the process at $t = T$ as shown in Fig. 4.35.

The control of heat and mass transfer is also not negatively influenced; after a transition period the particles possess the desired mean moisture content and mean temperature. For reasons of comparison the gas moisture content and temperature are also shown in Fig. 4.36 and Fig. 4.37. With varying gas inlet temperature and flow rate the maximum amount of moisture that can be absorbed by the gas, the saturation moisture content Y_{sat} , also varies.

The calculation time needed for one iteration of the control system is shown in Fig. 4.38: It consists of the time necessary to calculate an estimate of the number density function in the process, the solution of the non-linear optimisation programme to obtain the optimal process input and the calculations of the feedback controller for heat and mass transfer. It can be seen that the time needed is significantly smaller than the sampling time of the control system, i.e. a faster-than-real-time implementation is possible. As the main computational effort lies in the solution of the optimisation programme the sampling time can be increased in order to provide a larger time margin. This is possible as the particle growth dynamics are rather slow and the estimate of the number density function and the control of the heat and mass transfer are performed in a quasi-continuous manner.

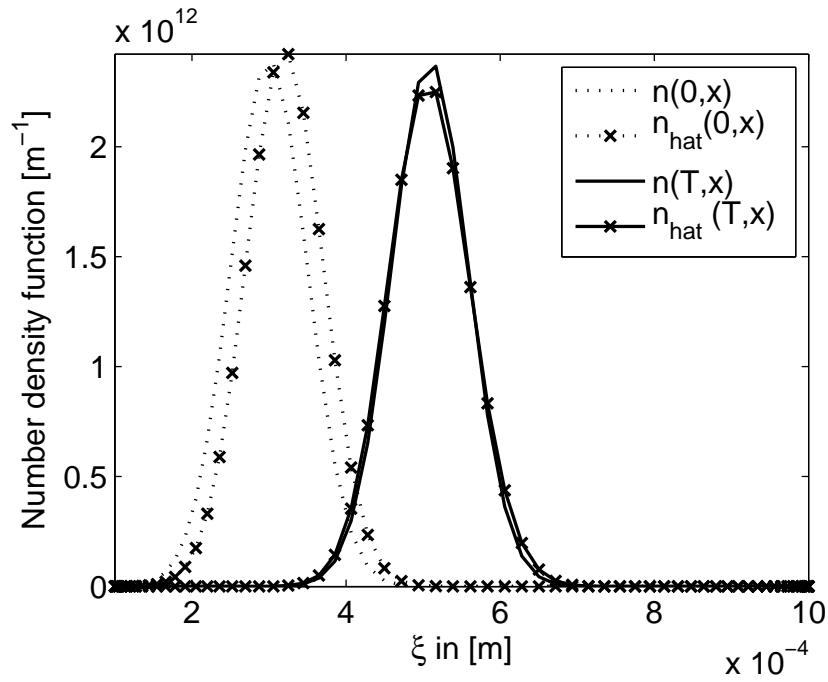


Figure 4.35: Plot of the number density functions in the process and the infinite-dimensional Luenberger observer at the beginning of the batch and at the end. Apart from a slight deviation in the magnitude the profiles are almost indistinguishable.

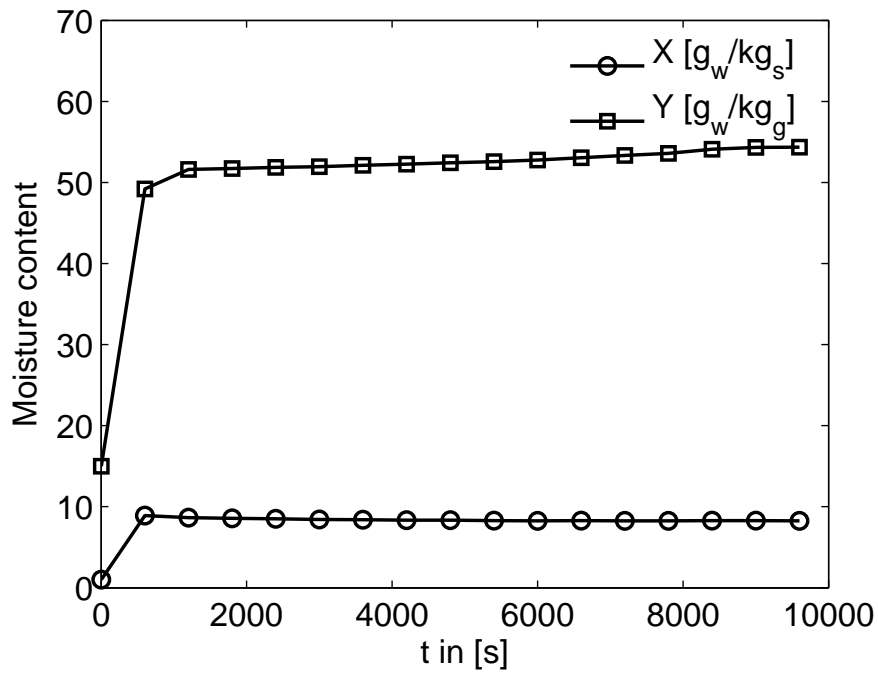


Figure 4.36: Evolution of the particle and gas moisture content. The required value is achieved under the constraints posed on the actuated process inputs.

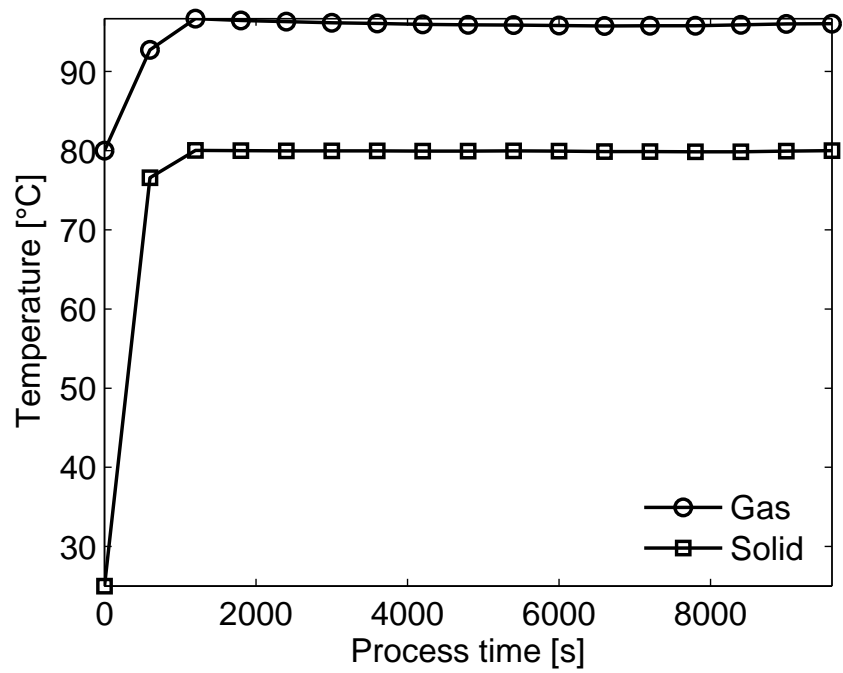


Figure 4.37: Plot of the particle and gas temperature during batch fluidised bed spray granulation. The desired value of 80 °C is achieved by a moderately higher gas temperature.

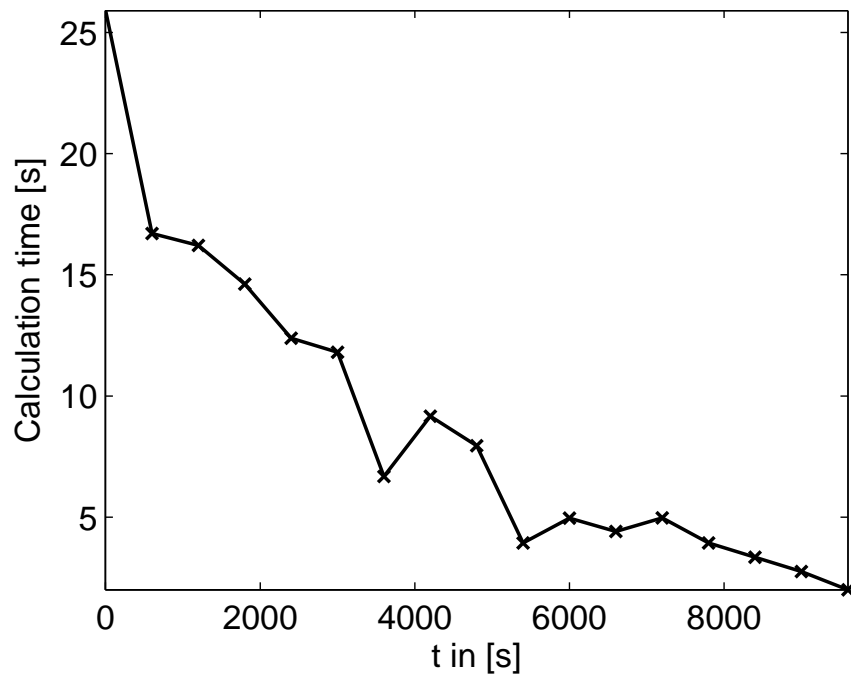


Figure 4.38: Computational time necessary for one cycle of the model-based control system. The time includes the estimation of the number density function and the calculation of the process inputs by a non-linear model-predictive and a linear multiple-input multiple-output controller, respectively.

4.5.2 Continuous fluidised bed spray granulation

For the task of stabilising an unstable steady-state number density function in the continuous spray granulation process with particle recycle, three controllers are available: linear-quadratic optimal controller, linear unconstrained model predictive controller, and linear constrained model predictive controller. From a practical point of view the constrained model predictive controller is of highest interest as it allows to incorporate explicitly various known process constraints. For that reason the focus in the test of a model-based control scheme for the stabilisation of unstable steady-states is laid on that type of controller.

As the controller is designed using a linear approximation of the model dynamics in the vicinity of a given steady-state number density distribution, feedback control of the non-linear process can only be successful if the process dynamics are approximately linear, i.e. the process must be sufficiently close to a steady-state.

In order to practically implement the designed constrained model predictive controller, information on the second moment μ_2 of the number density function in the process is required to evaluate the cost functional and to guarantee a zero steady-state error. Furthermore, the knowledge of the number density function in the process is needed to evaluate the control law, i.e. to calculate the necessary milling diameter ξ_M . If the number density function is known, all moments can be calculated, thus the reconstruction of the number density function from process measurements is necessary.

In the following it is assumed that the *mean diameter* of all particles in the process is available as a process measurement at discrete points in time $t_k = k T_{sample}$: $y_k = y(t_k) = \mu_1(t_k)/\mu_0(t_k)$. The measurements are taken with the same sampling time of the MPC algorithm T_{sample} . The reason for the choice of a time-discrete measurement is that it allows for a probe-internal averaging of quasi-continuous measurements and by this for a suppression of noise. The process parameters and design parameters are the ones reported in Tab. 4.1 (pg. 113), Tab. 4.2 (pg. 119), Tab. 4.3 (pg. 137).

The task therefore is to calculate an estimate of the number density function \hat{n} of the number density function n using the available process measurements y_k and using this information to calculate the control law and apply it to the non-linear process plant.

As the process has to be already in the vicinity of the steady-state in order to be stabilised by linear control, a linear time-discrete Luenberger observer is applied to estimate the number density function in the process from the time-discrete process measurements.

Although the process dynamics and the chosen observer possess a linear structure, the closed-loop dynamics is not linear, due to the presence of constraints in the controller calculation. Therefore the closed loop is non-linear, and the separation theorem does not hold in general, i.e. the stability of the closed-loop with an arbitrarily designed observer is not guaranteed in general; this would only be the case if no constraints are present in the controller formulation.

The initial deviation of the observer estimate from the process has to be such that in the simulation of the observer equations the process is also approximately linear; in that case the observer based on a linear model is able to correct dynamically the deviation.

In Fig. 4.39 – Fig. 4.42 the results of a test complying to these requirements are shown: There an initial number density distribution in the observer is chosen such that it deviates by two percent from the number density distribution in the process. The initial condition in the process is chosen such that it yields sustained oscillations in the number density function if it is not controlled (cf. Fig. 4.5).

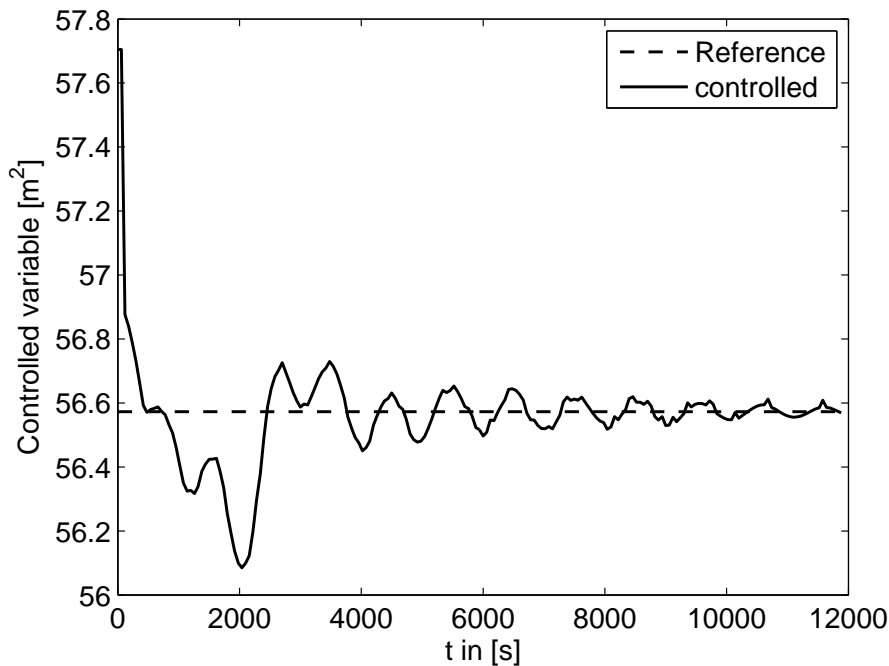


Figure 4.39: Evolution of the controlled output using the estimates provided by the time-discrete Luenberger observer in the calculation of the control law.

In the plot of the controlled output shown in Fig. 4.39 it can be seen that the output converges to the steady-state reference, i.e. the steady-state is stabilised by the model-based control scheme. It can be further observed that in comparison to the ideal case, i.e. the direct measurement of the number density function in the process (cf. Fig. 4.19), the convergence is slower. This is due to the initial deviation of the observer information from the process, that has to be corrected gradually with each available measurement. If the observer is sufficiently close to the process a convergence similar to the ideal case is achieved.

In the plot of the normalised error E_2 in the number density function it can be seen that the controller stabilises the unstable steady state in this integral measure: Apart from temporary increases which are due to the non-linearity of process, the time-discrete nature of the control inputs and state observations, the error is bounded, i.e. there is a bounded deviation of the number density function in the process from the required steady-state distribution.

In the snapshots of the number density function in the process taken at subsequent times (Fig. 4.41), it can be seen that the deviation is indeed bounded. The time necessary for the number density function to converge sufficiently close to the steady-state is increased due to the initial erroneous influence of the estimate provided by the state observer in the controller calculation.

The input trajectory calculated by the model predictive controller is shown in Fig. 4.42: Compared to the ideal case the input oscillates faster and the input constraints become active more often. This is also a result of the initial error in the estimate which yields more extreme results.

In summary, it can be stated that this configuration of a constrained model predictive controller and a linear Luenberger observer is able to stabilise a given unstable steady-state number density distribution.

If non-negligible measurement noise is present in the model-based control system, a decrease of control performance has to be expected. This is due to the influence of noise on the state correction

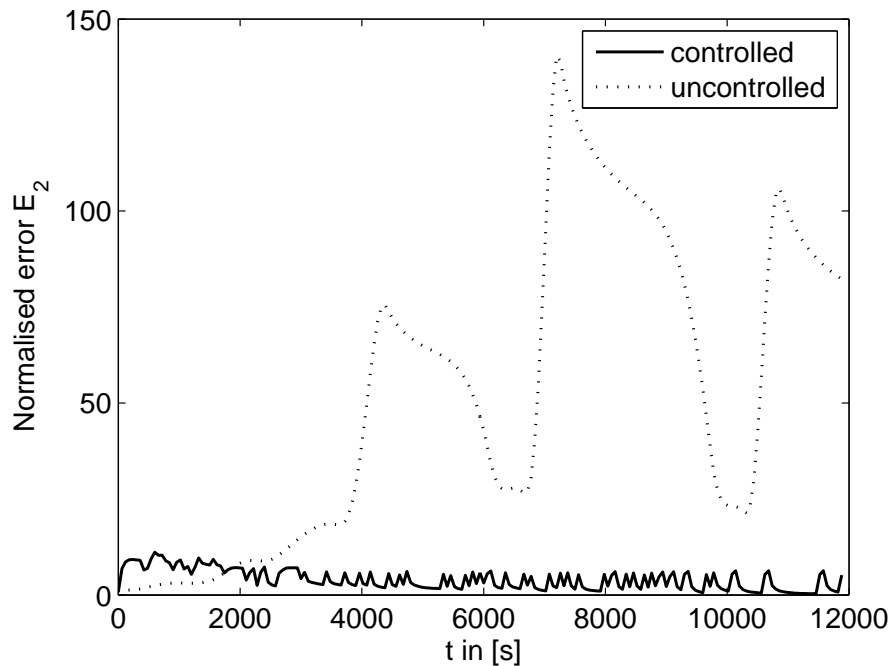


Figure 4.40: Plot of the normalised error E_2 : Despite the input constraints, it also converges to zero, i.e. the steady-state is stabilised by the constrained feedback controller.

as there the noise enters directly by the observer gain.

In Fig. 4.43 – Fig. 4.46 it is shown that the performance is indeed decreased: There the process measurement is subjected to additive zero-mean Gaussian noise before it is processed.

The controlled output now oscillates non-linearly around the reference value, i.e. a bounded non-zero steady error remains. The initial transition phase due to the error in the observer is not prolonged, however, the sustained influence of the measurement noise prevents a smooth convergence to the desired reference.

Same observations can be made in Fig. 4.44: There it can be seen that the integral error measure does not converge to zero but is stabilised at a non-zero value.

In the number density functions shown in Fig. 4.45 it can be seen that the results are still acceptable, especially if they are compared with the uncontrolled case or in case of using a PI input-output controller.

The effect of the measurement noise can be observed quite good in the computed input trajectory: The error in the estimate introduced by noise is processed in the prediction and thus accumulated. Depending on the sign of the error, the accumulation yields control inputs on the boundaries, i.e. the constraints are active.

This is an unwanted result, from a practical point of view, as operation of the actuator in its limits often yields material fatigue and a shortened actuator life-span. One possibility to decrease the influence of measurement noise is the use of averaging measurement filters that filter out the high-frequency noise. These can easily be implemented on-site if necessary. Another possibility is the use of a higher measurement sampling rate, which reduces the effect of an individual noise signal over the sampling horizon, especially in the case of high-frequency noise.

A third possibility is the use of state estimators that take into account the statistics of the noise to calculate an estimate, i.e. a filtered estimate is provided. One state estimator that is of particular

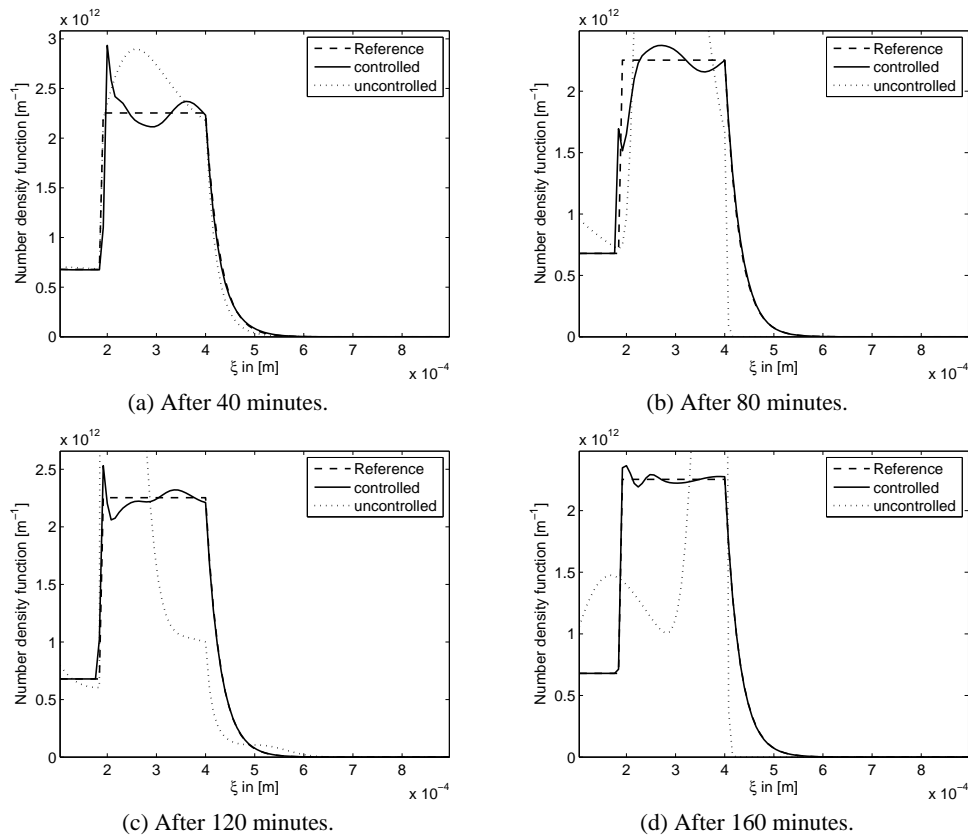


Figure 4.41: Snapshots of the number density function in the continuous spray granulation process with external classification and particle recycle under application of constrained model predictive control using a Luenberger observer for the reconstruction of the number density function from plant measurements of the mean particle diameter of all particles in the bed.

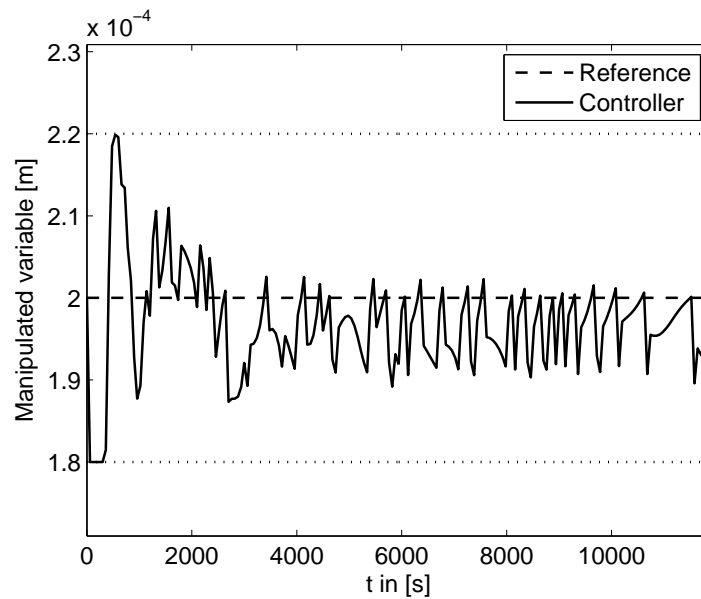


Figure 4.42: Input trajectory calculated by the mode-based control scheme using a constrained model predictive controller and a linear Luenberger observer. The input constraints are satisfied for all times.

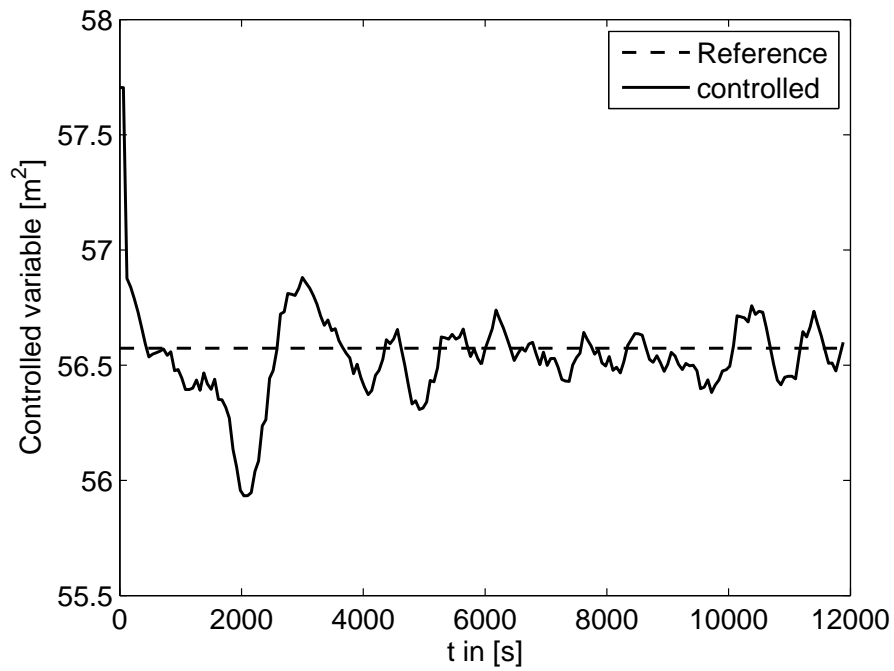


Figure 4.43: Controlled output by the model-based control system with measurement noise. The output does not converge to the reference value and a bounded steady-state error remains.

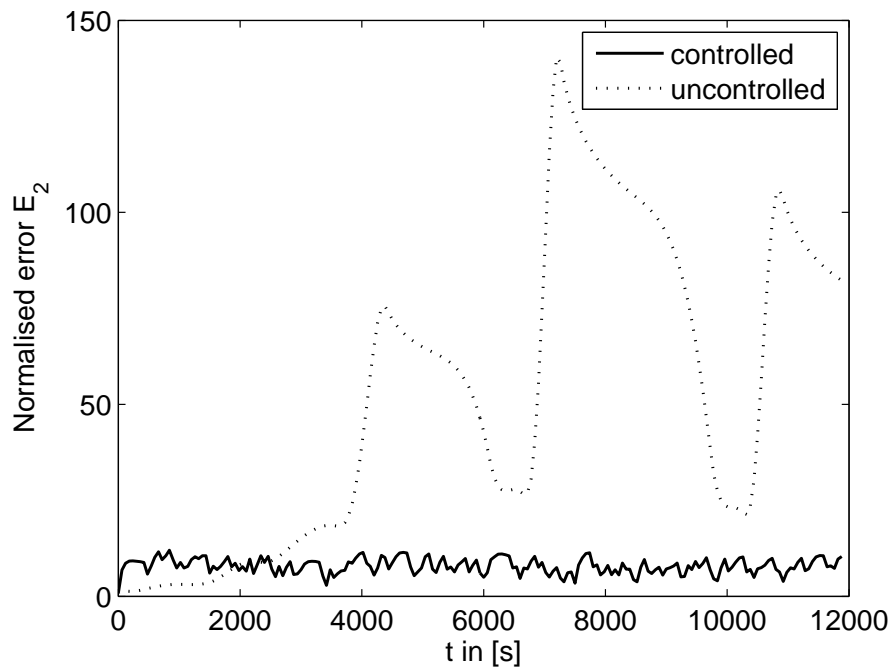


Figure 4.44: Plot of the normalised error E_2 : The error does not converge to zero but is stabilised at a not-zero value.

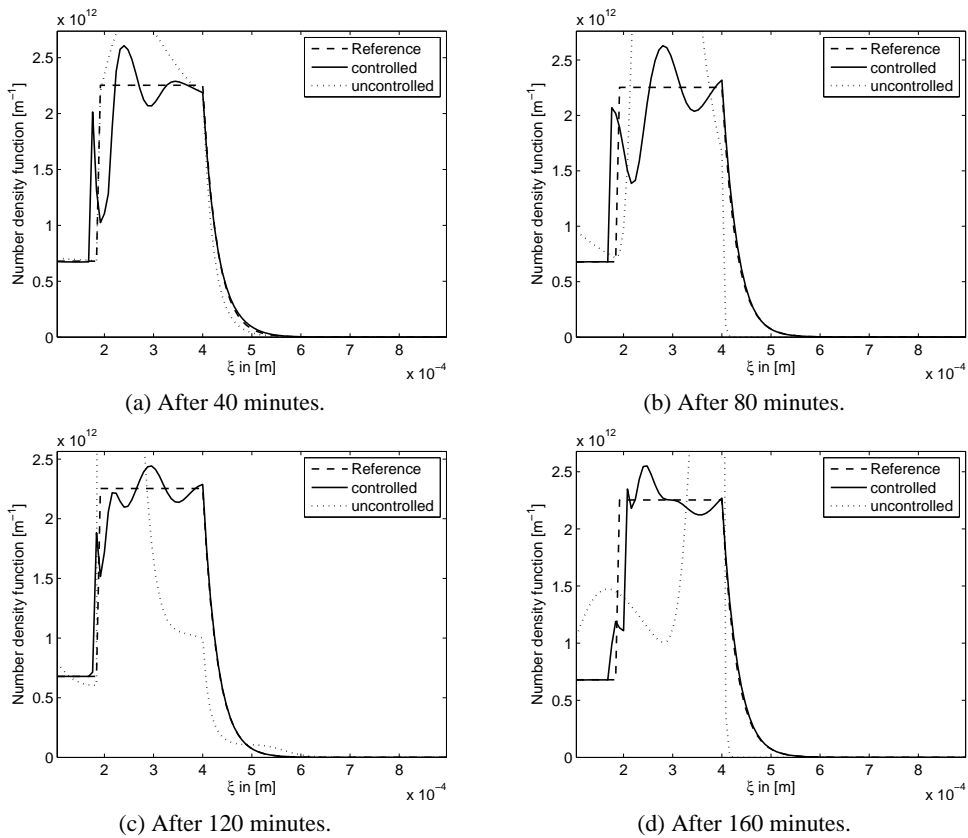


Figure 4.45: Snapshots of the number density function in the continuous process under application of model predictive control and a Luenberger observer. In this scenario the plant measurement is subjected to noise.

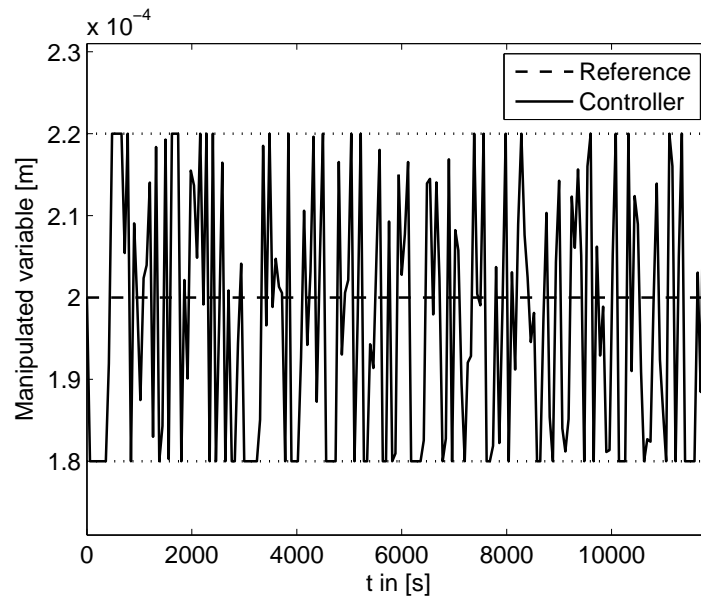


Figure 4.46: Input trajectory calculated on the basis of estimates subject to measurement noise.

interest in the application to non-linear process is the unscented Kalman filter (UKF). As was shown, it is able to provide reliable estimates in the non-linear process using measurements that are biased by noise. The practical implementation is hindered by two facts: The sampling time of the estimator has to be much shorter than the sampling time of the controller in order to provide a reliable estimate. This requires a permanent synchronisation of the measurement and control sampling times. Additionally, the computational effort to calculate an estimate of the number density function is significant: In tests up to eighty percent of the controller sampling interval is spent in the calculation of a state estimate, introducing a significant delay between the time a new measurement becomes available and the time the input to the process is calculated based on that state estimate.

For that reason a special implementation of this non-linear estimator is necessary using as much parallelisation of the algorithm as possible to reduce the computation time. This requires special hardware which may become a significant part of the total cost of the model-based control system.

In all applications of model predictive control in connection with a Luenberger observer the computational time for one control cycle is negligible, i.e. much smaller than one second. Therefore, if the process operates in the linear region of an unstable steady-state this configuration is preferred, possibly augmented by a moving-average measurement filter to further decrease the influence of noise on the estimate of the number density function in the process.

In summary, the combination of a constrained model predictive controller and a linear time-discrete Luenberger observer into a model-based control system yields acceptable results in the stabilisation of an unstable steady-state number density function.

As was motivated in the batch control application, the heat and mass transfer can be treated separately from the control of the dispersed phase. In all cases, the designed controllers are able to achieve the required values for the particle moisture content and temperature, as long as the references can be reached in compliance with the posed input constraints on the mass flow rate of gas and the gas temperature.

4.5.3 Summary

In this chapter feedback control methods for the stabilisation of unstable steady-state number density distributions in continuous fluidised bed processes with external classification and particle recycle were investigated. It was shown that simple input-output control by proportional-integral controllers does not achieve satisfying results. Thus state feedback control schemes were further investigated, namely linear-quadratic optimal control and model predictive control. It was shown that both schemes yield a stabilisation of unstable steady-states. From a practical point of view model predictive controllers are advantageous as they allow the incorporation of process and actuator constraints in the calculation of the control law.

In addition to the stabilisation an application of feedback control to a batch process was considered: Here the task was to achieve a given number density function at the end of the batch despite unmeasurable disturbances in the composition of the sprayed suspension. It was shown that a non-linear model predictive control scheme is successful.

Apart from the control of the number density distribution in the processes it was investigated how the particle moisture content and temperature, two other important product characteristics, can be influenced. Here, due to the stable open-loop behaviour and fast dynamics a linear multiple-input multiple-output controller with a proportional-integral structure was designed. In order to account for internal coupling of the process inputs and controlled outputs a decoupling network is designed that improves the controller performance.

In a last step the state feedback controllers were combined with state observers that allow to calculate estimates of the quantities required in the evaluation of the control laws, i.e. the number density function, from practically available measurements. It was shown that this combination yields acceptable results for the stabilisation of unstable steady-states in the continuous process as well as in the batch process.

Chapter 5

Summary

Particulate products play a major role in many industries, for instance pharmaceuticals, foods or fertilisers. Many product properties, for example the dissolution characteristic of a pill or the flowability of a powder, can be directly related to the particle properties.

As the particles in a powder often are not uniform, i.e. they differ in their characteristic properties, the product also is not uniform. Depending on the field of application, a property distribution is either undesired or only specific distributions are acceptable.

An important class of processes for the production of solid granular products from liquid raw materials, for example suspensions, or solutions where the solid is initially dissolved in a liquid, is fluidised bed spray granulation. These processes can be run either batch-wise or continuously, offering a wide-spread use of the process.

Depending on the process configuration, fluidised bed spray granulation processes can exhibit different dynamic behaviour, for instance in continuous mode unstable steady-states can occur. This may result in undesired product characteristics or irregular product flow.

A way to influence the dynamics of a process towards a desired behaviour is the use of process control. For fluidised bed spray granulation three properties are of most importance: the particle size distribution, the particle moisture content and the particle temperature as they have tremendous influence on the product properties and the necessary post-processing of the produced granules.

The major aim of this work therefore was to determine a process control strategy that allows to manipulate the particle properties in fluidised bed spray granulation towards desired product properties.

Spray granulation or layering granulation is a complex process involving particle formation as well as heat and mass transfer between multiple phases. A purposeful influence on the dynamics can therefore only be devised if a model of the dominant phenomena is available and used for controller design and implementation. This leads to the task of designing a model-based control system for the realisation of desired product characteristics in fluidised bed spray granulation processes, for batch as well as continuous operation.

To that aim in Chapter 2 a mathematical model for the description of the dynamic behaviour of the particle formation process and heat and mass transfer is derived. In order to account for the distributed character of the particle properties, especially the particle size, a macroscopic approach using population balances is used to describe the temporal evolution of the particles with respect to the property. For the case of particle growth by layering, i.e. the growth of the particles induced by the solid contained in the sprayed suspension, a growth rate is derived.

The considerations up to this point allow to describe the evolution of the particle size in a batch fluidised bed spray granulation process that is growth-dominated. For the description of a continuous process the external apparatuses which are required for particle re-cycle also have to be modelled. Here one specific type of continuous process with external product classification by screening and recycle of particles with milling of over-sized particles is considered, and a mathematical model for the particle size distribution of the particles is derived.

In comparison to the batch configuration this process is more complex due to the interaction of the screens, the mill, and the influence of the re-cycled particles on the particle growth in the process. An investigation of the process dynamics reveals that depending on the parametrisation of the screens and the mill, which is motivated by the desired product specification, unstable steady-states can occur. This means that even very small disturbances in the process lead to a loss of the operation at the desired steady-state and, thereby, to a loss in product quality.

The control task in this case is therefore the stabilisation of unstable steady-states in the continuous process with external classification and particle recycle. In the batch configuration a strategy to guarantee a desired product distribution at the end of the batch under process disturbances is to be derived.

The heat and mass transfer determines the two other product properties under consideration, i.e. the particle moisture content and the particle temperature. Here process controllers are to be used to guarantee a mean moisture content at a mean particle temperature. For controller design a simplified mathematical model based on mass and energy balances for the fluidised bed is derived.

In order to influence a process, information on the current state of the process has to be available. This can often be gathered by direct measurement of the interesting quantities, for instance the particle moisture or the particle temperature. In case of the particle size distribution the task is not simple: Although in-line as well as off-line methods for the characterisation of particles are available, the successful application is often hindered by technical aspects. In case of in-line measurement the calculation of the size distribution from the actually measured chord-length distribution is highly susceptible to measurement noise, possibly introducing large errors into the calculated result. Off-line methods are often more accurate than their *in situ* counterparts but they require a removal and transport of particles from the process to the measurement device introducing a large and often unacceptable time delay.

For that reason the use of model-based measurement systems is proposed in Chapter 3. They allow the reconstruction of not directly measurable quantities from more easily obtained measurement information by use of a mathematical process model. Facilitating an iterative approach, the estimation of the unmeasurable quantity is corrected on the basis of the available measurement information. After a presentation of the fundamentals of model-based measurement systems, several different approaches are presented and applied to the task of reconstructing the particle size distribution from limited process measurements in both configurations.

In simulation tests it was shown that the approach of model-based measuring is able to reconstruct the particle size distribution from limited measurement data, for instance the mean particle diameter of all particles in the process, to a sufficient degree. The choice of one specific method, and thereby the obtainable accuracy, is determined by the process configuration and conditions, for example batch or continuous mode or strong presence of measurement noise. If the continuous process is in the vicinity of a steady-state then an observer based on a linearised process model is able to reconstruct the number density function quite well. If the number density function is to be reconstructed during start-up of the process, then non-linear observers or estimators have to be used. The non-linear algorithms can also be used in steady-state operation but due to the higher computational costs, linear observers should be preferred. These results then allow the use of the

reconstructed particle size distribution for purposes of process monitoring or control.

The stabilisation of unstable steady-states is considered in Chapter 4. From the analysis of the process dynamics it can be derived that the stability strongly depends on the size of the milled particles that are re-cycled to the process. Therefore the size of milled particles is identified as a manipulated variable to the process. The controller then modifies temporarily the milling size to stabilise the unstable steady-state. Using the analytically derived knowledge on the steady-state number density function with respect to the process parameters, a linearised process model is used for controller design.

As a characteristic measure for the steady-state the total surface area of all particles in the process is identified. This quantity cannot be measured directly but can be calculated easily from the knowledge of the number density distribution, facilitating the use of a model-based measurement system in the implementation of the derived control law.

At first an output feedback controller of proportional-integral type, which is heavily used in industries and is widely accepted, is designed to stabilise a given unstable steady-state. In tests for the non-linear process it is revealed that the controller does only have limited influence, i.e. the use of a simple output feedback controller is not able to satisfactorily stabilise unstable steady-states.

This necessitates the application of more advanced control schemes using the knowledge of the complete process state and calculating appropriate values for the manipulated variable by state feedback. Two approaches, the linear-quadratic regulator and model predictive control, are investigated. Both methods are able to stabilise the unstable steady-states satisfactorily. Model predictive control has an advantage as it allows to explicitly incorporate constraints, for example in the actuator, in the calculation of the control law, additionally it has its roots in industry lowering the barriers in transporting this non-standard control approach to practical implementation. In summary, the unstable steady-states in the particle size distribution can be stabilised by the linear controllers derived for the continuous process.

The batch process is inherently non-linear, i.e. no steady-state can be derived and for control purposes the non-linear dynamic behaviour has to be taken into account. For the control task of guaranteeing a pre-specified product distribution at the end of the batch under process disturbances, for instance the composition of the sprayed suspension, a non-linear model predictive controller is designed and tested. In all simulations the controller was able to steer a given initial number density function sufficiently close to the desired final number density function, even when non-measured process disturbances were present.

Although the scenario seems to be simple, it highlights the strengths and weaknesses of non-linear model-predictive control especially in view of an application to the continuous process. The computational effort needed for the on-line solution of the non-linear optimisation programme, that yields the manipulated variables, is high which may lead to a violation of the constraint that the optimisation programme must be solved faster than real-time. Additionally, in the continuous process different model-based measurement schemes have to be used which also add to the computational effort.

In both particle formation processes heat and mass transfer occurs, determining the mean particle moisture content and the mean particle temperature. An analysis shows that the moisture content and the temperature are coupled, i.e. a change in one property also changes the other. For controller design it is assumed that the dynamics of heat and mass transfer are much faster in comparison to the growth of particles and always close to a steady-state. This motivates the use of a linearised process model in the design of a controller for the mean moisture content and the mean temperature of the particles.

Following, a multiple-input multiple-output controller of proportional-integral type is designed and tested. In order to increase the performance, an additional approximate decoupling network is designed that allows for an approximate independent control of the moisture content and the temperature. An application of this extended controller to the non-linear processes shows that indeed a better performance is achieved, i.e. specified set-points are reached without attaining critical product states, for example by over-heating or over-drying. This performance is however limited by actuator and hydro- and thermodynamic constraints.

In the end of Chapter 4 all components, i.e. the model-based measurement system, the controllers for the particle size distribution and the heat and mass transfer, are combined into one model-based process control scheme for a specific influence on the complete fluidised bed spray granulation process. It is tested for both configurations and it is shown that the designed scheme is able to achieve the required specifications.

In summary, in this thesis a model-based control scheme for important particle properties in fluidised bed spray granulation is developed. Novel contributions to that purpose are:

- Investigation of model-based approaches to reconstruct distributed particle properties, especially the particle size distribution, which are difficult to measure directly, from more easily measurable process data. This leads to an improvement in the on-line control of product quality, as undesired process states, for instance drift from the coating into the aggregation regime, can be identified directly during process monitoring from changes in the size distribution. Furthermore, the model-based measurement systems enable the use of the reconstructed size distribution in advanced control schemes in order to achieve required product specifications.
- Design of model-based controllers for batch and continuously operating spray granulation processes with a focus not only on integral measures of the property distribution, for instance total mass of product or hold-up, but also on the size distribution of the particles. This allows to formulate a process result on the basis of a desired size distribution. For feedback control of the size distribution model-predictive controllers are designed, permitting an optimal solution to the stated control problems, specifically the stabilisation of unsteady steady-states in continuously operating fluidised bed spray granulation, and control of the final size distribution in batch spray granulation. An additional virtue of this class of controllers, appealing to practical implementation, is the explicit consideration of process constraints, for instance in the manipulated variables.

Additionally, important thermal properties, the mean particle moisture content and mean temperature, are considered, posing in total a multiple-input multiple-output control problem to which solutions for this class of process and in this detail are not available.

- Combination of model-based measurement systems and model-predictive controllers into one model-based control scheme for fluidised bed spray granulation processes. The combination of the two components is not trivial due to the non-linear behaviour of each of them which may yield unacceptable results, even instability, if linked into one control system. By successfully realising this combination, it is possible to control the size distribution, the mean moisture content of the particles, and the mean particle temperature using only practically available, limited, and biased measurement data. Until now, for fluidised bed spray granulation such a model-based control scheme has not yet been available.

However, the results presented in this thesis are not the penultimate solution to the task of feedback control of particulate processes in fluidised beds. The processes in this thesis were investigated

using several assumptions and restrictions, for instance the process chamber was considered as a single compartment, a size-independent growth of the particles was assumed – realised by building up a compact layer of solid – and the possible influence of the drying conditions, i.e. the heat and mass transfer, on the growth rate was neglected.

The relaxation of these restrictions and assumptions, which will lead to an improvement in the description of experimental results, can be used as starting points for further research:

- **Size-dependent particle growth:** In experiments often a widening of the size distribution is observed. This cannot be represented by the size-independent growth law in the single compartment apparatus. For the description of the dispersion in the size distribution new approaches have to be found and to be parametrised in order to describe this effect. This necessitates further experimental investigations in order to identify the basic influences, as well as theoretical studies to derive extended growth laws.
- **Extension of the single-compartment description to multiple compartments:** In the single-compartment model the basic assumption is that all particles can be reached by the spray. In experiments at least two compartments can be identified: a spraying zone, where the particles receive new solid material from the nozzle, and a drying zone, where only evaporation of the sprayed liquid occurs. The division of the process chamber into multiple compartments yields interesting dynamic effects, for instance a widening of the size distribution can be observed even if a size-independent growth law is used. This widening is related to the residence times of a particle in the different compartments. The sizes of the compartments and the residence times of particles depend on the hydrodynamic state of the fluidised bed; in order to use multiple compartment models these dependencies have to be known. One way to gain insight is the use of computational fluid dynamics (CFD) and discrete element methods (DEM) to describe the particle motion inside the different compartments in relation to the gas flow in the process chamber.
- **Investigation of the influence of the drying conditions (the heat and mass transfer) on the particle growth kinetics,** for instance on the porosity of the formed layer. Experimental results show that heat and mass transfer and particle growth are coupled, i.e. they do not run on different time-scales and have to be considered in parallel. Until now, a functional relationship between the drying conditions and the resulting particle size, for instance in terms of the porosity of the solid layer is not known. For this, experiments have to be conducted in order to identify the process inputs influencing the characteristics of the formed layer. Afterwards, from the experimental data, and using theoretical knowledge of heat and mass transfer, functional relationships can be derived using parameter estimation methods.
- **Extension and application of the concepts to other classes of fluidised bed spray granulation processes,** for instance to horizontal fluidised beds or spouted beds. In case of horizontal fluidised bed the spatial distribution of the particle properties along the process chamber has to be considered, adding external coordinates to the model formulation, and increasing the model complexity. Spouted beds are used to fluidise particles of a different Geldart class, with a different hydrodynamic behaviour and thus, different particle dynamics, and heat and mass transfer. Both processes are heavily used in industries, and until now operated mainly by manual control. The introduction of model-based control schemes will be beneficial in terms of product quality and plant safety.

These extensions, used to describe the experimentally observed process dynamics, necessitate the incorporation of the full non-linear behaviour of particle formation and heat and mass transfer into

the process model. The non-linear model-predictive controller devised for the control of the final size distribution in the batch process may be extended in an elementary way when the functional relations are known.

For the continuous fluidised bed process the situation is more complex: The proposed controllers are only valid in the vicinity of a given steady-state. For tasks such as set-point changes, i.e. the transition from one steady-state to another, these can only be used if the new steady-state also lies in the vicinity of the steady-state the controller was designed for. By considering the coupling of heat and mass transfer with the particle growth dynamics, linear controllers may only give insufficient performance depending on the non-linearity of the coupling. A non-linear controller could be applied here, incorporating the non-linear process dynamics (and coupling) and thus guaranteeing a stabilisation of arbitrary unstable steady-states and allowing for the transition of the process between steady-states that do not lie within the vicinity of each other. However, in order to use non-linear model predictive control special algorithms for the solution of the optimisation programmes have to be devised in order to obtain a real-time applicable control law.

If the fully non-linear process is considered, non-linear model-based measurement systems must be incorporated into the model-based control system. As was mentioned in the discussion, this also requires a special implementation to reduce the tremendous computational effort in order to obtain a real-time applicable scheme.

Furthermore, the concepts presented in this work can be applied to other types of particulate processes, for instance aggregation and breakage which are heavily used in industries. The challenge here lies in the fact that aggregation and breakage are integral effects having completely different dynamics. Additionally, profound knowledge on the kinetics of these processes, in terms of mathematical relations, is rare and even the parametrisation is difficult. In addition to the control task the process has to be identified, not only in terms of parameters but also in terms of suitable manipulated variables.

The main results in this thesis are obtained from simulation studies. Thus, the experimental validation of the designed control systems has to serve as the ultimate test of functionality. There questions regarding the noise influence on measurements, the effect of process disturbances and deviations of the plant from the plant model used in the controller design are answered. The application of the model-based scheme developed in this thesis to the processes is therefore the next step in research on model-based measurement and control of fluidised bed spray granulation processes.

Appendix A

Hydro- and thermodynamics of fluidised bed processes

In this appendix all hydro- and thermodynamic correlations needed for the heat and mass transfer model of the fluidised bed spray granulation process are listed.

A.1 Hydrodynamic correlations

The *porosity* of a fluidised bed depends on the fluidisation gas velocity that has to lie between the minimum fluidisation gas velocity and the elutriation velocity. It can be calculated by a correlation given by Richardson and Zaki [122]:

$$\psi^n = \frac{\text{Re}_0}{\text{Re}_{elu}}. \quad (\text{A.1})$$

The exponent n can be calculated by an equation given by Martin [95]

$$n = \frac{\ln(\text{Re}_{mf}/\text{Re}_{elu})}{\ln \psi_{mf}}. \quad (\text{A.2})$$

The Reynolds number Re_0 is given by

$$\text{Re}_0 = \frac{u_0 d_p}{\nu_g}, \quad (\text{A.3})$$

where u_0 , the gas velocity in an empty tube (superficial velocity), can be calculated from

$$u_0 = \frac{\dot{M}_g}{\rho_g A_{bed}}. \quad (\text{A.4})$$

Reh [117] gives an equation for the calculation of the Reynolds number at the point of elutriation

$$\text{Re}_{elu} = \sqrt{\frac{4}{3} \text{Ar}}; \quad (\text{A.5})$$

the Reynolds number at minimum fluidisation velocity can be calculated from Martin [95]:

$$\text{Re}_{mf} = 42.9 (1 - \psi_{mf}) \left\{ \sqrt{\left[1 + \frac{\psi_{mf}^3}{(1 - \psi_{mf})^2} \frac{\text{Ar}}{3214} \right]} - 1 \right\}. \quad (\text{A.6})$$

In these two equations the Archimedes number Ar is defined by

$$Ar = \frac{g d_p^3 \rho_p - \rho_g}{\nu_g^2 \rho_g}, \quad (\text{A.7})$$

that depends only on material properties, with

$$d_p = \frac{6V_{bed}}{A_{bed}}. \quad (\text{A.8})$$

The porosity at the point of fluidisation ψ_{mf} lies in the range of [0.4, 0.7], practically. For all calculations the porosity at minimum fluidisation velocity is assumed to be $\psi_{mf} = 0.4$ (packed bed).

A.2 Heat and mass transfer correlations

A.2.1 Heat and mass transfer between particles and suspension gas

Reference: Gnielinski [48]

$$Re = \frac{Re_{mf}}{\psi_{mf}}, \quad (\text{A.9})$$

$$Sc = \frac{\nu_g}{\delta_{w,g}}, \quad (\text{A.10})$$

$$Sh_{lam} = 0.664 Re^{1/2} Sc^{1/3}, \quad (\text{A.11})$$

$$Sh_{tur} = \frac{0.037 Re^{0.8} Sc}{1 + 2.443 Re^{-0.1} (Sc^{2/3} - 1)}, \quad (\text{A.12})$$

$$Sh_{sphere} = 2 + \sqrt{Sh_{lam}^2 + Sh_{tur}^2}, \quad (\text{A.13})$$

$$Sh_{ps} = [1 + 1.5(1 - \psi_{mf})] Sh_{sphere}. \quad (\text{A.14})$$

The dimensionless Sherwood number Sh is defined as

$$Sh = \beta \frac{d_p}{\delta_g}. \quad (\text{A.15})$$

The dimensionless Nusselt number $Nu = \alpha d_p / \lambda$ can be calculated from the analogy of heat and mass transfer:

$$Nu = Sh Le^{-1/3}, \quad (\text{A.16})$$

$$Le = \frac{\lambda_g}{c_g \rho_g \delta_g}, \quad (\text{A.17})$$

with Le the (dimensionless) Lewis number.

A.2.2 Heat transfer between particles and wall

Reference: Martin [95]

$$Nu_{pw} = \frac{\alpha_{pw} d_p}{\lambda_g} = (1 - \psi) Z (1 - e^{-N}) \quad (\text{A.18})$$

$$N = \frac{\text{Nu}_{pw,max}}{C_K Z} \quad (\text{A.19})$$

$$Z = \frac{1}{6} \frac{\rho_p c_p}{\lambda_g} \sqrt{\frac{g d_p^3 (\psi - \psi_{mf})}{5(1 - \psi_{mf})(1 - \psi)}} \quad (\text{A.20})$$

$$C_K = 2.6 \quad (\text{A.21})$$

$$\text{Nu}_{pw,max} = 4 \left[\left(1 + \frac{2l}{d_p} \right) \ln \left(1 + \frac{d_p}{2l} \right) - 1 \right] \quad (\text{A.22})$$

$$l = 2 \left(\frac{2}{\gamma} - 1 \right) \Lambda \quad (\text{A.23})$$

$$\Lambda = \sqrt{\frac{2\pi \tilde{R} T}{\tilde{M}_g} \frac{\lambda_g}{P(2c_g - \tilde{R}/\tilde{M}_g)}} \quad (\text{A.24})$$

$$\lg \left(\frac{1}{\gamma} - 1 \right) = 0.6 - \left(\frac{1000K}{T_g} + 1 \right) \Big| C_A \quad (\text{A.25})$$

$$C_A = 2.8 \quad (\text{A.26})$$

A.2.3 Heat transfer between gas and wall

Reference: Baskakov [10]

$$\text{Nu}_{gw} = \frac{\alpha_{gwdp}}{\lambda_g} = \begin{cases} 0.009 \text{Pr}^{1/3} \text{Ar}^{1/2} \left(\frac{u}{u_{opt}} \right)^{0.3} & \text{for } u_{mf} < u_0 < u_{opt} \\ 0.009 \text{Pr}^{1/3} \text{Ar}^{1/2} & \text{for } u_{opt} < u_0 < u_{elu} \end{cases} \quad (\text{A.27})$$

$$\text{Re}_{opt} = \frac{u_{opt} d_p}{\nu_g} = 7.5 \left(\frac{g d_p^3}{\nu_g^2} \right)^{0.45} \quad (\text{A.28})$$

Reference: Shi [129]

$$\text{Nu}_{gw} = \left[0.005 \text{Re}_{elu} + 0.06 \text{Re}_{elu}^{1/3} \right] \text{Pr}^{1/3} \quad (\text{A.29})$$

A.2.4 Heat transfer between wall and environment

Reference: Churchill [24] (perpendicular plate)

$$\text{Nu}_{we} = \frac{\alpha_{we} L_{bed}}{\lambda_g} = (0.825 + 0.387[\text{Ra} f_1(\text{Pr})]^{1/8})^2 \quad (\text{A.30})$$

$$\text{Ra} = \text{Gr Pr} = \frac{\beta_g^* g L_{max}^3 (T_w - T_e)}{\nu_g} \quad (\text{A.31})$$

$$\beta_g^* = \frac{2}{T_w + T_e} \quad (\text{A.32})$$

$$f_1(\text{Pr}) = \left[1 + \left(\frac{0.492}{\text{Pr}} \right)^{9/16} \right]^{-16/9} \quad (\text{A.33})$$

The dimensionless numbers Pr (Prandtl number) and Gr (Grashof number) are defined by

$$\text{Pr} = \frac{\rho c_p \nu_g}{\lambda} = \frac{\nu_g}{\chi}, \quad (\text{A.34})$$

$$\text{Gr} = \frac{\beta_g^* g L_{max}^3 (T_w - T_e)}{\nu_g^2}. \quad (\text{A.35})$$

A.3 Material properties

In general the material properties are functions of the system pressure P and the temperature ϑ . In the following the dependency of the specific heat capacities, the thermal conductivity, and the dynamic viscosity of the gases on the pressure is neglected. Only for the mass density and the kinematic viscosity temperature and pressure dependencies are taken into account via the ideal gas law.

The material properties of liquid water are calculated considering the dependency on the temperature only.

The diffusion coefficient of water vapour in air $\delta_{w,g}$ and the saturation moisture content of air Y_{sat} are calculated as functions of pressure and temperature.

A.3.1 Material properties of dry air

Mean molar mass

Reference: Krauss [72]

$$\tilde{M}_g = 28.96 \text{ kg kmol}^{-1} \quad (\text{A.36})$$

Specific gas constant

Reference: Krauss [72]

$$R_g = 287.22 \text{ J kg}^{-1} \text{ K}^{-1} \quad (\text{A.37})$$

Mass density

$$\rho_g = \frac{P\tilde{M}_g}{\tilde{R}T_g} = \frac{P}{R_g(273.14\text{K} + \vartheta)} \quad (\text{A.38})$$

Unit: kg m^{-3} , $[P] = \text{Pa}$

Specific heat capacity

Reference: Glück [47]

$$\begin{aligned} c_g &= A + B\vartheta + C\vartheta^2 + D\vartheta^3 \\ A &= +1006.256 \times 10^0 \\ B &= +2.120536 \times 10^{-2} \\ C &= +4.180195 \times 10^{-4} \\ D &= -1.521916 \times 10^{-7} \end{aligned} \quad (\text{A.39})$$

Unit: $\text{J kg}^{-1} \text{ K}^{-1}$

Range of validity: $-20 \text{ }^\circ\text{C} \leq \vartheta \leq 200 \text{ }^\circ\text{C}$; $P = 100000 \text{ Pa}$

Maximum error: 0.05%

Thermal conductivity

Reference: Glück [47]

$$\begin{aligned} \lambda_g &= A + B\vartheta + C\vartheta^2 + D\vartheta^3 \\ A &= +24.52110 \times 10^{-3} \end{aligned} \quad (\text{A.40})$$

$$\begin{aligned}
 B &= +7.501414 \times 10^{-5} \\
 C &= -2.593344 \times 10^{-8} \\
 D &= +5.292884 \times 10^{-11}
 \end{aligned}$$

Unit: $\text{W m}^{-1} \text{K}^{-1}$

Range of validity: $-20\text{ }^\circ\text{C} \leq \vartheta \leq 200\text{ }^\circ\text{C}$; $P = 100000\text{ Pa}$

Maximum error: 0.08%

Dynamic viscosity

Reference: Glück [47]

$$\begin{aligned}
 \eta_g &= A + B\vartheta + C\vartheta^2 + D\vartheta^3 & (\text{A.41}) \\
 A &= +1.705568 \times 10^{-5} \\
 B &= +4.511012 \times 10^{-8} \\
 C &= -8.766234 \times 10^{-12} \\
 D &= -3.382035 \times 10^{-15}
 \end{aligned}$$

Unit: $\text{kg m}^{-1} \text{s}^{-1}$

Range of validity: $-20\text{ }^\circ\text{C} \leq \vartheta \leq 200\text{ }^\circ\text{C}$; $P = 100000\text{ Pa}$

Maximum error: 0.6%

Kinematic viscosity

$$\nu_g = \frac{\eta_g}{\rho_g} \quad (\text{A.42})$$

Unit: $\text{m}^2 \text{s}^{-1}$

A.3.2 Material properties of water

Mean molar mass

Reference: Wagner et al. [143]

$$\tilde{M}_w = 18.0153 \text{ kg kmol}^{-1} \quad (\text{A.43})$$

Specific gas constant

Reference: Wagner et al. [143]

$$R_w = 461.519 \text{ J kg}^{-1} \text{K}^{-1} \quad (\text{A.44})$$

Mass density

Reference: Glück [47]

$$\begin{aligned}
 \rho_{w,l} &= A + B\vartheta + C\vartheta^2 & (\text{A.45}) \\
 A &= +1006 \\
 B &= +0.26 \\
 C &= -0.0022
 \end{aligned}$$

Unit: kg m^{-3}

Range of validity: $-20\text{ }^\circ\text{C} \leq \vartheta \leq \vartheta_s$ or $200\text{ }^\circ\text{C}$

Maximum error: 0.16%

Specific heat capacity

Reference: Glück [47]

$$\begin{aligned}c_{w,l} &= A + B\vartheta + C\vartheta^2 + D\vartheta^3 & (\text{A.46}) \\A &= +4174.785 \times 10^0 \\B &= +1.785308 \times 10^{-2} \\C &= -5.097403 \times 10^{-4} \\D &= +4.216721 \times 10^{-5}\end{aligned}$$

Unit: $\text{J kg}^{-1} \text{K}^{-1}$

Range of validity: $10\text{ }^\circ\text{C} \leq \vartheta \leq \vartheta_s$ or $200\text{ }^\circ\text{C}$

Maximum error: 0.043%

Specific evaporation enthalpy

Reference: Glück [47]

$$\begin{aligned}\Delta h_v &= A + B\vartheta + C\vartheta^2 & (\text{A.47}) \\A &= +2.5 \times 10^6 \\B &= -2.0425 \times 10^3 \\C &= -3.813 \times 10^0\end{aligned}$$

Unit: J kg^{-1}

Range of validity: $10\text{ }^\circ\text{C} \leq \vartheta \leq 200\text{ }^\circ\text{C}$

Maximum error: 0.3%

Saturation pressure

Reference: Glück [47]

$$\begin{aligned}p_{sat} &= A \exp(B\vartheta_{sat} + C\vartheta_{sat}^2 + D\vartheta_{sat}^3 + E\vartheta_{sat}^4) & (\text{A.48}) \\A &= +611 \\B &= +7.257 \times 10^{-2} \\C &= -2.937 \times 10^{-4} \\D &= +9.810 \times 10^{-7} \\E &= -1.901 \times 10^{-9}\end{aligned}$$

Unit: Pa

Range of validity: $0.01\text{ }^\circ\text{C} \leq \vartheta_{sat} \leq 100\text{ }^\circ\text{C}$

Maximum error: 0.02% ($\equiv 7$ Pa)

A.3.3 Material properties of water vapour

Mass density

$$\rho_{w,g} = \frac{P \tilde{M}_w}{\tilde{R}T_g} = \frac{P}{R_w(273.14K + \vartheta)} \quad (\text{A.49})$$

Unit: kg m^{-3}

Specific heat capacity

Reference: Glück [47]

$$\begin{aligned} c_{w,g} &= A + B\vartheta + C\vartheta^2 + D\vartheta^3 & (\text{A.50}) \\ A &= +1.862 \times 10^3 \\ B &= +2.858485 \times 10^{-1} \\ C &= +6.148483 \times 10^{-4} \\ D &= -2.060606 \times 10^{-7} \end{aligned}$$

Unit: $\text{J kg}^{-1} \text{K}^{-1}$

Range of validity: $25^\circ\text{C} \leq \vartheta \leq 400^\circ\text{C}$; $100 \text{ Pa} \leq P \leq 1000 \text{ Pa}$

Maximum error: 0.06%

Thermal conductivity

Reference: Glück [47]

$$\begin{aligned} \lambda_{w,g} &= A + B\vartheta + C\vartheta^2 + D\vartheta^3 & (\text{A.51}) \\ A &= +0.0170 \times 10^0 \\ B &= +5.698384 \times 10^{-5} \\ C &= +1.297172 \times 10^{-7} \\ D &= -9.131313 \times 10^{-11} \end{aligned}$$

Unit: $\text{W m}^{-1} \text{K}^{-1}$

Range of validity: $25^\circ\text{C} \leq \vartheta \leq 400^\circ\text{C}$; $100 \text{ Pa} \leq P \leq 1000 \text{ Pa}$

Maximum error: 0.14%

Dynamic viscosity

Reference: Glück [47]

$$\begin{aligned} \eta_{w,g} &= A + B\vartheta + C\vartheta^2 + D\vartheta^3 & (\text{A.52}) \\ A &= +9.16 \times 10^{-6} \end{aligned}$$

$$\begin{aligned}
 B &= +2.781303 \times 10^{-8} \\
 C &= +4.626970 \times 10^{-11} \\
 D &= -5.054545 \times 10^{-14}
 \end{aligned}$$

Unit: $\text{kg m}^{-1} \text{s}^{-1}$

Range of validity: $25^\circ\text{C} \leq \vartheta \leq 400^\circ\text{C}$; $100 \text{ Pa} \leq P \leq 1000 \text{ Pa}$

Maximum error: 0.19%

Kinematic viscosity

$$v_{w,g} = \frac{\eta_{w,g}}{\rho_{w,g}} \quad (\text{A.53})$$

Unit: $\text{m}^2 \text{s}^{-1}$

Prandtl number

$$Pr_{w,g} = \frac{\eta_{w,g} c_{w,g}}{\lambda_{w,g}} \quad (\text{A.54})$$

Unit: –

Diffusion coefficient of water vapour in air

Reference: Schirmer [126]

$$\delta_{w,g} = \frac{2.252}{P} \left(\frac{\vartheta + 273.15\text{K}}{273.15\text{K}} \right)^{1.81} \quad (\text{A.55})$$

Saturation moisture content

$$Y_{sat} = 0.622 \frac{p_{sat}}{P - p_{sat}} \quad (\text{A.56})$$

Unit: $(\text{kg water}) (\text{kg dry air})^{-1}$

Saturation temperature The saturation temperature can be derived from an energy balance and yields a nonlinear system of equations for ϑ_{sat} and p_{sat} (via Y_{sat}) that has to be solved iteratively.

$$0 = c_{p,g} \vartheta_{g,in} + Y_{g,in} (c_{p,v} \vartheta_{g,in} + \Delta h_{evap}) - c_{p,g} \vartheta_{sat} + Y_{sat} (c_{p,v} \vartheta_{sat} + \Delta h_{evap}) \quad (\text{A.57})$$

Unit: $^\circ\text{C}$

Appendix B

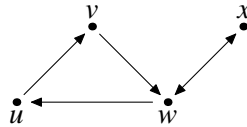
Elements of graph theory

The structural analysis of dynamic systems, as presented in chapter 3.2, relies on the mathematical theory of graphs and the investigation of information flows therein.

Graph theory is a complex mathematical field, therefore, in this appendix only concepts of importance for structural analysis are presented. The most important concept is the *directed graph*:

Directed graph [18, 109]. A directed graph (also: digraph), $G = [V, E]$ consists of a finite set V of vertexes (nodes) and a finite set of directed edges E . The edges are defined on the nodes of the graph, i.e. $E \subseteq V \times V$: $E = \{\dots, (v_j, v_k), \dots\}$, where $v_j, v_k \in V$. The notation (v_j, v_k) then means that there is a directed edge from vertex v_j to vertex v_k .

Example. The following graph G is given by the set of vertexes $V = \{u, v, w, x\}$ and the set of edges $E = \{(u, v), (v, w), (w, u), (w, x), (x, w)\}$:



An important tool for the abstract reasoning about graphs is the *adjacency matrix*:

Adjacency matrix [18, 109]. Given a directed graph $G = [V, E]$ with $V = \{v_1, \dots, v_n\}$, the matrix A with elements a_{ij}

$$a_{ij} = \begin{cases} 1, & (v_i, v_j) \in E \\ 0, & \text{otherwise} \end{cases} \quad i, j = 1, \dots, n \quad (\text{B.1})$$

is called the adjacency matrix of the digraph G .

If $a_{ij} = 1$, then there exists a direct connection between v_j and v_i , i.e. v_i is directly reachable from v_j . If there does not exist a direct connection between two vertexes, but a sequence of directed edges starting in v_j over some v_k to v_i , then v_i is reachable from v_j .

For the determination whether a vertex is reachable from another one, powerful algorithms exist, for instance the Moore algorithm [148].

The link to the structural matrices of a dynamic system can then be established as follows: If the states, the inputs and the outputs are considered as vertexes in a graph, and a value of 1 is assigned to all the direct connections between these vertexes, the structural matrices of the dynamic system are constructed. Additionally, the structural matrices are also the adjacency matrices for the graph. By this construction, all investigations concerning the flow of information, for example output-reachability, can be performed on the structural matrices.

Appendix C

Method of characteristics

The method of characteristics (abbr. MOC) [120, 38] is a method for the analytical solution of first order partial differential equations. The general idea is to reduce the partial differential equation to a set of ordinary differential equations by re-parameterisation of the solution domain. In many cases, the set of ordinary differential equations can be solved analytically, and a solution of the partial differential equation can be obtained. Even if the set of ordinary differential equations cannot be solved, important qualitative results on the solution can be obtained.

The method of characteristics can be applied to non-linear first order differential equations. It is not restricted to scalar equations, but can also be applied to systems of first order equations.

In the following, the special case of a quasi-linear scalar first order partial differential equation is considered. The independent variables are t and ξ , and the solution $z(t, \xi)$ of the following equation is sought:

$$a(t, \xi, z) \frac{\partial z}{\partial t} + b(t, \xi, z) \frac{\partial z}{\partial \xi} = c(t, \xi, z), \quad z(0, \xi) = \varphi(\xi). \quad (\text{C.1})$$

The term *quasi-linear* relates to the fact that the partial derivatives of z enter only linearly into the equation.

In order to solve this initial value problem, the solution domain described by t and ξ is re-parameterised by a set of curves, parameterised by two new variables θ and s : The initial point of the curve on the x -axis is parameterised by s ; the curve itself is parameterised by θ . This idea is visualised in Fig. C.1.

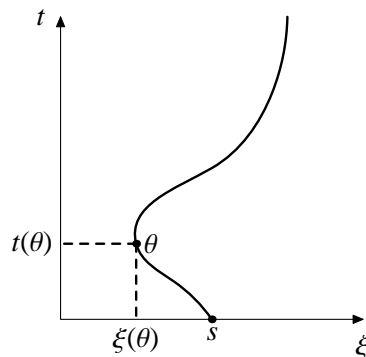


Figure C.1: Re-parameterisation of the solution domain by the method of characteristic.

The solution $z(t, \xi)$ is now investigated on these curves: On a curve t is a function of θ , $t = t(\theta)$;

the variable ξ is also a function of θ , i.e. $\xi = \xi(\theta)$. The variable s is considered as a parameter, henceforward. With these observations, the solution $z(t(\theta), \xi(\theta))$ can be expressed as a function of θ solely: $z(t(\theta), \xi(\theta)) = u(\theta)$.

Calculating the change of z on a curve under variation of θ yields:

$$\frac{dz}{d\theta} = \frac{\partial z}{\partial t} \frac{dt}{d\theta} + \frac{\partial z}{\partial \xi} \frac{d\xi}{d\theta}. \quad (\text{C.2})$$

Comparing the coefficients with the partial differential equation yields the following set of ordinary differential equations:

$$\frac{dt}{d\theta} = a(t, \xi, u), \quad t(\theta_0, s) = 0, \quad (\text{C.3})$$

$$\frac{d\xi}{d\theta} = b(t, \xi, u), \quad \xi(\theta_0, s) = s, \quad (\text{C.4})$$

$$\frac{du}{d\theta} = c(t, \xi, u), \quad u(\theta_0, s) = \varphi(s). \quad (\text{C.5})$$

This set of equations is called the *characteristic system* of the partial differential equations. The first and the second equation describe the parameterised curve, the characteristic. The third equation describes the evolution of the solution along this curve.

In order to obtain the solution of the partial differential equation, these equations have to be solved, to obtain $t(\theta, s)$, $\xi(\theta, s)$, and $u(\theta, s)$. In a last step the parameterisation of the curve has to be inverted, $\theta = \theta(t, \xi)$, and $s = s(t, \xi)$, in order to obtain the solution $z(t, \xi)$. This last step proves to be a most difficult one as the inversion is not always possible, for instance if two characteristic curves intersect.

Using the characteristic system many dynamical effects that may occur can be identified, for instance the occurrence of shocks in the solution – this can be attributed to the intersection of two characteristic curves. Also questions concerning the existence and uniqueness of the solution in the whole solution domain can be answered. For that reason, the method of characteristics found wide-spread application in process engineering, for instance in chromatography [120].

Appendix D

Discretisation of population balance equations

The dynamic modelling of property-distributed processes on the basis of the population balance approach [60, 114] yields a partial differential equation for the number density function, and is therefor, from a system-theoretic point of view, an infinite-dimensional system.

As the analytical solution of partial differential equations is often not possible, numerical methods have to be applied to obtain an approximation to the solution. Because of the limits of computer technology (especially limited memory), a finite-dimensional approximation of the infinite-dimensional system (the partial differential equation) is needed.

Approximation methods in use today either consider only integral values (e.g. moments) of the number density function, or approximate the number density function via discretisation.

The former class of methods is called *moment methods*, and are historically among the first approximation methods for population balance systems [60]. Here, instead of the number density function only a small, fixed set of moments are considered. For these dynamic equations are derived (from the balance equation), yielding a small set of ordinary differential equations, that is then solved numerically.

The two major problems with this approach are: (1) loss of information on the shape of the density function (this would in general require an infinite number of moments); (2) the danger that the set of moment equations cannot be closed, i.e. the dynamic relations between the moments cannot be expressed by a finite number of moments. In recent years, new moment methods have been derived that allow for an approximate closure of the moment equations, for instance QMOM [94] and DQMOM [93].

Moment methods are used in the solution of problems for which the exact form of the number density function is of less importance, for instance in CFD calculations. Here, only integral values (e.g. mass of particles) are of importance, and by considering only moments a tremendous reduction in computational effort is achieved.

For the direct approximation of the number density function, various methods are available, for instance finite-difference methods (FDM), finite-volume methods (FVM) [78], finite element methods (FEM) [59] and spectral methods (SM) [49, 137].

The general idea of these methods is to discretise the solution domain, and to approximate the density function at these discrete points (elements, nodes) in the domain. Then dynamic equations for the approximate values at the nodes are derived and solved. The solution between two nodes

is obtained by interpolation.

The methods vary in the detail of the discretisation, for instance semi-discrete or fully-discrete approximations of; also the treatment of the differential and integral operators is different – in some methods they are approximated directly, in others the approximation is the result of an optimisation problem. As a result the different numerical methods do have different properties, and are limited for the most part to special classes of problems.

One of these classes are convection-dominated processes (growth processes), to which the following discussion is restricted. For the handling of the population dynamic effects aggregation and breakage other methods are needed, for instance the Cell Average method [73] or the Fixed Pivot method [74].

In the following two important discretisation methods for the solution of growth-dominated population balance systems are presented: the finite volume method and a spectral method.

D.1 Finite volume method

The principle ideas of the finite volume method [78] are presented for the following scalar growth-dominated population balance equation:

$$\frac{\partial n}{\partial t} + \frac{\partial(Gn)}{\partial \xi} = p(t, \xi, n), \quad (Gn)(t, \xi_0) = B_0(t), \quad n(0, \xi) = \varphi(\xi). \quad (\text{D.1})$$

Here, one discretises the property coordinate ξ into N sub-intervals, as shown in Fig. D.1. To this purpose the interval $[\xi_0, \infty)$ has to be restricted to $[\xi_0, \xi_{\max}]$.

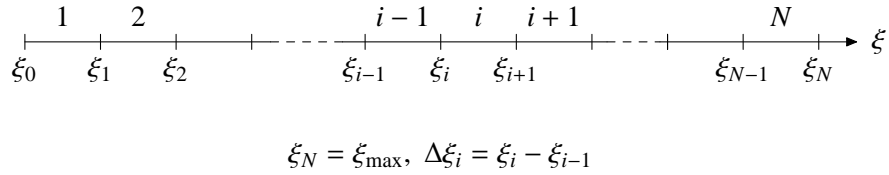


Figure D.1: Discretisation of the property coordinate ξ into N sub-intervals (finite volumes).

Then grid nodes $\bar{\xi}_i$ ($i = 1, \dots, N$) in the interior of the sub-intervals are defined, for instance in the middle of the interval. The number density function $n(t, \xi)$ is then expressed at this node as $n(t, \bar{\xi}_i) = n_i(t)$. In order to describe the temporal evolution of the value, a dynamic (balance) equation is derived by integrating the population balance equation over a sub-interval:

$$\int_{\xi_i}^{\xi_{i+1}} \frac{\partial n}{\partial t} d\xi = - \int_{\xi_i}^{\xi_{i+1}} \frac{\partial(Gn)}{\partial \xi} d\xi + \int_{\xi_i}^{\xi_{i+1}} p(t, \xi, n) d\xi. \quad (\text{D.2})$$

Interchanging differentiation and integration, and evaluating the first integral on the right-hand side by the Gauss theorem yields:

$$\frac{d}{dt} \int_{\xi_i}^{\xi_{i+1}} n d\xi = - (Gn)|_{\xi_i}^{\xi_{i+1}} + \int_{\xi_i}^{\xi_{i+1}} p(t, \xi, n) d\xi. \quad (\text{D.3})$$

Using this approach, the total flux (Gn) is conserved by the discretisation, i.e. the discretised problem will also obey a conservation law if the original problem obeys one (i.e. $p \equiv 0$). For this reason the finite volume methods are called *conservative*.

For further evaluation some assumptions on the profile on n and p in the interior of the interval have to be made, for instance that n and p are piece-wise constant in the interior, i.e. $n(t, \xi) = n_i(t, \bar{\xi}_i)$, $p(t, \xi, n) = p(t, \bar{\xi}_i, n_i) = p_i(t)$ for $\xi \in [\xi_i, \xi_{i+1}]$. Higher order approximations (e.g. linear, quadratic) are also possible. Use of these assumptions yields the set of ordinary differential equations:

$$\frac{dn_i}{dt} = -\frac{1}{\Delta\xi_i} (G_i n_i - G_{i-1} n_{i-1}) + p_i, \quad i = 1, \dots, N. \quad (\text{D.4})$$

Here the boundary fluxes $(Gn)(t, \xi_{i+1})$ and $(Gn)(t, \xi_i)$ are approximated by the so called up-wind scheme (see Fig. D.2): The fluxes at the boundaries are evaluated by a backward difference using the values of the number density function at the grid nodes in the interior of the cell, i.e. $(Gn)(t, \xi_{i+1}) \approx (Gn)(t, \bar{\xi}_i)$ and $(Gn)(t, \xi_i) \approx (Gn)(t, \bar{\xi}_{i-1})$.

The corresponding initial values $n_i(0)$ can be obtained from the initial number density function, i.e. $n_i(0) = \varphi(\bar{\xi}_i)$. This shift in the indexes necessitates a special treatment of the first equation by

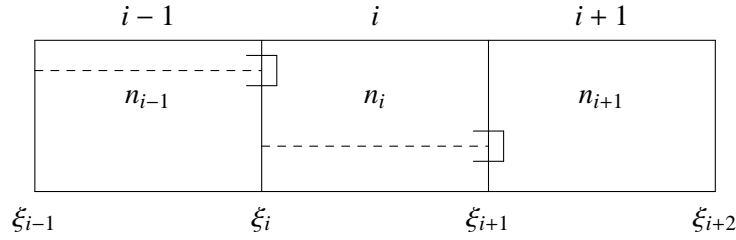


Figure D.2: Visualisation of the up-wind-scheme.

the explicit incorporation of the boundary value $(Gn)_0(t) = B_0(t)$:

$$\frac{dn_1}{dt} = \frac{1}{\Delta\xi_1} (G_1 n_1 - B_0(t)) + p_1. \quad (\text{D.5})$$

In total, the population balance equation is transformed into a set of coupled ordinary differential equations that can be solved numerically by standard methods.

Although the approximation was derived directly from the population balance equation, its solution does only in the limit $N \rightarrow \infty$ converge to the solution of the original population balance equation. It can be shown [78] that for finite N instead of the original equation the following equation is approximated with greater accuracy:

$$\frac{\partial n}{\partial t} + \frac{\partial(Gn)}{\partial \xi} = \nu(N) \frac{\partial^2 n}{\partial \xi^2} + p(t, \xi, n), \quad (\text{D.6})$$

i.e. a convection-diffusion equation is solved. The additional, purely numerical, diffusion term leads to a smoothing effect in the solution, known as *numerical diffusion*. The diffusion coefficient ν depends on the number of sub-intervals used in the discretisation. In the limit $N \rightarrow \infty$ the coefficient vanishes, i.e. the original problem is recovered.

As a result, by using a finite number N an approximation error is made. The specific choice of N strongly depends on the problem at hand, but generally, an increase of N will increase the accuracy but will also increase the computation time as the dimension of the system of ordinary differential equations increases. By using specialised higher-order methods, so called flux-limiters [70], the numerical diffusion can be decreased, but at a higher computational cost.

One class of methods that do not suffer as much from numerical diffusion as finite volume methods are the so called spectral methods.

D.2 Spectral methods

Spectral methods, like finite volume methods, approximate a partial differential equation by a finite set of ordinary differential equations, when applied to all but one of the coordinates of the problem. They allow for certain classes of (smooth) problems a stable and more accurate solution than finite volume methods, also in many cases less grid nodes have to be used to achieve this accuracy [49, 137]. This reduces the size of the system of ordinary differential equations, and may reduce thereby the computational time needed for the solution of the discretised problem.

In the following only the fundamental ideas are presented, details can be found in [49, 41, 137].

Spectral methods are closely linked to the theory of eigenfunctions of differential operators and are known in analysis since Euler and Fourier. They were first considered in numerical analysis in the 1970s and found wide-spread application, for example in fluid dynamics, or seismic explorations [49, 41].

Although these methods showed superior performance in many applications, interest decreased in the following years because of several problems: They were less intuitive than the finite difference, finite volume and finite element schemes available at this time and required more effort in programming. Additionally, the handling of complex computational geometries and process non-linearities was difficult.

Since the early 1990s new interest in these methods is shown, as evidenced for example by the works of Fornberg [41], Trefethen [137], Mantzaris et al. [92], and Dorao and Jakobsen [34].

A basic assumption in spectral methods is that the approximation can be expanded as a series:

$$n(t, \xi) \approx \sum_{i=0}^N a_i(t) \psi_i(\xi). \quad (\text{D.7})$$

In this equation, the $a_i(t)$ are the so called *spectral weights* of the *spectral modes* $\psi_i(\xi)$.

The functions ψ_i are chosen once for each problem and are defined on the whole region under consideration – possibly after appropriate rescaling of the problem. This is the main difference to finite volume methods where local approximations on some sub-interval are used.

The function set should consist of mutually orthogonal elements: Common choices are Fourier polynomials, for problems on periodic domains (periodic boundary conditions), or algebraic polynomials such as Chebyshev polynomials, for problems on non-periodic domains. If eigenfunctions for a given problem are known, then these can also be used to create a spectral method.

The approximation error made in the transition from the infinite dimensional problem to the finite dimensional problem is strongly influenced by the choice of the set of spectral modes and the number of modes N used in the approximation.

In order to determine the time-dependent spectral weights $a_i(t)$, the integral of the weighted residuals has to vanish:

$$\int_{\xi_0}^{\xi_{max}} \varrho(\xi) \left[\frac{\partial n}{\partial t} + \frac{\partial(Gn)}{\partial \xi} - p \right] d\xi = 0. \quad (\text{D.8})$$

Substituting n in this equation from Eq. (D.7) yields equations for the spectral weights $a_i(t)$, given the set of spectral modes and the weight function ϱ .

The choice of the weight function ϱ determines the type of spectral method. Choosing $\varrho = \delta(\xi - \xi_i)$ leads to *spectral collocation*, i.e. the spectral weights $a_i(t)$ are calculated such that the pseudo-

spectral approximation satisfies the population balance equation at the collocation points ξ_i ($i = 0, 1, \dots, N$).

The choice of collocation points is not arbitrary but depends on the spectral modes ψ_i . If algebraic polynomials are chosen then the collocation points must be distributed over the interval in a specific way to prevent numerical difficulties, for example Runge's phenomenon[41], in the approximation of the solution. For one specific method, the Chebyshev spectral method [137], the collocation point distribution is shown in Fig. D.3. It can be seen that the distribution of nodes

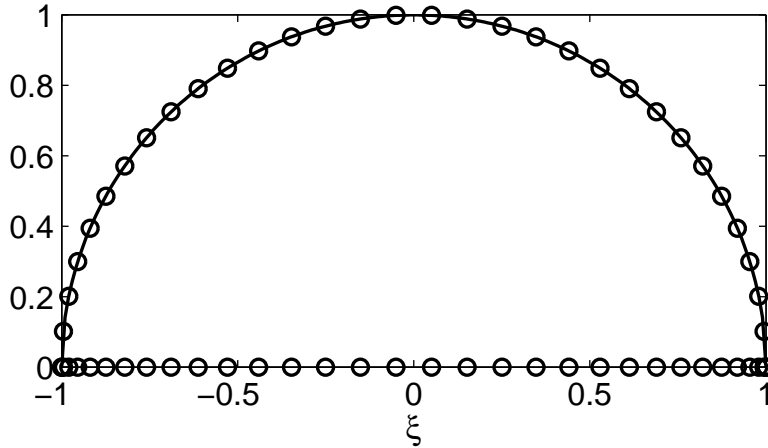


Figure D.3: Grid node distribution in the Chebyshev spectral method. The nodes are placed on the axis by first distributing them uniformly on the unit (semi-)circle and then projecting them orthogonally onto the axis. Nodes cluster at the boundaries of the interval yielding a coarser discretisation in the interior of the domain.

along the axis is not uniform. In fact, the nodes are uniformly placed on the unit circle and then projected onto the axis yielding a very fine discretisation at the boundaries of the interval.

The specific choice $\varrho = \delta(\xi - \xi_i)$ allows to calculate the values of the number density function at the grid nodes, i.e. $n_i(t)$, directly, without using Eq. (D.7). It is then possible to express differentiation as a matrix-vector multiplication

$$\frac{\partial n}{\partial \xi} \approx \frac{\partial n}{\partial \xi} = D_\xi n, \quad (\text{D.9})$$

$$n^T = [n_1(t), \dots, n_N(t)]. \quad (\text{D.10})$$

The information on the ψ_k is incorporated in the entries of the differentiation matrix D_ξ .

The advantage of spectral methods lies in the accuracy of approximation of derivatives. It can be shown that the approximation error decays faster than $O(N^{-m})$ for every m for sufficiently smooth functions (Trefethen [137]). This means that for a predefined accuracy considerably less number of grid nodes is needed, thus reducing the overall number of differential equations to be simulated. Further details on the derivation of the differentiation matrices (as a limiting case of finite difference methods) can be found in [137].

Inserting the approximation Eq. (D.9) into the population balance equation then leads to a set of ordinary differential equations for the spectral weights (resp. the values of the distribution at the collocation points) that can be solved by standard algorithms for differential equations.

A recent evaluation of the performance of spectral methods applied to the population balance equations of particulate processes can be found in [12].

D.3 Convergence of discretisations

The important question whether a discretised system correctly represents the temporal and property-related behaviour is in general very difficult to answer. However, in the limiting case $N \rightarrow \infty$ some statements can be made using the theorem of Lax and Wendroff:

Lax-Wendroff theorem [78]. Consider a sequence of grids indexed by $l = 1, 2, \dots$, with mesh parameters $k_l, h_l \rightarrow 0$ as $l \rightarrow \infty$. Let $u_l(x, t)$ denote the numerical approximation computed with a consistent and conservative method on the l th grid. Suppose that u_l converges to a function u as $l \rightarrow \infty$ in the 1-norm. Then $u(x, t)$ is a weak solution of the conservation law.

The two requirements for the application of the theorem are: (1) The problem must be written in flux-conservative form; (2) the time-stepping method has to be total-variation-diminishing (TVD), i.e. spurious oscillations have to be damped.

The finite volume method, as well as the spectral method can be written in flux-conservative form [78, 97]. The TVD-property can be guaranteed by the choice of the time-stepping method used to solve the set of ordinary differential equations, for instance the Euler method and certain Runge-Kutta methods [78, 134].

The Lax-Wendroff theorem thereby gives a justification of the use of discretised, finite-dimensional approximations to infinite-dimensional systems in various applications, for instance controller design.

Appendix E

Root-locus method for feedback controller design

The root-locus method, devised by W.R. Evans [39], is a descriptive and efficient graphical tool for the design of feedback controllers for linear time-invariant single-input single-output systems.

The basis for this method is the standard feedback control loop in the Laplace domain [83] with $d = 0$, depicted in Fig. E.1. Here, the open-loop transfer function is given by $G_o(s) = P(s)C(s)$, where $P(s)$ is the transfer function of the process to be controlled, and $C(s)$ is the transfer function of the controller to be designed. The transfer function of the closed-loop system (from reference r to controlled variable y) is given by

$$G_{ry}(s) = \frac{G_o(s)}{1 + G_o(s)} = \frac{P(s)C(s)}{1 + P(s)C(s)}. \quad (\text{E.1})$$

The stability and the dynamics of the closed-loop system are determined by the complex *roots* s_i of the characteristic polynomial

$$1 + P(s_i)C(s_i) = 0. \quad (\text{E.2})$$

The position of the s_i will move in the complex plane with variation of the controller parameters. In order to limit the number of parameters for the design process, often a controller with a fixed structure $\tilde{C}(s)$ is chosen such that $C(s) = k\tilde{C}(s)$. Here, k is an adjustable parameter, e.g. $k \in [0, \infty)$. The characteristic equation can then be written as

$$1 + kP(s_i)\tilde{C}(s_i) = 1 + k\tilde{G}_o(s_i) = 0. \quad (\text{E.3})$$

The trace of the roots of the characteristic equation in the complex plane (i.e. the geometric position) under variation of the parameter k is called the *root-locus*; one example is shown in Fig. E.2.

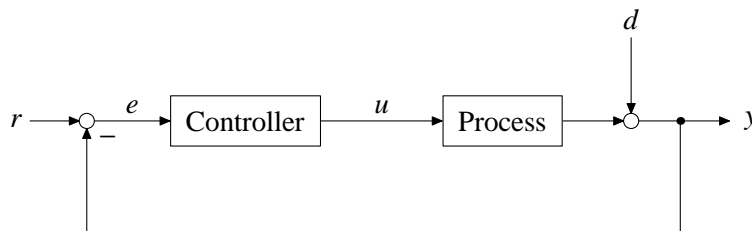


Figure E.1: Standard feedback control loop used in the derivation of the root-locus method.

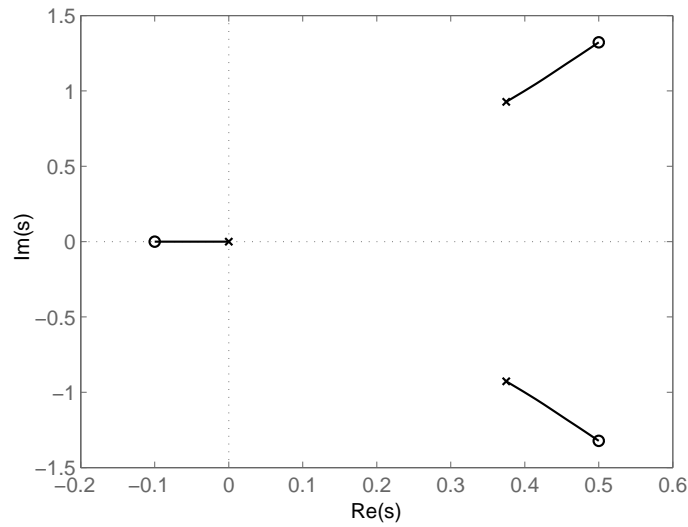


Figure E.2: Root-locus plot for an unstable, non-minimum phase open-loop system. Poles are denoted by \times , zeroes by \circ . The black lines are the root-loci obtained by variation of the parameter k from zero to infinity.

Often, the open-loop transfer function G_o can be written as:

$$G_o(s) = k\tilde{G}_o(s) = k \frac{\prod_{i=1}^q (s - n_i)}{\prod_{i=1}^n (s - p_i)}, \quad (\text{E.4})$$

where the n_i and p_i are the zeroes and the poles of the open-loop transfer function, respectively.

Rearranging the characteristic equation then yields

$$k \prod_{i=1}^q (s - n_i) + \prod_{i=1}^n (s - p_i) = 0. \quad (\text{E.5})$$

By inspection, one obtains that for $k = 0$ the root-locus starts at the poles of the open-loop transfer function. For $k \rightarrow \infty$ q branches of the root-locus end in the zeroes of the open-loop transfer function, and $n - q$ branches tend to infinity.

The rest of the root-locus can be constructed from the knowledge of the n_i and p_i by a set of graphical rules (or by using available software tools, e.g. Matlab). From the root-locus plot the controller gain k for a desired dynamic behaviour of the closed-loop system can be determined.

The root-locus method is most valuable if the poles and zeroes of the open-loop transfer function are known. It also allows the design of non-standard controllers by introducing additional poles and zeroes to shape the root-locus. The newly introduced poles and zeroes are then part of the designed controller.

Appendix F

Feedback control of bed mass in fluidised bed spray granulation

In this appendix a practical feedback controller for a continuous fluidised bed spray granulation process is designed and experimentally validated.

If a suspension or solution with a mass flow rate \dot{M}_{sus} and a solid mass fraction x_s is continuously sprayed into the process chamber and no solid is removed, then the bed mass at time t is given by

$$m_{bed}(t) = m(t = 0) + \int_0^t \dot{M}_{sus}(\tau)x_s(\tau) d\tau, \quad (\text{F.1})$$

which is monotonically increasing over time.

From practical aspects, e.g. hydro- and thermodynamics, a constant bed mass, or the tracking of the bed mass to a given reference is preferred. To that purpose an outlet tube is installed into the bottom of the process chamber.

In order to achieve the desired bed mass, a feedback controller can be applied. The current bed mass in the process can be determined from pressure drop measurements:

$$\Delta p = \frac{m_{bed} g}{A}, \quad (\text{F.2})$$

where g is the gravitational constant, and A the cross-sectional area of the process chamber.

As *manipulated variable* the flow rate of gas that can be supplied into the process chamber via the outlet tube is used. This gas flow has a classifying effect: If the gas velocity is higher than the sinking velocity of a particle entering the outlet tube, then the particle is transported back into the process chamber. If the sinking velocity, which depends on the particle size, is higher than the particle leaves the process chamber. A variation of the gas flow rate thus leads to a control of the particle outlet. By coupling of the gas flow rate with the bed mass measurements a feedback control system can be realised.

For the realisation of constant bed mass in continuous fluidised bed spray granulation process with external sieving and milling, a practical (linear) feedback controller had to be designed and implemented.

To that aim, at first the dynamic influence of the gas flow rate on the bed mass was experimentally identified. On the basis of this identified model a feedback controller was designed and tested in simulations as well as experiments.

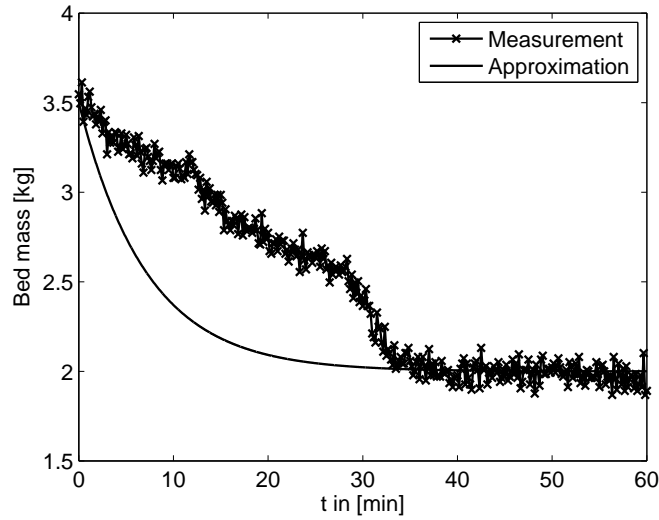


Figure F.1: Measured step response and approximation as a first-order time-lag system.

For the identification of a linear transfer function model describing the dynamic influence of the flow rate on the bed mass, a step-response experiment was performed: Particles with a certain bed mass were fluidised. The gas flow rate in the outlet tube was held constant until a constant bed mass was measured. Then the gas flow rate was decreased to a different value in one step. The development of the bed mass was registered until a new constant value was attained.

To the measured curve, depicted in Fig. F.1, a curve representing the step response of a first-order time-lag process (PT_1) was fitted, and the corresponding coefficients of the transfer function

$$P(s) = \frac{K_p}{T_1 s + 1} \quad (\text{F.3})$$

were determined: $K_p = 0.075 \text{ kg min}^{-1}$ and $T_1 = 7.15 \text{ min}$. Afterwards, the process was augmented by a measurement filter to limit the influence of measurement noise. The filter is also a first-order time-lag system with $K_f = 1$ and $T_f = 1/6 \text{ min}$. The feedback loop is closed with the filtered measurement signal, i.e. the complete process model then consists of a series of two first-order time-lag systems.

The controller was designed using the root-locus method (see Appendix E). The controller type was chosen to be proportional-integral, i.e.

$$C(s) = K \left(\frac{T_N s + 1}{T_N s} \right). \quad (\text{F.4})$$

This introduces two parameters into the design process. The parameter T_N can be removed by choosing it such that it compensates the dominating pole of the plant, or by positioning it left of the dominating pole. The former choice leads to a strongly damped and slow closed-loop system, the latter to a damped, oscillatory system. By a suitable choice of K the speed can be influenced, but care has to be taken with respect to overshooting. One possible choice is $K = 801 \text{ kg}^{-1} \text{ min}^{-1}$ and $T_N = 8 \text{ min}$.

As simulations performed were successful, the feedback controller was implemented in a fluidised bed spray granulation pilot plant. The controller was implemented in Matlab/Simulink and a communication link was established via an OPC-interface. This allowed the reading of measured values from the plant and the writing of set points for the gas flow rates to the mass flow controllers.

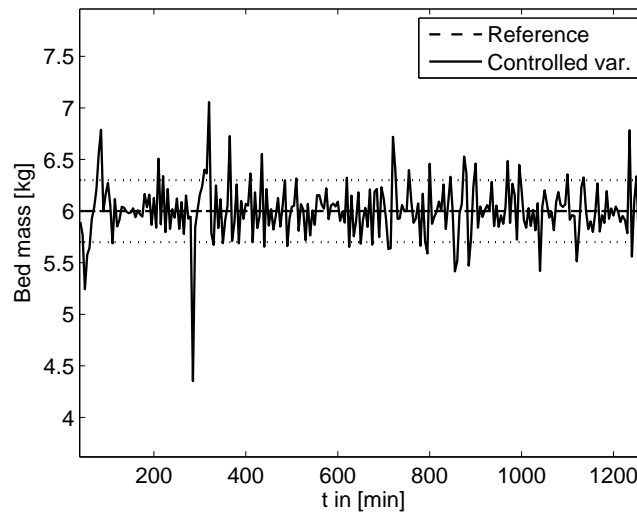


Figure F.2: Experimental results for the feedback control of bed mass in a continuous fluidised bed spray granulation process. Beside the measured bed mass and the reference value, the $\pm 5\%$ -band is also depicted.

Here, an important limitation of the controller came into action: Although it is able to remove mass from the process chamber, it is not able to insert mass directly. That means, if the controller acts too aggressively and the reference value is under-run, there is no other way than to increase the gas flow rate until the reference value is reached again by the spraying of suspension. As this is a rather slow process, the overall performance would be poor. For this reason the parameter $T_N = 133$ min is chosen much higher than T_1 , yielding a non-aggressive control behaviour. Additionally, the high value of T_N also improves the controller reaction to measurement noise by smoothing.

The controller was then tested in a long-time experiment on a continuous fluidised bed spray granulation process with external sieving, milling and particle recycle. In addition to the measurement equipment, an in-line probe for the measurement of particle moisture was installed. This probe empties its measurement volume by blowing out the particles by a flow of pressurised air, i.e. an additional variation in the bed mass measurement is introduced.

The result of the feedback control of bed mass using this setup is shown in Fig. F.2. Although only a coarse approximation to the dynamic behaviour was used in the controller design, a rather simple controller structure is used, and the measured variable is subject to severe measurement noise, the bed mass can be kept in a $\pm 5\%$ -band around the reference value for almost all times. The designed feedback control system can therefore be considered successful.

Bibliography

- [1] A -J , N., J , R., A -H A , M. Multivariable process identification and control of continuous fluidized bed dryers. *Drying Technology* 20(7) (2002), 1347–1377.
- [2] A -G , E., G ´ -S , J., G ´ -Á , V. PI controller design for a class of distributed parameter systems. *Chemical Engineering Science* 66 (2011), 4009–4019.
- [3] A , I., F , A., F F , J., W , J. LQ control design of a class of hyperbolic PDE systems: Applications to fixed-bed reactor. *Automatica* 45 (2009), 1542–1548.
- [4] A ¨ , F., F , R., N , Z. Nonlinear model predictive control: From theory to application. *J. Chin. Inst. Chem. Engrs.* 3 (2004), 299–315.
- [5] A , B., M , J. *Optimal control: Linear quadratic methods*. Dover Publications, 2007.
- [6] A , S., P , S., H , S. Breakage behaviour of agglomerates and crystals by static loading and impact. *Powder Technology* 206 (2011), 88–98.
- [7] A , M., M , S., G , N., C , T. A tutorial on particle filters for online nonlinear/non-Gaussian Bayesian tracking. *IEEE Trans. on Signal Processing* 50(2) (2002), 174–188.
- [8] B , M. Stable feedback control of linear distributed parameter systems: Time and frequency domain conditions. *Journal of Mathematical Analysis and Applications* 255 (1998), 144–167.
- [9] B , J. C., W , N. A. A comparison of some approximate methods for solving the aerosol general dynamic equation. *Journal of Aerosol Science* 29 (1998), 31–39.
- [10] B , H., B , B., V , O., F , N., K , V., G , J., M , V. Heat transfer to objects immersed in fluidized beds . *Powder Technology* 8 (1973), 273–282.
- [11] B , D., Z , M. Canonical form observer design for non-linear time-variable systems. *International Journal of Control* 38, 2 (1983), 419–431.
- [12] B ¨ , A., K , G., K , J., P , M., T , E. Numerical simulation of particulate processes for control and estimation by spectral methods. *AIChE Journal* (10.1002/aic.12757).

- [13] B^o, A., P^o, M., T^o, E., M^o, M., K^o, A. Model-based measurement of particle size distributions in layering granulation processes. *AIChE Journal* 57(4) (2011), 929–941.
- [14] B^o, J., T^o, E. Experimental investigation and modelling of continuous fluidized bed drying under steady-state and dynamic conditions. *Chemical Engineering Science* 57 (2002), 5021–5038.
- [15] C^o, E., B^o, C. *Model predictive control*. London: Springer, 1999.
- [16] C^o, C. *Zustands- und Parameterschätzung an einem katalytischen Festbettreaktor*. Düsseldorf: VDI-Verlag, 1988.
- [17] C^o, Y., L., S., P^o, L., S^o, R. Adjoint sensitivity analysis for differential algebraic systems: The adjoint DAE system and its numerical solution. *SIAM J. Sci. Comput.* 24(3) (2003), 1076–1089.
- [18] C^o, G. *Introductory graph theory*. Dover Publications, 1985.
- [19] C^o, H., A^o, F. Quasi-infinite horizon nonlinear model predictive control scheme with guaranteed stability. *Automatica* 34(10) (1998), 1205–1217.
- [20] C^o, T., C^o, P. Nonlinear control of particulate processes. *AIChE Journal* 45(6) (1999), 1279–1297.
- [21] C^o, P., D^o, P. Feedback control of hyperbolic PDE systems. *AIChE Journal* 42(11) (1996), 3063–3086.
- [22] C^o, P. D. Robust control of parabolic PDE systems. *Chemical Engineering Science* 53 (1998).
- [23] C^o, P. D. Control of nonlinear distributed process systems: Recent developments and challenges. *AIChE Journal* 47 (2001).
- [24] C^o, S., C^o, H. Correlating equations for laminar and turbulent free convection from a horizontal cylinder. *International Journal of Heat Mass and Transfer* 18 (1975), 1049–1053.
- [25] C^o, J.-P. *Process control: Theory and applications*. London: Springer, 2004.
- [26] C^o, R., M^o, K. Transfer functions of distributed parameter systems: A tutorial. *Automatica* 45 (2009), 1101–1116.
- [27] C^o, R., P^o, A. *Infinite dimensional linear systems theory*. Springer-Verlag, New York, 1978.
- [28] D^o, N., V S A^o, M., V H^o, M., K^o, J. Review of discrete particle modeling of fluidized beds. *Chemical Engineering Science* 62 (2007), 28–44.
- [29] D^o, M., P^o, M., T^o, E. A novel, structure-tracking Monte Carlo algorithm for spray fluidized bed agglomeration. *AIChE Journal* (10.1002/aic.13709).
- [30] D R^o, A., D M^o, F., G^o, R., F^o, B. DEM simulation of the mixing equilibrium in fluidized beds of two solids differing in density. *Powder Technology* 184 (2008), 214–223.

- [31] D , M., B , H., S , J., F , R., N , Z., A , F. Real-time optimization and nonlinear model predictive control of processes governed by differential-algebraic equations. *Journal of Process Control* 12 (2002), 577–585.
- [32] D , M., F , R., S , S., U , I., A , F., B , H., G , E., S , J. An efficient algorithm for nonlinear model predictive control of large-scale systems – Part 1: Description of the method. *at – Automatisierungstechnik* 50(12) (2002), 557–567.
- [33] D , J.-M., C , C., W , J. Generic properties and control of linear structured systems: A survey. *Automatica* 39 (2003), 1125–1144.
- [34] D , C., J , H. Hp-adaptive least squares spectral element method for population balance equations. *Applied Numerical Mathematics* 58 (2008), 563–576.
- [35] D , J., P , M., H , S., I , M., M , L. Investigating the dynamic behaviour of fluidized bed spray granulation processes applying numerical simulation tools. *Chemical Engineering Science* 60 (2005), 3817–3833.
- [36] D D , M., Y , B., F , M., L , B. Inventory control of particulate processes. *Computers and Chemical Engineering* 32 (2008), 46–67.
- [37] E , B., T , G., P , R. A microlevel-based characterization of granulation phenomena. *Powder Technology* 65 (1991), 257–272.
- [38] E , L. C. *Partial differential equations*. Providence, RI: American Mathematical Society, 2002.
- [39] E , W. Control system synthesis by root locus method. *Trans. AIEE* 69(1) (1950), 66–69.
- [40] F , C., P , M., T , E. Restoration of particle size distributions from fibre-optical in-line measurements in fluidized bed processes. *Chemical Engineering Science* 66 (2011), 2842–2852.
- [41] F , B. *A practical guide to pseudospectral methods*. Cambridge: Cambridge University Press, 1996.
- [42] F , D. Control of distributed parameter systems. *Regelungstechnik* 24(6) (1976), 109–144.
- [43] G , A., Ed. *Applied optimal estimation*. Massachusetts: MIT Press, 1979.
- [44] G , D. Types of gas fluidization. *Powder Technology* 7 (1973), 285–292.
- [45] G , E. *Systeme mit verteilten Parametern*. München: R. Oldenbourg Verlag, 1973.
- [46] G , T., S , C., W , F., C , I., L , J., P , J.-H., R , R., I , C., D III, F. Model predictive control of continuous drum granulation. *Journal of Process Control* 19 (2009), 615–622.
- [47] G , B., Ed. *Zustands- und Stoffwerte - Wasser, Dampf, Luft - Verbrennungsrechnung*, 3 ed. Berlin: VEB Verlag für Bauwesen, 1986.
- [48] G , V. *VDI-Wärmeatlas*, 9. ed. Düsseldorf: VDI-Verlag, 1980, ch. Wärme- und Stoffübertragung in Festbetten, pp. Gf1–Gf3.

- [49] G., D., O., S. *Numerical analysis of spectral methods*. Philadelphia: SIAM, 1977.
- [50] G., H., T., E. A new model for fluid bed drying. *Drying Technology* 15 (1997), 1687–1698.
- [51] H., S., K., G., M., L. Modelling of the batch treatment of wet granular solids with superheated steam in fluidized beds. *Chemical Engineering and Processing* 38 (1999), 131–142.
- [52] H., S., P., M., I., M., M., L. Particle population modeling in fluidized bed spray granulation – Analysis of the steady state and unsteady behavior. *Powder Technology* 130 (2003), 154–161.
- [53] H., R., K., A. Nonlinear controllability and observability. *IEEE Transactions on Automatic Control* 20, 5 (1977), 728–740.
- [54] H., H. *Lehrbuch der Analysis Teil 2*. Stuttgart: B.G. Teubner Verlag, 1991.
- [55] H., T., P., M., T., E. Investigation of growth kinetics for the fluidised bed spray granulation. In *Proceedings of the 8th European Congress of Chemical Engineering* (2011).
- [56] H., T., P., M., T., E. Prozessdynamik der Wirbelschichtgranulierung. *Chemie Ingenieur Technik* 83(5) (2011), 658–664.
- [57] H., Q., R., S., J., A. Modelling and optimization of seeded batch crystallizers. *Computers and Chemical Engineering* 29, 4 (2005), 911–918.
- [58] H., X., M., M., K., A., G., E. D. State profile estimation of an autothermal periodic fixed-bed reactor. *Chemical Engineering Science* 53 (1998), 47–58.
- [59] H., T. *The finite element method*. Mineola: Dover Publications, 1987.
- [60] H., H. M., K., S. Some problems in particle technology: A statistical mechanical formulation. *Chemical Engineering Science* 19 (1964), 555–574.
- [61] I., E. *Ordinary differential equations*. Mineola: Dover Publications, 1956.
- [62] I., S., L., J., H., K., E., B. Nucleation, growth and breakage phenomena in agitated wet granulation processes: A review. *Powder Technology* 117 (2001), 3–39.
- [63] J., G., V., Y., D., M. Simple conditions for the appearance of sustained oscillations in continuous crystallizers. *Chemical Engineering Science* 38, 10 (1983), 1675–1681.
- [64] J., S., U., J. K., D.-W., H. F. A new method for the nonlinear transformation of means and covariances in filters and estimators. *IEEE Transactions on Automatic Control* 45, 3 (Mar 2000), 477–482.
- [65] J., S. J., U., J. K. Unscented filtering and nonlinear estimation. *Proceedings of the IEEE* 92(3) (2004), 401–422.

- [66] K , N., M , W., B , H. Estimation of particle size distributions from focused beam reflectance measurements based on an optical model. *Chemical Engineering Science* 64 (2009), 984–1000.
- [67] K , A., C , P. Nonlinear control of spatially inhomogenous aerosol processes. *Chemical Engineering Science* 54 (1999), 2669–2678.
- [68] K , R. E. A new approach to linear filtering and prediction problems. *Trans. ASME – J. Basic Eng* 82 (1960).
- [69] K , M. Implementation of distributed parameter state observer. *Distributed Parameter Systems: Modelling and Identification, Proceedings of the IFIP working Conference Rome, Italy* (1978).
- [70] K , B. *Notes on Numerical Fluid Mechanics*, vol. 45. Braunschweig: Vieweg, 1993, ch. A robust upwind discretization method for advection, diffusion and source terms, pp. 117–138.
- [71] K , S. R., E , D. L., T , T. J. Observability of nonlinear systems. *Inform. Contr.* 22 (1973), 89–99.
- [72] K , R. *VDI-Wärmeatlas*, 9 ed. Düsseldorf: VDI-Verlag, 1994, ch. Stoffwerte von Luft, pp. Dbb1–Dbb13. ISBN 3-540-41201-8.
- [73] K , J., P , M., W , G., H , S., M , L. Improved accuracy and convergence of discretized population balance for aggregation: The cell average technique. *Chemical Engineering Science* 61 (2006), 3327–3342.
- [74] K , S., R , D. On the solution of population balance equations by discretization – I. A fixed pivot technique. *Chemical Engineering Science* 51(8) (1996), 1311–1332.
- [75] K , D., L , O. *Fluidization engineering*. Boston: Butterworth-Heinemann, 1991.
- [76] L , K., M , T. Simultaneous coagulation and break-up using constant-*N* Monte Carlo. *Powder Technology* 110 (2000), 82–89.
- [77] L , S.-J., S , R., K , S. The stability and dynamic behavior of a continuous crystallizer with a fines trap. *AIChE J.* 17, 6 (1971), 1459–1470.
- [78] L V , R. *Numerical methods for conservation laws*. Basel: Birkhäuser, 1992.
- [79] L , J., F , B., W , C., L , J. A general compartment-based population balance model for particle coating and layering granulation. *AIChE Journal* (10.1002/aic.12678).
- [80] L , D. Observing the state of a linear system. *IEEE Trans. on Military Electronics* (1964), 74–80.
- [81] L , D. Observers for multivariable systems. *IEEE Trans. on Automatic Control AC-11(2)* (1966), 190–197.
- [82] L , D. An introduction to observers. *IEEE Trans. on Automatic Control AC-16(6)* (1971), 596–602.

- [83] L *Skog*, J. *Regelungstechnik 1*. Berlin: Springer-Verlag, 2006.
- [84] L *Skog*, J. *Regelungstechnik 2*. Berlin: Springer-Verlag, 2006.
- [85] M *Wang*, D., T *Chen*, D., B *Chen*, R. High-resolution simulation of multidimensional crystal growth. *Industrial and Engineering Chemistry Research* 41 (2002), 6217–6223.
- [86] M *Wang*, A., E *Kang*, F., F *Chen*, H. Direct simulation Monte Carlo for simultaneous nucleation, coagulation, and surface growth in dispersed systems. *Chemical Engineering Science* 59 (2004), 2231–2239.
- [87] M *Wang*, M. Use of a Kalman filter to reconstruct particle size distributions from fbrm measurements. *Chemical Engineering Science* 70, 1 (2012), 99–108.
- [88] M *Wang*, M., B *Chen*, A., H *Chen*-R *Chen*, R. Passivity based control of a distributed PEM fuel cell model. *Journal of Process Control* 20 (2010), 292–313.
- [89] M *Wang*, M., B *Chen*, A., S *Chen*, R., S *Chen*, C., V *Chen*, A., S *Chen*, K. Two state estimators for the barium sulfate precipitation in a semi-batch reactor. *Chemical Engineering Science* 64(4) (2009).
- [90] M *Wang*, M., L *Chen*, G., S *Chen*, J., Z *Chen*, M., G *Chen*, E. State and parameter estimation for adsorption columns by nonlinear distributed parameter state observers. *Journal of Process Control* 4(3) (1994), 163–172.
- [91] M *Wang*, M., S *Chen*, C., N *Chen*, B., V *Chen*, A., S *Chen*, K. Methods of state estimation for particulate processes. In *Proceedings of the 16th European Symposium on Computer Aided Process Engineering and 9th International Symposium on Process Systems Engineering* (2006), W. Marquardt and C. Pantelides, Eds., Elsevier B.V.
- [92] M *Wang*, N., D *Chen*, P., S *Chen*, F. Numerical solution of multi-variable cell population balance models: I. Finite difference methods. *Computers and Chemical Engineering* 25 (2001), 1411–1440.
- [93] M *Wang*, D., F *Chen*, R. Solution of population balance equations using the direct quadrature method of moments. *Journal of Aerosol Science* 36(1) (2005), 43–73.
- [94] M *Wang*, D., P *Chen*, J., F *Chen*, R., V *Chen*, R., B *Chen*, A. Quadrature method of moments for population-balance equations. *AIChE Journal* 49(5) (2003), 1266–1276.
- [95] M *Wang*, H. *VDI-Wärmeatlas*, 9 ed. Düsseldorf: VDI-Verlag, 1994, ch. Wärmeübergang in Wirbelschichten, pp. Mf1–Mf8. ISBN 3-540-41201-8.
- [96] M *Wang*, D., R *Chen*, J., R *Chen*, C., S *Chen*, P. Constrained model predictive control: Stability and optimality. *Automatica* 36 (2000), 789–814.
- [97] M *Wang*, D., B. Flux-corrected pseudospectral method for scalar hyperbolic conservation laws. *Journal of Computational Physics* 82(2) (1989), 413–428.
- [98] M *Wang*, D., K *Chen*, C. Monte Carlo simulation for the solution of the bi-variate dynamic population balance equation in batch particulate systems. *Chemical Engineering Science* 62 (2007), 5295–5299.
- [99] M *Wang*, H. *Particle size measurements – Fundamentals, practice, quality*. Dordrecht: Springer Science+Business Media B.V., 2009.

- [100] M^o, L., H^o, S., P^o, M. *Granulation*. Amsterdam: Elsevier B. V., 2007, ch. Fluidized Bed Spray Granulation, pp. 21–188.
- [101] N^o, H., S^o, A. J. *Nonlinear dynamical control systems*. New York: Springer, 1991.
- [102] N^o, J., W^o, S. *Numerical optimization*. London: Springer Science+Business Media, LLC, 2006.
- [103] Ö^o, H. H^∞ optimal controller design for a class of distributed parameter systems. *International Journal of Control* 58(4) (1993), 739–782.
- [104] P^o, S., K^o, A. Stabilization of continuous fluidized bed spray granulation – a Lyapunov approach. In *Proceedings of the 8th IFAC Symposium on Nonlinear Control Systems* (2010).
- [105] P^o, S., K^o, A. Stabilization of continuous fluidized bed spray granulation with external product classification. *Chemical Engineering Science* 70(5) (2012), 200–209.
- [106] P^o, M., A^o, S., J^o, M., P^o, S., H^o, S., T^o, E. *Modern Drying Technology*, vol. 3. Weinheim: Wiley-VCH, 2011, ch. Determination of physical properties of particles, nanoparticles and particle beds, pp. 295–379.
- [107] P^o, M., C^o, U., T^o, E. An analytical solution of population balance equations for continuous fluidized bed drying. *Chemical Engineering Science* 66 (2011), 1916–1922.
- [108] P^o, M., K^o, J., H^o, S., W^o, G., T^o, E., M^o, L., W^o, B. A generic population balance model for simultaneous agglomeration and drying in fluidized beds. *Chemical Engineering Science* 62 (2007), 513–532.
- [109] P^o, J. *Graphentheorie: Grundlagen und Anwendungen*. Wiesbaden: Akademische Verlagsgesellschaft, 1981.
- [110] P^o, M., O^o, B., A^o, A., E^o, B. Model-based control of a granulation system. *Powder Technology* 108 (2000), 192–201.
- [111] P^o, D., R^o, B., C^o, C. Dynamic Matrix Control Method. *United States Patent # 4,349,869 (Sep. 14, 1982)* (1982).
- [112] R^o, C., G^o, B., K^o, J. Large-scale powder mixer simulations using massively parallel GPU architectures. *Chemical Engineering Science* 65 (2010), 6435–6442.
- [113] R^o, R., M^o, T., K^o, A., H^o, S., P^o, M., M^o, L. A numerical bifurcation analysis of continuous fluidized bed spray granulation with external product classification. *Chemical Engineering and Processing* 45 (2006), 826–837.
- [114] R^o, D. *Population balances: Theory and application to particulate systems in engineering*. New York: Academic Press, 2000.
- [115] R^o, A., L^o, M. *Theory of particulate processes: Analysis and techniques of continuous crystallization*. Academic Press, 1972.
- [116] R^o, C., R^o, J. Constrained process monitoring: Moving-horizon approach. *AIChE Journal* 48(1) (2002), 97–109.

- [117] R , L. Trends in research and industrial application of fluidization. *Verfahrenstechnik 11* (1977), 381–384.
- [118] R , J. Representation and H^∞ -control of LTI spatially distributed systems. *Automatisierungstechnik 52(1)* (2004), 23–29.
- [119] R , K. J. *Multivariable control – A graph theoretic approach*. Berlin: Akademie-Verlag, 1988.
- [120] R , H.-K., A , R., A , N. *First-order partial differential equations*, vol. 1. Dover Publications, 1986.
- [121] R , J., O’D , D. *Predictive functional control*. London: Springer, 2009.
- [122] R , J., Z , W. Sedimentation and fluidization: Part I. *Transactions of the Institution of Chemical Engineers 32* (1954), 35–53.
- [123] R , D. G., L , J. H., R , J. B. A moving horizon-based approach for least-squares estimation. *AIChE Journal 42* (1996), 2209–2224.
- [124] R , A., W , J., M , M. Modeling and experimental analysis of PSD measurements through FBRM. *Part. Part. Syst. Charact. 17* (2000), 167–179.
- [125] S , S. *Nonlinear systems: Analysis, stability and control*. New York: Springer-Verlag, 1999.
- [126] S , R. Die Diffusionszahl von Wasserdampf-Luftgemischen und die Verdampfungsgeschwindigkeit. *VDI Beiheft Verfahrenstechnik* (1938), 170.
- [127] S , E.-U., T , E. *Wärmeübertragung in Festbetten, durchmischten Schüttgütern und Wirbelschichten*. Stuttgart: Georg Thieme Verlag, 1988.
- [128] S , H., F , J., G , M. Feedback control of hyperbolic distributed parameter systems. *Chemical Engineering Science 60* (2005), 969–980.
- [129] S , D. *Fluidodynamik und Wärmeübergang in einer zirkulierenden Wirbelschicht*. Düsseldorf: VDI-Verlag, 1997.
- [130] S , D., E-F , N., L , M., M , P., C , P. Predictive control of particle size distributions in particulate processes. *Chemical Engineering Science 61* (2006), 268–281.
- [131] S , D. *Optimal state estimation – Kalman, H_∞ , and nonlinear approaches*. Hoboken: John Wiley & Sons, Inc, 2006.
- [132] S , M., M , T. Constant-number Monte Carlo simulation of population balances. *Chemical Engineering Science 53(9)* (1998), 1777–1786.
- [133] S , J., B , R. *Introduction to numerical analysis*. New York: Springer-Verlag, 2002.
- [134] T , E. Total-variation and error estimates for spectral viscosity approximations. *Mathematics of Computation 60* (1993), 245–256.
- [135] T -V , K., P , M., T , E. Investigation of the kinetics of fluidized bed spray agglomeration based on stochastic methods. *AIChE Journal 57(11)* (2011), 3012–3026.

- [136] T , F. Observing the state of non-linear dynamic systems. *International Journal of Control* 17(3) (1973), 471–479.
- [137] T , L. *Spectral methods in MATLAB*. Philadelphia: SIAM, 2000.
- [138] T , E., M , A., Eds. *Modern Drying Technology*, vol. 1–5. Weinheim: Wiley-VCH, 2007.
- [139] M , R., W , E. A. The square-root unscented Kalman filter for state and parameter estimation. *International Conference on Acoustics, Speech, and Signal Processing, Salt Lake City, Utah* (2001).
- [140] V , J., D , S., W , H., Y , W., R , R. Distributed parameter control of a batch fluidised bed dryer. *Control Engineering Practice* 17 (2009), 1096–1106.
- [141] V , U., R , J. Population balance modelling and H_∞ -controller design for a crystallization process. *Chemical Engineering Science* 57 (2002), 4401–4414.
- [142] V , A., L , C., H , M. A basic population balance model for fluid bed spray granulation. *Chemical Engineering Science* 64 (2009), 4389–4398.
- [143] W , W., K , A., Eds. *Properties of water and steam. The industrial standard IAPWS-IF97*, 3 ed. Berlin: Springer-Verlag, 1998.
- [144] W , F., C , I. Review and future directions in the modelling and control of continuous drum granulation. *Powder Technology* 124 (2002), 238–253.
- [145] W , H., D , T., S , P., R , R., Y , W. Modelling of batch fluidised bed drying of pharmaceutical granules. *Chemical Engineering Science* 62 (2007), 1524–1535.
- [146] W , L. *Model predictive control system design and implementation using MATLAB*. London: Springer, 2009.
- [147] W , P. On the feedback control of distributed parameter systems. *International Journal of Control* 3(3) (1966), 255–273.
- [148] W , H.-D. *Strukturelle Analyse linearer Regelungssysteme*. München: R. Oldenbourg Verlag, 1993.
- [149] W , D. M. *State space and linear systems*. New York: McGraw-Hill, 1971.
- [150] W , E. Relationship between particle-size and chord-length distributions in focused beam reflectance measurement: Stability of direct inversion and weighting. *Powder Technology* 133 (2002), 125–133.
- [151] Z , M. *Nichtlineare Beobachter für chemische Reaktoren*. Düsseldorf: VDI-Verlag, 1977.
- [152] Z , M. Beobachter mit verteilten Parametern. In *GMA Workshop Theoretische Verfahren der Regelungstechnik, Interlaken* (1998).
- [153] Z , H., M , A., M , T., Z , C. Analysis of four Monte Carlo methods for the solution of population balances in dispersed systems. *Powder Technology* 173 (2007), 38–50.
- [154] Z , G. State observation by on-line minimization. *International Journal of Control* 60(4) (1994), 595–606.

Co-supervised theses

The following theses were co-supervised by the author of this thesis:

Name	Title of thesis	Type
Jue Qian	State Estimation in Fluidized Bed Granulation Batch Processes	Master thesis
Günter Klaunick	Numerische Lösung von Populationsbilanzen durch Spektralmethoden	Pre-diploma thesis
	Anwendung von Spektralmethoden auf Partikelprozesse	Diploma thesis
Hung Minh Quang Tran	Grundlegende Gestaltung eines Berechnungstools zur Simulation von Wirbelschicht-Sprühgranulationsprozessen für variable Anlagenkonfigurationen	Diploma thesis

Curriculum vitae

Name	Andreas Bück
Date of birth	June 3rd, 1982
Place of birth	Magdeburg, Germany
Education	
1989-1993	Elementary school “Düppler Mühle”, Magdeburg
1993-2001	Gymnasium “Bettina von Arnim”, Magdeburg
2001-2002	Gymnasium “Albert Einstein”, Magdeburg
Military service	
2002-2003	Conscripted military service, Luftwaffe (German Air Force)
Higher Education	
2003-2008	Otto von Guericke University, Magdeburg, Diploma studies “Systemtechnik und Technischen Kybernetik” Academic degree: Diplomingenieur (Dipl.-Ing.)
Doctoral studies	
since 09/2008	Otto von Guericke University, Magdeburg, Chair of Thermal Process Engineering, Scientific assistant “InnoProfile-Nachwuchsforschungsgruppe” NaWiTec